Schweizerische Eidgenossenschaft
Confédération suisse
Confederazione Svizzera
Confederaziun svizra

Eidgenössisches Departement für Umwelt, Verkehr, Energie und Kommunikation UVEK
Département fédéral de l'environnement, des transports, de l'énergie et de la communication DETEC
Dipartimento federale dell'ambiente, dei trasporti, dell'energia e delle comunicazioni DATEC

Bundesamt für Strassen
Office fédéral des routes
Ufficio federale delle Strade

Static effects, feasibility and execution of drainages in tunnelling

Statische Auswirkung, Machbarkeit und Ausführungsaspekte von Gebirgsdrainagen im Untertagbau

L'effet statique, des aspects de la faisabilité et de la mise en œuvre des drainages lors des travaux souterrains

ETH Zürich, Institut für Geotechnik, Professur für Untertagbau
Dr. Sara Zingg
Prof. Dr. Georg Anagnostou

Forschungsprojekt FGU 2010/004 auf Antrag der Arbeitsgruppe Tunnelforschung (AGT)

Dezember 2016 **1587**

Schweizerische Eidgenossenschaft
Confédération suisse
Confederazione Svizzera
Confederaziun svizra

Eidgenössisches Departement für Umwelt, Verkehr, Energie und Kommunikation UVEK
Département fédéral de l'environnement, des transports, de l'énergie et de la communication DETEC
Dipartimento federale dell'ambiente, dei trasporti, dell'energia e delle comunicazioni DATEC

Bundesamt für Strassen
Office fédéral des routes
Ufficio federale delle Strade

Static effects, feasibility and execution of drainages in tunnelling

Statische Auswirkung, Machbarkeit und Ausführungsaspekte von Gebirgsdrainagen im Untertagbau

L'effet statique, des aspects de la faisabilité et de la mise en œuvre des drainages lors des travaux souterrains

ETH Zürich, Institut für Geotechnik, Professur für Untertagbau
Dr. Sara Zingg
Prof. Dr. Georg Anagnostou

Forschungsprojekt FGU 2010/004 auf Antrag der Arbeitsgruppe Tunnelforschung (AGT)

Dezember 2016 **1587**

Impressum

Forschungsstelle und Projektteam
Projektleitung
Prof. Dr. Georg Anagnostou

Mitglieder
Dr. Sara Zingg

Begleitkommission
Präsident
Felix Amberg

Mitglieder
Martin Bosshard
Alain Jeanneret
Dr. Alex Schneider
Heinz Dicht
Urs Kost

Antragsteller
Arbeitsgruppe Tunnelforschung (AGT)

Bezugsquelle
Das Dokument kann kostenlos von http://www.mobilityplatform.ch heruntergeladen werden.

Table of contents

Summary

This research project investigates the effectiveness of drainage measures with respect to three particularly important problems associated with tunnelling through water-bearing, weak ground: the stability of tunnel faces, the stability and deformation of grouting bodies and the water pressure acting on tunnel linings. Water is an adverse factor with respect to the stability and deformation of underground structures due to, (i), the pore water pressure and, (ii), the seepage forces associated with seepage flow towards the tunnel. Drainage boreholes reduce the pore water pressure and the seepage forces in the vicinity of the cavity. Furthermore, loss of pore water pressure increases the effective stresses and thus the shearing resistance of the ground (‘consolidation’), which is favourable in terms of the deformation occurring during and after tunnelling. The goal of the research project is to improve the understanding of the static impacts of drainage measures and to provide design aids for the tunnel engineer.

The study of *face stability* is organised in four chapters. The first chapter investigates the effectiveness of various advance drainage schemes with respect to face stability in ground of uniform permeability. A suite of computations is carried out to quantify the effects of the geometric parameters of several different drainage schemes. The seepage forces, which are considered in the limit equilibrium computations, are determined numerically through a steady-state, three-dimensional seepage flow analysis which takes account of the characteristics of a given drainage scheme. A dimensionless formulation of the required support pressure (or the required cohesion of the ground) is developed in order to produce design nomograms that can provide a quick assessment of face stability in cases involving partial pore pressure relief in advance of excavation.

Hydraulic heterogeneity due to alternating aquifers and aquitards may result in a hydraulic head field which is particularly adverse for face stability due to high gradients close to the face. In the second chapter, a suite of stability analyses are carried out in order to quantify the effects of the orientation, thickness, location, number and permeability ratio of the ground layers, paying particular attention to the effectiveness of a common advance drainage measure consisting of six axial boreholes drilled from the tunnel face. The computational results provide valuable information about whether and to what extent the required support pressure is higher or lower than in the case of uniformly permeable ground; which ground structures are critical for face stability and necessitate a higher support pressure; the extent to which advance drainage allows for a reduction in support pressure; and where the drainage boreholes have to be arranged in order to be most effective.

Several other factors may impose limits on pore pressure relief in the ground around advance drainage boreholes and thus limit their effectiveness with respect to face stability: (i) the hydraulic capacity of the drainage boreholes hindering full pressure relief in highly permeable ground at high water table; (ii) the casings required for stabilizing the borehole, but which in turn restrict pore pressure relief to small openings; (iii) the lead-time in a poorly permeable ground where pore pressure relief by advance drainage may take a prohibitively long time to work; (iv) environmental constraints with respect to the drawdown of the water table; (v) the magnitude of settlements, which may impose limits on the amount of admissible pore pressure relief and, (vi) the pumping capacity available on site, which may limit the quantity of water inflow. In the third chapter, the hydraulic capacity of the drainage boreholes is investigated by means of an equivalent conductivity model taking account of pipe- and open-channel flow hydraulics within the drainage borehole. The model makes it possible to determine the maximum ground permeability for which it is safe to consider the borehole wall as a seepage face. In addition, the minimum requirements for casings are elaborated based upon face stability considerations. The fourth chapter discusses the time required for lowering the hydraulic head field to practically steady state conditions and analyses the magnitudes of drawdown, settlement and water discharge caused by advance drainage boreholes drilled from the tunnel face. The computational results provide useful insights into

potential risks related to advance drainage measures for face stability and indicate the limits of applicability of the design nomograms.

The *stability of grouting bodies* is studied for two crucial drainage measures: (i) drainage of the inner part of a grouting body to decrease the load and the risk of inner erosion due to the action of high hydraulic gradients, (ii) advance drainage of the area of future grouting bodies to increase the effective stresses and lead to consolidation of the ground prior to injection. A cylindrical tunnel is assumed to be excavated in ground considered as a porous, elasto-plastic medium obeying the principle of effective stress and Coulomb's failure criterion and taking the seepage forces into account. For the virtual case of ideal drainage, i.e. complete pore pressure relief, an analytical solution is derived for plane strain conditions. Several specific arrangements of drainage boreholes are studied by means of hydraulic-mechanical coupled FE-modelling and the deviations from the analytical solutions are elaborated. The effect of the drainage measures is discussed by means of the characteristic line, i.e. stress as a function of the displacement at the excavation boundary of the tunnel and the degree of plastification of the grouting body, which may serve as another dimensioning criterion for stability. The computational results provide valuable information about the static effects of number, length and spacing of drainage boreholes arranged inside and outside the grouting body.

The study of the *tunnel lining* quantifies (i) the residual water pressure developing on the impermeable tunnel lining in the presence of permanent drainage measures, as well as (ii) the discharge of water resulting from the drainage measures. The three-dimensional, numerical seepage flow analyses in a homogeneous, isotropic medium obeying Darcy's law at steady-state conditions take account of two drainage layouts: radial drainage borehole arrangements drilled through the impermeable tunnel lining and ring-shaped drainage gaps arranged in the lining. Design charts are provided, which allow a quick assessment of the residual water pressure and of the inflow resulting from several different drainage layouts and thus represent a useful design aid for tunnel engineers.

In summary, the contribution of this report is the detailed investigation of the static effects of drainage measures during tunnelling with respect to the stability of both the tunnel face and the grouting body, as well as the pressure acting on the tunnel lining. Design aids are supplied, which are capable of providing a quick assessment of face stability when considering a number of advance drainage schemes, and which quantify the residual water pressure and inflow when considering several different permanent drainage measures.

Zusammenfassung

Das Forschungsprojekt untersucht die Auswirkung von Drainagemassnahmen auf drei grundlegende, tunnelbauliche Problemstellungen durch wasserführendes Gebirge von geringer Festigkeit: die Stabilität der Ortsbrust, Stabilität und Verformungen eines Injektionskörpers, sowie der Wasserdruck auf die Tunnelschale. Wasser hat eine ungünstige Wirkung auf Stabilität und Verformungen von Tunnelbauten zum einen wegen dem Porenwasserdruck, und zum andern wegen den Strömungskräften, die sich aus der Sickerströmung in Richtung Tunnel ergeben. Drainagebohrungen reduzieren sowohl den Porenwasserdruck als auch die Strömungskräfte rund um den Hohlraum. Zudem erhöht der Porenwasserdruckabbau die effektiven Spannungen und somit die Scherfestigkeit des Baugrundes („Konsolidation"), was sich günstig auf die Verformungen während und nach dem Tunnelbau auswirkt. Das Ziel des Forschungsprojektes ist es, das Verständnis der statischen Auswirkungen von Drainagemassnahmen zu verbessern und dem praktischen Ingenieur Hilfsmittel für Planung und Ausführung zur Verfügung zu stellen.

Die Untersuchung der *Ortsbruststabilität* ist in vier Kapitel gegliedert. Das erste Kapitel untersucht die Wirksamkeit von verschiedenen, vorauseilenden Drainageanordnungen im homogen durchlässigen Baugrund. Die geometrischen Parameter der unterschiedlichen Drainageanordnungen werden variiert und ihr Einfluss quantifiziert. Die Strömungskräfte, die in die Gleichungen des Grenzgleichgewichts eingehen, werden für jede einzelne Drainageanordnung numerisch mittels stationärer, dreidimensionaler Strömungsanalyse bestimmt. Eine dimensionslose Formulierung des erforderlichen Stützdrucks (oder der Baugrundkohäsion) wird entwickelt sowie Dimensionierungs-Nomogramme erarbeitet, die eine rasche Beurteilung der Ortsbruststabilität unter Berücksichtigung der vorauseilenden Drainagemassnahme erlauben.

Bei einer Wechsellagerung von Aquiferen und Aquitarden kann eine Druckverteilung entstehen, die in Ortsbrustnähe grosse Gradienten aufweist und darum besonders ungünstig ist für die Ortsbruststabilität. Im zweiten Kapitel wird die hydraulische Heterogenität am Beispiel einer gängigen Drainageanordnung (sechs Drainagebohrungen ab der Ortsbrust) diskutiert und der Einfluss von Orientierung, Dicke, Ort, Anzahl und Durchlässigkeitsverhältnis der Baugrundschichten auf die Ortsbruststabilität untersucht. Die Berechnungsresultate liefern wertvolle Informationen darüber, ob und um wieviel der erforderliche Stützdruck von jenem in homogenem Baugrund abweicht; welche Baugrundmodelle einen höheren Stützdruck erfordern und somit kritisch sind für die Ortsbruststabilität; welche Stützdruckreduktion durch Drainagemassnahmen erreichbar ist und wo die Drainagebohrungen angeordnet werden müssen, damit sie möglichst ihre volle Wirkung entfalten.

Es gibt eine Reihe von Faktoren, die den erreichbaren Porenwasserdruckabbau rund um Drainagebohrungen einschränken können: (i) im hochdurchlässigen Baugrund tief unterhalb des Bergwasserspiegels können die Wasserzutritte die hydraulische Kapazität der Bohrungen erreichen, womit sich in den Drainagebohrungen ein Wasserdruck aufbaut; (ii) in instabilen Bohrlöchern erforderliche Hüllrohre verringern die für den Druckabbau zur Verfügung stehende Fläche auf kleine Öffnungen, was eine verminderte Drainagewirkung zur Folge hat; (iii) die Vorlaufzeit bis zum Erreichen des gewünschten Drucks kann in geringdurchlässigem Baugrund zu lange sein; (iv) eine Absenkung des Grundwasserspiegels kann aufgrund von Umweltauflagen problematisch sein; (v) im überbauten Gebiet kann ein Porenwasserdruckabbau zu unzulässigen Setzungen führen und; (vi), die verfügbare Pumpkapazität auf der Baustelle kann die abführbare Wassermenge begrenzen. Diese limitierenden Faktoren werden anhand der Problemstellung der Ortsbruststabilität untersucht. Im dritten Kapitel wird ein Modell zur Erfassung der hydraulischen Kapazität von Drainagebohrungen erarbeitet, das das turbulente Druck- und Freispiegelabflussverhalten im Drainagerohr mittels eines porösen Mediums von äquivalenter Durchlässigkeit abbildet. So kann die maximale Baugrunddurchlässigkeit bestimmt werden, für welche die Annahme von atmosphärischem Druck entlang der Bohrlochwand noch zulässig ist. Weiter werden hydraulische Mindestanforderungen an Hüllrohre erarbeitet, die eine ausreichende Drainagewirkung sicherstellen. Im vierten

Kapitel wird schliesslich die zum Erreichen einer nahezu stationären Porenwasserdruckverteilung erforderliche Zeit quantifiziert. Im Weiteren werden die aus Drainagebohrungen resultierende, zusätzliche Grundwasserspiegelabsenkung, die Setzung der Geländeoberfläche und der Wasserzutritt analysiert. Die Berechnungsresultate liefern wichtige Hinweise auf die potentiellen Risiken von vorauseilenden Drainagemassnahmen und zeigen die Anwendungsgrenzen der entwickelten Dimensionierungs-Nomogramme auf.

Die *Stabilität von Injektionskörpern* wurde anhand von zwei Drainageanordnungen untersucht: (i) der Drainage des zentralen Bereichs eines Injektionskörpers mit dem Ziel, die Beanspruchung sowie das Risiko der inneren Erosion infolge grosser hydraulischer Gradienten zu reduzieren; und (ii), der vorauseilende Drainage des gesamten Bereiches des zukünftigen Injektionskörpers, um die effektiven Spannungen zu erhöhen und so den Baugrund vor der Injektionsmassnahme zu konsolidieren. Betrachtet wird ein kreisförmiger Tunnel im wasserführenden Baugrund, der wiederum als elasto-plastisches, poröses Medium unter Gültigkeit des Prinzips der effektiven Spannungen und der Coulomb'schen Bruchbedingung angesehen wird. Für den theoretischen Fall der vollständigen Drainage, d.h. der Porenwasserdruckabsenkung auf atmosphärischen Druck, wird eine analytische Lösung hergeleitet. Praxisnahe Drainageanordnungen werden mittels hydraulisch-mechanisch gekoppelter FE-Modellierung untersucht und die Unterschiede zur analytischen Lösung aufgezeigt. Die Auswirkungen der Drainagemassnahmen werden anhand der Kennlinien, also des Ausbauwiderstands als Funktion der Verschiebung am Tunnelausbruchrand, diskutiert. Daneben wird der Plastifizierungsgrad erfasst, der ein Dimensionierungskriterium gegen innere Erosion darstellen kann. Die Resultate liefern wertvolle Informationen über die statische Wirkung von Anzahl, Länge und Abstand der Drainagebohrungen, welche inner- und ausserhalb eines Injektionskörpers angeordnet werden.

Die Studie zum *Tunnelausbau* quantifiziert die Wirkung von zwei permanenten Drainagemassnahmen: (i) radiale Drainagen, die durch den undurchlässigen Ausbau gebohrt werden und (ii), Drainageschlitze (Ringfugen), die den ansonsten undurchlässigen Ausbau in regelmässigen Abständen unterbrechen. Der Restwasserdruck auf den Tunnelausbau und die abzuführenden Wassermengen werden mittels stationärer, dreidimensionaler Strömungsanalyse nach Darcy in einem homogenen, isotropen Medium ermittelt. Die Resultate werden in Dimensionierungs-Diagrammen präsentiert, welche eine rasche und einfache Beurteilung von Wasserdruck und Zufluss dieser Drainageanordnungen erlauben und so ein nützliches Hilfsmittel für den praktizierenden Ingenieur darstellen.

Zusammenfassend liegt der Beitrag dieses Forschungsberichts in der detaillierten Untersuchung der statischen Effekte von Drainagemassnahmen im Tunnelbau bezüglich der Ortsbruststabilität, der Stabilität von Injektionskörpern und der Belastung der Tunnelschale. Es werden Dimensionierungshilfen erarbeitet, die eine rasche Beurteilung der Ortsbruststabilität unter Berücksichtigung verschiedener, vorauseilender Drainageanordnungen erlauben, sowie Wasserdruck und Zufluss infolge permanenter Drainagemassnahmen durch den Tunnelausbau quantifizieren.

Résumé

Ce projet de recherche analyse l'efficacité des mesures de drainage en ce qui concerne les trois problèmes les plus importants associés aux travaux souterrains dans des roches faibles à conducteurs d'eau : la stabilité du front de taille, la stabilité et les déformations d'un corps d'injection et la pression de l'eau sur le revêtement du tunnel. L'eau est un facteur défavorable en ce qui concerne la stabilité et les déformations des structures souterraines à cause (i) de la pression de l'eau interstitielle, et (ii) de la force de l'écoulement associée à un flux d'écoulement en direction du tunnel. Les forages de drainage réduisent la pression de l'eau interstitielle et les forces d'écoulement dans les environs du tunnel. En outre, la perte de la pression de l'eau interstitielle augmente les contraintes effectives et ainsi la résistance au cisaillement du sol (« consolidation »), ce qui est favorable en termes de déformations avant ainsi qu'après l'excavation du tunnel. L'objectif de ce projet de recherche est d'améliorer la compréhension des effets statiques des mesures de drainage afin de fournir des outils pratiques aux ingénieurs spécialistes des tunnels.

L'analyse de la *stabilité du front de taille* est divisée en quatre chapitres. Le premier chapitre analyse l'efficacité de plusieurs configurations différentes de drainages dans un sol de perméabilité uniforme. Les paramètres géométriques de différentes configurations de drainage sont variés afin de quantifier leur effet sur la stabilité du front de taille. Les forces d'écoulement, qui sont considérées dans les équations de limite d'équilibre, ont été déterminées pour chaque configuration de drainage en exécutant une analyse tridimensionnelle d'écoulement stationnaire. Une formulation sans dimension de la pression de soutien (ou de la cohésion du sol) nécessaire a été développée afin d'élaborer des nomogrammes de dimensionnement permettant une évaluation rapide de la stabilité du front de taille considérant des mesures de drainage avant l'excavation du tunnel.

L'hétérogénéité hydraulique due à une alternance d'aquifères et d'aquitards peut mener à une distribution de pression défavorable caractérisée par des gradients hydrauliques considérables étant orientés vers le front de taille. Le second chapitre traite l'influence de l'orientation, l'épaisseur, l'emplacement, le nombre ainsi que le rapport de perméabilité entre les couches de sol sur la stabilité du front de taille, en tenant compte d'un arrangement courant des drainages (six forages de drainage réalisés depuis le front de taille). Les résultats de ces calculs fournissent des informations précieuses sur les points suivants : si ou dans quelle mesure, la pression de soutien diffère de celle nécessaire dans un sol homogène ; quelles structures du sol nécessitent une pression de soutien plus élevée et sont ainsi plus critiques en vue de la stabilité du front de taille ; quelle réduction de la pression de soutien est réalisable grâce aux mesures de drainage ; et où est-ce que les drainages doivent être forés afin que leur efficacité soit maximale.

Plusieurs facteurs peuvent limiter la réduction de la pression de l'eau interstitielle et ainsi l'efficacité des forages de drainage en ce qui concerne la stabilité du front de taille : (i) dans des sols très perméables ayant un niveau d'eau très élevé, la pénétration d'eau peut atteindre la capacité hydraulique des forages, ce qui a pour conséquence qu'une pression d'eau se forme dans les forages de drainage ; (ii) les gaines, nécessaires pour stabiliser le trou du forage, réduisent la surface disponible pour la réduction de pression à des petites ouvertures, ce qui engendre un effet de drainage réduit ; (iii) dans des sols peu perméables, le délai nécessaire afin d'atteindre la pression désirée peut être trop long ; (iv) l'abaissement de la nappe phréatique peut être problématique en raison de réglementations environnementales ; (v) en zone urbaine, la réduction de la pression de l'eau interstitielle peut engendrer des tassements inadmissibles et (vi) ; la capacité des pompes disponible sur le chantier peut limiter la quantité d'eau d'écoulement. Dans le troisième chapitre, la capacité des forages de drainage est analysée à l'aide d'un modèle de conductivité équivalente qui considère l'hydraulique d'écoulement en conduites et à surface libre dans les forages de drainage. C'est ainsi que la perméabilité maximale du sol peut être déterminée, pour laquelle une pression atmosphérique le long de la paroi du drainage peut être assumée. En outre, les exigences hydrauliques minimales pour les

gaines sont développées en considérant la stabilité du front de taille. Le quatrième chapitre traite le temps nécessaire afin d'obtenir une distribution de la pression de l'eau interstitielle quasiment stationnaire et analyse l'abaissement de la nappe phréatique, le tassement de surface et l'entrée d'eau suite aux forages de drainage. Les résultats de ces calculs fournissent des informations importantes sur les risques potentiels des mesures de drainage et démontrent les limites d'application des nomogrammes de dimensionnement développés.

L'analyse de la *stabilité de corps d'injection* a été effectuée pour deux configurations de drainage : (i) un drainage de la partie intérieure du corps d'injection afin de réduire la force et le risque de l'érosion interne due à des gradients hydrauliques élevés ; et (ii), un drainage préliminaire des zones du futur corps d'injection afin d'augmenter les contraintes effectives et ainsi consolider le sol avant les travaux d'injection. Un tunnel cylindrique excavé dans un sol saturé d'eau est analysé. Celui-ci est considéré comme poreux et élastoplastique en obéissant aux principes des contraintes effectives et au critère de défaillance de Mohr-Coulomb, considérant les forces de l'écoulement. Pour le cas virtuel d'un drainage idéal, c'est-à-dire soumis à une pression de l'eau interstitielle atmosphérique, une solution analytique a été dérivée pour l'état de déformations planes. Plusieurs configurations de drainages spécifiques ont été étudiées à l'aide de modèles numériques couplés avec l'hydraulique et la mécanique et les différences de la solution analytique sont démontrées. L'effet des mesures de drainage est discuté à l'aide de la courbe caractéristique, c'est-à-dire la relation entre les contraintes et les déplacements à la bordure du tunnel et du degré de plasticité du corps d'injection, qui peut servir de critère de dimensionnement. Les résultats des calculs fournissent des informations importantes sur les effets statiques du nombre, de la longueur et l'espacement des forages de drainage arrangés à l'intérieur ainsi qu'à l'extérieur du corps d'injection.

L'étude du *revêtement du tunnel* quantifie (i) la pression d'eau résiduelle qui se développe sur un revêtement de tunnel imperméable en présence de mesures de drainages permanentes ainsi que (ii) l'écoulement d'eau qui résulte des mesures de drainage. Les analyses d'écoulement numériques et tridimensionnelles considérant un médium homogène et isotrope obéissant à la loi de Darcy en condition d'écoulement stationnaire, tiennent compte de deux configurations de drainages : des configurations radiales de drainage foré à travers le revêtement imperméable du tunnel et des espaces de drainage de forme annulaire arrangés dans le revêtement. Des tableaux de dimensionnement ont été conçus, qui permettent une évaluation rapide de la pression d'eau restante ainsi que l'écoulement d'eau qui résulte de plusieurs configurations différentes de drainage. Ces tableaux offrent un outil pratique aux ingénieurs spécialistes des tunnels.

En résumé, la contribution de ce rapport est une étude détaillée des effets statiques des mesures de drainage pour des tunnels par rapport à la stabilité du front de taille et du corps d'injection ainsi que la pression d'eau résiduelle sur un revêtement de tunnel. Le rapport fournit des aides de dimensionnement qui permettent une évaluation rapide de la stabilité du front de taille (considérant plusieurs configurations de drainage préliminaire) et de la pression d'eau résiduelle et de l'écoulement d'eau (considérant différentes mesures permanentes de drainage).

1 Introduction

1.1 Problem statement

Tunnelling in water-bearing, low strength ground represents an engineering challenge. A key factor is water, which has a negative effect on the stability or deformation of underground openings due to the pore water pressure and the seepage forces associated with seepage flow towards the cavity. Thus, for example, a high pore pressure and/or a high hydraulic gradient may endanger the stability of the working face or favour the development of large convergences. Drainage of the ground decreases both the pore pressure and its gradient in the vicinity of the cavity. The consolidation that occurs due to the pore pressure relief is favourable with respect to the stability and deformation because it increases the mean effective stress in the ground and thus also its stiffness and resistance to shearing.

The improvement of ground behaviour by means of drainage measures is well known from tunnelling practice. Although it is important to understand and quantify the static effects of pore pressure and drainage for rational decision-making in design and construction, relatively few investigations have been made (as shown below) into the interaction of seepage flow, pore pressure and ground response to tunnel excavation. Even fewer publications deal specifically with the effect of drainage. This was the motivation for the present research report, which investigates the stabilizing effect of drainage measures on three selected tunnelling problems: (i) the stability of the tunnel face, (ii) the deformation of the excavation boundary of a grouting body in geological fault zones and (iii) the pressure acting on the tunnel lining. The goal of the research project is to improve the understanding of the static impacts of drainage measures and to provide design aids for the tunnel engineer.

The report deals with static effects, the feasibility and execution of drainages measures in tunnelling. The first key word points to the objective of elaborating a detailed understanding of the interrelationships between drainage measures and the stability of the tunnel face, grouting body or tunnel lining. In the first step, examination is based on the simplifying assumption of ideal drainage, *i.e.* complete pore pressure relief. In the second step, focus is placed on aspects of feasibility, execution and/or design, which may limit drainage effectiveness with regard to static effects. Factors limiting pore pressure relief achieved by drainage measures may include geometric restrictions concerning the arrangement of drainage boreholes (*e.g.* location, number, length of the boreholes), constraints due to the ground encountered on site (*e.g.* non-uniform permeability rendering some boreholes ineffective; high permeability causing the boreholes to reach hydraulic capacity; unstable borehole walls requiring casings), as well as limitations due to environmental reasons (*e.g.* admissible groundwater drawdown or settlement) or operational reasons (*e.g.* lead-time or pumping capacity available on site).

1.2 State of research

1.2.1 Face stability

One of the most serious risks in tunnelling through weak ground is collapse of the tunnel face. The favourable effect of advance drainage on face stability is well known from tunnelling experience (*e.g.* [1], [2], [3], [4], [5], [6], [7]). Although there are many publications addressing face stability in water-bearing ground (*e.g.* [8], [9], [10], [11], [12], [13], [14], [15], [16], [17], [18], [19]), few research works deal specifically with the effect of advance drainage measures on face stability, and those that do focus mainly on ground of uniform permeability ([20], [21], [22]).

Tunnelling in weak water-bearing ground is demanding particularly under high water pressures and in heterogeneous formations exhibiting variable permeability. The hydraulic heterogeneity may result in locally high hydraulic gradients or impair effectiveness of advance drainage. The literature on face stability in water-bearing ground of non-uniform permeability deals mainly with tunnelling through fault zones (*e.g.* [23], [24], [25]); specific case histories (*e.g*. [26], [27], [28], [29], [1], [2], [3]); or specific aspects such as the effect of pre-support (pipe roof) and grouting in fractured zones [30] or the mechanism of punching failure [5].

As shown later in Chapters 4 and 5, the literature on situations where multiple factors are conspiring to limit the effectiveness of drainage measures is sparse and does not refer to face stability.

1.2.2 Grouting body

Water-bearing fault zones consisting of crushed rock or soil-like material with little or no cohesion represent a major challenge for the design and construction of deep tunnels. Sudden water and mud inflows as well as high ground and water pressures can have a disastrous impact on tunnelling operation and safety (see *e.g.* [31] for a historic example). Therefore, the timely application of special measures (or combinations thereof) such as grouting, systematic drainage or even artificial ground-freezing is required ([24], [32]).

Grouting bodies usually have an increased strength and stiffness and, due to the filling of the pores by grout, lower permeability than untreated ground. The induced hydraulic heterogeneity of the ground may result in locally high hydraulic gradients and pore pressures. Both in turn may endanger stability and favour the development of large convergences: the pore pressure reduces effective stresses and thus the shear resistance of the ground; the gradients may overstress the grouted body or cause its inner erosion. Drainage is an effective measure for preventing these water-related dangers in ground behaviour.

Previous investigations considered two borderline cases of grouting body drainage: a perfectly sealing (*i.e.* fully impermeable) and an ideally drained (*i.e.* fully permeable) grouting body. The stability of grouting bodies for these borderline cases was extensively investigated *e.g.* by [33], [34], [35], [36], [37], [38], [39], [40], [41] or [42]. Some case histories are reported using grouting bodies in combination with drainage measures ([43], [6]). Focusing ond seepage analysis only, Nasberg and Ilyushin [44] derived approximated analytical solutions for considering several different drainage borehole arrangements, but there is a lack of research with respect to the effect of specific drainage borehole arrangements on the stability of grouting bodies.

1.2.3 Tunnel lining

There are three concepts of dealing with water in the operational stage of a tunnel: (i) in case of a sealing lining, the lining has to withstand potentially high pressures caused by the water head; (ii) in case of a partially sealed lining, the admissible water pressure is limited to a predefined level, above which the pressure is relieved by drainage (so-called "smart drainage control system"); and (iii) in case of a permeable lining, there is no water pressure acting on the lining, but high water inflow may develop.

Several case histories of failures of the tunnel lining caused by water pressure are reported, especially when tunnelling in Karst formations (*e.g.* [45], [46], [47]). The residual water pressure on a permeable tunnel lining was investigated by means of (approximated) analytical or numerical solutions (*e.g.* [48], [49], [50], [51]). Pressure relief resulting from coaxial drainage boreholes drilled around an example of a subsea-tunnel is illustrated by Hong *et al*. [52]. A systematic study of the water pressure on the lining when considering several different drainage arrangements was presented by Nasberg and Ilyushin ([44]; referring themselves to previous research of Pavlovskii or Nasberg of the 1960's), who presented analytical expressions approximating the seepage flow towards drainage boreholes drilled around a tunnel in a low-permeable grouting body. These results, which apply also for uniformly permeable ground, were verified by experimental investigations of Beruchashvili [53] and extended by Bukhairov [54], but these works are unfortunately neither well-known in the field of tunnelling, nor presented in an easily accessible manner.

1.3 Structure of the report

The report is organized in seven Chapters. After the introduction, Chapters 2-5 focus on face stability, Chapter 6 deals with the stability and deformation of the grouting body and Chapter 7 presents the findings of permanent drainage measures with respect to the tunnel lining.

1.3.1 Face stability

The pore water pressure relief resulting from advance drainage measures may be overestimated due to several simplifying or common assumptions (Table 1.1). These factors are discussed individually with respect to tunnel face stability. Chapter 2 starts with face stability analysis in ground of uniform permeability and investigates the effectiveness of various advance drainage schemes (item *iv* in Table 1.1). The effects of the geometric parameters for each drainage scheme are discussed assuming the borehole walls as seepage faces under atmospheric pressure. A dimensionless formulation of the required support pressure (or the required cohesion of the ground) is developed in order to produce design nomograms capable of providing a quick assessment of face stability for a series of advance drainage layouts in tunnelling.

***Table 1.1** Common or simplifying assumptions when modelling drainage boreholes*

Simplifying or common assumptions:	*But:*	
The borehole walls represent seepage faces under atmospheric pressure.	(*i*)	High permeability and water table may result in pressure development inside the boreholes, thus resulting in reduced pore pressure relief in the surrounding ground.
	(*ii*)	If the boreholes have casings, only their openings will represent seepage faces and consequently the pore pressure relief will be reduced.
Sufficient time is available for pore pressure relief.	(*iii*)	The time available may be limited, with the consequence that pore pressures ahead of the face will be higher than at steady state conditions.
Sufficient number and/or length of boreholes to achieve the desired pore pressure relief.	(*iv*)	Geometric constraints: The equipment may impose constraints on the number and/or locations of boreholes, thus resulting in reduced pore pressure relief.
	(*v*)	Heterogeneous ground: Boreholes within aquitards are less effective. Heterogeneous ground may necessitate a large number of boreholes; otherwise the pore pressure relief will be less than in homogeneous ground.
	(*vi*)	Drawdown of water table: If the water table experiences an inadmissible drawdown, then the number and/or length of boreholes may have to be limited, which in turn results in reduced pore pressure relief.
	(*vii*)	Settlements: If the consolidation-induced settlements are inadmissible (independently of whether the water table experiences a drawdown or not), then the number and/or length of the boreholes may have to be limited, which in turn results in reduced pore pressure relief.
	(*viii*)	Water discharge: If the amount of water inflow is too large to be handled by the pumping system, the number and/or length of boreholes may have to be limited, which in turn results in reduced pore pressure relief.

Hydraulically heterogeneous formations (item *v* in Table 1.1) may originate from tectonic or formation history, as the latter may cause variations in the degree of fracturation or in the lithological composition and grain size distribution of the ground (for an overview, for example, see Anagnostou *et al*. [55]). Hydraulic heterogeneity may occur at different scales. Aquifers and aquitards may have a thickness ranging from decimetres to decametres and be oriented vertically, horizontally or with an arbitrary inclination to the tunnel axis. Frequently alternating sub-vertical zones of variable strength and permeability, for instance, result in great variability in the geotechnical behaviour of the ground during tunnelling, thus rendering the timely application of adequate auxiliary measures difficult. Single weak zones consisting of crushed rock or soil-like material of low cohesion, if encountered suddenly, may result in large-scale instability and subsequent inundation of a long portion of the tunnel. All alternating aquifers and aquitards may lead to hydraulic head distributions that are particularly challenging for face stability. Chapter 3 investigates the effects of the orientation, thickness, location, number and permeability ratio of ground layers with regard to the effectiveness of a common advance drainage measure consisting of six axial boreholes drilled from the tunnel face. Useful guide values are indicated as to potentially critical situations, the effectiveness of advance drainage and the adequate arrangement of drainage boreholes.

The combination of very high hydraulic gradients and highly permeable ground (*e.g.* in a subaqueous tunnel) may result in quantities of water inflow so high that advance drainage becomes ineffective with respect to pore pressure relief (item *i* in Table 1.1). The flow regime within the borehole changes from open-channel to pipe flow and the water pressure developing within the boreholes may result in reduced pore pressure relief in the surrounding ground. In Chapter 4, an equivalent permeability[1] model is developed which considers the hydraulic capacity of the drainage boreholes. The model allows a numerical determination of the interaction between seepage flow in the ground and turbulent pipe flow in the boreholes. The computational results provide an insight into factors influencing face stability under high inflow conditions and allow a determination to be made of the range of conditions (water level, ground permeability) for which advance drainage measures are fully effective with respect to pore pressure relief and thus nomograms provided in Chapter 2 are thus applicable here. In addition, Chapter 4 investigates the limited capacity of drainage boreholes in cases where casings become necessary because the borehole walls are unstable (item *ii* in Table 1.1). The screen of the casings impedes pore pressure relief by restricting the passage of water to small openings. The investigations indicate the minimum requirements for casings in order to account for pore pressure relief comparable to the relief when assuming the borehole wall is a seepage face.

Chapter 5 completes the study on the remaining factors of Table 1.1 and deals with operational and environmental limits on pore pressure relief and their impact on face stability. Focus is placed on a common advance drainage scheme consisting of axial boreholes from the tunnel face:

- In ground of low permeability, pore pressure relief by advance drainage boreholes may take a long time to occur (item *iii* in Table 1.1). The lead-time required for the hydraulic head to fall far enough for the face stability considerations according to Chapter 2 is analysed.
- In order to avoid disturbance to hydrogeological conditions, it may be necessary to limit groundwater drawdown (item *vi* in Table 1.1). The additional drawdown due to drainage measures is studied and estimates of groundwater drawdown are provided for specific drainage arrangements.
- Drainage increases the pore pressure relief and may thus lead to inadmissible settlements of the ground surface (item *vii* in Table 1.1). Potential consolidation settlement is estimated assuming linear-elastic ground behaviour. The investigations indicate the settlement due to the additional pressure reduction induced by drainage measures.
- In the case of high water inflow (item *viii* in Table 1.1), the pumping system installed on site may become a limiting factor. The amount of water discharge from the tunnel face and from the boreholes is quantified for variable ground permeability considering the borehole walls as seepage faces.

[1] Strictly speaking: “hydraulic conductivity”. Note that within this report, the term “permeability” is used interchangeable with “hydraulic conductivity”.

1.3.2 Grouting body

The completion of tunnel sections in water-bearing fault zones is often possible only after strengthening and sealing the ground around the opening by grouting, which is carried out ahead of the tunnel excavation. Chapter 6 of the present research project picks up the investigations of Anagnostou and Kovári [40], but with point to three crucial aspects of drainage measures:

- The effect of local drainage of the inner part of a grouting body to decrease the load and the risk of inner erosion due to the action of high hydraulic gradients;
- Advance drainage of the entire area of the future grouting body to increase the effective stresses and lead to consolidation of the ground prior to injection;
- Consideration of both the virtual case of ideal drainage (*i.e.* complete pore pressure relief) and the effects of several different borehole arrangements (*i.e.* considering the geometric constraints on the number, length and/or locations of the boreholes).

The chapter starts with the virtual case of ideal drainage, for which analytical solutions are derived. The partial pore pressure relief resulting from several different arrangements of drainage boreholes is then studied using hydraulic-mechanical coupled FE-modelling. The effect of the drainage measures is discussed by means of the characteristic line, *i.e.* stress as a function of the displacement at the excavation boundary of the tunnel. Another dimensioning criterion for grouting body stability may be the extent of the plastic zone developing due to overstressing of the grouting body. Therefore, the degree of plastification is evaluated as a function of the lining support pressure.

The computational results provide valuable information about the number, length and spacing of drainage boreholes arranged inside and outside of grouting body and quantify the derivation of the specific drainage measures compared to the ideal drainage case.

1.3.3 Tunnel lining

In tunnels crossing highly permeable ground deep under the water table, the water pressure may be too high in case of an impermeable tunnel lining, but the inflow too large in case of a permeable lining. Hence, the combination of a sealing tunnel lining combined with discrete drainage measures may be the method of choice. The water pressure acting on the lining is reduced compared to the sealing tunnel; and the water inflow is potentially smaller than when considering a permeable lining (of course, the water discharge may be additionally reduced by grouting).

Chapter 7 quantifies the residual water pressure acting on the tunnel lining and the amount of water inflow for the following two drainage cases:

- drainage via radial boreholes drilled through an impermeable lining (*i.e*. largely similar drainage arrangements as in Nasberg and Ilyushin [44]; but analysed numerically instead of developing an approximate formulae);
- a tunnel lining consisting of impermeable blocks separated by ring-shaped drainage gaps (*e.g.* Tunnel Engelberg in Switzerland; see later Section 7.1).

The numerical computations consider steady state conditions and assume sufficient drainage capacity. The residual water pressure and the inflow resulting from a series of drainage measures *(i.e*. several number, length, diameter and spacing of the drainage boreholes) for a wide range of tunnel depth and diameter are presented in design charts.

1.4 Research methods and limitations

1.4.1 Methods

The *stability of the tunnel face* is analysed after Anagnostou and Kovári [9] by considering the limit equilibrium for a failure mechanism consisting of a wedge ahead of the tunnel face and a prism extending up to the surface. The computational model takes account of the mechanical action of the groundwater, (i) by analysing the limit equilibrium in terms of effective stress, and (ii) by introducing the seepage forces that act on the wedge and the prism into the equilibrium equations. The seepage force at any point of the sliding bodies is equal to the gradient of the pore pressure field. The latter is determined by means of three-dimensional, numerical seepage flow analyses assuming Darcy's law when taking account of a specific advance drainage layout (performed with the finite element code COMSOL® [55]).

The *stability and deformation of the grouting body* is analysed after Anagnostou and Kovári [40] by considering a cylindrical tunnel, surrounded by a grouting body in the form of a thick-walled cylinder. Both treated and untreated ground is considered as a porous, elasto-plastic medium obeying the principle of effective stress, Coulomb's failure criterion and taking account of the seepage forces according to Darcy's law. Analytical solutions are derived for the virtual case of ideal drainage in a system fulfilling the condition of rotational symmetry. The effect of several different drainage borehole arrangements are studied by means of hydraulic-mechanical coupled FE-modelling (performed with the finite element code COMSOL® [55]).

The water pressure acting on the *tunnel lining* as well as the inflow resulting from the drainage measures are determined by means of three-dimensional, numerical seepage flow analyses in a homogeneous, isotropic medium obeying Darcy's law at steady-state conditions (performed with the finite element code COMSOL® [55]).

1.4.2 Limitations of scope

The report focuses on numerical modelling of the static effects of drainage measures in tunnelling. Research intended to develop or improve the application-oriented, technological implementation of drainage boreholes was not part of this study. No operational handling is therefore addressed in terms of drainage boreholes in tunnelling practice (such as drilling, insertion or monitoring the effectiveness of drains).

The applicability of the results is discussed by means of analytical considerations and application examples of tunnels. No work was undertaken in field or laboratory testing.

The study considers the ground as a porous medium obeying Darcy's law. In fractured rock, preferential seepage flow along the rock joints is to be expected. The stabilizing effect of drainage boreholes that consider such flow patterns is not part of the research project.

1.5 Contributions and publications

Besides the authors, several undergraduate students of the Department of Civil Engineering at the ETH Zurich participated to the numerical analyses either in the framework of their Master's theses (D. Bronzetti with preliminary numerical studies for Chapter 2, D. Herzig with preliminary numerical studies for Chapter 3; F. Flütsch and R. Gallus with numerical studies for Chapter 6) or as teaching assistant (A. Baumann with numerical studies for Chapter 7) under the lead and with close support of S. Zingg. Finally, the editorial assistance of R. Poggiati preparing this report is greatly appreciated.

Extensive parts of the present report have already been made accessible for the engineering community by means of scientific publications. Major parts of Chapter 2 have been published in Zingg and Anagnostou [56] and preliminary results have been presented in Anagnostou and Zingg [57], Zingg and Anagnostou [58], [59] and Zingg *et al.* [60]. Preliminary results of Chapter 3 have been published in Zingg and Anagnostou [61]. In addition, Chapters 2 to 6 are based upon Zingg [62].

2 An investigation into efficient drainage layouts for the stabilisation of tunnel faces in homogeneous ground

2.1 Introduction

Drainage measures comprise horizontal or inclined boreholes that are drilled either directly from the face (Fig. 2.1a) or from lateral niches or enlarged cross-sections (Fig. 2.1b). Deep below the water table, the equipment has to be protected against high water pressure by means of so called "preventers". The installation of advance drainage boreholes from the tunnel face interferes with tunnel excavation and support installation. In addition, technical equipment and procedures limit the length of the drainage boreholes and thus the time available for pore pressure relief, which is a critical factor in low permeability grounds. Advance drainage from niches (Fig. 2.1b) in combination with directional drilling (allowing for longer boreholes) remedies these problems. Another option is to employ a pre-existing underground opening, such as a pilot tunnel inside or outside the cross-section of the main tunnel (Fig. 2.1c and d) or – in the case of twin tunnels – the tube constructed first (Fig. 2.1e). The drainage action of a pre-existing underground opening can be enhanced by drilling sufficiently long radial boreholes, *i.e.* extending beyond the axis of the main tunnel (Fig. 2.1d). Such drainage curtains are of course essential for pore pressure relief where the lining of the pre-existing opening is watertight (*e.g.* a TBM-driven safety gallery with a sealed segmental lining).

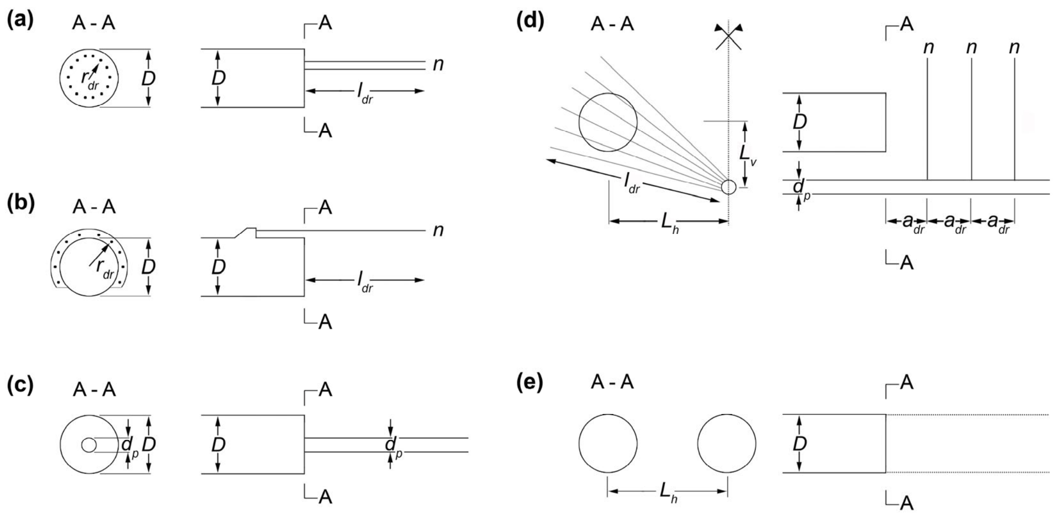

***Figure 2.1** Drainage via: (a) boreholes from the tunnel face; (b) boreholes from a niche or from a locally enlarged cross-section; (c) a co-axial pilot tunnel; (d) boreholes from an external pilot tunnel; (e) the first tube of a twin tunnel*

This chapter extends the face stability model of Anagnostou and Kovári [9] to include pore pressure relief due to advance drainage. It analyses and presents design nomograms for the most common drainage layouts (Fig. 2.1). The chapter considers ground of uniform permeability sufficiently high for the necessary drainage time not to be a limiting factor (*cf.* Table 1.1). This condition is fulfilled where ground permeability is higher than about 10^{-8} m/s ([9], [22]). In addition, uncased drainage boreholes of sufficient hydraulic capacity are considered.

After outlining the computational model (Section 2.2), basic aspects of the different drainage layouts in Figure 2.1 are discussed in Section 2.3 through comparative analyses of a cylindrical tunnel (Fig. 2.2). Section 2.4 presents dimensionless design nomograms allowing a quick estimate to be made of the necessary face support pressure in the presence of drainage measures. The practical applicability of the nomograms is illustrated in Section 2.5, making reference to two tunnelling projects.

2.2 Computational model

Face stability is analysed after Anagnostou and Kovári [9], which considered a failure mechanism consisting of a wedge and a prism (Fig. 2.2), determined the seepage forces by means of numerical, steady state seepage flow analyses assuming Darcy's law, and introduced these into the equilibrium equations. There are only two differences to the model of Anagnostou and Kovári [9]: (i) The latter takes the ratio of horizontal to vertical stresses which governs the frictional part of the shear resistance at the vertical slip planes of the failure mechanism to $\lambda_p = 0.8$ for the prism and $\lambda_w = 0.4$ for the wedge. Here, slightly higher values are considered (1.0 and 0.5, respectively), based on recent results in Anagnostou [63][2]. (ii) For the determination of the seepage forces, Anagnostou and Kovári [9] considered the hydraulic head field that prevails when drainage occurs only through the tunnel face. Here, the effect of advance drainage measures (Fig. 2.1) on the hydraulic head field is taken into account.

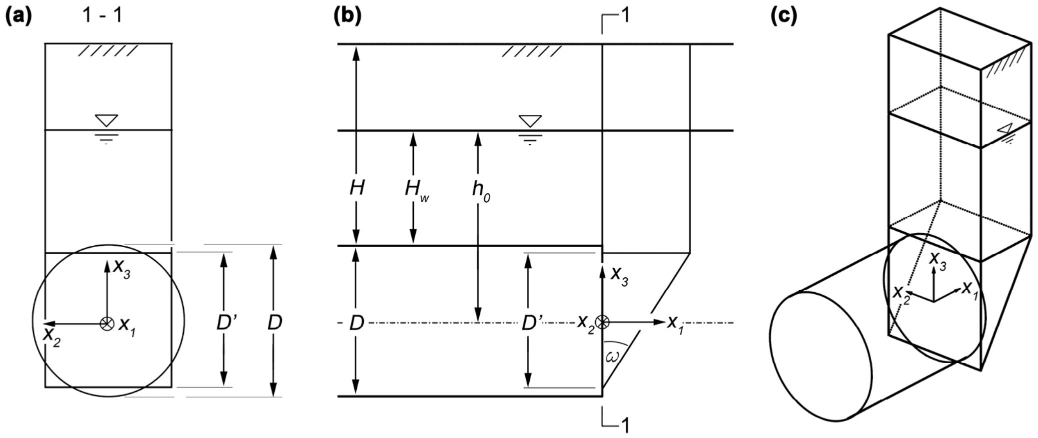

Figure 2.2 *Failure mechanism (after Anagnostou and Kovári [9]): (a) cross-section, (b) longitudinal section and (c) axonometric projection*

2.2.1 Seepage flow analyses

The seepage flow domain extends either up to the ground surface H (subaqueous tunnels) or up to the groundwater table H_w. The upper boundary of the numerical model is thus located at distance $T = \min(H, H_w)$ above the tunnel crown. The hydraulic head at the far-field boundaries is taken equal to the initial hydraulic head h_0, which is equal to the elevation of the water table above the tunnel axis. The water table is assumed to remain constant in spite of the drainage action of the tunnel. This assumption is true in the case of sufficient groundwater recharge from the surface and conservative in the case of a drawdown.

The tunnel face and the walls of the drainage boreholes are taken as seepage faces under atmospheric pressure, while the tunnel boundary is considered impervious up to the face (no-flow boundary condition, Fig. 2.3). Investigations by Wongsaroj [68] indicated that seepage flow through the lining can be neglected if the lining permeability is lower than 0.1 $K_g \cdot d_{lin}/T$, where K_g and d_{lin} denote the ground permeability and the lining

[2] The shear resistance of the vertical slip surfaces depends essentially on the horizontal stresses, which cannot be determined from the equilibrium equations. The assumed value of $\lambda_p = 1$ for the prism is according to Janssen's classic silo-theory [64] and was also proposed by Terzaghi and Jelinek [65] on the basis of trap-door tests. The assumption of a half-as-high coefficient λ_w for the wedge is based upon comparative analyses with the method of slices (see end of section 2 in [66]). A detailed investigation of this issue as well as comparisons with other methods and experimental results, which show the adequacy of $\lambda_p = 1$ and $\lambda_w = 0.5$, can be found in Anagnostou [63] as well as in section 4 of Perazzelli and Anagnostou [67].

thickness, respectively (*cf.* also [69]). Even if for a low permeability ground (K_g = 10^{-7} m/s), a large cover (T = 250 m) and a thin lining (d_{lin} = 0.2 m), the threshold lining permeability amounts to about 10^{-11} m/s. Well applied shotcrete exhibits a lower permeability (10^{-12} m/s; [70]) and can, therefore, be considered as practically impermeable. Low-quality shotcrete may exhibit a higher permeability (in the order of 10^{-10} m/s; [71]) and allow for some additional drainage and pore pressure relief. This is particularly true for a perforated shotcrete lining or an open shield. In such cases, the no-flow boundary condition represents a simplification on the safe side.

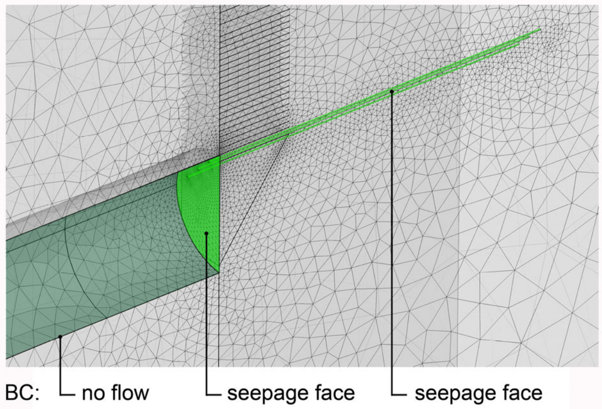

Figure 2.3 *Example of spatial discretisation and hydraulic boundary conditions for advance drainage according to Figure 2.1a*

2.2.2 Support pressure

The support pressure that is needed in order to stabilize a specific wedge (characterized by the angle ω; Fig. 2.2) for given drainage measures can be expressed as follows (for detailed derivation see Zingg [62]; or in condensed form in Zingg and Anagnostou [56]):

$$s_\omega = N_{\gamma\omega}\gamma' D - N_{c\omega}\, c + N_{h\omega}\, \gamma_w h_0 \ , \tag{2-1}$$

where c, h_0, γ' and γ_w denote the ground cohesion, the depth of the tunnel axis underneath the water table (Fig. 2.2), the submerged unit weight of the ground and the unit weight of the water, respectively. $N_{\gamma\omega}$, $N_{c\omega}$ and $N_{h\omega}$ are dimensionless coefficients, which depend on the numerically computed hydraulic head field (and thus on the drainage layout), the friction angle φ, the normalized cohesion $c/\gamma'D$, the ratio of dry unit weight γ_d to γ', the normalized overburden H/D, the normalized in situ head $\gamma_w h_0/\gamma'D$ and the angle ω between the tunnel face and the inclined slip surface of the wedge (hereafter referred to as "wedge angle").

The critical wedge angle ω_{cr}, *i.e.* the angle that results in the maximum support pressure s, is determined iteratively by repeating the computation for different values of ω.

2.3 Comparative analyses

2.3.1 Introduction

We consider the example of a 100 m deep subaqueous cylindrical tunnel (Fig. 2.4). The assumed parameters are given in Table 2.1. The effectiveness of each drainage scheme (Fig. 2.1) is evaluated in terms of the face support pressure s that is needed for stability. For the purposes of comparison we first consider the following two borderline cases (Section 2.3.2): (i) no drainage measures, *i.e.* pore pressure relief only due to the natural drainage action of the open tunnel face; (ii) ideal drainage, *i.e.* complete pore pressure relief in the ground ahead of the tunnel face. These two borderline cases bound the range of face support pressures that would be needed in combination with non-ideal, real world advance drainage. They thus serve as reference cases for an evaluation of the effectiveness of the various drainage layouts in Figure 2.1.

Subsequently (in Section 2.3.3), we show the effect of the number, length and location of drainage boreholes drilled either directly from the tunnel face (Fig. 2.1a) or from lateral niches or enlarged cross-sections (Fig. 2.1b). Sections 2.3.4 and 2.3.5 deal with the drainage action of a pilot tunnel (located inside or outside the cross-section of the main tunnel) or of the first tube of a twin tunnel, respectively. Finally, Section 2.3.6 investigates drainage curtains (Fig. 2.1d).

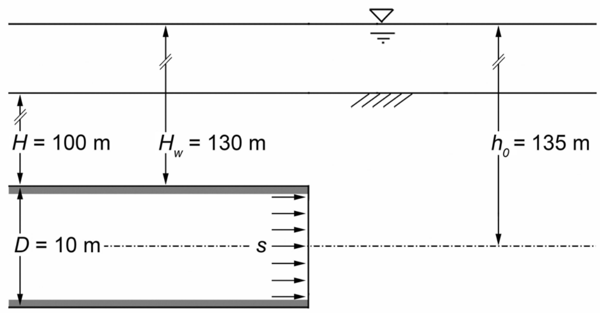

Figure 2.4. *Problem setup for the comparative analyses*

Table 2.1 *Parameters for the comparative analyses*		
Problem layout		
Depth of cover	H	100 m
Elevation of water table	Hw	130 m
Tunnel diameter	D	10 m
Ground		
Effective cohesion	c	0-400 kPa
Angle of eff. internal friction	φ	30°
Submerged unit weight	γ'	12 kN/m^3
Unit weight water	γ_w	10 kN/m^3
Shear resistance of the vertical slip surfaces		
Coefficent of lateral stress in wedge	λ_w	0.5
Coefficent of lateral stress in prism	λ_p	1.0
Drainage boreholes		
Diameter	d_{dr}	0.1 m
Length	l_{dr}	0.5-30 m
Number	n	0-12
Distance from tunnel axis	r_{dr}	1.5-11 m
Drainage via a pilot tunnel or another tunnel		
Diameter of coaxial pilot tunnel	d_p	0.5-5 m
Diameter of adjacent tunnel	d_p	1-10 m
Vertical centre distance	L_v	14-92 m
Horizontal centre distance	L_h	14-90 m
Distance of drainage curtains	a_{dr}	4-20 m

2.3.2 Reference cases

Figure 2.5a shows the support pressure needed for face stability in a cohesionless ground as a function of the wedge angle ω in the case of ideal drainage (lower curve) and in the absence of drainage measures (upper curve). In the first case, the pore pressure in the wedge is atmospheric; seepage forces have to be taken into account only for the overlying prism. In the second case, the wedge is acted upon by seepage forces which are directed towards the tunnel face, thus leading not only to a considerably higher necessary support pressure (s = 770 vs. 100 kPa), but also a more extended unstable region (critical wedge angle ω_{cr} = 63° vs. 30°). It is, nevertheless, remarkable that even in the absence of drainage measures the necessary support pressure is considerably lower than the initial hydrostatic pressure (s = 770 vs. 1400 kPa). This is due to the natural drainage action of the tunnel heading, which inevitably leads to some pore pressure relief in the ground ahead of the face.

The practical significance of these results becomes evident when we consider the fact that face support pressures of more than 200 kPa cannot be managed in conventional tunnelling, even with heavy face bolt reinforcement [72]. In the present example, ground improvement by grouting or freezing would be indispensable in the absence of drainage measures. In the case of complete pore pressure relief by advance drainage, the face would still need support, but this would be technically feasible considering the relatively moderate support pressure of about 100 kPa that is required.

The required support pressure (for the critical wedge) decreases with increasing cohesion of the ground (Fig. 2.5b). In the case of complete pore pressure relief, cohesion of just 45 kPa would be sufficient for the tunnel face to remain stable without support (point A). Without drainage measures the cohesion required for an unsupported face increases to 330 kPa (point B); even with heavy bolt reinforcements (s = 180 kPa), the ground would need a cohesion of at least 240 kPa (point C).

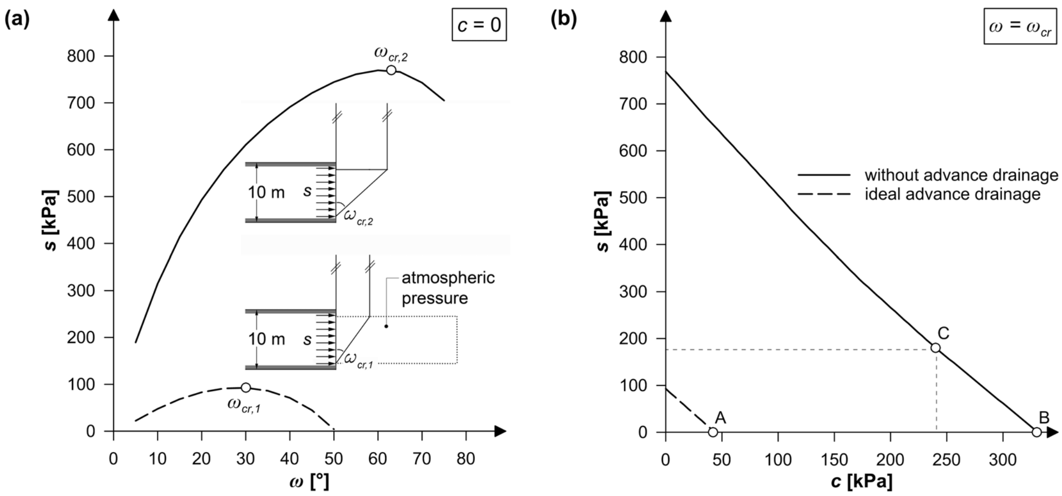

***Figure 2.5** (a) Required support pressure s as a function of the angle ω for a cohesionless ground with ideal advance drainage (lower curve) and without drainage (upper curve); (b) required support pressure s for the critical wedge as a function of the cohesion c (parameters according to Fig. 2.4 and Table 2.1)*

2.3.3 Drainage via boreholes from the tunnel face or niches

We consider horizontal boreholes of uniform diameter (d_{dr} = 10 cm) and investigate successively the effect of their number n, location, length l_{dr} and distance r_{dr} from the tunnel axis (Figs. 2.1a and 2.1b).

2.3.3.1 Number of drainage boreholes

The effect of the number of boreholes is investigated assuming that they are 30 m long and located at r_{dr} = 3.8 m. Figure 2.6 shows the distribution of the hydraulic head along the x_1-axis ahead of the tunnel face and along the x_3-axis above the tunnel for 2 to 12 boreholes (dashed lines) as well as for the reference case without drainage boreholes (solid line). It is remarkable that just 2 to 4 boreholes result in considerable pore pressure relief, particularly ahead of the tunnel face (x_1-axis in Fig. 2.6). Advance drainage

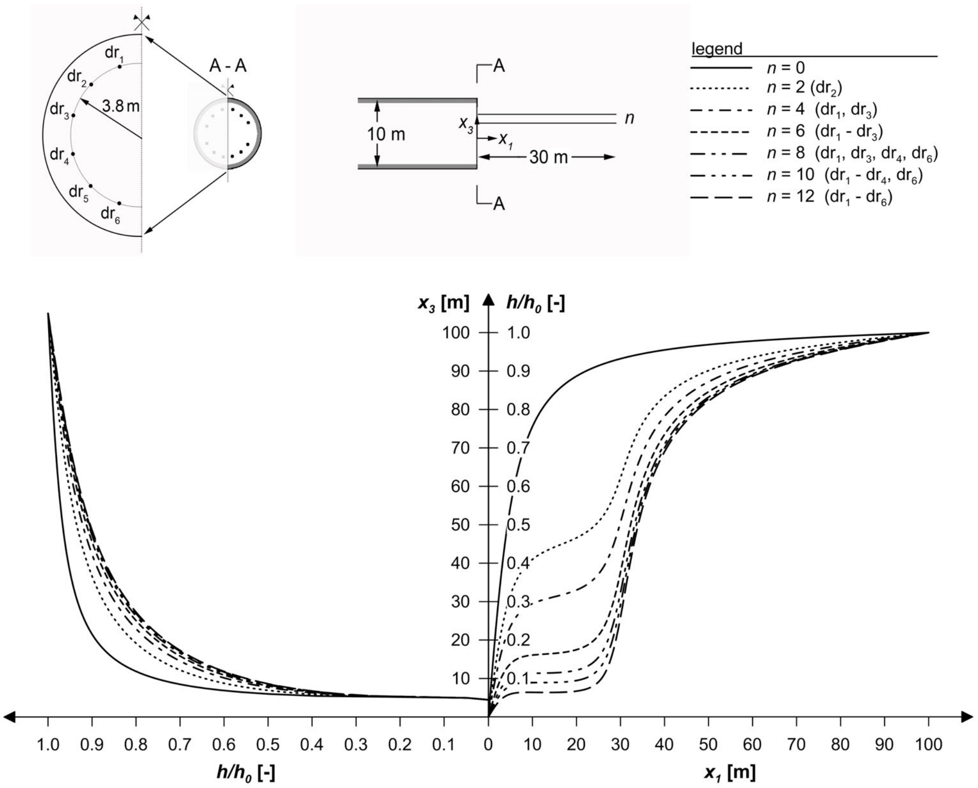

Figure 2.6 *Distribution of the hydraulic head* h *above (l.h.s.) and ahead of (r.h.s) the tunnel face (parameters according to Fig. 2.4 and Table 2.1)*

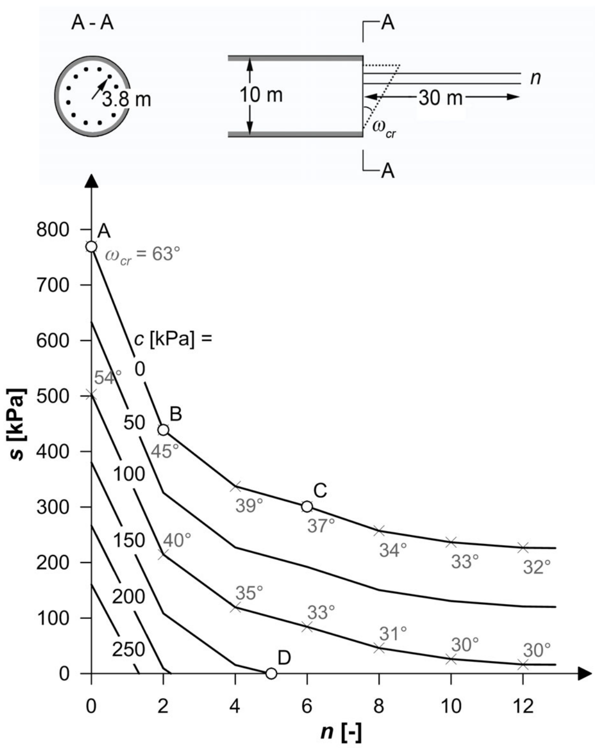

Figure 2.7 *Required support pressure* s *as a function of the number of drainage boreholes* n *(borehole locations see Fig. 2.8; parameters according to Fig. 2.4 and Table 2.1)*

decreases the hydraulic head gradients close to the face (they occur only at a greater distance), which leads to narrower critical wedges and a substantial reduction in the required support pressure (Fig. 2.7). In a cohesionless ground, advance drainage with just two boreholes decreases the required support pressure to about 60% of the reference pressure, *i.e.* the pressure required in the absence of boreholes (compare points A and B in Fig. 2.7). The addition of four more drainage boreholes (point C in Fig. 2.7) leads to a further reduction in the support pressure to about 40% of the reference pressure; marginal utility diminishes with further boreholes. In a weak rock exhibiting a cohesion of 150 kPa, 6 boreholes would suffice for face stability (point D in Fig. 2.7). Trading the feasible pore pressure relief against the drilling effort, 4 - 6 drainage boreholes can be recommended as an efficient face stabilization measure in homogeneous ground.

2.3.3.2 Location of drainage boreholes

The exact location of the boreholes is of secondary importance for the required support pressure, provided that at least two boreholes are located in the upper third of the tunnel face and the remaining boreholes either arranged in the upper section or distributed evenly over the face (for details see Zingg [62]). Figure 2.8 indicates the borehole locations which are taken into account for further consideration in the following sections.

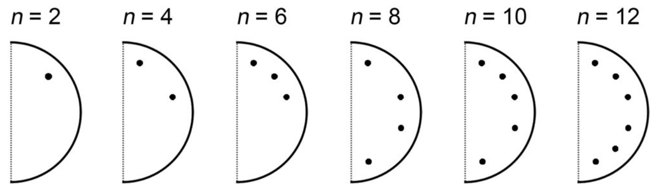

***Figure 2.8** Locations of very effective drainage boreholes*

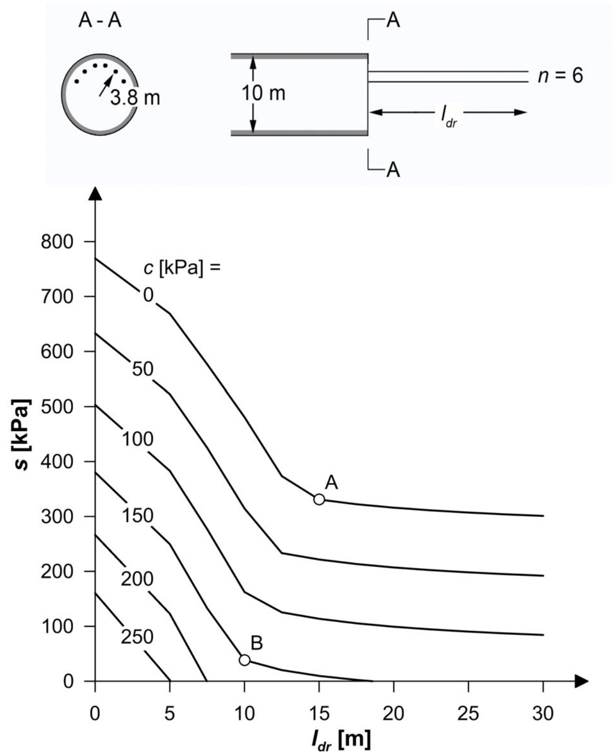

***Figure 2.9** Required support pressure s as a function of the borehole length l_{dr} (borehole locations see inset; parameters according to Fig. 2.4 and Table 2.1)*

2.3.3.3 Length of drainage boreholes

We discuss the effect of borehole length l_{dr} for the case of 6 boreholes (Fig. 2.9) considering the effective borehole location indicated in Figure 2.8. The required support pressure decreases rapidly with increasing borehole length l_{dr} until the latter reaches about 15 m (point A in Fig. 2.9), *i.e.* until the boreholes extend sufficiently ahead of the largest critical wedge (remember that in the absence of drainage the critical angle ω_{cr} is equal to about 63°). Longer boreholes provide no benefit, because they cause pore pressure relief far ahead of the tunnel face (in a zone that is anyway non-critical for face stability; see below). In the present example (10 m diameter tunnel), 30 m long boreholes (a technically feasible length) every 15 m (one and a half tunnel diameters) would be a sensible choice. Longer boreholes would be advantageous in medium to low permeability ground because they provide a longer drainage period in advance of excavation. However, they may present execution difficulties due to instabilities or deformations in the borehole walls, friction when using casings or drilling accuracy.

An increase of the borehole length beyond a certain value (hereafter referred to as "characteristic borehole length $l_{dr,char}$") does not increase face stability, because it causes pore pressure relief in the ground far away from the tunnel face, which is anyway non-critical for stability. The characteristic borehole length corresponds to the extent of the potentially unstable zone ahead of the face, *i.e.* to the depth $D'\tan\omega_{cr}$ of the critical wedge (where $D' = 0.89D$ denotes the side length of equivalent rectangle to the tunnel diameter D and ω_{cr} the critical wedge angle). As the critical wedge angle does not depend on D (for a specific drainage layout and given ratios for horizontal to vertical stress (λ_w, λ_p) it is $\omega_{cr} = f(\varphi, \overline{H}, \overline{\gamma}_d, \overline{c}, \overline{h}_0)$; [62]), $l_{dr,char}$ is proportional to D.

These relations are shown in Figure 2.10 for our tunnel example. Figure 2.10a shows the required support pressure s as a function of the wedge angle ω when considering no drainage boreholes. The critical wedge angle ω_{cr} decreases with increasing ground cohesion c (Fig. 2.10b), thus also the characteristic borehole length $l_{dr,char}$ (Fig. 2.10c). Figure 2.10d finally superimposes the characteristic borehole length (indicated with crosses) with Figure 2.9, which leads to the recommendation of always maintaining a minimum borehole length of 1.5 D (*e.g.* by drilling 3 D long boreholes every 1.5 tunnel diameter). This proposal covers even the worst-case of cohesionless ground.

Of course, the critical wedge angle (and thus the characteristic borehole length) increases with increasing hydraulic gradient. In case of $T/D > 5$ and considering cohesionless ground as decisive, the dependencies of the critical wedge angle simplify to $\omega_{cr} = f(\varphi, \overline{h}_0)$. Figure 2.11 shows the normalized characteristic borehole length for a wide range of normalized hydraulic head $\overline{h}_0$ and three angles of internal friction of the ground φ. The normalized characteristic borehole length clearly increases with increasing normalized head and slightly with decreasing friction angle (Fig. 2.11).

(Our conclusions about the minimum borehole length agree with those of Atwa *et al.* [73], who studied the hydraulic head field close to the tunnel face (without considering its stability) and found that the hydraulic gradients do not change with the borehole length anymore if the latter is greater than $2D$.)

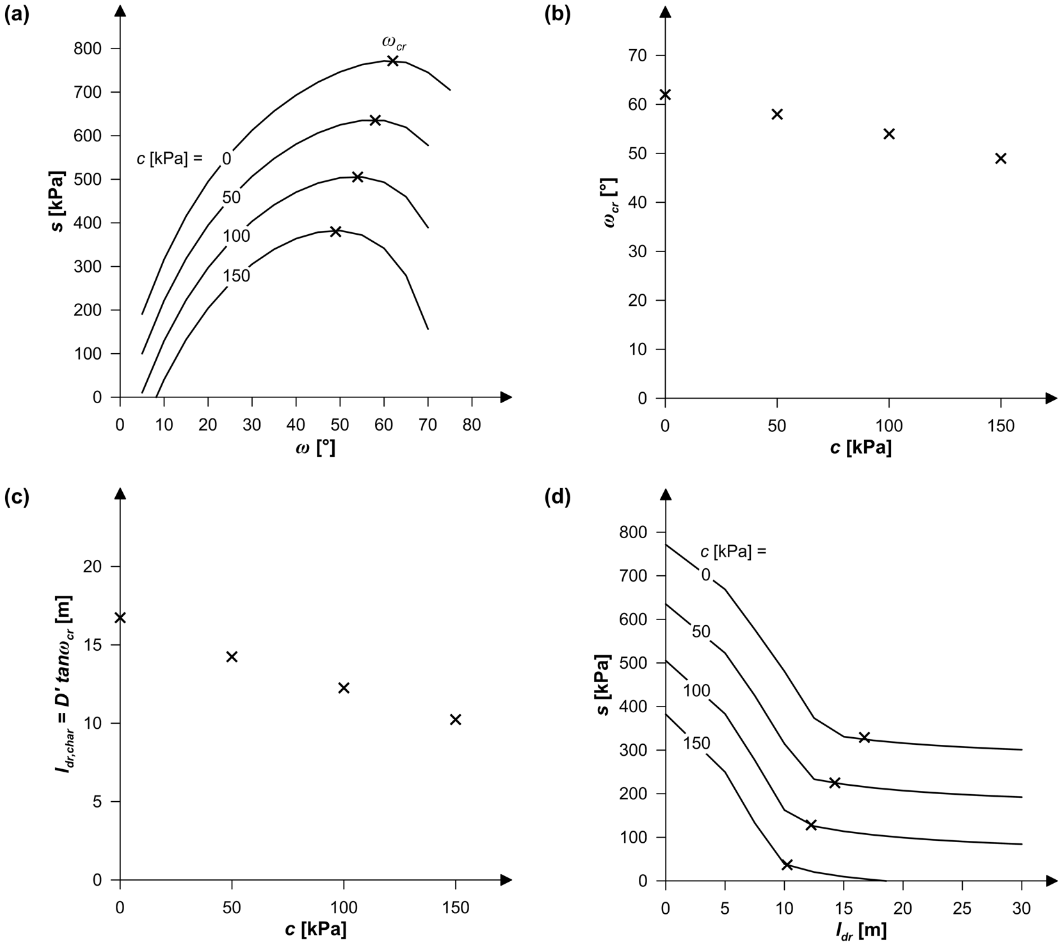

Figure 2.10 *(a) Support pressure s as a function of the wedge angle ω when considering no drainage boreholes, (b) critical wedge angle ω_{cr} as a function of ground cohesion c, (c) characteristic borehole length $l_{dr,char}$ as a function of ground cohesion c, (d) superimposing Fig. 2.9 with the characteristic borehole length $l_{dr,char}$ (indicated with crosses; parameters according to Fig. 2.4 and Table 2.1)*

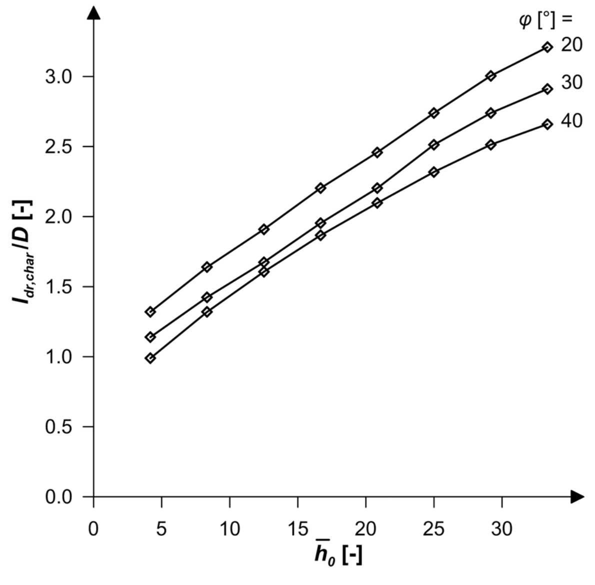

Figure 2.11 *Normalized characteristic borehole length $l_{dr,char}$ as a function of the normalized hydraulic head $\bar{h}_0$ for selected friction angle φ*

2.3.3.4 Radial distance of drainage boreholes

Finally, we investigate whether there is any optimisation potential with respect to the distance r_{dr} of the boreholes from the tunnel centre. We consider six, 30 m long drainage boreholes located at distances of 1.5 - 11 m from the tunnel centre (the distances $r_{dr} > D/2 = 5$ m apply to boreholes drilled from niches), which are located either at the upper part of the cross-section or laterally in groups of three (see inset in Fig. 2.12, l.h.s. and r.h.s cross-section, respectively). Figure 2.12 shows the required support pressure s as a function of r_{dr} for these two arrangements (solid and dashed lines, respectively). As the dashed and solid lines are very close together but all curves exhibit a minimum at $r_{dr} = 5$ - 7 m, the conclusion is that the drainage boreholes should be arranged close to the periphery of the tunnel cross-section, while draining from a niche above the roof or from a lateral niche does not make any difference.

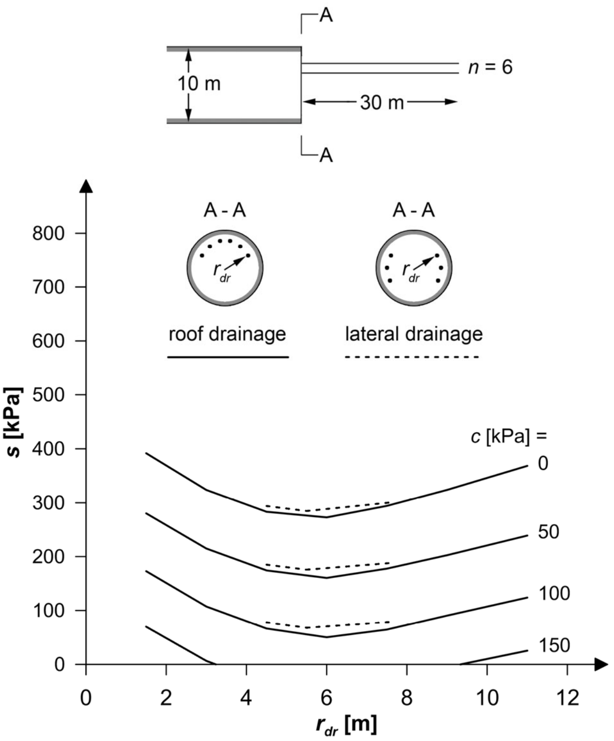

***Figure 2.12** Required support pressure s as a function of the borehole location r_{dr} (borehole locations see inset; parameters according to Fig. 2.4 and Table 2.1)*

2.3.4 Drainage action of a pilot tunnel

We consider first a pilot tunnel that is coaxial with the main tunnel. Figure 2.13 shows the required face support pressure s as a function of the diameter d_p of the pilot tunnel for different values of the cohesion c. In order to determine the required face support pressure, failure mechanisms involving the entire face or parts thereof were considered (mechanisms I, II and III in the inset in Fig. 2.13). Mechanism III proved to be decisive. The pore pressure relief from the pilot tunnel has a significant stabilizing effect. For example, face stability in a weak rock exhibiting a cohesion c of 150 kPa would require a very high support pressure of about 400 kPa in the absence of drainage measures (point A in Fig. 2.13). A 3 m diameter pilot tunnel would, however, provide sufficient pore pressure relief in advance of profile enlargement for the face to be stable without support (point B in Fig. 2.13).

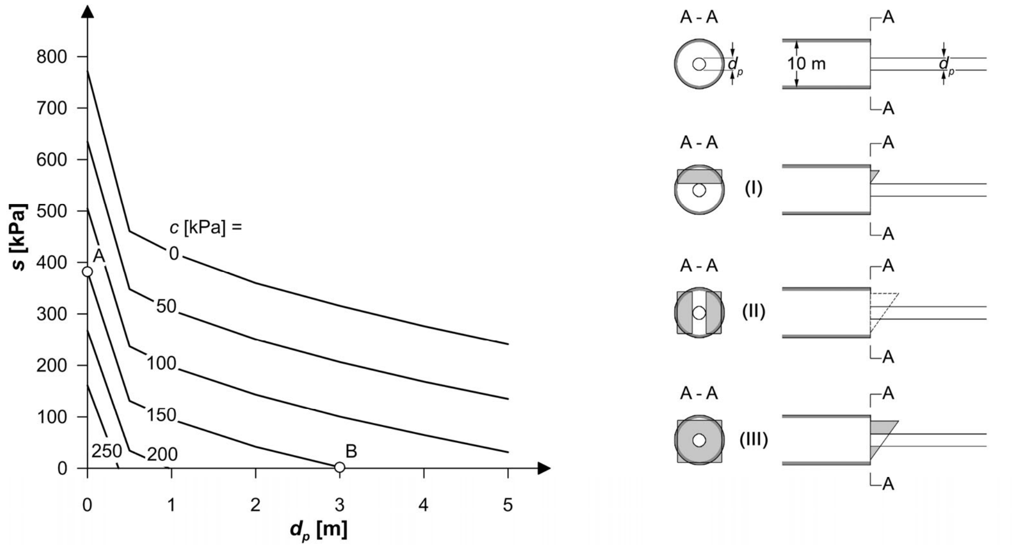

***Figure 2.13** Required support pressure s as a function of the pilot tunnel diameter d_p (inset: the considered failure mechanisms; parameters according to Fig. 2.4 and Table 2.1)*

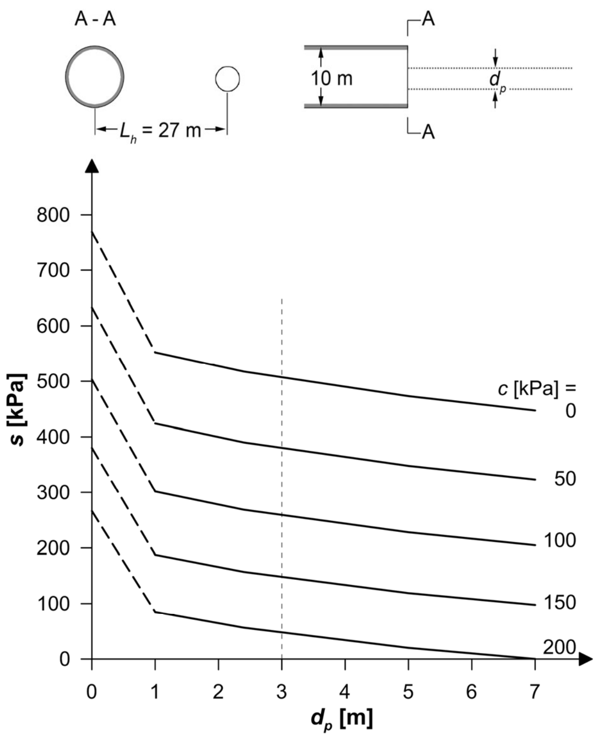

***Figure 2.14** Required support pressure s as a function of the diameter d_p of an external pilot tunnel (parameters according to Fig. 2.4 and Table 2.1)*

The drainage effect of a pilot tunnel outside the cross-section of the main tunnel (Fig. 2.14) is, as might be expected, less pronounced than that of a coaxial pilot tunnel. It is still remarkable, however, considering the relatively long distance from the main tunnel (27 m in the example in Fig. 2.14). A 3 m diameter pilot tunnel causes a reduction in the required support pressure by 34 - 80% depending on the cohesion of the ground (compare points at $d_p = 0$ with points at $d_p = 3$ m in Fig. 2.14). In the case of a weak rock exhibiting cohesion of 150 - 200 kPa, for example, the necessary face support pressure can be reduced to a technically feasible level of 50 - 150 kPa by pre-constructing a pilot tunnel of 3 - 4 m diameter.

According to Figures 2.13 and 2.14, the drainage effect of a pilot tunnel is considerable even if its diameter is very small (as is the case with micro-tunnelling). The form of the s (d_p) curves also shows that the benefit of excavating a larger diameter pilot tunnel is relatively small. In addition, the stability of the face in a larger diameter pilot tunnel may itself be problematic. (For small tunnel diameters, drainage measures alone often suffice for stability, even in ground of low cohesion; see also Zingg and Anagnostou [59].) From the point of view of face stability, a pilot tunnel of small diameter is therefore clearly preferable.

2.3.5 Drainage action of the first tube of a twin tunnel

The solid curves in Figure 2.15 show the support pressure s required for face stability of the second tube as a function of its distance L from the first tube. The crosses apply to the tube constructed first. The advance drainage of the ground due to the first tube has a marked effect on the face stability of the second tube even if the distance of the two tubes is relatively large (L = 50-70 m; compare solid lines with crosses in Fig. 2.15).

For a typical spacing of L_h = 30 m, the drainage action of the first tube leads to a reduction in the necessary face support pressure in the second tube of 44 – 77% depending on the cohesion of the ground. The construction of the second tube is, therefore, considerably easier than that of the first tube. Consider, for example, a twin tunnel in weak rock exhibiting a cohesion c of 200 kPa. Face stabilization in the first tube would require a barely feasible support pressure of more than 200 kPa (point B in Fig. 2.15), or, alternatively, advance drainage by means of boreholes from the face, ground improvement by grouting or combinations thereof. In the second tube, however, the face would be stable without any support s (point C in Fig. 2.15).

It should be noted that the decisive parameter for the drainage action of the first tube is the distance L, irrespective of the vertical or horizontal offset of the two tubes. This is illustrated by the dashed lines in Figure 2.15, which applies to the theoretical case of vertically arranged tunnel tubes with zero horizontal offset.

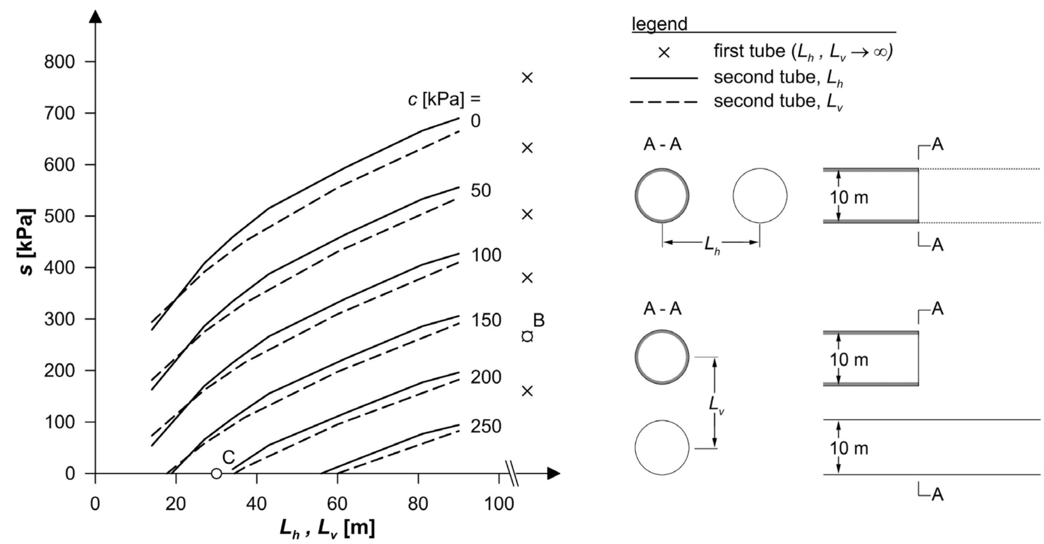

Figure 2.15 *Required support pressure s as a function of the centre distance L of two twin tunnels (parameters according to Fig. 2.4 and Table 2.1)*

2.3.6 Effect of drainage curtains from a pilot tunnel

Taking into account the results of the previous sections, we consider a pilot tunnel of 3 m diameter. The geometric parameters for drainage curtains are: their spacing a_{dr}, the number n and the location of the boreholes of each curtain (Fig. 2.16). The length and the diameter of the boreholes are taken equal to 30 m and 10 cm, respectively. Both the case of a single tunnel (Fig. 2.16a) and that of a twin tunnel will be considered (Fig. 2.16b). The horizontal and vertical offsets of the pilot tunnel are taken equal to 20 m and 10 m, respectively, which mean that the drainage curtains reach the entire cross section of the main tunnel(s).

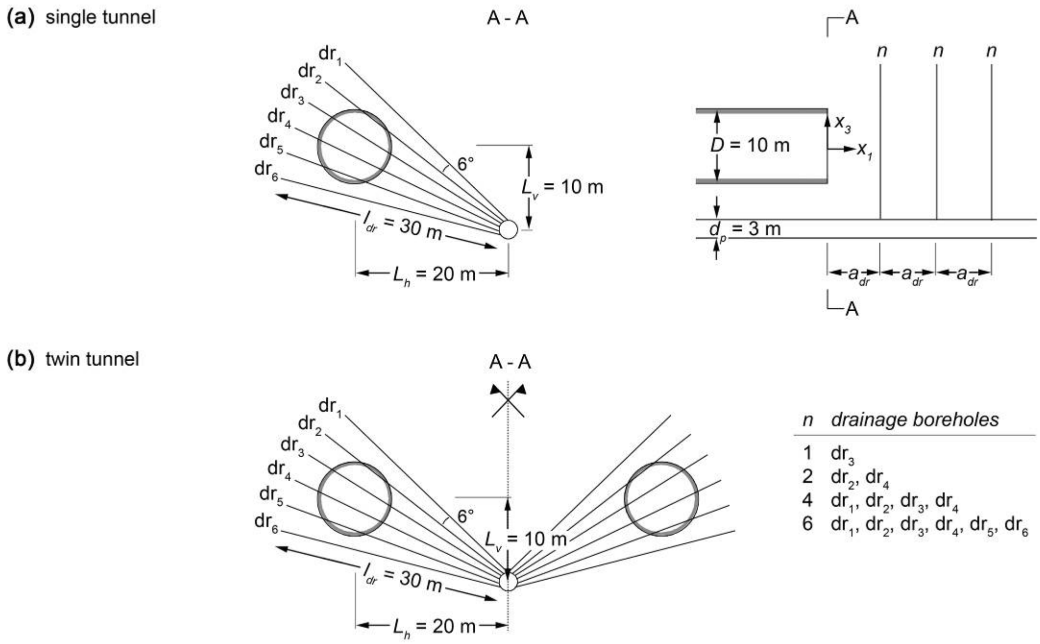

Figure 2.16 *Location of the most effective boreholes (dr_1 - dr_6) of the drainage curtain*

The numerical investigations were carried out for two different pilot tunnel linings: an impermeable lining (*e.g.* a sealed segmental lining) and a permeable lining (*e.g.* a shotcrete lining with pore pressure relief holes). In the first case, drainage occurs solely via the face of the main tunnel and via the radial boreholes. In the second case, pore pressure relief also occurs due to drainage through the pilot tunnel walls.

The computations were carried out for 1, 2, 4 or 6 boreholes per curtain; the benefit of a larger number of boreholes per curtain is marginal (*cf.* Section 2.3.3.1). For any specific number of boreholes per curtain, computations for different borehole arrangements in the plane of the tunnel cross-section were carried out to identify the one with the lowest necessary support pressure (see example in Zingg *et al.* [60]). The table in Figure 2.16 shows the optimum borehole arrangements.

The diagrams in Figure 2.17 apply to the case of a single tunnel (Fig. 2.16a) and show the distribution of the hydraulic head in the axial direction ahead of the tunnel face for 1, 2, 4 or 6 boreholes per curtain (diagrams from the top down) and a sealed (l.h.s. diagrams) or draining (r.h.s. diagrams) pilot tunnel lining. The curves in every diagram apply to curtain spacings $a_{dr} = 4$ - 20 m (Fig. 2.16). The diagrams also show for comparison the head distribution without drainage curtains (upper line in every diagram). The hydraulic head is lower in the case of a draining pilot tunnel lining (r.h.s. diagrams), exhibits local minima at the locations of the drainage curtains and decreases with decreasing curtain spacing and with increasing number of boreholes per curtain. It is remarkable that just 2 boreholes per curtain spaced at 10 m intervals in the longitudinal direction suffice to reduce the hydraulic head to 45 – 60 % of its initial value in the vicinity of the face (see red curves in Figs. 2.17b and 2.17f). Considering the high cost but limited additional benefit of very closely spaced curtains, a spacing of 10 m (*i.e.* one tunnel diameter) represents a reasonable choice. Figure 2.18 shows the required support pressure s for this spacing as a function of the cohesion c for curtains consisting of 1, 2, 4 or 6 boreholes for an impermeable (Fig. 2.18a) and a permeable (Fig. 2.18b) pilot tunnel lining, a single tunnel (black lines) and a twin tunnel (red lines). The difference between single and twin tunnels is small (*e.g.* for $c = 0$: 3-12% for an impermeable, 3-7% for a permeable pilot tunnel lining).

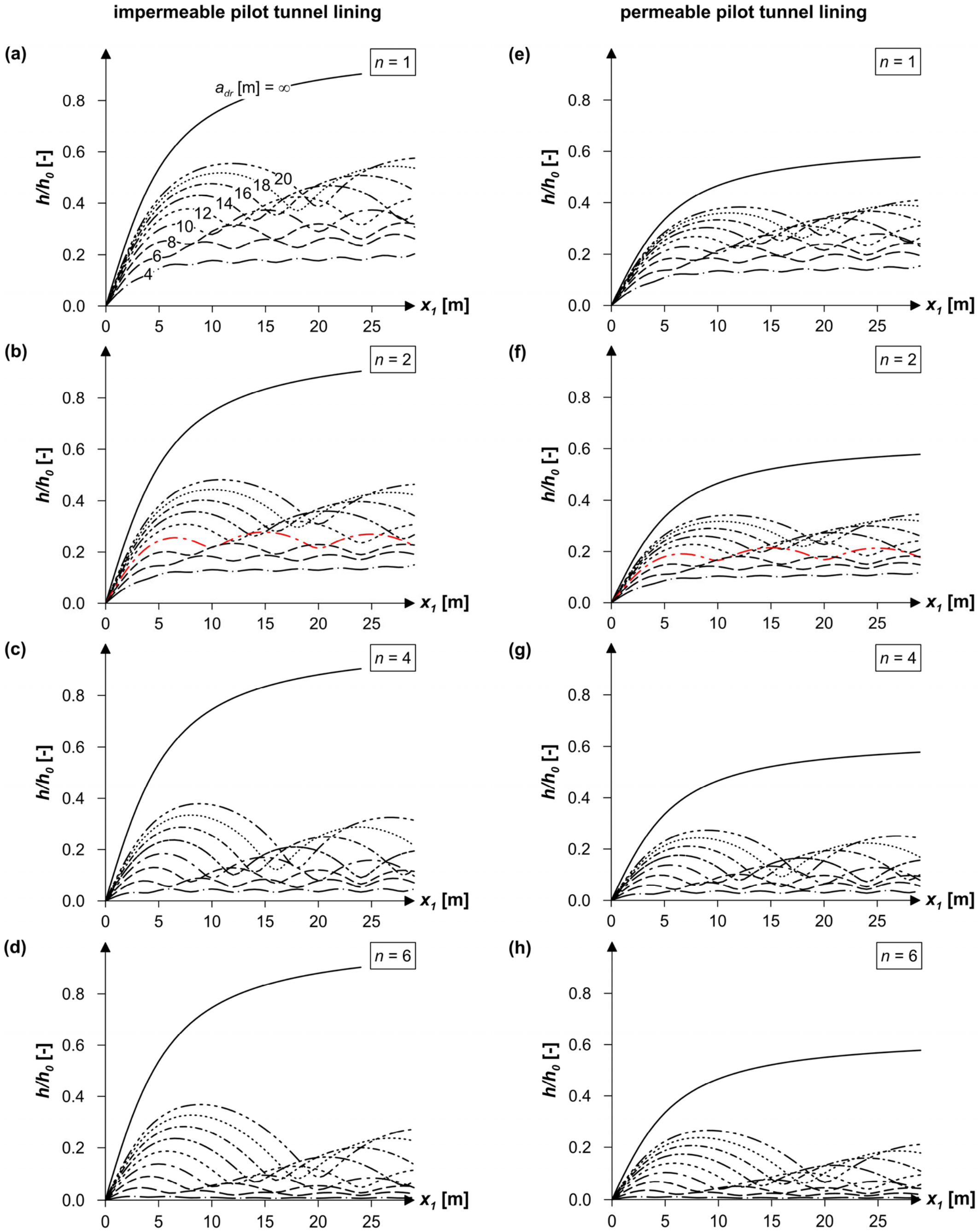

Figure 2.17 *Axial distributions of the normalized hydraulic head* h *ahead of the face of the main tunnel (borehole locations according to table in Fig. 2.16, parameters according to Table 2.1)*

In order to illustrate the significance of these results from the practical engineering point of view, consider a single tunnel crossing weak rock exhibiting a cohesion of 100 - 150 kPa. In the absence of drainage measures, the required support pressure would be 400 - 500 kPa (point A in Fig. 2.18a). This value, which is unfeasible in conventional tunnelling, can be reduced to a manageable level (of about 100 kPa) by drainage curtains consisting of 2-4 boreholes each (points B and C, Fig. 2.18a). In combination with a permeable pilot tunnel lining (Fig. 2.18b), the drainage curtains would even allow an unsupported face, and this in spite of the combination of weak ground with high *in situ* hydrostatic pressure.

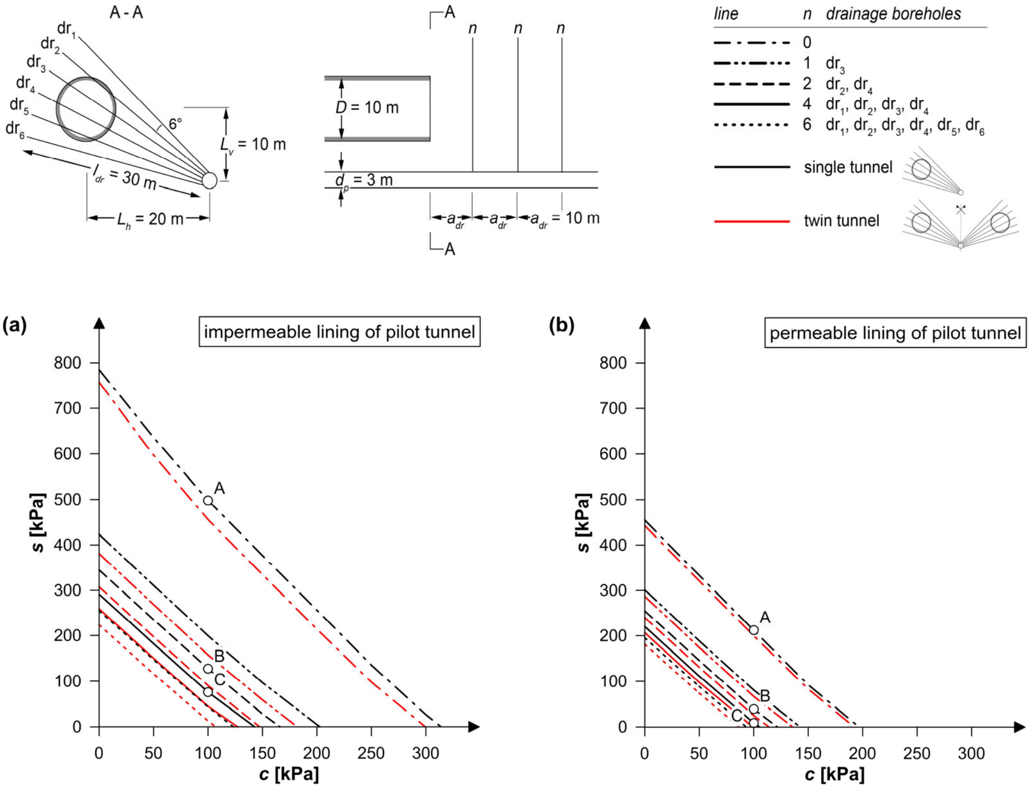

Figure 2.18 *Required support pressure s as a function of cohesion c for n = 0 to 6 drainage boreholes per curtain: (a) impermeable, (b) permeable pilot tunnel lining (borehole locations according to table in Fig. 2.16, parameters according to Fig. 2.4 and Table 2.1)*

2.4 Design equation

Provided that the upper boundary of the seepage flow domain is not too close to the tunnel crown (specifically, that $\min(H, H_w) > 5D$), the required face support pressure can be approximated by the following equation, which is sufficiently accurate for practical design purposes:

$$\frac{s}{\gamma' D} = F_0 - F_1 \frac{c}{\gamma' D} + \left(F_2 - F_3 \frac{c}{\gamma' D} \right) \frac{\gamma_w h_0}{\gamma' D} \quad , \tag{2-2}$$

where the dimensionless coefficients F_0 to F_3 depend only on the friction angle φ and the drainage layout. The coefficients were determined by means of a comprehensive parametric study and can be depicted from the design nomograms of Figures I.1 to I.7 of Appendix I. Each figure applies to a different drainage layout; Table 2.2 provides an overview.

Details of the development of the design equation (2-2), the determination of the coefficients F_0 to F_3 and the applicability limits of the presented nomograms are given in Zingg [62] or in condensed form in Zingg and Anagnostou [56].

***Table 2.2** Drainage layouts and belonging design nomograms*

Drainage layout	*Nomogram of Appendix I*
None (only drainage action of the tunnel face)	Figure I.1 (n = 0)
Axis-parallel, long boreholes through the tunnel face (l_{dr}/D = 1.5)	Figure I.1
Axis-parallel, short boreholes through the tunnel face (l_{dr}/D = 3)	Figure I.2
Axis-parallel boreholes from niches	Figure I.3
Co-axial pilot tunnel	Figure I.4
First tube of twin tunnel	Figure I.5
External pilot tunnel with permeable lining	Figure I.6 (n = 0)
Radial boreholes from external pilot tunnel with permeable lining	Figure I.6
Radial boreholes from external pilot tunnel with impermeable lining	Figure I.7

2.4.1 Applicability limits of the nomograms

The nomograms assume that $T = min(H, H_w) > 5D$. This condition is fulfilled by subaqueous tunnels ($H_w > H$) with an overburden H of minimum 5 times the tunnel diameter D and by mountain tunnels ($H_w < H$) at a depth H_w of minimum 5 D underneath the water table. For $T/D < 5$, the nomograms underestimate the support pressure. This can be compensated by increasing the coefficient F_2 roughly by 20%. Of course, the nomograms are not applicable where there is no seepage flow.

The nomograms were developed for a normalized borehole diameter $d_{dr}/D = 0.01$, which is typical for usual borehole and traffic tunnel diameters, but they are sufficiently accurate in the range $d_{dr}/D = 0.005 – 0.020$, *i.e.* for most practical purposes.

The nomograms provide an estimate of the required support pressure that is slightly on the safe-side for the practically relevant ranges of cohesion and support pressure ($c/\gamma' D \geq 0.2$, $0 \leq s/\gamma' D \leq 4$) and up to very high hydraulic heads ($\gamma_w h_0/\gamma' D \leq 30$).

2.4.2 Use of the nomograms

The use of the nomograms is straightforward: choose the applicable nomogram according to the intended drainage scheme (Figs. I.1 to I.7 of Appendix I); read out the values of the coefficients F_0 to F_3; and calculate the required support pressure s by means of design equation (2-2). Safety factors can easily be taken into account by using reduced shear strength parameters (c, $tan\varphi$) or a higher hydraulic head h_0.

Consider, for example, the problem of Section 2.3 (Fig. 2.4) with 6 axial drainage boreholes drilled from the face ($d_{dr}/D = 0.01$, $l_{dr}/D = 3$) and the ground parameters φ = 30°, c = 100 kPa, γ' = 12 kN/m^3 and γ_w = 10 kN/m^3. The applicable nomograms are given in Figure I.2. For $\varphi = 30°$ and $n = 6$, the coefficients are: $F_0 = 0.15$, $F_1 = 1.9$, $F_2 = 0.21$ and $F_3 = 0.007$. Inserting these values in Eq. (2-2) results in a support pressure of 104 kPa.

The design equation (2-2) can be used in an inverse way to estimate the critical cohesion *c* (*i.e.* the cohesion that would render face support measures unnecessary). Solving Eq. (2-2) with respect to c for $s = 0$ results in a critical cohesion of 152 kPa for the example considered. If the cohesion is higher than this value, then advance drainage would suffice for face stability.

2.5 Application examples

2.5.1 Albula tunnel

The planned Albula II railway tunnel will run at an axial distance of 30 m parallel to the historic Albula I tunnel, a UNESCO engineering landmark built about 110 years ago in Switzerland (Fig. 2.19). Albula I became famous because of the difficulties experienced during construction through the so-called rauwacke formation [31]. The latter consists of cellular dolomite, a weak rock exhibiting a porous, sponge-like structure with pore dimensions in the range of millimetres. Close to the boundary with the next geological unit, the rauwacke formation contains a network of what are probably tubular cavities with fine-grained infillings. The locally almost cohesionless ground in combination with the high water table (initially about 120 m above the alignment) resulted in instabilities with several instances of material inrush and tunnel flooding. Overcoming the rauwacke formation, which was only 110 m long, caused a delay of 11 months in construction.

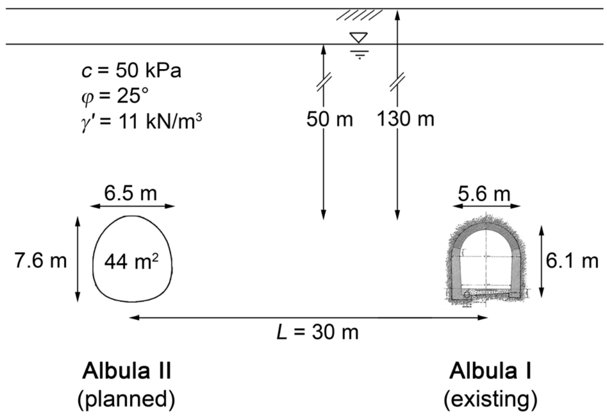

Figure 2.19 *Problem layout of application example Albula*

On account of the previous tunnelling experience, the rauwacke formation is also expected to be challenging in the construction of Albula II. According to recent geological investigations, the infillings of the voids appear – when drained – to be "a stiff to weak, strongly silty sand with some gravel", but under seepage conditions become flowing slurry [74]. Advance drainage therefore represents a construction option, alone or in combination with ground improvement by grouting or freezing, provided of course that the environmental impact of drainage can be accepted.

In the following paragraphs, we investigate the effectiveness of some possible drainage schemes with respect to the stabilization of the tunnel face by using the design equation (2-2). For this purpose, the egg-shaped cross-section of the planned tunnel is approximated by a circular cross-section of same area (44 m^2, diameter 7.5 m). The shear strength parameters for the ground depend on the degree of disintegration and on the fraction of voids with soft infillings. The friction angle φ of the rauwacke is in the range of 25-30°, while the cohesion amounts to 5-10 kPa for the infillings and to 500-1000 kPa for the rock [74]. The computations were carried out assuming overall values representing a weakly consolidated rauwacke formation with a high fraction of infillings (φ = 25°, c = 50 kPa). According to recent measurements, the current piezometric head is about 50 m above the tunnel. Due to the drainage action of Albula I, this value is probably lower than the undisturbed head that prevailed before its construction (estimated to 120 m).

Table 2.3 shows the coefficients F_0 to F_3 as well as the support pressure s after Eq. (2-2). Without drainage measures the necessary support pressure amounts to 191 kPa (Table 2.3, row 1). Such high support pressure is barely feasible with face bolts: Consider, for example, a dense face reinforcement consisting of fully grouted bolts spaced at 1 m (*i.e.*, a bolt density n_b of 1 bolt/m^2) and a wedge with an inclined slip surface forming an angle of 45º-φ/2 = 32.5º to the vertical direction (Fig. 2.20). Where the bolts are sufficiently long, the limiting factor for the support force offered by the reinforcement is the anchorage length of the bolts inside the wedge [72]. For the wedge under consideration, the average anchorage length amounts to about 2.1 m. Taking the diameter d_b of the grouted bolt boreholes equal to 0.1 m and the bond strength τ_m of the grout–ground interface equal to maximum 150 - 200 kPa, the support pressure offered by the reinforcement amounts at most to $n_b \cdot \pi \cdot d_b \cdot \tau_m$ = 100 - 130 kPa, which is considerably lower than the necessary support pressure.

***Table 2.3** Coefficients F_0 to F_3 and resulting support pressure s for the example Albula*

	Drainage layout	F_0	F_1	F_2	F_3	s [kPa]
1	None (Fig. I.1, n = 0)	0.134	2.241	0.552	0.014	191
2	2 axis-parallel boreholes through the face (Fig. I.1, n = 2, l_{dr} = 1.5D = 11.3 m)	0.154	2.145	0.377	0.016	103
3	4 axis-parallel boreholes through the face (Fig. I.1, n = 4, l_{dr} = 1.5D = 11.3 m)	0.189	2.218	0.292	0.016	57
4	6 axis-parallel boreholes through the face (Fig. I.1, n = 6, l_{dr} = 1.5D = 11.3 m)	0.199	2.251	0.268	0.013	43
5	Co-axial pilot tunnel of 3 m diameter (Fig. I.4)	0.177	2.231	0.244	0.001	20
6	Face of 3 m diameter pilot tunnel d_p (Fig. I.1, n = 8, l_{dr} = 1.5d_p = 4.5 m)	0.216	2.331	0.232	0.008	4
7	Drainage curtains spaced at 7.5 m, each having 6 boreholes, executed from Albula I (Fig. I.7)	0.190	2.391	0.191	0.005	0

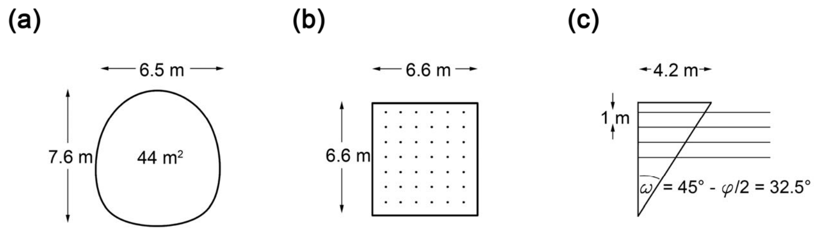

***Figure 2.20** Estimate of the support pressure provided by face reinforcement: (a) actual tunnel cross-section; (b) equivalent square cross-section; (c) geometry of the wedge in longitudinal section*

According to rows 2 to 4 of Table 2.3, which apply to the case of advance drainage via 2 to 6 boreholes from the tunnel face, four drainage boreholes, each a minimum of 11 m long, would be sufficient to reduce the necessary support pressure to an acceptable level. A considerable reduction in the necessary support pressure could also be achieved by first excavating a 3 m diameter coaxial tunnel (Table 2.3, row 5). Stabilization of the pilot tunnel's face would, nevertheless, require advance drainage by at least 8 boreholes (Table 2.3, row 6).

Alternatively, drainage of the ground ahead of the excavation face of Albula II tunnel could be carried-out by means of about 30 m long boreholes from the existing Albula I tunnel (Table 2.3, row 7). As the latter is lined by a stonework arch, the necessary support pressure can be estimated with the coefficients F_0 to F_3 according to Figure I.6 (permeable lining). In the present case, we used Figure I.7, which applies to an impermeable lining, because the drainage effect of the existing tunnel is taken into account by considering the current piezometric head (50 m) instead of the initial, undisturbed head. It should be noted that the support pressure computation with the nomograms in Figure I.7 is sufficiently accurate in spite of the differences between the actual geometry and the geometry underlying the nomograms (smaller tunnel spacing, symmetrically arranged drainage curtains). This was confirmed by a numerical seepage flow analysis that was carried-out considering the actual geometry (Fig. 2.21). According to Table 2.3, row 7, drainage curtains (spaced at 7.5 m and each consisting of six boreholes) are sufficient for face stability. This solution would thus not only avoid the interference between excavation and drainage work, but also render unnecessary any other stabilization measures. On the other hand, the execution of drainage work from the existing tunnel would impose constraints on railway operations.

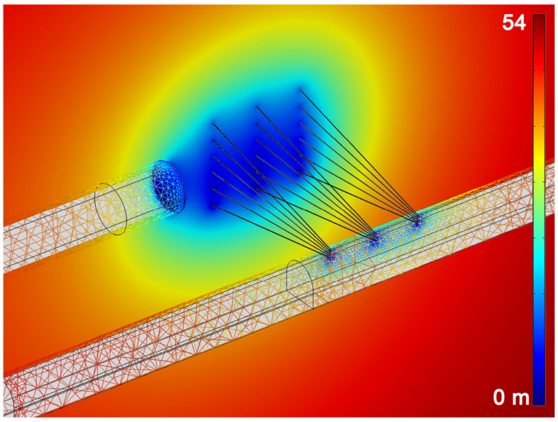

Figure 2.21 *Axonometric projection of the hydraulic head field of application example Albula in the presence of drainage curtains*

2.5.2 Lake Mead Intake No. 3 Tunnel

The Lake Mead Intake Tunnel No. 3 belongs to Las Vegas' water supply scheme. It is 4.7 km long and has a diameter of 7.22 m. Tunnel excavation was recently completed using a convertible hybrid TBM capable of boring in open mode or in closed mode as a slurry shield [75]. The ground consists of metamorphic and tertiary sedimentary rocks (conglomerates, breccias, sandstones, siltstones and mudstones of very variable quality) with several fault zones probably recharged directly from the lake (Fig. 2.22). The maximum hydrostatic pressure amounts to about 14 bar. Due to the lack of experience with closed-mode operation under such high pressures and the very poor local ground quality, it was necessary to design face stabilisation measures such as advance drainage and pre-excavation grouting that would allow for open mode operation.

In the first part of the alignment through metamorphic rocks, considerable difficulties were encountered due to the unfavourable combination of high water pressure, extremely high rock permeability (10^{-4} to 10^{-5} m/s) and the presence of an unexpected fault zone subparallel to the tunnel [77]. The fault, consisting of almost cohesionless material, made it necessary to operate in closed mode at 14 bar for several hundred metres. Attempts to bring the slurry pressure below the hydrostatic pressure resulted in extremely high, barely manageable quantities of water inflow (up to 1100 m^3/hour; [78]). Advance drainage under such conditions was ineffective.

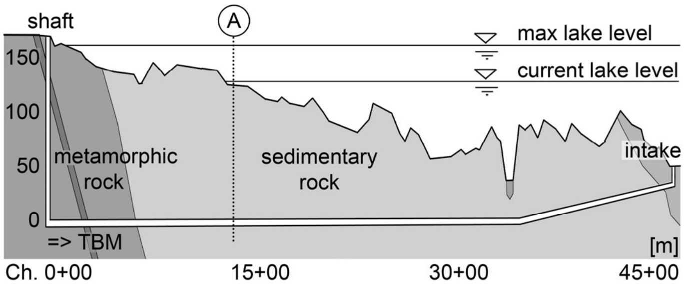

Figure 2.22 *Geological profile of the Lake Mead Intake No. 3 tunnel (after Feroz et al, [76])*

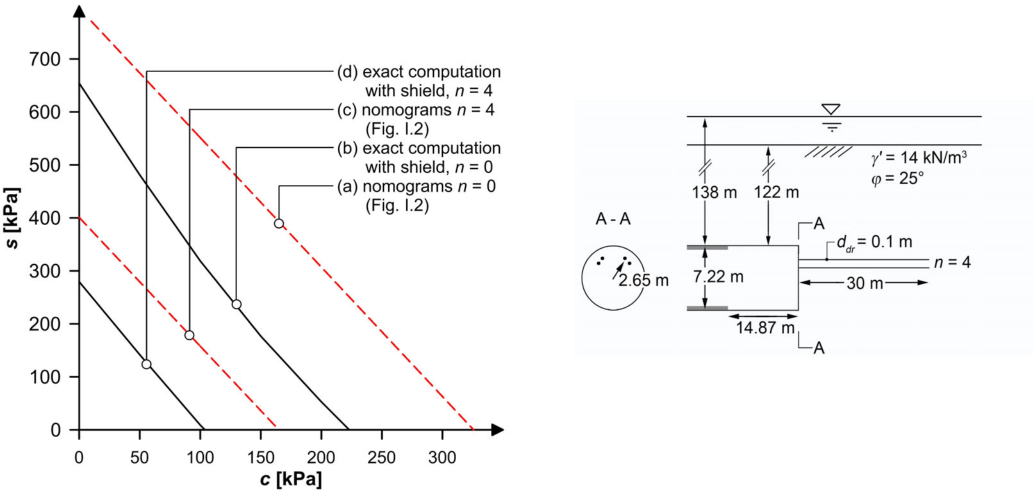

Figure 2.23 *Lake Mead Intake No. 3 tunnel, Ch. 12+60 (point A in Fig. 2.22): Support pressure s as a function of the cohesion c*

The sedimentary rocks exhibited a medium to low permeability (10^{-6} to 10^{-10} m/s) and proved sufficiently stable at least in short term. The TBM was operated mainly in open mode in combination with 3 boreholes drilled through the cutter head for advance probing and drainage. The boreholes were 30-45 m long and overlapped by 10 m. In order to ensure stability during longer standstills (of more than two days), 2 to 3 additional boreholes of at least 10 m were drilled.

The advance drainage in the Lake Mead tunnel has considerably widened the feasibility range of open mode TBM drives and atmospheric interventions in the working chamber for inspection and maintenance. Related studies can be found elsewhere ([22], [55]). Here, we focus on one peculiarity of shielded TBMs in order to show a limitation of the proposed design nomograms. In a shielded TBM, water inflows occur not only from the tunnel face and the drainage boreholes, but also from the rock around the shield. The shield of the Lake Mead TBM is 14.87 m long, which means that the total area of the seepage face is 337 m^2 larger than the tunnel face (41 m^2). As larger seepage face areas obviously favour pore pressure relief, the question arises as to how much the nomograms (which assume no flow through the tunnel periphery) underestimate stability in such cases.

Figure 2.23 shows the relationship between the necessary support pressure s and the cohesion c for the following drainage cases: (a) from the tunnel face only (based on the nomograms in Fig. I.2); (b) from the tunnel face and the shield area (based on a numerical seepage flow analysis taking account of the additional seepage face around the shield); and (c) from the tunnel face and from four advance drainage boreholes (based on the nomograms in Fig. I.24); (d) from the tunnel face, the shield area and four advance drainage boreholes (based on a numerical seepage flow analysis taking account of the additional seepage face around the shield as well as the exact locations, length and diameter of the boreholes according to the inset in Fig. 2.23).

Without the boreholes, drainage through the additional seepage face around the shield reduces the necessary support pressure by about 200 kPa or, for the given support pressure, the necessary cohesion by about 100 kPa (compare a to b in Fig. 2.23). In the case of advance drainage by 4 boreholes, disregarding the drainage in the shield area overestimates the necessary support pressure and cohesion by about 125 kPa and 60 kPa, respectively (compare c to d in Fig. 2.23). This example shows that the nomograms should be used with care where the seepage flow conditions are very different from the ones assumed by the nomograms.

2.6 Conclusions

Advance drainage greatly improves tunnel face stability because it reduces pore pressures and their gradients in the ground ahead of the face. The study in hand quantifies the effects of various advance drainage schemes by means of limit equilibrium computations which take account of the steady-state, three-dimensional seepage flow conditions prevailing in a homogenously permeable ground.

Four to six drainage boreholes (from the tunnel face or a niche) with a minimum length of one and a half tunnel diameters will generally be enough to reduce the necessary face support pressure significantly or even to render support unnecessary. The marginal utility of advance drainage diminishes for more or longer boreholes. The boreholes are more effective if they are located in the upper part and close to the periphery of the tunnel cross-section, but their exact positioning (roof or lateral) is not so important.

The drainage effect of a pilot tunnel (located either inside or outside the main tunnel cross-section) is also considerable. Even a very small diameter coaxial pilot tunnel brings so much pore pressure relief that the face of the main tunnel may be stable without additional auxiliary measures. Sparsely arranged drainage curtains (*e.g.* spaced at about one diameter intervals along the tunnel and consisting of two to four drainage boreholes each) improve the drainage effectiveness of adjacent tunnels.

In the case of twin tunnels, the drainage action of the first tube is important with respect to face stability of the second tube, even if the distance of the two tubes is relatively large (4-7 tunnel diameters).

A design equation has been developed which makes it possible to assess the stabilizing effect of drainage and study the various options rapidly, thus providing a very valuable design aid. The coefficients that appear in this equation depend on the friction angle and the geometric parameters for the drainage layout. They can be depicted using the dimensionless nomograms worked out by analysing the computational results of a comprehensive parametric study incorporating a wide parameter range and several advance drainage schemes.

The nomograms provide an estimate of the required support pressure that is slightly on the safe-side for the practically relevant ranges of cohesion and support pressure ($c/\gamma'D \geq 0.2$, $0 \leq s/\gamma'D \leq 4$) and up to very high hydraulic heads ($\gamma_w h_0/\gamma'D \leq 30$). The nomograms assume that the seepage flow domain is not too close to the tunnel crown ($T = min(H, H_w) > 5D$), otherwise they underestimate the support pressure. The nomograms were developed for a normalized borehole diameter $d_{dr}/D = 0.01$, but they are sufficiently accurate in the range $d_{dr}/D = 0.005 – 0.020$, *i.e.* for most practical purposes.

3 Effectiveness of drainage measures for tunnel face stability in ground of non-uniform permeability

3.1 Introduction

Chapter 3 aims to improve understanding of the differences in face stability and drainage effectiveness between ground of uniform and non-uniform permeability, hereinafter referred to as “homogeneous” and “heterogeneous” ground, respectively. It analyses a series of formations, exhibiting heterogeneity at various scales and consisting of alternating horizontal or vertical aquifers and aquitards intersecting or being in close proximity to the tunnel face (Fig. 3.1). The performed analyses provide valuable information about whether and to what extent the required support pressure is higher or lower than in the case of homogeneous ground; which ground structures are critical for face stability and necessitate a higher support pressure; to which extent advance drainage does allow for reduction in support pressure; and where the drainage boreholes have to be arranged in order to be most effective.

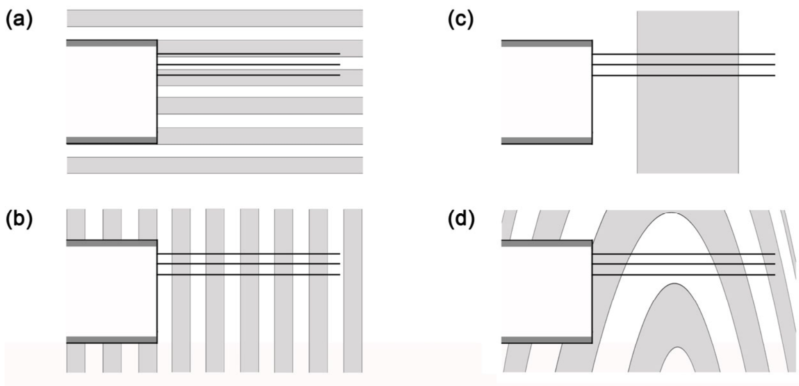

Figure 3.1 *Formations consisting of alternating aquifers and aquitards: hydraulic heterogeneity due to horizontal (a) and vertical (b) layers; (c) a single fault zone or (d) variation in the longitudinal direction due to intensive folding*

Sections 3.2 to 3.5 investigate face stability in a horizontally stratified ground (Fig. 3.1a). Horizontal layers of variable permeability may be present in quaternary formations due to the sedimentation sequence; in sedimentary rocks (*e.g.* alternating layers of marl and sandstone); or – more rarely – in the case of sub-horizontal faults (such a fault was encountered, *e.g.* in the Bodio Section of the Gotthard Base Tunnel; [79]). A wide range of the heterogeneity scale characterized by layer thicknesses from decimetres to decametres is considered, first by analysing the case of tunnelling close to the horizontal interface of two differently permeable formations (Section 3.2). Then a single layer exhibiting a higher or a lower permeability than the surrounding ground will be considered, paying attention to the effect of its elevation and thickness (Section 3.3) and at variable elevation (Section 3.4). Finally, the case of alternating thin horizontal layers will be discussed, which can be treated as a homogeneous anisotropic medium (Section 3.5).

Sections 3.6 to 3.9 investigate cases of a permeability variation in the horizontal direction, which is caused by a sequence of practically vertical, alternating zones with different lithological or structural characteristics. This situation is encountered typically when approaching the interface of an aquifer with an aquitard (Fig. 3.1b), in fault zones (Fig. 3.1c) or in intensively folded formations (Fig. 3.1d). Single fault zones, consisting of crushed rock or soil-like material of low cohesion, if encountered suddenly, may result in a large-scale instability and subsequent inundation of a long portion of the tunnel

(Fig. 3.2a). For example, during construction of the Albula railway tunnel in the beginning of 20th century in the Swiss Alps, it took almost one year to overcome a 113 m long tunnel section through "a ground consisting of finest dolomite sand" (so-called "running ground") under a water pressure of about 12 bar ([80], [31]); the water in this zone was infiltrating from all sides and washed out big quantities of sand. Considerable problems with water and mud inrushes occurred also in the Sampuoir section of the Engadine power station, where competent rock alternated with up to 2 m wide zones filled with loose material (Fig. 3.2b; [26], [81]). A recent case of particularly demanding heterogeneous ground is that of the Lake Mead Intake No. 3 tunnel, where a fault striking almost parallel to the tunnel axis was encountered unexpectedly and made it necessary to realign the tunnel (e.g. [82], [55], [82], [83]). Faults occur alone or in a group (Fig. 3.3a and b, respectively) and are in some cases accompanied laterally by heavily jointed and fractured rock (referred to as "damage zone" by Faulkner *et al*. [84]; see Fig. 3.3), while in other cases the transition to the surrounding rock is sharp [26]. They often exhibit permeability contrasts of several orders of magnitude ($10\text{-}10^4$; [85]), which result in considerable anomalies in the pore pressure distribution ([86], [87], [84]). In the case of faults in hard brittle rocks, the fault zones are often blocky, brecciated and due to the fracture connectivity more permeable than the surrounding rock. On the other hand, in intensively sheared and weathered rocks, the fault core will be mostly fine-grained (clayey or silty) and less permeable than its surroundings. Therefore, both low- and high-permeability fault zones will be investigated. Section 3.6 starts with an investigation of tunnelling close to the vertical interface of two differently permeable formations. Section 3.7 will focus on face stability when entering a vertical fault zone. Finally, the case of multiple vertical layers (including that of thin alternating layers, which can be modelled as a homogeneous, anisotropic medium) will be investigated (Section 3.8).

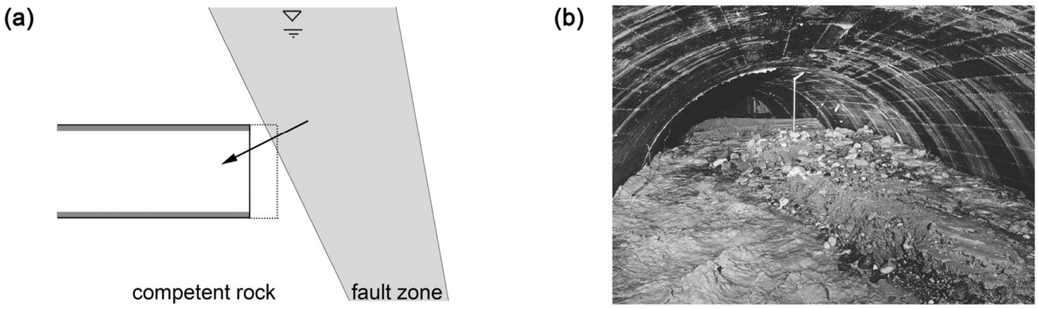

Figure 3.2 *(a) Collapse in water-bearing fault zone; (b) Water and mud inflows during construction of a tunnel for the Engadin power station at Sampuoir*

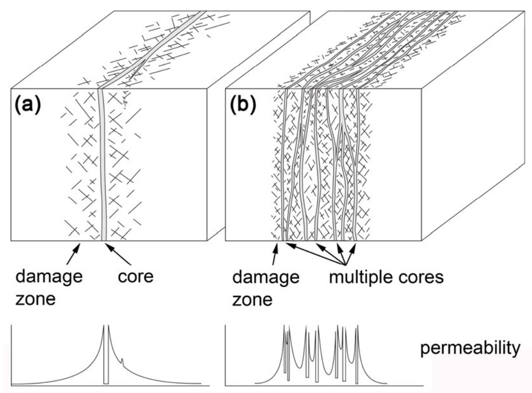

Figure 3.3 *Permeability distributions in a fault zone, (a), with a single core and, (b), with multiple cores (Faulkner et al. [84])*

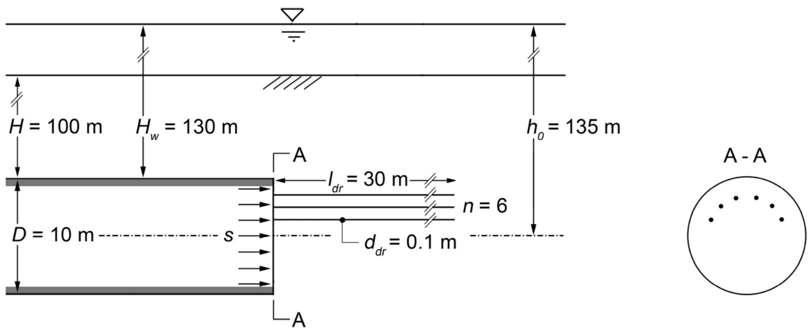

Figure 3.4 *Problem setup of the comparative analyses*

For all geological situations mentioned above, the effect of permeability heterogeneity on face stability will be quantified in terms of the support pressure that is required for stabilizing the face. The example of a subaqueous cylindrical tunnel will be studied, either without or with advance drainage measures according to Figure 3.4. The considered drainage layout of six axial boreholes was proved to be the most effective in homogeneous ground (Section 2.3.3.2).

As in Chapter 2, the estimate of the required face support pressure is based upon the model of Anagnostou and Kovári [9]. The seepage forces, which have to be introduced into the equilibrium equations, are determined by numerical three-dimensional, steady-state seepage flow analyses taking account of both the heterogeneity of the ground and the presence of the drainage boreholes, assuming that their hydraulic capacity allows water discharge under atmospheric pressure. The tunnel lining is taken impervious; no drawdown of water table is considered. For simplicity and as this research project focuses on hydraulic effects, uniform shear strength is assumed[3] (with one exception in Section 3.8.2); keeping in mind that layers of different permeability may exhibit different shear strength as well. Table 3.1 summarizes the parameters assumed for the seepage flow and limit equilibrium analyses.

Table 3.1 *Parameters for the comparative analyses*		
Problem layout		
Depth of cover	H	100 m
Elevation of water table	H_w	130 m
Tunnel diameter	D	10 m
Thickness of layer or zone	d_L	0-100 m
Ground		
Effective cohesion	c	0-500 kPa
Angle of eff. internal friction	φ	30°
Submerged unit weight	γ'	12 kN/m^3
Unit weight water	γ_w	10 kN/m^3
Shear resistance of the vertical slip surfaces		
Coefficient of lateral stress in wedge	λ_w	0.5
Coefficient of lateral stress in prism	λ_p	1.0
Drainage boreholes (location see Fig. 3.4)		
Diameter	d_{dr}	0.1 m
Length	l_{dr}	0-30 m
Number	n	6
Permeability of the ground		
Permeability ratio (layer to host rock)	k_L/k	0.01 - 100
Degree of anisotropy	k_p/k_n	0.01 - 100

[3] For formations with horizontal layers, also failure mechanisms involving only an individual layer were considered. However, as the shear strength of the ground is taken uniform, the failure mechanism that comprises the entire face requires the highest support pressure and thus was decisive.

3.2 Tunnelling close to the horizontal interface of aquitard and aquifer

Assume tunnelling close to a horizontal permeability interface (Fig. 3.5a) when considering no or six advance drainage boreholes (red and blue lines, respectively). Figure 3.5b shows the support pressure, which is required for face stability, as a function of the distance between the tunnel axis and the interface of the two zones. The permeability contrast was taken equal to 100; the reference case of uniform permeability is also included in the diagram. For simplicity, the figures discussed in detail assume ground without any cohesion (denoted with support pressure s_0). An increase in ground cohesion c might be approximated by the equations inside the diagram for support pressures s (confirmation of the roughly linear shift downwards of the curves of Figure 3.5b and the subsequently discussed Figures 3.7, 3.9, 3.15, 3.16, 3.20 and 3.23 is given in Zingg [62]).

The heterogeneous structure of the ground has a remarkable effect on face stability, if the tunnel is closer than about to diameters to the interface of aquifer to aquitard. Two potentially critical situations are indicated with point A and B in Figure 3.5b. The corresponding hydraulic head fields are given in Figure 3.6.

In both cases A and B, the tunnel is located completely within the aquitard, but very close to the aquifer. In case A (aquitard above of aquifer), the interface of the two formations is at the tunnel floor (case A in Fig. 3.6). In case B (aquifer above of aquitard), the interface of the two formations is located at the tunnel crown (case B in Fig. 3.6). As the tunnel does not intersect the aquifer and the latter is by factor 100 more permeable than the aquitard; the pore pressure within the aquifer remains practically hydrostatic in spite of the drainage action of the tunnel face and of the boreholes (compare head fields in Fig. 3.6b and Fig. 3.6c, respectively). Consequently, the hydraulic head at the interface of the two zones is practically equal to the initial head and since the interface is located close to the tunnel, the pore pressure inside the aquitard and around the face are higher than in the case of homogeneous ground (compare also solid to dashed lines in Fig. 3.6a).

The distance between the red and blue lines in Figures 3.5 and 3.6 represents a measure of the effectiveness of the drainage boreholes in terms of support pressure and pore pressure relief, respectively. In homogeneous ground, the drainage boreholes would cause a pore pressure relief by about 75% in front of the face and reduce also the hydraulic head gradient above the tunnel (Fig. 3.6a), which results in a decrease in the required support pressure by about 450 kPa (Fig. 3.5). In heterogeneous ground, the drainage boreholes reduce the required support pressure by 250 - 500 kPa, *i.e.* as much as an increase in cohesion by 100 – 200 kPa (*e.g.* by grouting; Fig. 3.5). However, their effectiveness is lower if they are drilled within the aquitard and the aquifer is either just above the tunnel (point B in Fig. 3.5) or just underneath the boreholes (between point A and C in Fig. 3.5). Boreholes reaching the aquifer would be significantly more effective (see later Section 3.4.2.3).

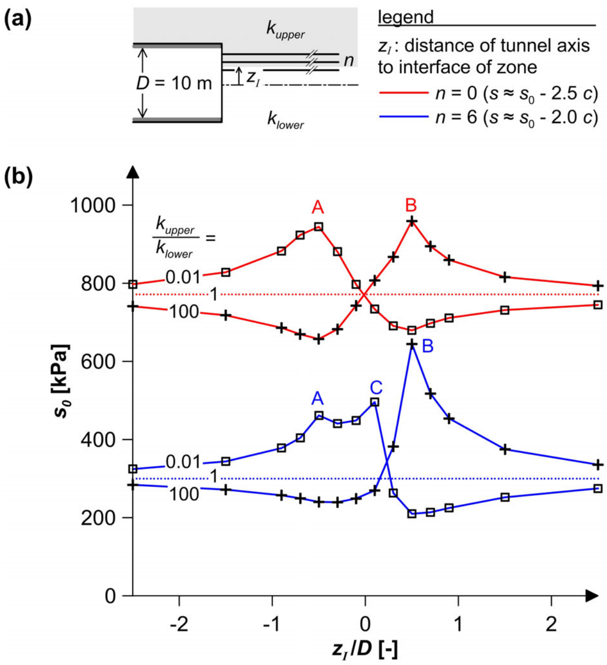

Figure 3.5 *(a) Two differently permeable zones with horizontal interface and (b) required support pressure s_0 as a function of the distance z_I in ground without any cohesion c (permeability contrast k_{upper}/k_{lower} = 0.01, 1, 100; parameters according to Table 3.1)*

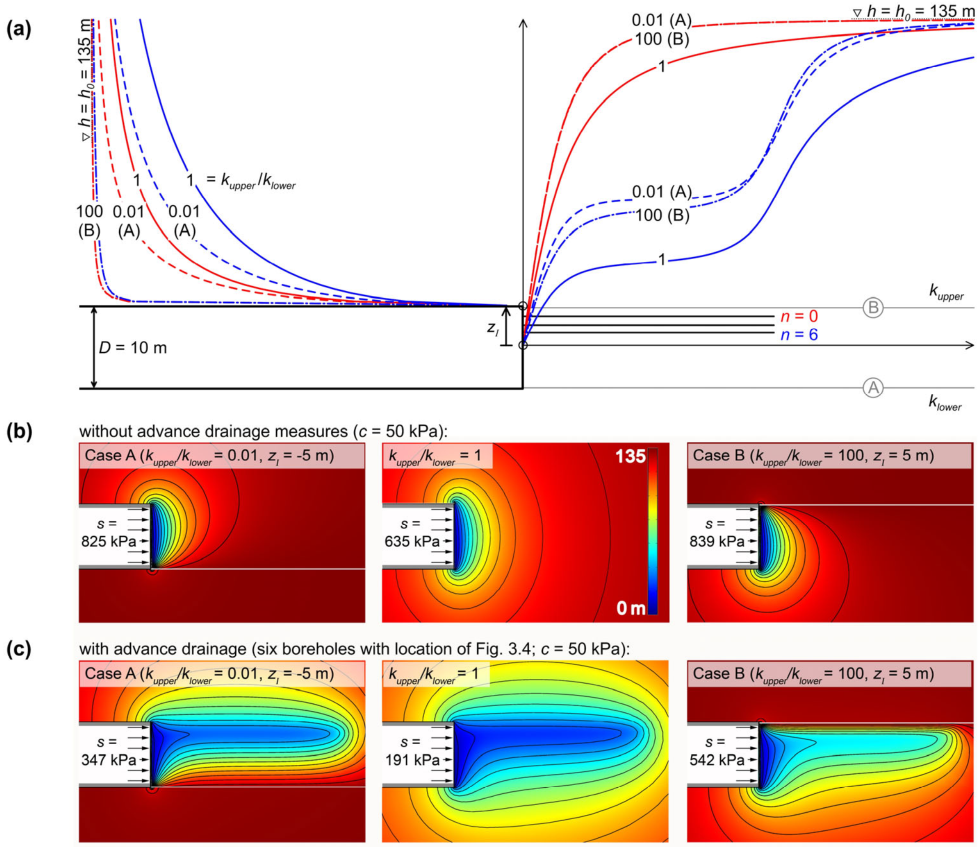

Figure 3.6 *(a) Distribution of the hydraulic head h along two lines above and ahead of the tunnel face for two horizontal zones of different permeability (cases A and B of Fig. 3.5). Belonging surface plots of the hydraulic head field as well as required support pressure s (b) without advance drainage measures and (c) with six axial drainage boreholes (c = 50 kPa, other parameters according to Table 3.1)*

3.3 A single, horizontal aquifer or aquitard symmetric to the tunnel axis

Complexity of permeability heterogeneity increases when considering one high- or low-permeability layer of variable thickness on the tunnel axis (Fig. 3.7a). Figure 3.7b shows the required support pressure s_0 for face stability as a function of the normalized layer thickness d_L in ground without any cohesion.

A single high- or low-permeability layer has a considerable effect on the required face support pressure even if it is relatively thick (Fig. 3.7b): the support pressure tends to the value of homogeneous ground only for very large layers ($d_L/D > 7$). The heterogeneity effect is biggest when the layer thickness is equal to the tunnel diameter (cases A and B in Fig. 3.7; the corresponding hydraulic head fields are given in Fig. 3.8).

Overall, a low-permeability layer increases support demand compared to homogeneous ground, while a high-permeability layer is more favourable for stability. The aquitard acts as a hydraulic barrier and the hydraulic head is higher than in homogeneous ground both ahead and above of the tunnel face (compare dashed to solid lines in Fig. 3.8a and surface plots of case A in Fig. 3.8b and c). The aquifer acts as a natural advance drainage, which reduces the hydraulic head in relation to homogeneous ground both ahead and above of the tunnel face (compare dash-dotted to solid lines in Fig. 3.8a and surface plots of case B in Fig. 3.8b and c). It is remarkable that in the absence of drainage boreholes, even a very thin high-permeability layer results in a significant reduction of the required support pressure (case C in Fig. 3.7b).

Drainage boreholes reduce the required face support pressure by 300 – 500 kPa depending on the layer thickness (compare red to blue lines in Fig. 3.7). In case of a low-permeability layer, the drainage boreholes cause an additional pore pressure relief only inside the layer (case A in Fig. 3.8c). The hydraulic head in the surrounding aquifer is not affected by the drainage boreholes (compare red and blue dashed lines in l.h.s. of Fig 3.8a) and is clearly higher than in homogeneous ground (compare dashed to solid blue lines in Fig. 3.8a). Therefore, the support pressure is very high (upper blue line in Fig. 3.7b). Note that another arrangement of boreholes (such as they reach the aquifer) would increase effectiveness of the drainage measure (see later Section 3.4.2.3).

In the presence of a high-permeability layer, the additional pore pressure relief and support pressure reduction due to the drainage boreholes is smaller than in homogeneous ground, because the aquifer layer acts as a natural advance drainage, which anyway reduces pore pressures and face support pressure (compare case B in Fig. 3.8b to 3.8c).

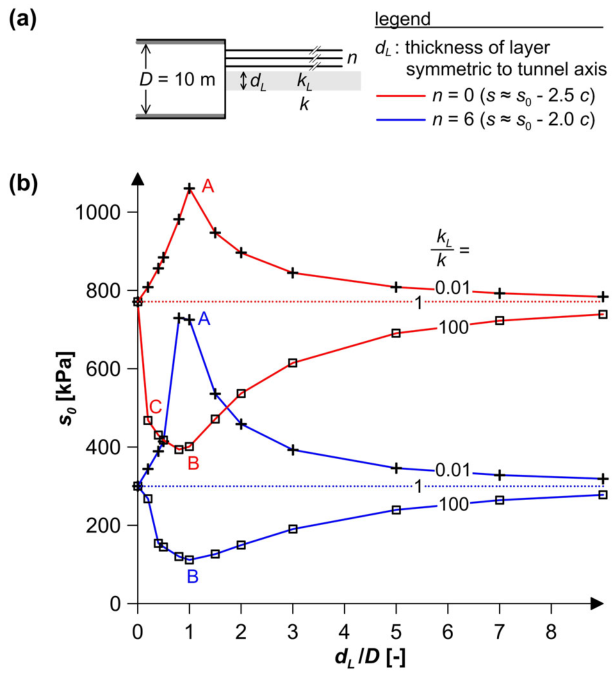

Figure 3.7 *(a) Single horizontal layer coaxial to the tunnel axis and (b) required support pressure s_0 as a function of the thickness of the layer d_L in ground without any cohesion c (permeability contrast k_L/k = 0.01,1,100; parameters according to Table 3.1)*

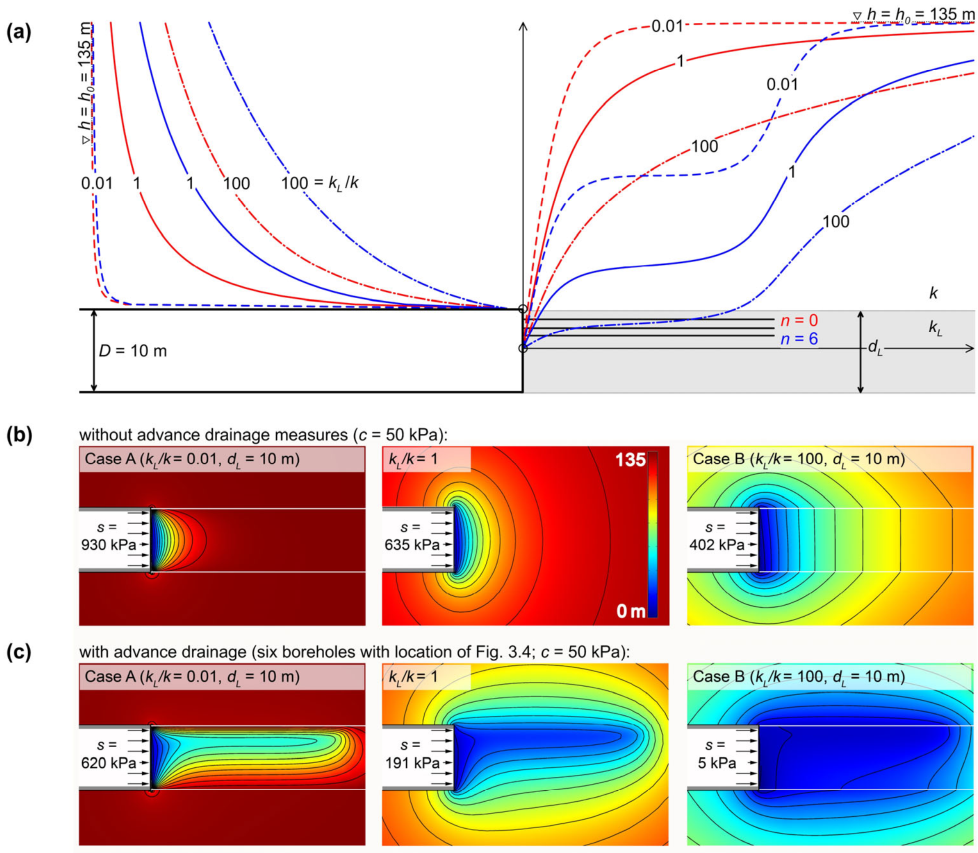

Figure 3.8 *(a) Distribution of the hydraulic head h along two lines above and ahead of the tunnel face for a single horizontal layer coaxial to the tunnel axis (cases A and B of Fig. 3.7). Belonging surface plots of the hydraulic head field as well as required support pressure s (b) without advance drainage measures and (c) with six axial drainage boreholes (c = 50 kPa, other parameters according to Table 3.1)*

3.4 A single horizontal layer of variable elevation and thickness

3.4.1 Support pressure and hydraulic head field

Permeability heterogeneity of a single horizontal layer is characterized by the permeability ratio k_L/k, the layer thickness d_L and elevation z_b (Fig. 3.9a). Figure 3.9 shows the results of a parametric study into these effects on the required support pressure as a function of the permeability ratio k_L/k for a 2 m and a 5 m thick layer, respectively. The markers indicate different ground models of layer elevation from tunnel invert to slightly above the roof (layers located outside that range have a negligible influence on face stability; see also Fig. 3.5 or Fig. 3.7). The ground models, which can be summarized as unfavourable (A, B) and favourable (C, D) concerning face stability, are sketched for each extremal permeability ratio in Figure 3.9b.

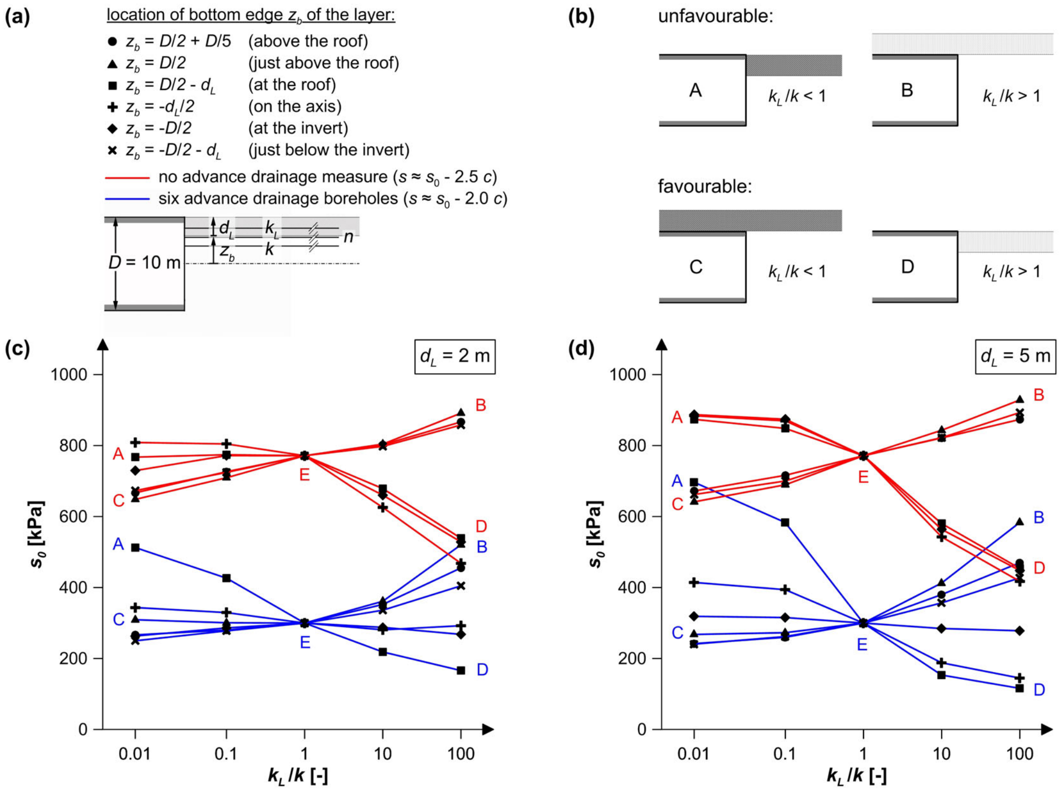

Figure 3.9 *(a) Parametric study of a single horizontal layer of variable elevation and thickness. (b) Unfavourable and favourable ground models concerning face stability. Required support pressure s_0 as a function of the permeability contrast k_L/k in ground without any cohesion c for (c) a 2 m thick layer and (d) a 5 m thick layer (blue: no drainage measure; red: six drainage boreholes; other parameters according to Table 3.1)*

In case of a low-permeability layer ($k_L/k < 1$), all ground models require roughly the same support as in homogeneous ground. Distinctive exception is the case of advance drainage with a barrier layer at the roof, where a considerably higher support pressure is necessary (compare blue A to E in Fig. 3.9c and d). In case of a high-permeability layer ($k_L/k > 1$), a clearly lower support pressure than in homogeneous ground is required in case where the layer is within the tunnel face (compare *e.g.* D to E in Fig. 3.9c and d). On the other hand, remarkable more support pressure than in homogeneous ground is required in case of lacking connection of the layer to a seepage face (compare *e.g.* B to E in Fig. 3.9). Assuming for example a ground of cohesion $c = 150$ kPa and considering 6 drainage boreholes, the tunnel face in homogeneous ground would be stable, while in case of a 2 m thick high-permeability layer at the tunnel roof, still 200 kPa support pressure would be required [62].

The hydraulic head field of the (un-)favourable cases concerning support pressure (A to E in Fig. 3.9) are given in Figures 3.10 and 3.11. As the typical characteristics do not change with increasing layer thickness (the thicker the layer, the more pronounced is the effect of permeability contrast; compare Fig. 3.9c to d), we limit our discussion below to a 2 m thick layer.

3.4.1.1 Layer at the tunnel roof

A low-permeability layer at the tunnel roof ($k_L/k < 1$) hinders pressure relief above the tunnel face (compare dashed to solid lines in Fig. 3.10a). In case without advance drainage, the barrier-effect of the low-permeability layer is of subordinate importance with respect to the required support pressure, because the hydraulic head distribution ahead of the face is practically the same as in homogeneous ground (case A and E in Fig. 3.10b). In case with advance drainage boreholes however, the required support pressure is significantly higher than in homogeneous ground, because the boreholes are not able to relief the pressure above of the aquitard (case A and E in Fig. 3.10c).

A high-permeability layer at the tunnel roof ($k_L/k < 1$) acts as natural drainage and is favourable for both cases with and without drainage. Especially compared to no advance drainage measure, the drainage boreholes allow for a drastic reduction of the required support pressure by about 85% (from 403 to 58 kPa; case D in Fig. 3.10b and c).

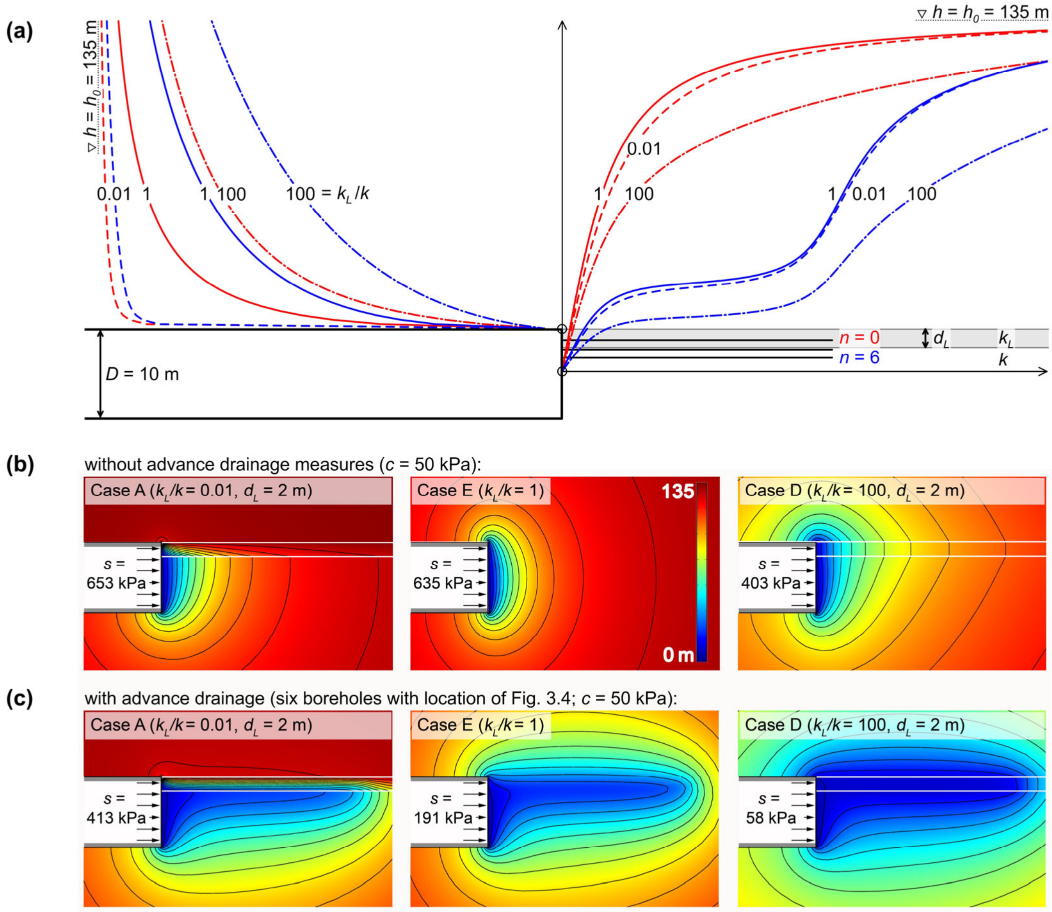

***Figure 3.10** (a) Distribution of the hydraulic head h along two lines above and ahead of the tunnel face in the case of a 2 m thick layer at the tunnel roof (cases A, D and E of Fig. 3.9c). Belonging surface plots of the hydraulic head field as well as required support pressure s (b) without advance drainage measures and (c) with six drainage boreholes (c = 50 kPa, other parameters according to Table 3.1)*

3.4.1.2 Layer just above the tunnel roof

Compared to the hydraulic head field in homogeneous ground, a low-permeability layer above the tunnel roof ($k_L/k < 1$) is favourable ahead, but not above of the tunnel face (compare dashed to solid lines in Fig. 3.11a). The pore pressure dissipates mostly within the layer and the hydraulic head above the aquitard is practically equal to the initial hydraulic head. However for face stability considerations, the distance of the hydraulic gradients to the tunnel face is large enough and the support pressures required are similar to the ones required in homogeneous ground (compare cases C to E in Fig. 3.11).

A high-permeability layer ($k_L/k > 1$) just above the tunnel roof cannot act as natural drainage due to the lack of connection to a seepage face, be that the drainage boreholes or the tunnel face (case B in Fig. 3.11). The hydraulic head is higher than in homogeneous ground both ahead and above the tunnel face (compare dash-dotted to solid lines in Fig. 3.11a) and thus significant more support pressure is necessary for face stability (case B in Fig. 3.9).

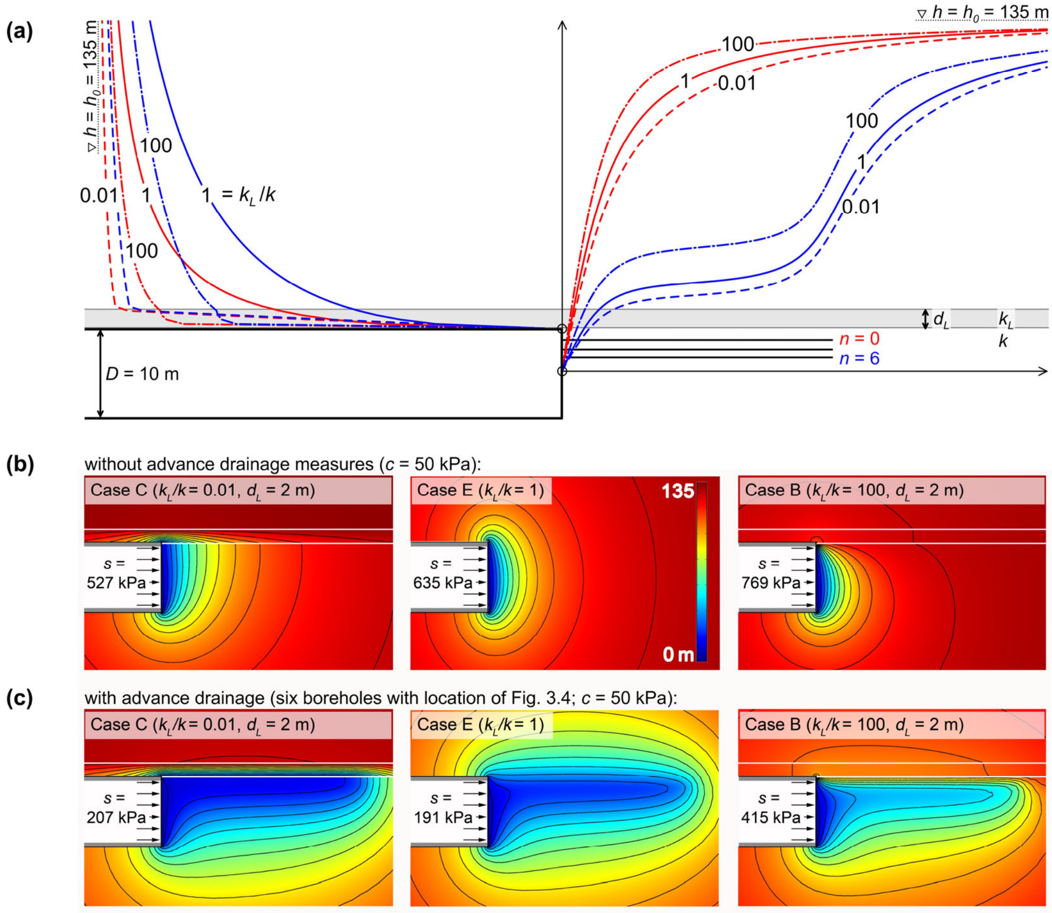

Figure 3.11 *(a) Distribution of the hydraulic head h along two lines above and ahead of the tunnel face in the case of a 2 m thick layer just above the tunnel roof (cases B, C and E of Fig. 3.9c). Belonging surface plots of the hydraulic head field as well as required support pressure s (b) without advance drainage measures and (c) with six drainage boreholes (c = 50 kPa, other parameters according to Table 3.1)*

3.4.2 Optimizing the drainage borehole layout

The effectiveness of advance drainage can be increased by optimizing the borehole layout such as at least some boreholes intersect the more permeable layer. In fact, by shifting two of the lower boreholes upwards into the overlying aquifer (by drilling from a niche as in Fig. 3.12b, or by drilling steeply inclined boreholes as in Fig. 3.12c), the hydraulic barrier effect of the aquitard can be defused. In case of a low-permeability layer in the tunnel face (central column in Fig. 3.12; corresponding to case A in Fig. 3.9c and Fig. 3.10c), about half the support pressure of the standard drainage layout is required (216-239 instead of 413 kPa; Fig. 3.12). In case of a high-permeability layer without connection to a seepage face (right column in Fig. 3.12; corresponding to case B in Fig. 3.9c and Fig. 3.10c), the support pressure decreases even more (from 415 to 69-127 kPa; Fig. 3.12) and is lower than the support pressure required in homogeneous ground (of 191 kPa). Thus for both unfavourably situated low- and high-permeability layer, a wise borehole arrangement levels the support pressure needed to about the values required in homogeneous ground.

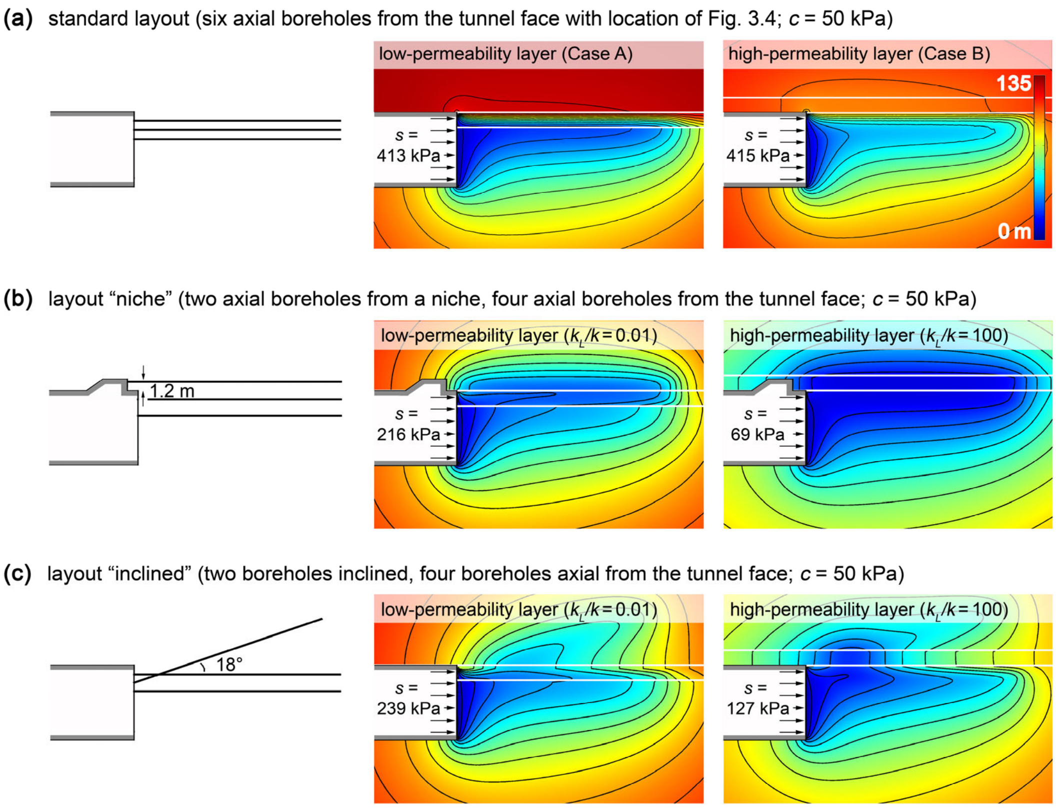

Figure 3.12 *Surface plots of the hydraulic head field as well as required support pressure s for the cases A and B of Figure 3.9c (a) with the standard drainage layout, (b) with drainage from a niche (c) with inclined drainage boreholes (other parameters according to according to Table 3.1)*

3.4.3 Application example

The practical significance of these results is discussed for an exemplary tunnel in ground of very low cohesion ($c = 50$ kPa). A marginally inclined, 2 m thick layer crosses the alignment such as the previously discussed ground models apply with sufficient accuracy (longitudinal section in Fig. 3.13a). The required support pressure s for face stability when approaching a high-permeability layer is shown in Figure 3.13b; approaching a low-permeability layer is plotted in Figure 3.13c. Each figure shows the support pressure required when considering no advance drainage measure (red line), advance drainage with six axial boreholes (blue) and advance drainage with optimized borehole location (green; two boreholes arranged in the more permeable ground as discussed in Section 3.4.2).

When crossing a high-permeability layer without advance drainage measures, an overall very high support pressure is required, which shows high sensitivity to the variability of the ground (347 - 769 kPa; red in Fig. 3.13b). As a face support pressure of about 200 kPa would yet necessitate heavy face reinforcement (grey area in Fig. 3.13b) and pressures of more than 300 kPa cannot be materialized (Section 2.5.1), auxiliary measures such as grouting or freezing would be necessary to stabilize the face. Advance drainage by axial boreholes from the face would reduce the required support pressure mostly to a technically manageable level (58 – 415 kPa; blue in Fig. 3.13b). Optimizing the borehole arrangement by drilling two boreholes in the more permeable ground would finally decrease the support overall to a feasible range (57 – 243 kPa; green in Fig. 3.13b).

The support pressure when crossing a low-permeability layer without advance drainage measures is less variable, but yet too high for conventional tunnelling (527 - 673 kPa; red in Fig. 3.13c). Advance drainage with axial boreholes decreases the required support pressure down to the feasible range of face bolts with only exception of the previously discussed situation of a barrier layer in the tunnel face (141 – 413 kPa; blue in Fig. 3.13c). Optimizing the borehole arrangement and dewatering the permeable ground above the layer, also these pressures would be reduced to a technically manageable level (59 – 191 kPa; green in Fig. 3.13c).

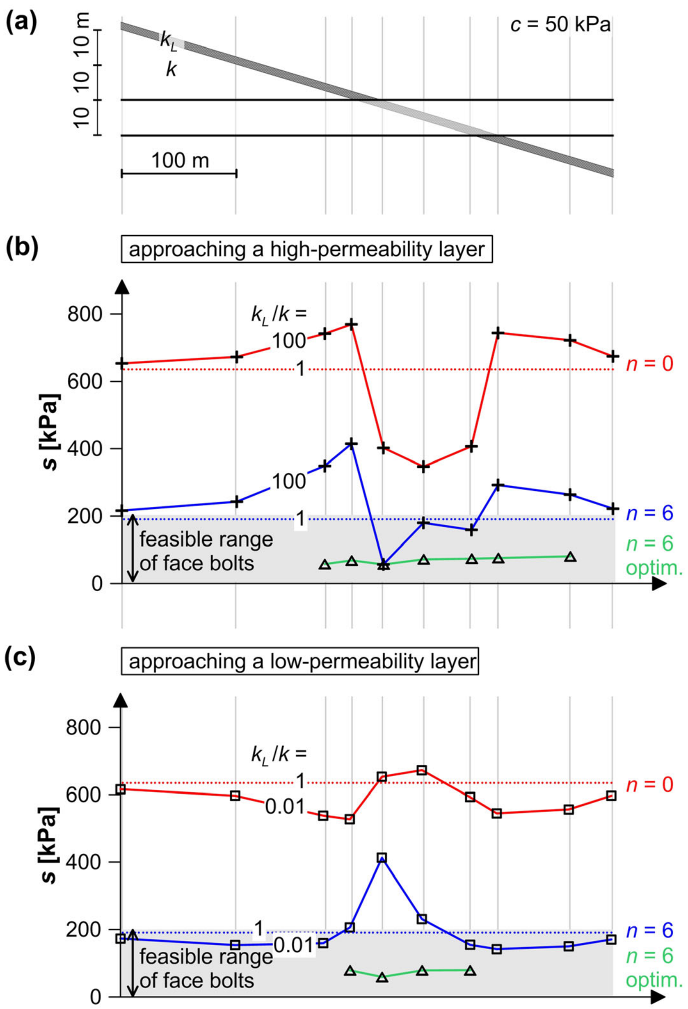

Figure 3.13 *(a) Longitudinal section of a tunnel crossing a marginally inclined, 2 m thick layer in ground of cohesion c = 50 kPa. Required support pressure s (b) when approaching a high-permeability layer and (c) when approaching a low-permeability layer (blue: no drainage measure; red: six axial boreholes according to Fig. 3.4; green: optimized drainage layout with two boreholes shifted in the more permeable ground; other parameters according to Table 3.1)*

3.5 Thinly interbedded horizontal aquifers and aquitards

3.5.1 Homogenisation to an equivalent anisotropic model

Sedimentary deposits (heterogeneous quaternary soils or sedimentary rocks) have often a considerably higher permeability in the horizontal than in the vertical direction. If the layer thickness is small in relation to the size of the tunnel cross-section, the ground can be considered as a homogeneous medium of anisotropic permeability. The equivalent permeability parallel and normal to the strata are (*e.g.* [88]):

$$k_p = a_1 k_1 + a_2 k_2 \quad , \tag{3-1}$$

$$k_n = \left(\frac{a_1}{k_1} + \frac{a_2}{k_2} \right)^{-1} \quad , \tag{3-2}$$

where a_i and k_i denote the fraction and the permeability of the layer i, and are considered in an orthotropic permeability matrix. The steady state hydraulic head field depends on the degree of anisotropy, expressed by the ratio

$$\frac{k_p}{k_n} = 1 + a_1 \left(1 - a_1\right) \left(\frac{k_1}{k_2} + \frac{k_2}{k_1} - 2 \right) \quad , \tag{3-3}$$

but not on the individual values of k_p and k_n.

3.5.2 Maximum layer thickness

The equivalent homogeneous anisotropy model allows neglecting numerical expensive, discretely depicted layers in an FE-model. In order to determine the maximum layer thickness for which homogenisation to an equivalent homogeneous anisotropy model is possible, Figure 3.14 shows the required face support pressure s as a function of the normalized layer thickness d/D (ground without any cohesion). The results of stratified media consisting of discretely modelled layers are indicated as black crosses (inset in Fig. 3.14a); the equivalent anisotropic medium is shown in red.

The range of required support pressure (which is due to the upmost layer at the face acting as a hydraulic barrier or as a natural drainage) decreases with decreasing layer thickness (highlighted in grey in Fig. 3.14b). The face support needed in an equivalent anisotropic medium (s = 555 kPa) is nearly identical to the one required when modelling discrete layers of adequately thin strata (s = 514 - 610 kPa for d/D = 0.2; Fig. 3.14b). The support pressure for thicker layers deviates more than 10% from the pressure required considering the equivalent anisotropic permeability model and is not safe-side.

3.5.3 Effect of permeability anisotropy

The effect of permeability anisotropy on face stability is discussed for an increasing degree of anisotropy (Fig. 3.15a). Figure 3.15b shows the required support pressure s_0 as a function of the permeability ratio k_1/k_2 and the degree of anisotropy k_p/k_n for cohesionless ground. The solid red line applies to no advance drainage measures, the blue to advance drainage with six axial boreholes. The dotted lines indicate the support pressure required in isotropic ground. Figure 3.15c shows the belonging distribution of the hydraulic head h along two lines above and ahead of the tunnel face.

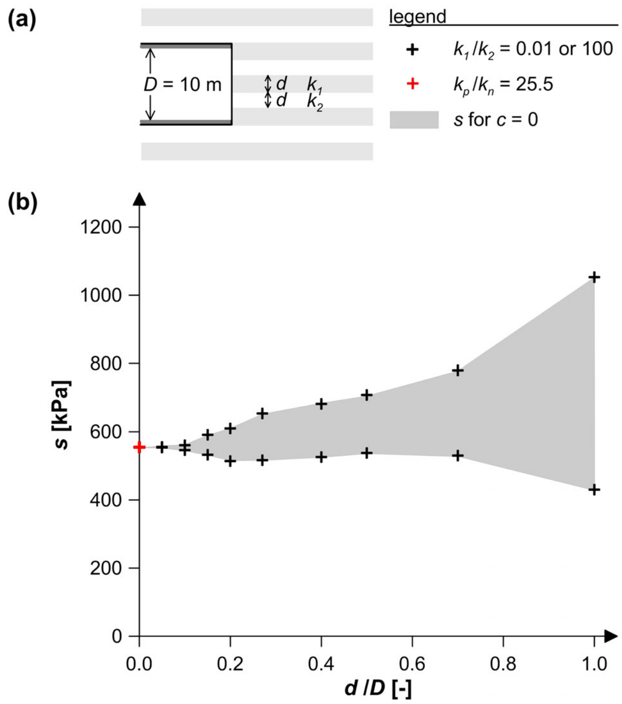

Figure 3.14 *(a) Multiple horizontal layers and (b) required support pressure s as a function of the layer thickness d in ground without any cohesion c (black: discretely modelled layers of permeability contrast k_1/k = 0.01 and 100; red: equivalent anisotropic model; other parameters according to Table 3.1)*

3.5.3.1 Without advance drainage measure

The required support pressure decreases with increasing degree of anisotropy (red in Fig. 3.15b). An increase of k_p/k_n from 1 to 10 (which corresponds to a permeability ratio of $k_1/k_2 = 38$ in a thin-layered ground) leads to a support pressure reduced by $\Delta s = 178$ kPa. However, the required support pressure is far above the feasible range of about 200 kPa (*cf*. Section 2.5.1). Yet in a ground of higher cohesion (*e.g.* $c = 250$ kPa; [62]), no face support would be required due to this moderate permeability anisotropy.

The favourable effect of permeability anisotropy is due to the pore pressure dissipating mainly in the lower permeable direction. Indeed, the hydraulic head above of the tunnel is higher than in the isotropic case (compare red lines in l.h.s. of Fig. 3.15c). But the seepage area of the tunnel face, perpendicular to the more permeable direction, favours the pore pressure relief ahead of the face (compare red lines in r.h.s. of Fig. 3.15c) and leads to lower support pressures.

3.5.3.2 With advance drainage boreholes

The support pressure for face stability slightly increases with increasing degree of anisotropy (blue in Fig. 3.15b). However, the increase is small ($\Delta s = 32$ kPa for an increase of k_p/k_n from 1 to 10) and the required support pressure is still remarkably lower than without boreholes (compare blue to red lines in Fig. 3.15b).

When considering anisotropic permeability, the hydraulic head above of the tunnel is higher than in the isotropic case (blue lines in l.h.s. of Fig. 3.15c). But compared to without drainage measure, trend reverses ahead of the tunnel, where the hydraulic head is also higher as the isotropic case (blue lines in r.h.s. of Fig. 3.15c). Due to the lower permeability in vertical direction, the horizontal seepage faces of the drainage boreholes are less efficient than in isotropic ground.

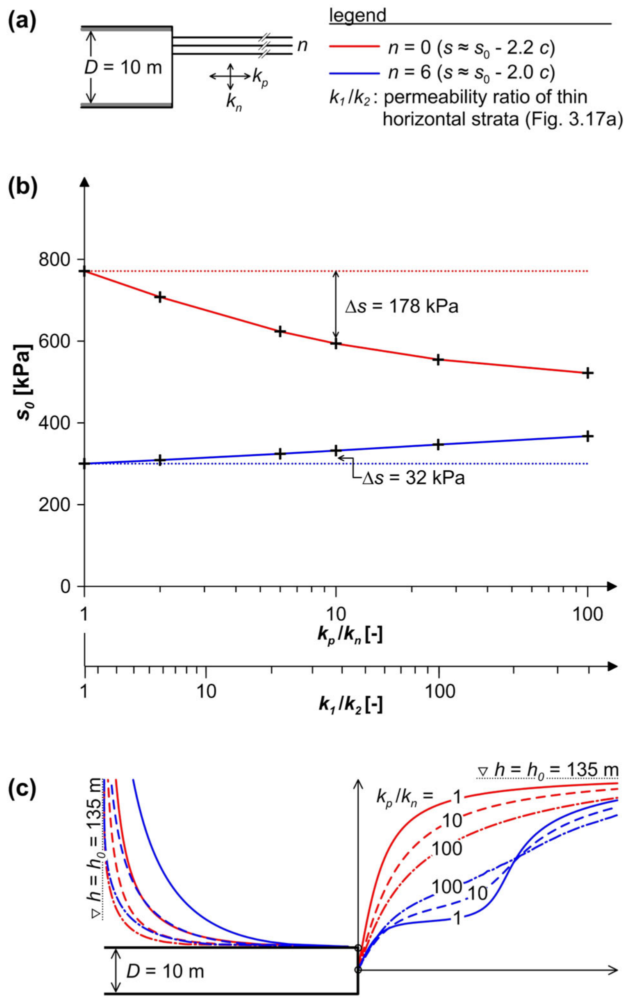

Figure 3.15 *(a) Permeability anisotropy of the equivalent homogeneous model representing very thin horizontal layers. (b) Required support pressure s as a function of the permeability ratio k_1/k_2 and the degree of anisotropy k_p/k_n at logarithmic scale in ground without any cohesion c and (c) belonging distribution of the hydraulic head h along two lines above and ahead of the tunnel face (blue: no drainage measure; red: six drainage boreholes; parameters according to Table 3.1)*

3.6 Tunnelling close to the vertical interface of an aquitard or an aquifer

Assume tunnelling close to a vertical permeability interface of an aquifer and an aquitard (Fig. 3.16a). Figure 3.16b evaluates the required support pressure s_0 as function of the distance of permeability-interface to tunnel face x_{If} in cohesionless ground. Again, the permeability contrast was taken equal to 100; the case of uniform permeability is added for comparison.

Without advance drainage, the required support pressure is highly sensitive to permeability heterogeneity if the tunnel face is close to the permeability-interface ($3 \geq x_{If}/D \geq -1$ for red line in Fig. 3.16b). Approaching an aquifer requires a distinctive higher support pressure (*e.g.* point A in Fig. 3.16b) than approaching an aquitard (point B in Fig. 3.16b). The maximum support pressure of 1.6 times the value required in homogeneous ground is necessary if the aquifer is very close the tunnel face ($x_{If}/D = 0.1$ in Fig. 3.16b).

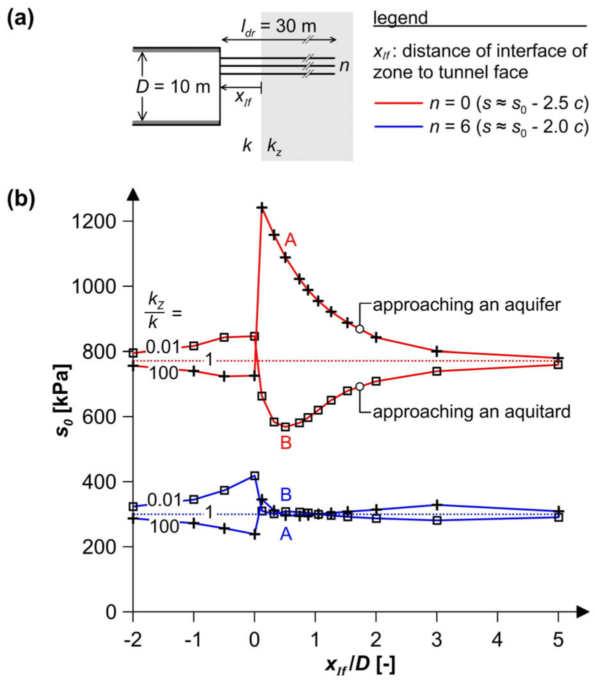

Figure 3.16 *(a) Two differently permeable zones with vertical interface and (b) required support pressure s_0 as a function of the distance x_{If} in ground without any cohesion c (permeability contrast k_z/k = 0.01, 1, 100; parameters according to Table 3.1)*

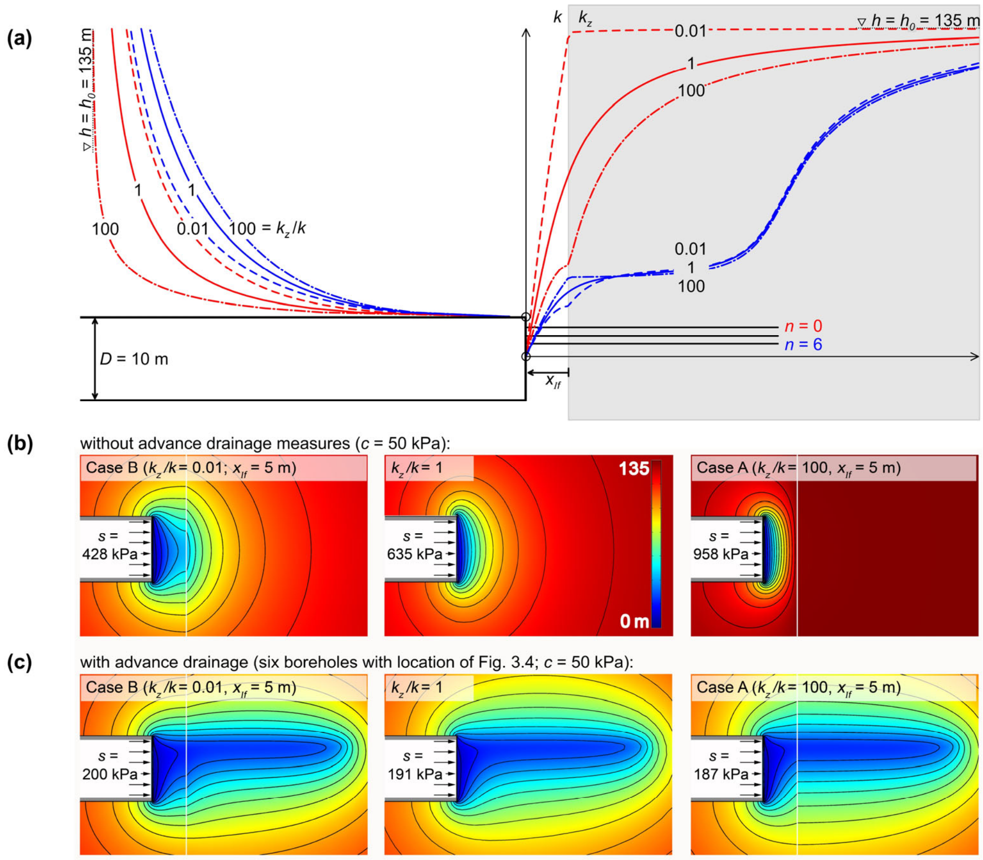

Figure 3.17 *(a) Distribution of the hydraulic head h along two lines above and ahead of the tunnel face for cases A and B of Figure 3.16. Belonging surface plots of the hydraulic head field as well as required support pressure s (b) without advance drainage measures and (c) with six axial drainage boreholes (c = 50 kPa, other parameters according to Table 3.1)*

Advance drainage boreholes reduce the sensitivity to variability of the ground remarkably (blue lines in Fig. 3.16b). The required support pressure is nearly the same as in homogeneous ground and has small peaks only when the interface is at or just behind the tunnel face ($0 \geq x_{If}/D \geq -1$).

The hydraulic head field of the potential critical situations indicated with A and B in Figure 3.16 are given in Figure 3.17. When the tunnel face without advance drainage gets close to an aquifer, the face itself is located within the lower permeable zone, where most of the pore pressure dissipates (case A in Fig. 3.17b). The hydraulic head at the interface of the two zones is virtually equal to the initial head (red dashed line in r.h.s. of Fig. 3.17a). This leads to unfavourable hydraulic gradients and a pronounced higher required support pressure than in homogeneous ground. The hydraulic head distribution is by far more favourable when the tunnel face gets close to an aquitard (case B in Fig. 3.17b), where the pore pressure dissipates mainly within the aquitard itself and the hydraulic head is lower above and particularly ahead of the tunnel face (compare dash-dotted with solid red lines in Fig. 3.17a).

Because the advance drainage boreholes pierce both zones of different permeability, they lead to a uniformly favourable hydraulic head field in vicinity of the tunnel face, independently of approaching and aquifer or an aquitard (Fig. 3.17c). The hydraulic head distribution both ahead and above the tunnel face is about the same for cases A and B or homogeneous ground (compare blue lines in Fig. 3.17a) and thus the required support pressure is hardly affected by permeability heterogeneity.

3.7 Entering a single vertical zone

3.7.1 Hydraulic head field

When entering a single vertical fault zone, the hydraulic head field depends on the zone thickness d_L, the ratio of permeability of zone to host rock k_L/k and on the drainage measures, especially on the length of the boreholes l_{dr} (Fig. 3.18a). The distribution of the hydraulic head is discussed in Figure 3.18, considering a representative example of entering a 10 m thick fault zone without drainage measures (red lines) and with six advance drainage boreholes of different length (blue lines in Fig. 3.18a).

3.7.1.1 Without advance drainage measures

As the head difference between the far field and tunnel face dissipates mainly within the less permeable zone, a low-permeability fault (red dashed line in Fig. 3.18a) “attracts” a higher head gradient than a high-permeability fault (red dash-dotted line in Fig. 3.18a). The narrower the lower-permeability zone, the higher the gradient and the more adverse will be the situation.

For the example a 10 m thick low-permeability zone ($k_L/k = 0.01$ in Fig. 3.18b), the average head gradient in the fault is by 30% higher than in homogenous ground (or in terms of required support pressure to 836 instead of 635 kPa; Fig. 3.18b). In case of the high-permeability zone ($k_L/k = 100$ in Fig. 3.18b), pore pressure relief takes places mainly ahead of the fault zone, the average gradient in the fault is by 40% lower than in homogenous ground and hence favourable in terms of support pressure (332 to 635 kPa in Fig. 3.18b).

3.7.1.2 With advance drainage boreholes

In case of a low-permeability zone (blue dashed lines in Fig. 3.18a), the drainage boreholes must reach at least 1-2 m in the rock behind the fault in order to reduce the water pressure acting on the zone. If they do not intersect the interface to the more permeable rock, they have nearly no effect (compare dark to light blue lines in Fig. 3.18a and l.h.s. of Fig. 3.18c to d and e).

In the case of a high-permeability zone (blue dash-dotted lines in Fig. 3.18a), the pore pressure dissipates mainly within the rock ahead of the fault. Therefore, the borehole length is less important (and partially superimposed by the drainage effect of the tunnel face). The boreholes should intersect the interface of the fault zone, but they do not offer any value for face stability if extending deeper into the surrounding (compare r.h.s. of Fig. 3.18c to d and e).

Note that even in homogeneous ground, a minimum drainage length (of about 1.5 times the tunnel diameter; compare central column of Fig. 3.18c to d and e; *cf.* Section 2.3.3.3) should be provided at any time in order to avoid face instabilities due to an insufficient shift of the maximum hydraulic gradients into the ground.

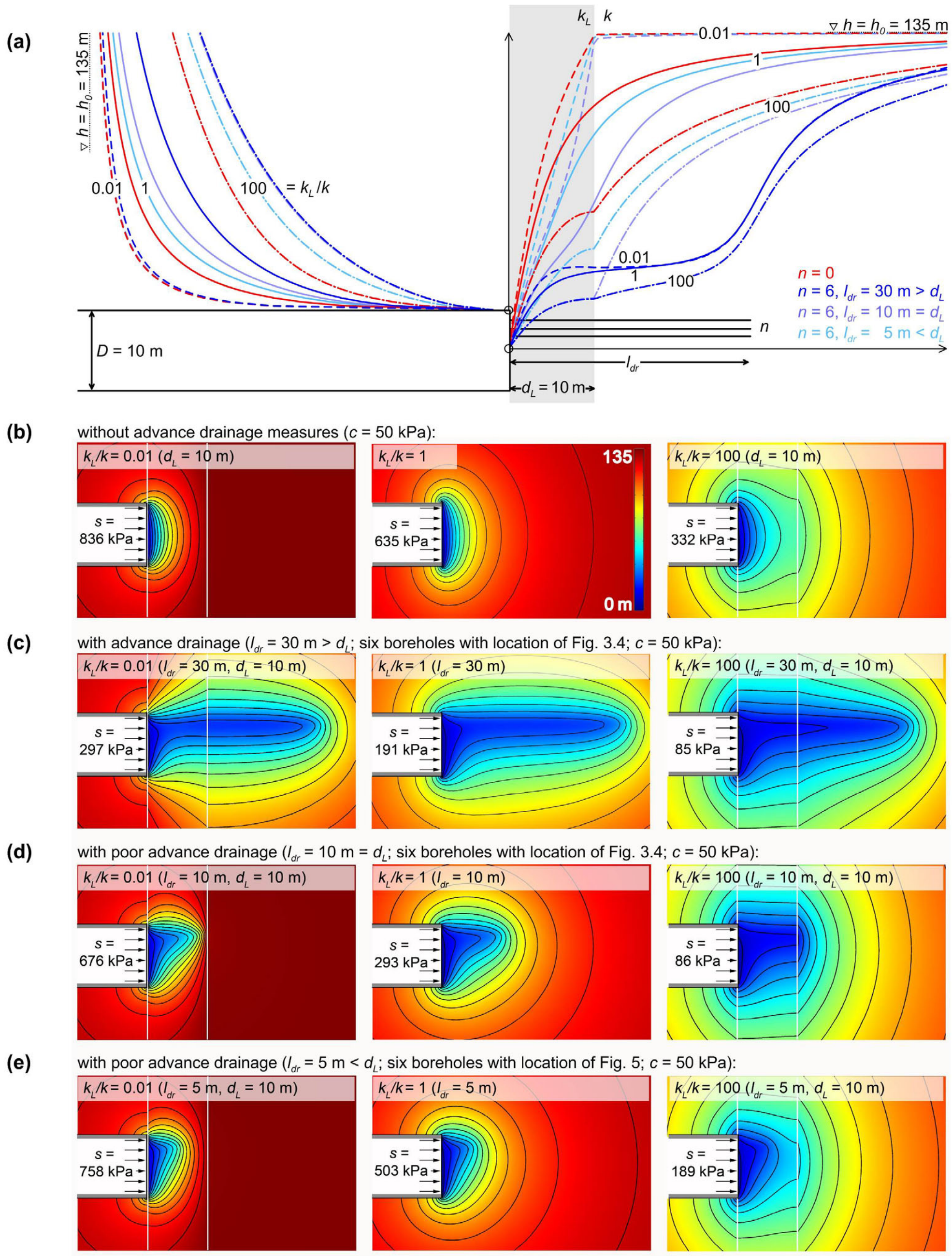

***Figure 3.18** (a) Distribution of the hydraulic head h along two lines above and ahead of the tunnel face when entering in a fault zone of different permeability. Belonging surface plots of the hydraulic head field as well as required support pressure s (b) without advance drainage measures; with six axial drainage boreholes of length (c) l_{dr} = 30 m; (d) l_{dr} = 10 m and (e) l_{dr} = 5 m (c = 50 kPa, other parameters according to Table 3.1)*

3.7.2 Support pressure

3.7.2.1 Unstable or stable neighbouring rock

In contrast to the previous sections, we investigate both cases of neighbouring stable and unstable rock when entering a vertical fault zone. Thus the stability conditions are different from those prevailing in homogeneous ground not only due to the anomaly of the hydraulic head distribution that is induced by the permeability variation, but also because the extent of the potentially unstable region ahead of the face might be limited by the thickness of the zone.

The effect of the thickness of the zone d_L is explained by means of Figure 3.19 showing the support pressure s needed in the reference case of homogeneously permeable ground ($c = 0$; other ground parameters see Table 3.1).

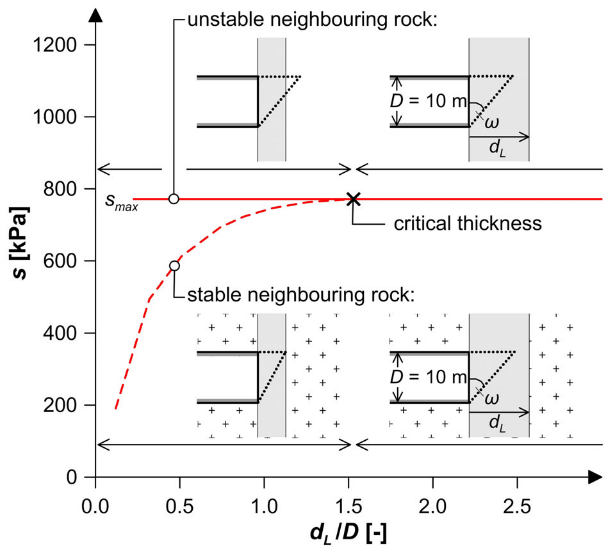

***Figure 3.19** Required support pressure s as a function of the vertical layer thickness d_L in ground without any cohesion c (homogeneous permeability; no drainage measure; other parameters according to Table 3.1)*

Unstable neighbouring rock

Entering a fine-grained fault zone in a highly fractured rock might be considered as homogeneous ground from mechanical point of view, as both rock and fault have the same ground parameters c, φ. The neighbouring rock is unstable and the failure angle ω can develop over both fault zone and rock (upper insets in Fig. 3.19). The required support pressure always reaches its maximum value s_{max} as both rock and fault zone fail (solid line in Fig. 3.19).

Stable neighbouring rock

Entering a fault surrounded by stable rock, the required support pressure for face stability is not only determined by the hydraulic head distribution, but also by the geometry of the fault (*e.g.* entering a brecciated fault zone in a competent, solid rock with different ground parameters c, φ; lower insets in Fig. 3.19). The wedge angle ω is limited by the thickness of the fault zone ($\omega \leq \arctan(d_L/D)$) and thus the support pressure cannot reach its maximum s_{max} (dotted line in Fig. 3.19). However this is true only if the fault zone is narrower than a critical thickness (indicated by the cross symbol in Fig. 3.19). For thicker zones, the thickness ceases to play a role and the support pressure reaches the maximum value s_{max}.

3.7.2.2 Parametric study

Figure 3.20 shows the results of a parametric study into the effects of permeability heterogeneity and stable or unstable neighbouring rock on the required face support s_0 when entering a single vertical zone of variable thickness d_L in cohesionless ground. The cases of unstable and stable neighbouring rock are plotted with solid and dashed lines, respectively. Four permeability ratios are considered (for better readability, the ratios $k_L/k = 0.1$ and 10 are plotted in light colour) in addition to the reference case of uniform permeability.

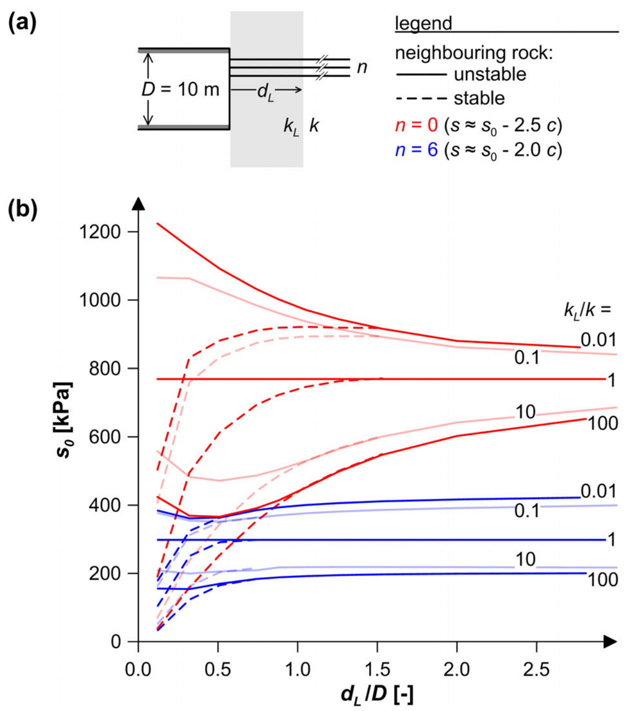

Figure 3.20 *(a) Parametric study of a single vertical layer of variable thickness. (b) Required support pressure s_0 as a function of the layer thickness d_L in ground without any cohesion c (permeability contrast k_L/k = 0.01-100; blue: no drainage measure; red: six drainage boreholes; parameters according to Table 3.1)*

Without drainage measure

The required support pressure is sensitive to permeability heterogeneity, but does not increase linearly with growing permeability ratio (compare red lines for $k_L/k = 1$ to $k_L/k = 0.1$ or 0.01 in Fig. 3.20b). Face support in large faults is similar to the one required in homogeneous ground (asymptotically converging curves for $d_L/D \geq 2.5$), but clearly different for low fault thicknesses $d_L/D < 1$-1.5.

In *unstable neighbouring rock* (solid red lines in Fig. 3.20b), all curves would start at the value of homogeneous ground for $d_L/D = 0$ (which is not pictured for the sake of simplicity), but then rapidly diverge. In a narrow low-permeability zone ($k_L/k < 1$), considerably higher support pressures than in homogeneous ground are required for face stability. The fault zone itself acts as a hydraulic barrier, within which unfavourable high hydraulic gradients develop. The gradients and thus the required support pressure decrease with increasing zone thickness. In case of a very narrow high-permeability zone ($k_L/k > 1$), high gradients develop immediately after the zone, but still within the potentially unstable wedge (which is *e.g.* $\omega = 65°$ for $d_L/D = 0.1$). At a fault thickness of about half the tunnel face ($d_L/D = 0.5$), the draining action of the tunnel face leads to a favourably reduced pore pressure distribution all-over the zone such as the support pressure decreases to a local minimum, before increasing again with increasing zone thickness.

In *stable neighbouring rock*, the support pressure for narrow faults is lower than for unstable rock due to the limited extent of failure (compare dashed to solid red lines in

Fig. 3.20b). In case of a low-permeability zone ($k_L/k < 1$), the support over the thickness exhibits a flat maximum due to the competing effects of permeability heterogeneity (the required support pressure decreases with increasing thickness) and geometry (the support increases with the thickness). In case of a high-permeability zone ($k_L/k > 1$), the support pressure is lower compared to homogeneous ground due to the favourable hydraulic head field.

With advance drainage boreholes

On account of the structural complexity of geological faults, permeability estimates are highly uncertain [84]. Figure 3.20b shows that advance drainage substantially reduces the sensitivity of the support pressure with respect to permeability contrasts: the differences between the five permeability cases are considerably smaller in the presence of drainage boreholes than they are without advance drainage (compare blue to red lines in Fig. 3.20b especially for narrow faults).

In *unstable neighbouring rock* (solid blue lines in Fig. 3.20b), the extrema observed when considering no drainage measure (solid red lines in Fig. 3.20b) disappear in the presence of advance drainage. Sufficiently long advance drainage boreholes eliminate especially the maxima predicted for low-permeability faults; because it uniformly relieves the pore pressure both in rock and fault zone (see also l.h.s. of Fig. 3.18c).

Also in *stable neighbouring rock* (dashed blue lines in Fig. 3.20b), less support pressure is required when considering zones of a thickness up to about one tunnel diameter. For thicker zones, the support pressures coincide with the ones required assuming unstable neighbouring rock.

3.7.3 Application example

The practical significance of these findings is discussed for an exemplary tunnel in a vertically stratified ground of uniform, very low cohesion (c = 50 kPa; other parameters see Table 3.1). The tunnel crosses 5 m tick layers oriented perpendicular to the tunnel axis (Fig. 3.21a). The permeability contrast of 100 leads to distinctively changing water inflows, but also to variable support pressure required to stabilize the tunnel face. The support pressure s when repeatedly crossing high- and low-permeability layers is shown in Figure 3.21b as a function of the position of the tunnel face x_f. Face stability considering no advance drainage measure is marked as red line; advance drainage with six axial boreholes in blue (borehole layout see Fig. 3.4).

Without drainage measure, face stability is highly sensitive to both permeability heterogeneity and location of the tunnel face within the layers. In conventional tunnelling, the tunnel face would collapse without an extremely heavy and practically unfeasible additional support. Entering a high-permeability zone requires lower support pressure than homogeneous ground (compare dotted to solid red line in Fig. 3.21b at x_f = 0). The closer the tunnel faces gets to the low-permeability layer ($0 \leq x_f \leq 5$ m), the more increases the support pressure. This is due to high hydraulic gradients developing in the upcoming low-permeability layer, which are still within the potentially unstable wedge (*cf.* Section 3.7.2.2). Due to the hydraulic barrier effect of the low-permeability zone, the highest support pressure is required immediately before leaving the low-permeability layer (1086 kPa at x_f = 8.75 m in Fig. 3.21b).

With advance drainage boreholes, the sensitivity to both permeability heterogeneity and location of the tunnel face within the layer is substantially reduced (blue solid line in Fig. 3.21b). The support pressure required within the high-permeability layer is lower than the one within the low-permeability layer, which is due to the preferential steeper hydraulic gradients within the aquitard. Overall, the support pressures required are within the feasible range of face bolting ($s \leq 200$ kPa) and thus prove feasibility of the tunnel example only by help of sufficiently long advance drainage boreholes.

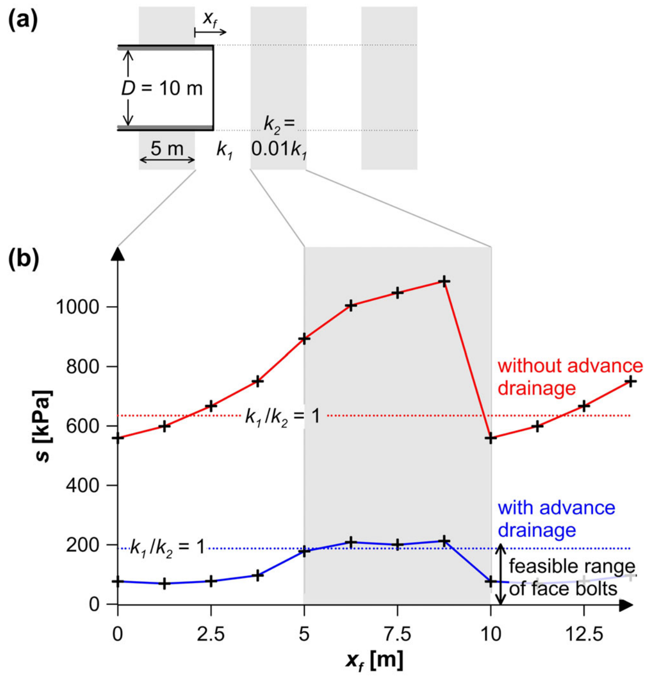

Figure 3.21 *(a) Longitudinal section of a tunnel crossing 5 m thick vertical layers of permeability contrast $k_1/k_2 = 100$. (b) Required support pressure s as a function of the position of the tunnel face x_f in ground of cohesion c = 50 kPa (blue: no drainage measure; red: six drainage boreholes; parameters according to Table 3.1)*

3.8 Thinly interbedded vertical aquifers and aquitards

3.8.1 Homogenisation to an equivalent anisotropic model

In cases where sedimentary deposits undergo intense folding, thin aquifers and aquitards might become vertical (Fig. 3.2d). As explained in Section 3.5.1, the ground consisting of sufficiently thin layers can be considered as homogeneous medium of orthotropic permeability. The equivalent permeability is then calculated according to Eqs. (3-1), (3-2) and the hydraulic head field of the equivalent anisotropic model is governed by the degree of anisotropy (Eq. (3-3)).

3.8.2 Maximum layer thickness

The maximum layer thickness for which homogenisation is possible is determined by Figure 3.22. It shows the required face support pressure s as a function of the normalized layer thickness d/D (c = 0, other ground parameters see Table 3.1). The support pressure[4] needed when considering stratified media consisting of discretely modelled layers are indicated as black crosses (inset in Fig. 3.22a); the equivalent anisotropic medium is shown in red.

The difference in required support pressure of each layer thickness (highlighted in grey in Fig. 3.22b) originates from a high- or a low-permeability layer immediately at the tunnel face. The thinner the discretely modelled strata, the smaller are the ranges and the higher are the resulting support pressures (barrier effect of a low-permeability layer close to the face, *cf.* Section 3.7.2.2). The required face support pressure when modelling discrete, thin layers of $d/D \leq 0.05$ (s = 1039 - 1144; Fig. 3.22b) is within 10% accuracy of the face

[4] Please note that the present study considers the failure mechanism of wedge and prism (Fig. 2.2), but does not consider potential failure of individual layers such as spalling or buckling.

support needed in an equivalent anisotropic medium (s = 1135 kPa). For thicker layers, the support pressure considering the equivalent anisotropic permeability model overestimates the face support needed.

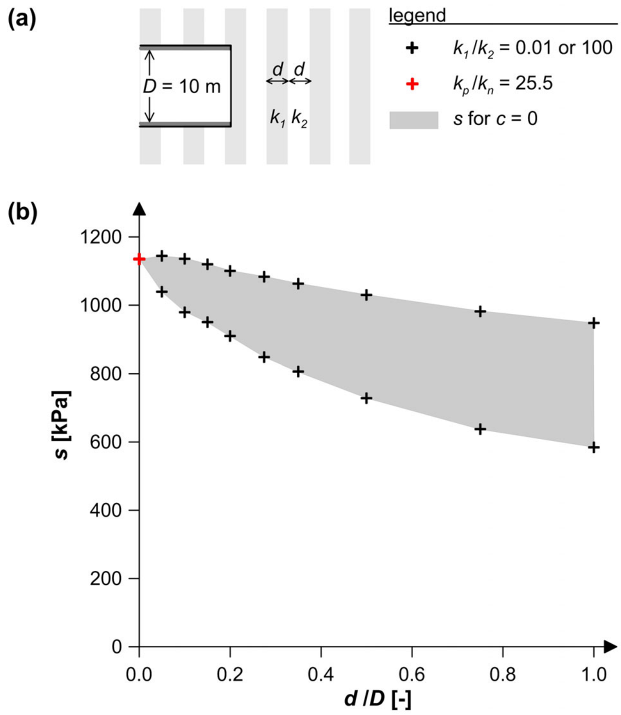

Figure 3.22 *(a) Multiple vertical layers and (b) required support pressure s as a function of the layer thickness d in ground without any cohesion c (black: discretely modelled layers of permeability contrast k_1/k = 0.01 and 100; red: equivalent anisotropic model; other parameters according to Table 3.1)*

3.8.3 Effect of permeability anisotropy

The effect of permeability anisotropy representing very thin vertical layers on face stability is discussed in Figure 3.23. Figure 3.23b shows the required support pressure s_0 as a function of the degree of anisotropy k_p/k_n (and the permeability ratio k_1/k_2) when assuming cohesionless ground. The solid red line applies to no advance drainage measures, the blue line to six axial advance drainage boreholes. The dotted lines indicate the support pressure required in isotropic ground. Figure 3.23c shows the belonging distribution of the hydraulic head h along two lines above and ahead of the tunnel face.

3.8.3.1 Without advance drainage measure

The required support pressure increases with increasing degree of anisotropy (red in Fig. 3.23b) and is overall far above the feasible range of about 200 kPa (Section 2.5.1). An increase of k_p/k_n from 1 to 10 (which corresponds to a permeability ratio of k_1/k_2 = 38 in a thin-layered strata) requires an additional support pressure of Δs = 295 kPa.

The hydraulic head distribution above of the face is unaffected of permeability anisotropy (compare red lines in l.h.s. of Fig. 3.23c). Ahead of the face, the open tunnel face reliefs pore pressure not as effective as in isotropic ground, because the seepage face is perpendicular to the lower permeable direction and high hydraulic gradients result (compare red lines in r.h.s. of Fig. 3.23c).

3.8.3.2 With advance drainage boreholes

The support pressure for face stability only marginally increases with increasing degree of anisotropy (blue; Δs = 29 kPa for an increase of k_p/k_n from 1 to 10 in Fig. 3.23b).

Again, the hydraulic head distribution above of the face is nearly unaffected of permeability anisotropy (compare blue lines in l.h.s. of Fig. 3.23c). Immediately ahead of the tunnel face, the drainage boreholes are not able to reduce the hydraulic head as effective as in isotropic ground (due to the diminished seepage action of the tunnel face). However, in some distance of the tunnel face, the drainage boreholes are even more effective than in isotropic ground due to their seepage faces being perpendicular to the more permeable direction (blue lines in r.h.s. of Fig. 3.23c).

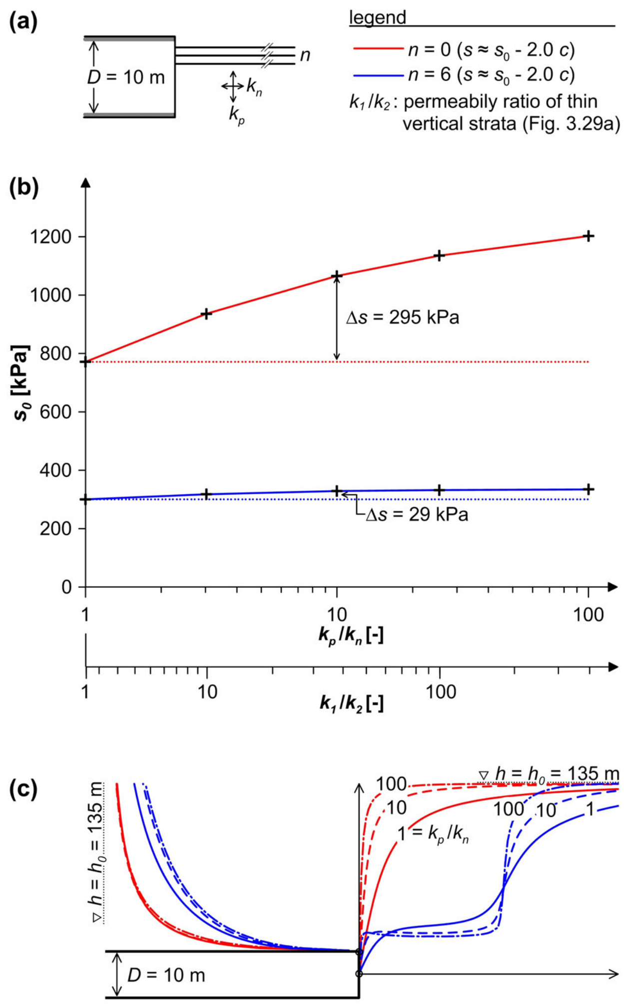

Figure 3.23 *(a) Permeability anisotropy of the equivalent homogeneous model representing very thin vertical layers. (b) Required support pressure s as a function of the permeability ratio k_1/k_2 and the degree of anisotropy k_p/k_n at logarithmic scale in ground without any cohesion c and (c) belonging distribution of the hydraulic head h along two lines above and ahead of the tunnel face (blue: no drainage measure; red: six drainage boreholes; parameters according to Table 3.1)*

3.9 Conclusions

In water-bearing ground of non-uniform permeability, the hydraulic head distribution is decisive for face stability. The head distribution depends on the permeability ratio of layer and surrounding rock; the orientation, elevation and thickness of the layer and the arrangement of the advance drainage boreholes.

Advance drainage boreholes may suffice to lower the pore water pressure such that both the risk of face instability and the sensitivity to permeability contrast is clearly reduced. Furthermore, the boreholes may serve as hydraulic exploration of the ground by capturing changes in water ingress at different borehole depth during drilling (of course protected against high water pressures by means of a so-called "preventer") and thus provides useful information about the permeability distribution of the upcoming ground.

When tunnelling in a ground containing *horizontal layer(s)*, less support pressure than in the reference case of homogeneous ground is required when a high-permeability layer intersects a seepage face and thus acts as natural advance drainage. Unfavourable are layers acting as a hydraulic barrier and thus hindering pore pressure relief above of the tunnel face (*e.g.* a low-permeability layer in the upper part of the tunnel face or a high-permeability layer above the tunnel roof, *i.e.* without connection to a seepage face). Six axial *advance drainage boreholes* in the upper part of the tunnel face reduce the required support pressures by about 60%. The arrangement of the boreholes should aim to reduce the pore pressure as widely as possible above and ahead of the tunnel face. This can be achieved by wisely arranging the boreholes such as they reach into the permeable rock above or below a low-permeability layer (*e.g.* by drilling two horizontal boreholes from a roof niche or by drilling them inclined from the tunnel face).

When tunnelling in a ground containing *vertical fault zone(s)*, less support pressure than in the reference case of homogeneous ground is required when encountering an aquifer connected to a seepage face (*i.e.*, the tunnel face or drainage boreholes; of course at the expense of potentially high water inflow). Highly unfavourable concerning face stability is a low-permeability zone at or around the tunnel face acting as hydraulic barrier and “attracting” high hydraulic gradients. Six axial *advance drainage boreholes* improve stability remarkably if the boreholes reach into the rock ahead of the fault zone. Moreover, by uniformly lowering the hydraulic head both in fault zone and surrounding ground, the risk of other possible failure mechanism such as punching decreases.

In case of adequately thin-layered ground relatively to the tunnel diameter ($d/D \leq 0.2$ for horizontal stratified ground, $d/D \leq 0.05$ for vertical strata), it is suitable to use an *equivalent homogeneous anisotropic model* for calculating the seepage flow condition. This is numerically faster than to model discretely layered ground and yet provides face-stability results of at least 10% accuracy to the equivalent anisotropic medium. Again, advance drainage boreholes reduce sensitivity to permeability heterogeneity clearly.

Permeability heterogeneity in ground may be *anthropogenic* when bearing in mind *e.g.* a sealing grouting body. In cases where the low-permeability grouting body comprises the entire potential failure volume around the tunnel face, a hydraulic head field comparable to homogeneous ground develops. But in cases where limiting accessibility render impossible executing a full grouting body, horizontal low-permeability layer(s) may results and unfavourable hydraulic head distributions might develop similarly to the ones discussed.

4 Effect of the capacity of drainage boreholes on tunnel face stability

4.1 Introduction

Chapter 4 focuses on the limited effectiveness of drainage measures with respect to face stability in cases where the drainage borehole walls do not to represent seepage faces under atmospheric pressure and studies: (i) the capacity of the drainage boreholes hindering full pressure relief in highly permeable ground under a high water table; and (ii) casings required for stabilizing the borehole, but which in turn restrict pore pressure relief to small openings (*cf*. Table 1.1).

The limited capacity of a drainage borehole may become significant in highly permeable ground and at great elevation of the water table. Large inflow may change the flow regime within the borehole from open-channel (free surface or gravity flow; Fig. 4.1b and 4.1c) to pipe flow (pressurized flow, Fig. 4.1a). The pressure developing within the borehole results in reduced pore pressure relief in the surrounding ground. Literature about the limited capacity of advance drainage boreholes is very scanty and to the author's knowledge there are only Hong *et al.* [52] who calculated for a simplified example the maximum borehole length which provides full pipe flow capacity (but without reference to face stability). Much more attention was paid to hydraulic capacity of boreholes in related fields such as Karst, well or petroleum engineering, but mainly focusing on large scale. Reference here is restricted to works, supporting the author's approach described in Section 4.2.2, where it was shown that turbulent flow hydraulics formulae are appropriate for approximating flow in Karst conduits (*e.g.* [89], [90], [91]) and where the suitability of equivalent permeability models for considering pipe flow was shown: Halford [92] simulated laminar and turbulent flow in and towards a well by considering an "equivalent hydraulic conductivity" which depends on the Reynolds number and – for turbulent flow – on the pipe friction factors. Shoemaker *et al.* [93], [94] slightly modified the turbulent equivalent hydraulic conductivity in order only to depend

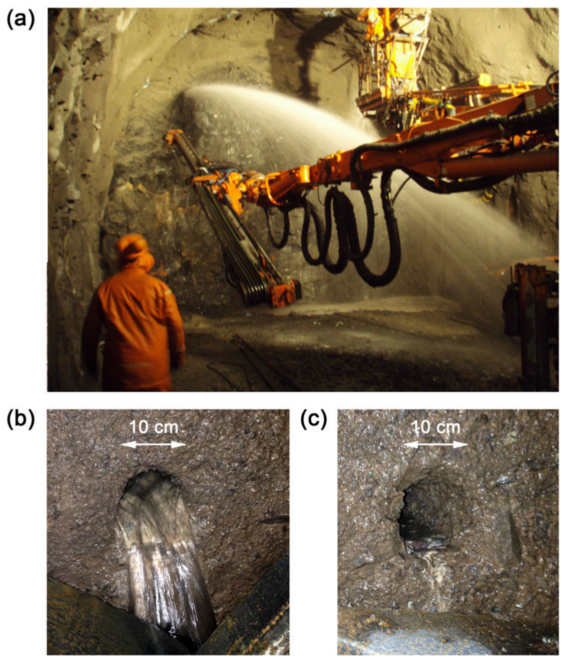

Figure 4.1 *(a) Pressurized flow from a borehole during construction of Olafsfjödur street tunnel, Island (courtesy of Karl Gunnar Holter) and outflow of drainage borehole of (b) discharge of about 0.25 m^3/h and (c) dripping only (Lake Mead Intake No. 3)*

on the Reynolds-Number (but not on pipe friction data) and pointed out the importance of considering turbulent flow when modelling preferential groundwater flow layers. Birch *et al.* [95] assigned "values of an equivalent hydraulic conductivity along the length of the well screen that would simulate the head losses associated with pipe flow" for simulating flow rates in horizontal wells. Chen *et al.* [96] focused on a single horizontal well, where an equivalent hydraulic conductivity represented laminar and turbulent flow, and found good agreement of his laboratory study with the numerical findings. Wang and Zhang [97] continued numerical investigations similar to Chen *et al.* [96], but with a slightly different coefficient of friction and Li *et al.* [98] applied the same approach to an example of drain pipes below a concrete channel. Section 4.2 investigates an equivalent permeability model considering pipe- and open-channel flow equations for determining the hydraulic capacity of drainage boreholes and revolves around the following leading questions: How does tunnel face stability change when the limited flow capacity of the drainage boreholes is considered? What is the maximum permeability of the ground for which it is safe to assume a seepage face at the borehole wall?

Drainage effectiveness may also be limited by *borehole casings* becoming necessary when the borehole walls are unstable. These casings typically restrict the passage of water to small openings and therefore impede pore pressure relief around the boreholes, which in turn reduces the effectiveness of the drainage measure with respect to face stability (Section 4.3).

4.2 Flow capacity of the drainage boreholes

4.2.1 Introduction

The goal of this Section is to investigate face stability taking account of the effect of the limited flow capacity of the boreholes on the pore pressure relief. The detailed flow regime within the borehole can be neglected, as focus is on pore pressure relief in the surrounding ground. Instead, considering *averaged coaxial flow velocities* within the borehole at *steady state* is sufficient (no need for computational fluid dynamics, CFD). This reduces the complexity considerably and allows making use of empirical equations of pipe flow and open-channel flow hydraulics.

Section 4.2.2 shows how the pipe and open-channel flow within the boreholes can be considered as flow through a porous medium of equivalent permeability (also known as "equivalent hydraulic conductivity"; here used interchangeably). Section 4.2.3 considers the simplest possible borehole-ground seepage flow interaction problem (a single drainage borehole) and presents some characteristic results on the effect of ground permeability, initial water head and surface roughness of the single borehole. Section 4.2.4 quantifies the reduced drainage effectiveness with respect to tunnel face stability considering a common advance drainage layout (six axial boreholes drilled from the face) and discusses the applicability of the design nomograms (Chapter 2).

4.2.2 Equivalent permeability

4.2.2.1 Borehole with pressurized pipe flow

Drainage boreholes are straight pipes of circular cross-section. Within the pipe, laminar or turbulent flow develops, depending on the Reynolds number

$$\mathrm{Re} = \frac{v_x \cdot d_{dr}}{\upsilon} \tag{4-1}$$

relating the product of pipe diameter d_{dr} and axial flow velocity v_x (averaged over the pipe cross-section) to the kinematic viscosity of the water υ. Laminar flow usually evolves in small diameter pipes and for low flow velocities ($\mathrm{Re} < 2300$). For higher Reynolds numbers, first transitional then fully turbulent flow develops. Considering a typical borehole diameter of $d_{dr} = 0.1$ m and the kinematic viscosity of water ($\upsilon = 1.307 \cdot 10^{-6}$ m^2/s at 10°C), turbulent flow develops already for flow velocities v_x superior to about 0.03 m/s. These flow velocities are easily reached within drainage pipes, even in low permeable ground [62]. Therefore, turbulent flow only is considered below.

In a drainage borehole, water inflow takes place along its entire shell surface. Here we consider the borehole as a pipe consisting of sequential segments, each of section length Δx, and assume inflow taking place only at the connection points (*i.e*. the nodes).

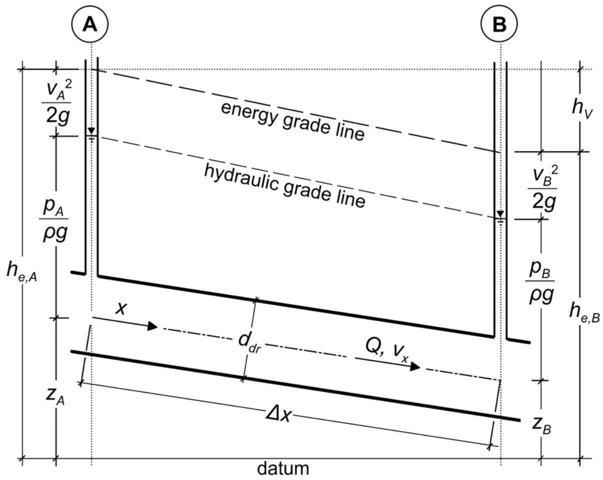

Figure 4.2 *Pipe flow*

The flow in a completely filled (pressure) pipe of section length Δx and of constant diameter d_{dr} is assumed as incompressible, steady and turbulent between locations *A,B* (Fig. 4.2; for detailed derivation see Zingg [62]). According to the conservation of energy, energy head at point *A* ($h_{e,A}$) has to be equal to the sum of stored energy at point *B* ($h_{e,B}$) and the head loss h_V due to friction. For constant drainage pipe diameter and taking account of the empirical equation of head loss according to Darcy-Weisbach and the empirical friction coefficient as suggested by Colebrook-White [99], we obtain the averaged flow formula for turbulent pipe flow

$$v_x = -K_x I_x \quad , \tag{4-2}$$

with

$$K_x = K_{x,pipe} = 2 \cdot \log_{10}\left(\frac{2.51\upsilon}{d_{dr} \cdot \sqrt{2g \cdot d_{dr} \cdot I_x}} + \frac{k_{s,eq}}{3.71 d_{dr}} \right) \sqrt{\frac{2g \cdot d_{dr}}{I_x}} \quad . \tag{4-3}$$

Eq. (4-2) is formally the same as a non-linear Darcy's law. This allows modelling the pipe as an equivalent porous medium with head gradient-dependent hydraulic conductivity $K_{x,pipe}$.

The equivalent sand roughness $k_{s,eq}$ quantifies roughness and texture of the borehole wall and amounts from $k_{s,eq} = 15$ mm (rock excavation; "hydraulically very rough") to 5 mm (smooth rock excavation or highly incrusted steel pipe; "hydraulically rough") and for comparison to 0.05 mm (a surface smooth as a newly rolled steel pipe; "hydraulically smooth"; [100]).

4.2.2.2 Borehole with open-channel flow

Open-channel flow must be considered if a borehole is not filled completely, because friction develops only along the contact surface between pipe wall and fluid. Comparison of the results considering pipe- and open-channel flow to the results taking account of pipe-flow only shows that the latter is sufficiently accurate for the purpose of investigating face stability (*cf.* Zingg [62]). Therefore, the flow in the boreholes is considered as seepage flow in an equivalent porous medium obeying a non-linear Darcy law (Eq. (4-2)). The non-linearity is due to the dependency of the equivalent permeability K_x on the head gradient I_x (Eq. (4-3)).

For $I_x = 0$, the permeability according to Eq. (4-3) becomes infinite, but this is irrelevant as there is no seepage flow in this case. To avoid division by zero, an arbitrary value (*e.g.* $K_x = 100$ m/s) can be assigned to the permeability if $I_x = 0$.

4.2.2.3 Transverse permeability

Equation (4-2) describes flow as seepage flow through an equivalent porous medium in the axial pipe direction only. In the absence of ground - pipe interaction it would be sufficient to model the boreholes by linear (one-dimensional) elements. Seepage flow in the ground around the boreholes (and water discharge into the boreholes) depends however on the borehole radius. Therefore the boreholes have to be modelled as three-dimensional objects (Fig. 4.3a), which necessitates an assumption about the permeability of the equivalent porous medium in the plane of the borehole cross-section (*i.e.* perpendicular to the borehole axis). The transverse permeability is taken here 100 times higher than the ground permeability K_g, ensuring a uniform pressure distribution in the cross-section plane of the borehole. Comparative computations showed that this assumption is not essential. Consider for example the numerical results of Figure 4.3, which were obtained taking the transverse permeability either equal to the ground permeability K_g, or 100 times higher than K_g: in both cases, the velocity distribution is approximately uniform over the borehole cross-section; the hydraulic head field in the ground around the borehole does not depend on the transverse permeability.

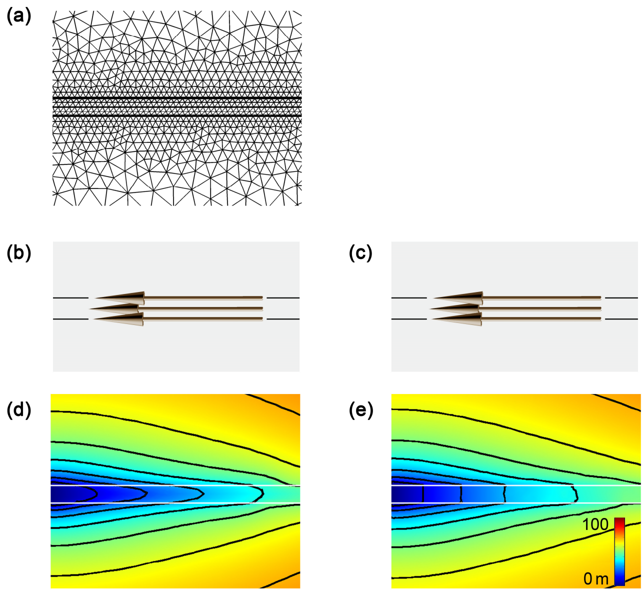

Figure 4.3 *(a) Spatial discretization of borehole and surrounding ground. Seepage flow velocity vectors inside the borehole for transverse permeability (b) equal to K_g and (c) equal to 100 K_g. Hydraulic head field for transverse permeability (d) equal to K_g and (e) equal to 100 K_g*

4.2.3 Ground - single drainage borehole interaction

First, the simplest problem of a single drainage borehole is considered in order to capture the leading factors of the interaction of seepage flow in both borehole and ground.

4.2.3.1 Computational model

A single, 30 m long, 0.1 m diameter drainage borehole is considered (Fig. 4.4). The seepage flow domain extends up to the 100 m ahead and around the borehole. The hydraulic head at the far-field boundaries is taken equal to the initial hydraulic head h_0. The outlet of the drainage borehole represents the only seepage face under atmospheric pressure. The interior of the borehole is modelled as an equivalent porous medium (Section 4.2.2). The ground is considered as isotropic porous medium obeying Darcy's law with the permeability K_g. Table 4.1 summarizes the assumed parameters.

Note that in highly permeable ground well below the water table, turbulent flow conditions may prevail even in the ground itself: during construction of Intake No. 3 at Lake Mead, 3.7 m^3/s water discharge was measured collected from a seepage area of about 360 m^2 [78]. The average inflow velocity of 0.01 m/s indicates clearly turbulent seepage flow within the pores of the ground (turbulent flow for $\mathrm{Re} > 1$). However, assuming Darcy's law is an assumption on the safe side for flow in highly permeable ground, because the linear increase of filter velocity with hydraulic gradient overestimates both filter velocity and water inflow into the boreholes.

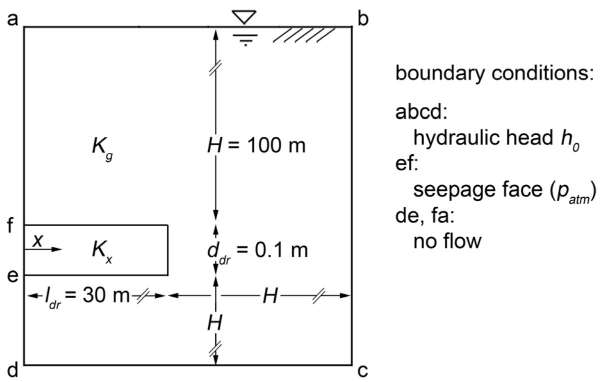

Figure 4.4 *Problem setup for the comparative analysis of a single drainage borehole*

Table 4.1 *Parameters for the comparative analyses of the ground - single drainage borehole interaction*

Problem layout		
Depth of cover	H	100 m
Initial hydraulic head	h_0	50, 100, 200 m
Borehole diameter	d_{dr}	0.1 m
Borehole length	l_{dr}	30 m
Ground		
Permeability	K_g	10^{-7}-10^{-3} m/s
Borehole		
Equivalent permeability	K_x	Eq. (4-3)
Kinematic viscosity water	υ	$1.307 \cdot 10^{-6}$ m^2/s
Equivalent sand roughness	$k_{s,eq}$	0.05-15 mm

4.2.3.2 Characteristic results

Figures 4.5a and b show the pressure p (normalized by the initial pressure p_0) along the borehole axis x and the hydraulic head field, respectively, for several values of ground permeability K_g. The numerical results were validated by comparison with an approximated analytical solution in Zingg [62].

In a highly permeable ground ($K_g \geq 1 \cdot 10^{-4}$ m/s), pore pressure relief is limited to the vicinity of the outlet. The length of the borehole becomes irrelevant as it is not able to induce any pressure reduction deep into the ground (compare head fields of $K_g \leq 1 \cdot 10^{-4}$ to $K_g > 1 \cdot 10^{-4}$ in Fig. 4.5b). In moderately permeable ground, advance drainage reduces the pressure to less than 10% of its initial value along the borehole axis x as well as in its vicinity ($K_g = 1 \cdot 10^{-5}$ m/s in Fig. 4.5). For lower permeability, the drainage borehole lowers the initial pressure to nearly zero ($p/p_0 \leq 0.003$ for $K_g \leq 1 \cdot 10^{-6}$ m/s in Fig. 4.5).

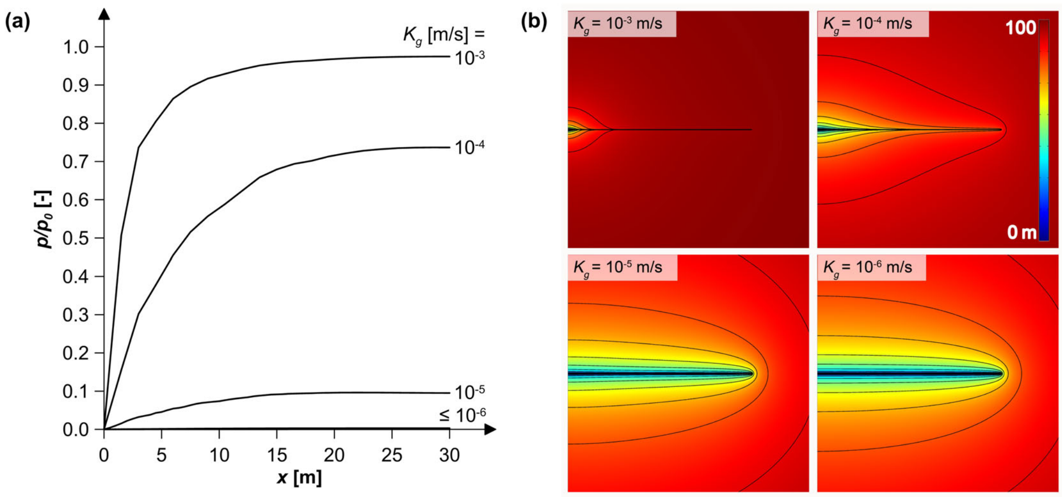

Figure 4.5 *(a) Pressure p normalized by the initial pressure p_0 along the borehole axis x and (b) the belonging hydraulic head fields for selected ground conductivity K_g ($k_{s,eq}$ = 5 mm, h_0 = 100 m, other parameters according to Table 4.1)*

The higher the initial head h_0, the higher is the pressure p developing in the borehole (Fig. 4.6). In highly permeable ground solely pipe-flow develops (Fig. 4.6a; markers added for orientation indicating the averaged pressure of a just filled borehole). At lower ground permeability, however, the section of open-channel flow increases with decreasing initial head (Fig. 4.6b).

The roughness of the borehole walls is captured by the value of equivalent sand roughness $k_{s,eq}$. Figure 4.7 shows the pressure distribution along the borehole axis for rough ($k_{s,eq}$ = 5-15 mm; "hydraulically rough behaviour") and smooth borehole walls ($k_{s,eq}$ = 0.05 mm; "hydraulically smooth behaviour"). The latter is plotted for comparative purposes only, because such smooth surfaces are achievable only by using borehole casings, which however reduce inflow remarkably (*cf.* Section 4.3). The rougher the borehole wall (*i.e.* the higher $k_{s,eq}$), the higher is the pressure developing within the borehole. However, the effect of surface roughness is of secondary importance compared to that of the ground permeability (compare pressure distributions for $k_{s,eq}$ = 5 mm to $k_{s,eq}$ = 15 mm in both Fig. 4.7a,b).

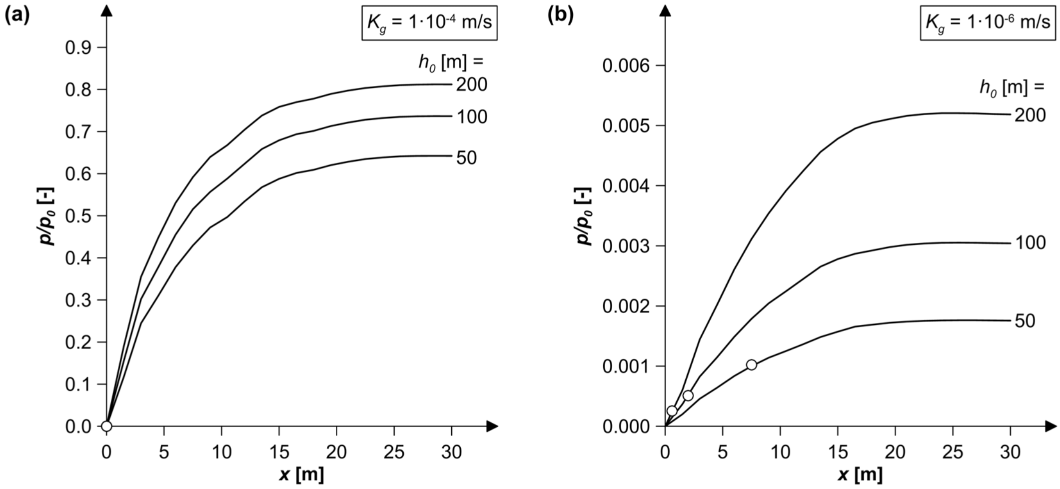

Figure 4.6 *Pressure p normalized by the initial pressure p_0 along the borehole axis x for variable initial hydraulic head h_0 in (a) highly permeable and (b) medium permeable ground with markers indicating the transition point from open-channel to pipe flow ($k_{s,eq}$ = 5 mm, other parameters according to Table 4.1)*

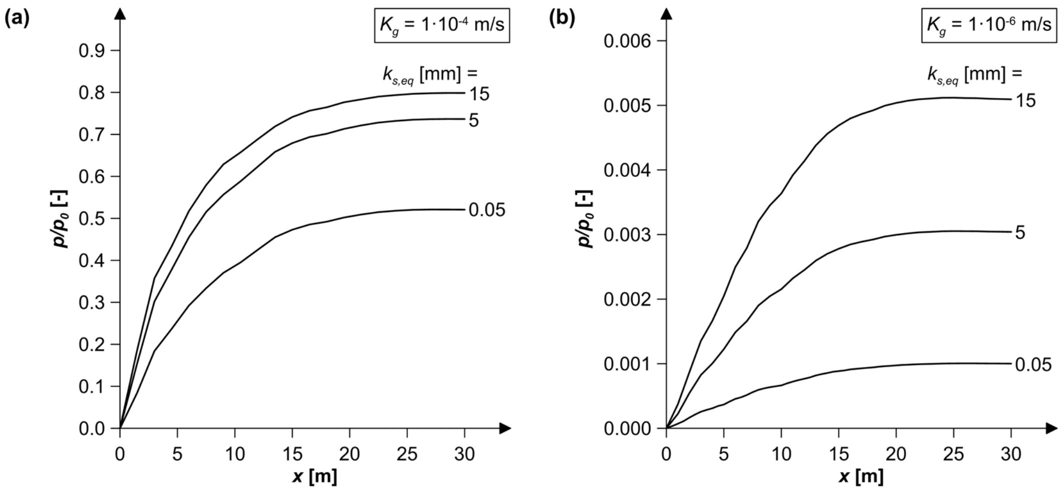

Figure 4.7 *Pressure p normalized by the initial pressure p_0 along the borehole axis x for variable surface roughness $k_{s,eq}$ of the borehole in (a) highly permeable and (b) medium permeable ground (h_0 = 100 m, other parameters according to Table 4.1)*

Figure 4.8 shows the water discharge Q from the borehole as a function of the permeability of the ground K_g in a double logarithmic scale. At low permeabilities, where the water inflows to the borehole are so small that pressure in the borehole is practically atmospheric, Q increases linearly with K_g. At high K_g, pressure develops within the borehole and therefore Q increases sub-linearly with K_g. Discharge is lower than when assuming sufficient drainage capacity (*i.e.* atmospheric boundary condition prevailing at the borehole wall; dotted in Fig. 4.8).

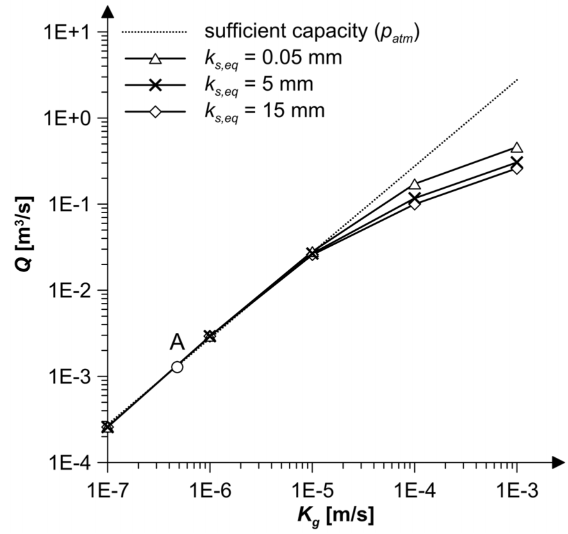

Figure 4.8 *Discharge Q from a single borehole as a function of the permeability of the ground K_g for variable borehole surface roughness $k_{s,eq}$ (h_0 = 100 m, other parameters according to Table 4.1)*

4.2.4 Face stability

4.2.4.1 Computational model

Face stability is analysed for a tunnel example considering six axial drainage boreholes drilled from the face (Fig. 4.9; limit equilibrium model described in Section 2.2). The numerical model contains the boreholes as porous material of equivalent permeability according to Eq. (4-3); the permeability orthogonal to the borehole axis is taken 100 times higher than that of the ground K_g. The tunnel lining is considered as waterproof up to the face (no-flow boundary condition); the tunnel face including the borehole outlets are considered as seepage faces (atmospheric pressure). The water table is assumed to remain constant in spite of the drainage action of the tunnel (no drawdown). Table 4.2 summarizes the parameters assumed for the seepage flow and limit equilibrium analyses.

4.2.4.2 Characteristic results

The impact of the hydraulic capacity of the boreholes on the face support pressure that is needed for stability is shown in Figure 4.10. The range of face support pressures that would be needed if pressure develops inside the boreholes is bounded by the two borderline cases of, (i) no drainage boreholes at all, *i.e.* pore pressure relief only due to the natural drainage action of the tunnel face; and, (ii) boreholes of sufficient capacity, *i.e.* the borehole wall is under atmospheric pressure (marked by triangles and crosses in Fig. 4.10).

Figure 4.10a shows the support pressure s required for face stability in a cohesionless ground as a function of the wedge angle ω for several ground permeabilities K_g. In ground of high ground permeability, considerably more support pressure is required (s = 702 vs. 300 kPa for $K_g = 1 \cdot 10^{-3}$ vs. $K_g \leq 1 \cdot 10^{-5}$ m/s) and the unstable region is extended (critical angle ω_{cr} = 62° vs. 35°). In medium or low permeability ground ($K_g \leq 1 \cdot 10^{-5}$ m/s), the necessary support pressure is identical to that obtained assuming that the borehole walls represent seepage faces. Figure 4.10b shows that this is also true for higher ground cohesion c.

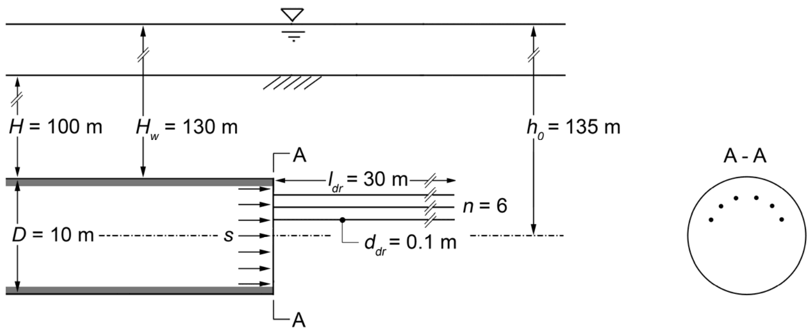

Figure 4.9 *Problem setup for the comparative analysis of the tunnel example*

Table 4.2 *Parameters for the comparative analyses of the hydraulic capacity in the tunnel example*

Problem layout		
Depth of cover	H	100 m
Elevation of water table	H_w	130 m
Tunnel diameter	D	10 m
Ground		
Effective cohesion	c	0-300 kPa
Angle of eff. internal friction	φ	30°
Submerged unit weight	γ'	12 kN/m^3
Unit weight water	γ_w	10 kN/m^3
Permeability	K_g	10^{-7}-10^{-3} m/s
Shear resistance of the vertical slip surfaces		
Coeff. of lateral stress wedge	λ_w	0.5
Coeff. of lateral stress prism	λ_p	1.0
Drainage boreholes		
Diameter	d_{dr}	0.1 m
Length	l_{dr}	30 m
Number	n	0, 6
Equivalent permeability	K_x	Eq. (4-3)
Kinematic viscosity water	υ	$1.307\cdot10^{-6}$ m^2/s
Equivalent sand roughness	$k_{s,eq}$	0.05-15 mm

Figure 4.10c shows the relationship between discharge Q and ground permeability K_g in a double logarithmic scale. The solid lines indicate the discharge when considering the hydraulic capacity; the dotted line is added for orientation and indicates the total discharge when assuming sufficient capacity in the boreholes. Up to a permeability of $K_g = 1\cdot10^{-5}$ m/s, most of the discharge accumulates from the drainage boreholes (ratio $Q_{dr}/Q_{tot} \approx 70\%$ in Fig. 4.10c, where "Q_{tot}" denotes the total discharge and "Q_{dr}" indicates the sum of discharge of all six drainage boreholes). For higher ground permeability, the effectiveness of the drainage boreholes with respect to pore pressure relief decreases, which results in less discharge from the boreholes. In extremely permeable ground ($K_g = 1\cdot10^{-3}$ m/s), inflow from the boreholes is only 23% of the total inflow, while large discharge from the tunnel face is predicted ($Q_{face} = 3.3$ m^3/s in Fig. 4.10c; keeping in mind the possible overestimation of Q_{face} due the assumption of laminar flow in the ground may, *cf.* Section 4.2.3.1). In conventional tunnelling practice, such a large discharge is probably too high and additional sealing measures such as grouting would be required. The latter would reduce ground permeability and thus result in lower borehole pressures or even change in the flow regime within the boreholes.

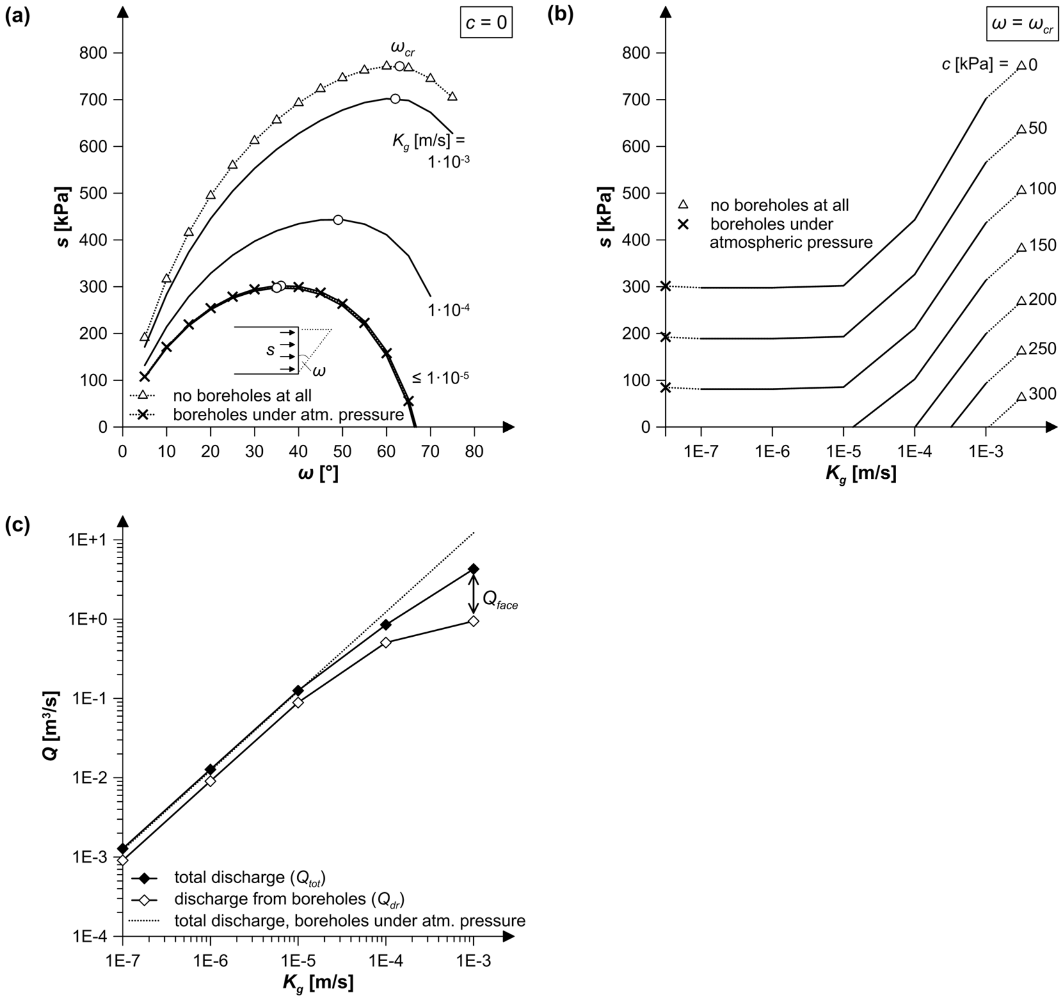

***Figure 4.10** Face stability and water discharge of the tunnel example ($k_{s,eq}$ = 5 mm, other parameters according to Table 4.2): (a) required support pressure s as a function of failure angle ω and (b) as a function of the permeability of the ground K_g; (c) water discharge Q as a function of the permeability of the ground K_g on a logarithmic scale*

4.2.4.3 Applicability of nomograms

Chapter 2 provides nomograms for calculating the required support pressure under the assumption of sufficient capacity of the drainage boreholes. Question arises about the applicability of these nomograms in the case of pressure developing in the drainage boreholes.

Figure 4.11 shows the required support pressure s considering hydraulic capacity as a ratio of the support pressure according to the nomograms s_{nomo}, plotted as a function of the ground permeability K_g for our tunnel example. Several values of roughness of the borehole wall $k_{s,eq}$ (Fig. 4.11a), of the ground cohesion c (Fig. 4.11b), of the elevation of water table H_w (Fig. 4.11c) and of the drainage borehole length l_{dr} (Fig. 4.11d) were considered. Overall for $K_g \leq 1 \cdot 10^{-5}$ m/s, the same face support is needed as when assuming sufficient hydraulic capacity in the boreholes. But in extremely permeable ground ($K_g = 1 \cdot 10^{-3}$ m/s), the hydraulic capacity of the boreholes limits their effectiveness considerably. The deviation in support pressure slightly increases with the roughness of the borehole walls (Fig. 4.11a). Crucial is though the deviation in support pressure for increasing ground cohesion: in ground with $c = 100$ kPa is five times more support required ($K_g = 1 \cdot 10^{-3}$ m/s in Fig. 4.11b). In ground of even higher cohesion, there is no additional face support necessary according to the nomograms (thus it is not any more possible to determine a ratio s/s_{nomo}), but considering hydraulic capacity results in a considerable support pressure (*e.g.* about 300 kPa for $c = 150$ kPa in Fig. 4.10b). On the other hand, the deviation in support pressure with increasing elevation of the initial water table (Fig. 4.11c) as well as with increasing borehole length (Fig. 4.11d) is of secondary importance.

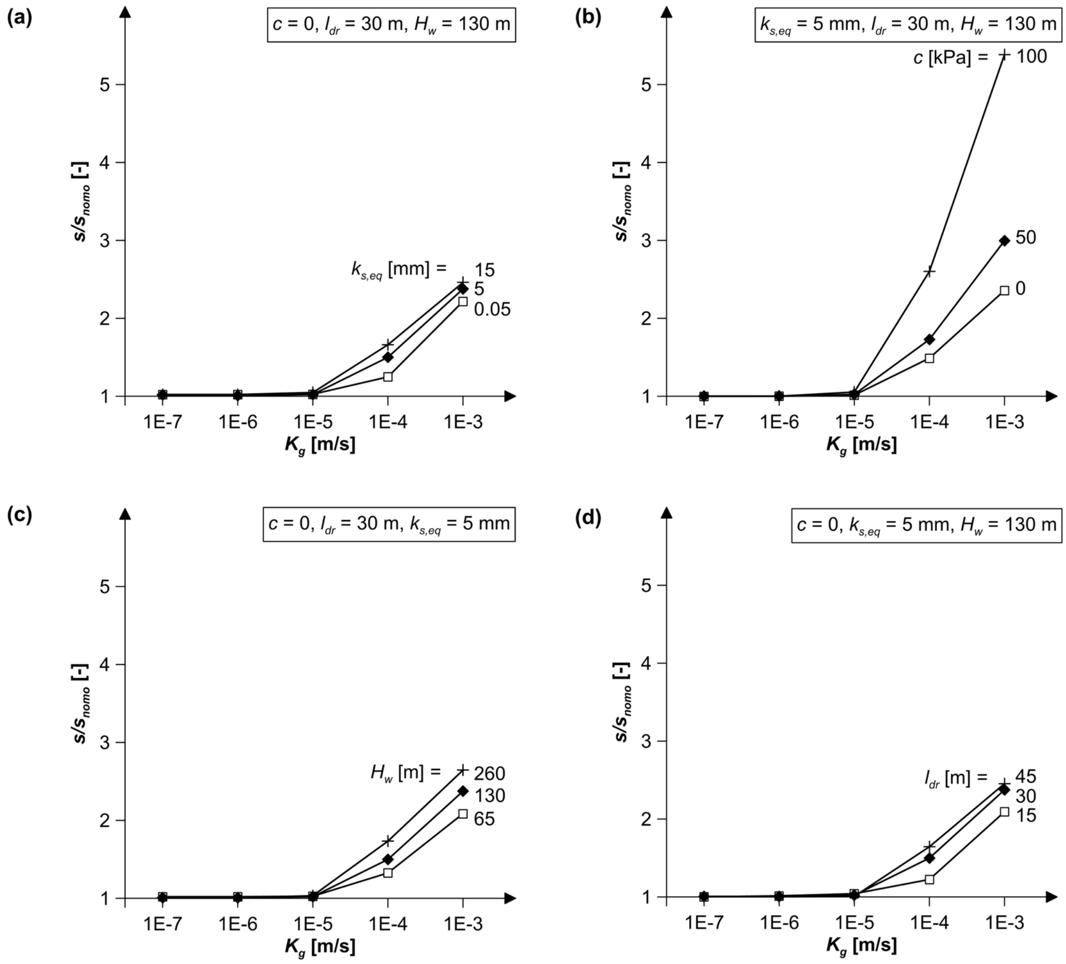

Figure 4.11 *Required support pressure s normalized by the support pressure according to the nomograms s_{nomo} as a function of the permeability of the ground K_g for (a) variable surface roughness $k_{s,eq}$ of the borehole, (b) ground cohesion c, (c) elevation in water table H_w and (d) borehole length l_{dr} (other parameters according to Table 4.2)*

In order to make a reasonably conservative statement about the applicability range of the nomograms in a more universal way, Zingg [62] derived for small admissible hydraulic gradients i_{adm} the following relationship for the admissible ground permeability:

$$K_g = n\left(i_{adm}\frac{gD}{8}\right)^{0.5}\left(\frac{l_{dr}}{D}\right)^{-1}\left(\frac{d_{dr}}{D}\right)^{2.5}\left(\frac{h_0}{D}\right)^{-1}\ln\frac{2h_0}{D}\log_{10}\frac{3.71\,d_{dr}}{k_{s,eq}} \quad . \tag{4-4}$$

The higher the admissible permeability of the ground, the larger is the range of applicability of the nomograms provided in Chapter 2. The admissible permeability of the ground K_g decreases and the situation becomes less favourable with

- increasing normalized initial head h_0/D;
- decreasing number of boreholes n;
- increasing normalized borehole length l_{dr}/D;
- decreasing borehole diameter d_{dr};
- increasing roughness $k_{s,eq}$;
- increasing tunnel diameter D;
- decreasing admissible gradient i_{adm}.

Figure 4.12 shows the permeability of the ground K_g as a function of the admissible hydraulic gradient i_{adm}. Three cases of normal, favourable and adverse drainage situations are considered (Table 4.3). The highlighted area indicates the range of admissible permeability of each drainage case when considering the upper and lower bound of normalized hydraulic head $h_0/D = 5$ and 40, respectively. In the normal drainage case, ground permeabilities $K_g = 1$ to $3 \cdot 10^{-5}$ m/s are admissible even for low hydraulic gradient $i_{adm} = 0.1$ (which is in accordance with the FEM-results previously discussed in Fig. 4.10). In the favourable drainage case, the admissible ground permeability increase to $K_g = 1 \cdot 10^{-4}$ m/s, while in the adverse case only $K_g = 1 \cdot 10^{-7}$ m/s are admissible ($i_{adm} = 0.1$).

In conclusion, the provided nomograms of Chapter 2 can be used in normal drainage cases (Table 4.3) up to moderately permeable ground ($K_g \leq 1 \cdot 10^{-5}$ m/s). In that wide range, the nomograms are valid even when considering the hydraulic flow capacity of the drainage boreholes.

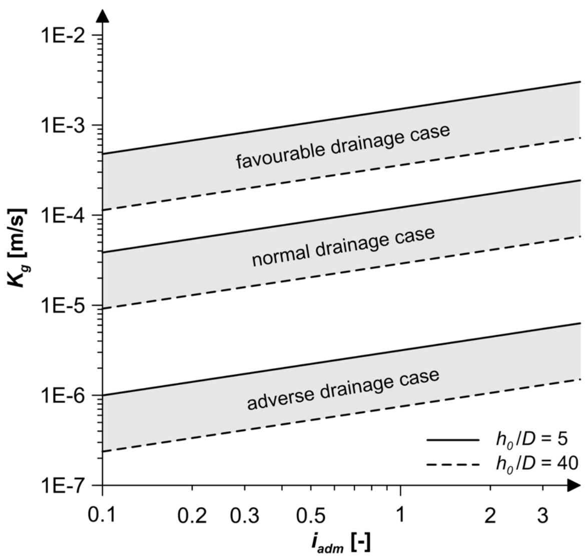

Figure 4.12 *Admissible permeability of the ground K_g as a function of the admissible hydraulic gradient i_{adm} providing sufficient capacity in the drainage boreholes (drainage cases see Table 4.3)*

Table 4.3 *Values of the considered drainage cases*

Parameters of drainage cases:		normal	adverse	favourable
Number of drainage boreholes	n [-]	6	4	12
Diameter of drainage boreholes	d_{dr} [m]	0.1	0.06	0.12
Equivalent sand roughness	$k_{s,eq}$ [m]	0.005	0.015	0.001
Tunnel diameter	D [m]	10	15	6
Length of drainage boreholes	l_{dr}/D [-]	1.5	3	1.5
Initial hydraulic head	h_0/D [-]	5, 40	5, 40	5, 40

4.3 Borehole casings

A common measure when encountering unstable drainage borehole walls is using casings (Fig. 4.13). The latter may cause difficulties in drilling (*e.g.* jamming of the casing or failure of the joints of two casing segments due to high friction at the borehole as shown in Fig. 4.13d) and thus trial drilling may be necessary. In terms of hydraulic head field, the casing screens reduce the effectiveness of the drainage measures as they impede pore pressure relief around the boreholes due to the restricted passage of water to small openings. The present section quantifies that effect for the borehole screens sketched in Figure 4.14a representing fairly sealed casings (compare to Fig. 4.13).

4.3.1 Computational model

Face stability is analysed for the tunnel example of Figure 4.9 and according to the limit equilibrium model described in Section 2.2. The water table is assumed to remain constant in spite of the drainage action of the tunnel (no drawdown). The tunnel lining is considered as waterproof up to the face (no-flow boundary condition); the tunnel face is considered as seepage faces (atmospheric pressure). The casing is taken as an impervious boundary with the exception of its openings (Fig. 4.14a), which are considered as seepage faces under atmospheric pressure. Possible local losses in hydraulic potential due to water entering the openings are neglected (for considerations of local losses at well screens see *e.g.* [101], [102], [103]). Table 4.4 summarizes the parameters assumed for the seepage flow and limit equilibrium analyses.

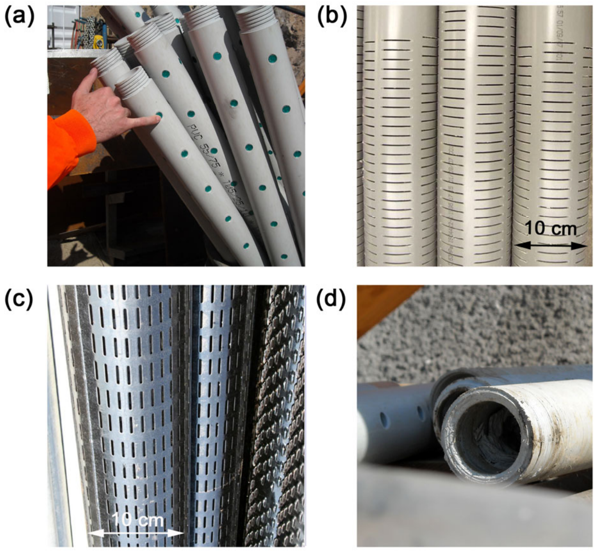

Figure 4.13 *Exemplary screens of drainage casings: (a) perforated, (b) slotted (courtesy of Baosu Pipe), (c) oblong slotted (courtesy of Pancera Tubi e Filtri S.r.l.). (d) Failure of the screw thread at the joint of the segmental casings*

4.3.2 A single cased drainage borehole

Figure 4.14b shows the distribution of the pressure p (normalized by the initial pressure p_0) along the cased borehole wall of the boreholes screens according to Figure 4.14a. The pressure minimum and maximum occur at the opening of the casings and at the midpoint between the openings, respectively. The larger the spacing x_s of the openings and the lower the opening ratio R_s, the higher is the intermediate pressure. Increasing the opening ratio (compare *e.g.* black to blue dashed lines in for screen C and G in Fig. 4.14b: twice the draining area leads to 1.5 times lower intermediate pressures) has about the same effect as decreasing the spacing (compare *e.g.* screen D to G: half the spacing leads to a 1.5 times lower intermediate pressures). A pressure reduction to about

$p/p_0 \approx 0.1$ is possible when using fairly dense slotted or perforated borehole casings (*e.g.* slotted borehole screen A, B; *e.g.* perforated borehole screen E of Fig. 4.14a).

4.3.3 Face stability

Face stability is analysed for the most efficient screens A, B, C, E, F and G of Figure 4.14a and compared to the support pressure required for face stability when considering no casings (*i.e.* seepage faces under atmospheric pressure at all borehole wall).

(a) slotted borehole screen (not at scale) perforated borehole screens (not at scale)

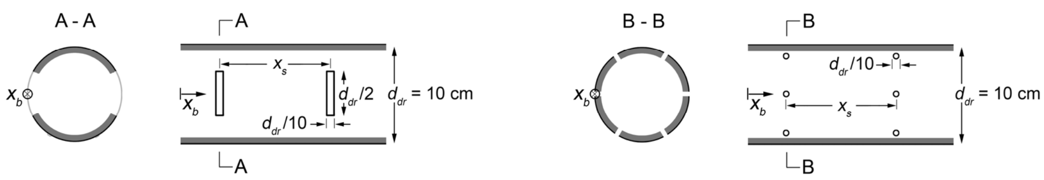

	spacing d_{dr}/x_s [-]	opening ratio R_s [%] *
screen A	4	12.7
screen B	3	9.6
screen C	2	6.4
screen D	1	3.2

	spacing d_{dr}/x_s [-]	opening ratio R_s [%]
screen E	4	6.0
screen F	3	4.5
screen G	2	3.0
screen H	1	1.5

* R_s = seepage area / borehole shell surface

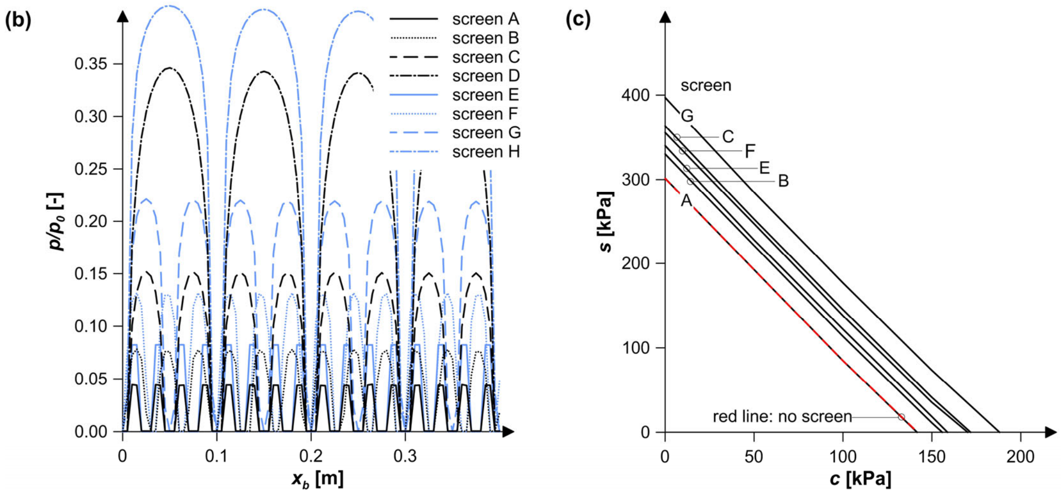

Figure 4.14 *(a) Screens of the considered drainage casings. (b) Pressure p normalized by the initial pressure p_0 along the borehole axis x for the single cased borehole. (c) Required support pressure s as a function of the ground cohesion c for the tunnel example (parameters according to Table 4.4)*

The effect of the borehole casings is evaluated in terms of the face support pressure s that is needed for stability as a function of the ground cohesion c (Fig. 4.14c). In case using a very densely slotted casing (screen A of Fig. 4.14), the same support pressure is required as when considering uncased boreholes (red dashed line in Fig. 4.14c). But the required support pressure increases fast for more sealed casings (compare *e.g.* slotted screens A to B to C in Fig. 4.14c). In ground of cohesion $c = 150$ kPa, the more sealed casings require additional face support, while with the densely slotted screen A the tunnel face is stable without additional support.

Thus the use of the nomograms provided in Chapter 2 is recommended for densely slotted or perforated screens only (*e.g.* slotted screen A of Fig. 4.14a: spacing $x_s \leq d_{dr}/4$, opening ratio $R_s \geq 12\%$; the same effect results when using a screen with about double the perforations of screen E).

Table 4.4 *Parameters for the comparative analyses*

Problem layout		
Depth of cover	H	100 m
Elevation of water table	H_w	130 m
Tunnel diameter	D	10 m
Ground		
Effective cohesion	c	0-200 kPa
Angle of eff. internal friction	φ	30°
Submerged unit weight	γ'	12 kN/m^3
Unit weight water	γ_w	10 kN/m^3
Shear resistance of the vertical slip surfaces		
Coeff. of lateral stress wedge	λ_w	0.5
Coeff. of lateral stress prism	λ_p	1.0
Drainage boreholes		
Diameter	d_{dr}	0.1 m
Length	l_{dr}	30 m
Number	n	6

4.4 Conclusions

Limited flow capacity of the drainage boreholes may be expressed as flow in porous media according to Darcy's law of a non-linear, equivalent permeability derived by considering pipe-flow equations. It allows for numerical determination of the hydraulic head field when considering the interaction between seepage flow in the ground and turbulent pipe flow in the borehole. The FEM-results are in good agreement with an analytical solution derived in the report.

For ground of permeability $K_g \leq 1 \cdot 10^{-5}$ m/s, flow capacity does not limit drainage effectiveness, independently of the initial hydraulic head, the surface roughness of the borehole wall, the drainage borehole length or the ground cohesion. It is thus safe to assume sufficient drainage capacity (*i.e.* atmospheric pressure acting at the borehole walls in numerical modelling) and the design aids for evaluating face stability provided in Chapter 2 are applicable. For higher ground permeabilities however, flow capacity forces a several times higher support pressure for face stability, tending to the values required without any drainage measures. Due to the high water discharge from the open tunnel face in such permeable ground, probably additional sealing measures such as grouting would be needed to provide safe work-conditions at the tunnel face. Obviously, permeability would thus change to more favourable conditions again.

Drainage success may also be limited by borehole casings. Densely slotted or perforated screens do not limit drainage effectiveness in terms of face stability. More sealing casings (*i.e.* spacing $x_s > d_{dr}/4$, ratio of seepage area $R_s < 13\%$; *cf.* Fig. 4.14) should be handled with particular caution as they necessitate an increase of the support pressures given in the nomograms of Chapter 2.

5 Other operational and environmental factors limiting the effectiveness of advance drainage measures for face stability

5.1 Introduction

Chapter 5 successively studies following operational and environmental factors of Table 1.1, which may reduce the effectiveness of the drainage measures with respect to face stability: (i) the lead-time in poorly permeable ground, where pore pressure relief by advance drainage may take a prohibitively long time to work; (ii) environmental constraints with respect to the drawdown of the water table, or (iii) the magnitude of settlements, which may impose limits on the amount of admissible pore pressure relief, and finally (iv) the quantity of water inflow, which may be restricted due to the pumping capacity on site.

In ground of low permeability, pore pressure relief by advance drainage boreholes may take a prohibitively long time to occur. The *lead-time* for reaching practically stationary condition in a Darcy-material is discussed in literature *e.g.* for drawdown of the water table due to wells, but not when considering drainage measures for increasing the stability of a tunnel face. Section 5.2 closes this knowledge gap and quantifies the time required until the hydraulic head is lowered sufficiently to be taken into account for face stability considerations according to Chapter 2.

Drainage-induced pore pressure relief may be undesirable for environmental reasons such as the disturbance of the hydrogeological conditions due to the *drawdown in water table* or the admissible *subsidence of ground*. Operational constraints such as the pumping capacity available on site may additionally limit the amount of admissible *water inflow* (*e.g.* as encountered during construction of Lake Mead Intake No. 3; [78]). Water inflow to wells is widely discussed in tunnelling literature (starting with Theis [104]; see for example Coli and Pinzani [105] for a recent state of the art), but mostly limited to tunnel cross-sections far away of the face (*i.e.* two-dimensional consideration only). Heuer [106], [107] estimated the inflow at the tunnel face (which needs to be considered in three dimensions) to about 1-5 times higher as the cross-sectional discharge. This is in good agreement with the inflow calculated by Anagnostou [108], where additionally the groundwater drawdown due to tunnelling with an open tunnel face was quantified. Atwa *et al.* [73] computed the drawdown of the water table for a single shallow tunnel example with advance drainage boreholes of unusually large drainage diameters, which probably overestimate the drainage effect (diameter of boreholes 0.2 m, diameter of tunnel 5 m).

In Section 5.3, the additional groundwater drawdown caused by axial boreholes from the tunnel face is quantified. Then, the settlement induced by pore water relief resulting from drainage measures is discussed for both situations of continuous groundwater recharge and groundwater drawdown (Section 5.4). Finally, the water inflow arising from drainage measures is analysed in Section 5.5.

5.2 Time dependency

5.2.1 Problem

Previous investigations considered stationary conditions of the hydraulic head field. But in ground of low permeability, achieving this state might require inadmissible time during the construction process.

Imagine tunnelling in competent rock and approaching a weak zone (of equal permeability as the competent rock), where an advance drainage measure is required for ensuring face stability (Fig. 5.1a). In order to relief the destabilizing gradients (temporally and spatially) sufficiently ahead of the tunnel face, drainage boreholes are drilled in some distance to the weak rock (Fig. 5.1b). Then, excavation proceeds by turns with the drilling operations of the drainage boreholes (No.1 and 2, respectively, in Fig. 5.1c and 5.1d).

Before drilling the boreholes into the weak rock, the pore pressure ahead of the tunnel face is at least partially relieved due to the previous drainage stage (indicated with dotted line in Fig. 5.1c and 5.1d). However and with respect to the lead-time required until a drainage measure reaches practically stationary conditions, the most critical situation would be drilling the drainage boreholes and neglecting the pore pressure relief resulting from the previous drainage stage. Thus the section in hand assumes a standstill long enough to lead to a virtually steady state head field around the open tunnel face. Then the drainage boreholes are immediately enabled and the time-dependent relief of pore water pressure is analysed. Two drainage schemes are considered: the borderline case of ideal drainage (Fig. 5.2b) and a common drainage scheme of axial drainage boreholes drilled from the tunnel face (Fig. 5.2c).

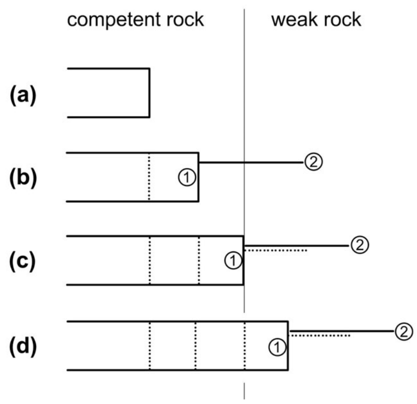

Figure 5.1 *Sketches of the construction process of tunnel excavation (No. 1) and subsequent drilling works of drainage boreholes (No. 2) when approaching a weak rock requiring drainage measures for face stability*

5.2.2 Computational model

The seepage flow analyses are performed for the example of a deep cylindrical tunnel (Fig. 5.2a). The hydraulic head at the far-field boundaries is taken equal to the initial hydraulic head h_0 (*i.e.* equal to the elevation of the water table above the tunnel axis). The water table is assumed to remain constant in spite of the drainage action of tunnel face and boreholes (no drawdown). The tunnel lining is considered as impervious up to the face (no-flow boundary condition). The borehole walls are considered as seepage faces under atmospheric pressure (which presupposes uncased boreholes of sufficient hydraulic capacity).

The time-development of the hydraulic head field is determined by numerical, three-dimensional analyses assuming Darcy's law for the following cases: ideal advance drainage (complete pore pressure relief in the ground ahead of the tunnel face, Fig. 5.2b) and advance drainage via axial boreholes from the tunnel face (Fig. 5.2c). The seepage flow analysis consists of two steps: in the first step, the steady state hydraulic head field is computed considering the tunnel face as a seepage face. In the second step, the drainage measure is activated and a transient analysis starting from the hydraulic head field prevailing after step 1 is carried out.

Table 5.1 summarizes the assumed parameter values.

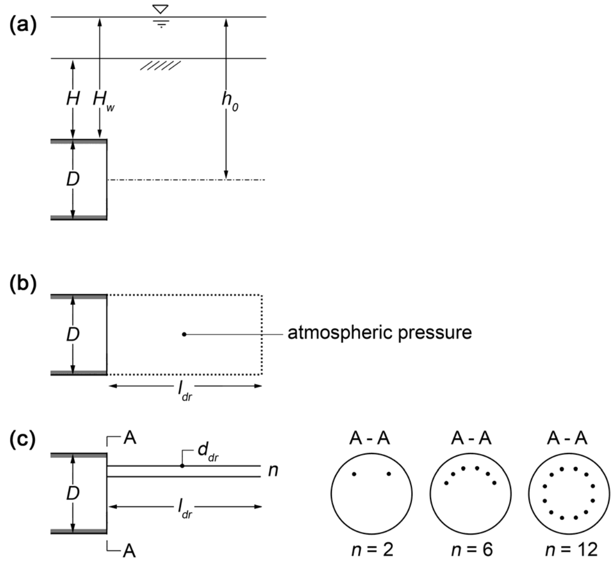

***Figure 5.2** (a) Problem setup with drainage schemes considered of (a) no advance drainage, (b) ideal advance drainage by means of complete pore pressure relief in the ground ahead of the tunnel face and (c) advance drainage by means of axial boreholes from the face*

***Table 5.1** Parameters for the comparative analyses of the degree of pore pressure relief*

Problem layout		
Distance ($T = \min(H,H_w)$ in Fig. 5.2a)	T	50-400 m
Tunnel diameter	D	10 m
Hydraulic properties of the ground		
Ratio permeability to storage	K_g/S_s	10^{-7}-10^{3} m^2/s
Drainage boreholes		
Diameter	d_{dr}	0.1 m
Length	l_{dr}	30 m
Number	n	2,6,12

***Table 5.2** Typical values of permeability K_g and specific storage S_s*

Typical values (after Younger [109])	S_s [m^{-1}]	K_g [m/s]	K_g/S_s [m^2/s]
Clay	10^{-2}	10^{-9}	10^{-7}
Sand (fine)	10^{-5}	10^{-6}	10^{-1}
Gravel (medium)	10^{-5}	10^{-2}	10^{3}
Rock (highly fissured)	10^{-5}	10^{-4}	10^{1}
Rock (unfissured)	10^{-8}	10^{-10}	10^{-2}

5.2.3 Characteristics of time-dependent behaviour

Figure 5.3a illustrates the typical time-development of the hydraulic head field h (normalized by the initial head h_0) considering the borderline case of ideal drainage ahead of a subsea tunnel (inset in Fig. 5.3a). The initial state is marked with $t = 0$. As time passes ($t = 0$ to 27 h in Fig. 5.3a), the hydraulic head field approaches the stationary distribution ($t = \infty$). The average hydraulic head above the tunnel face

$$B(t) = \frac{1}{H} \int_{D/2}^{H+D/2} h(t, x_3)\, dx_3 \qquad \text{(5-1)}$$

serves as time-dependent measurement of drainage progress when considering a specific drainage scheme. The degree of pore pressure relief of a drainage scheme at any specific time t is evaluated as

$$M_{\text{eff}}(t) = \frac{B(t) - B(0)}{B(\infty) - B(0)} \qquad \text{(5-2)}$$

and runs from zero (no pore pressure relief for initial state at $t = 0$) to one (full pressure relief for stationary conditions at $t = \infty$).

For a homogeneous, isotropic porous media obeying Darcy's law, the time-dependent hydraulic head field $h(t,x_3)$ appearing in Eq. (5-1) is governed by the diffusion equation

$$S_s \frac{\partial h}{\partial t} = K_g \nabla^2 h \quad , \qquad \text{(5-3)}$$

according to which the ratio of conductivity K_g to specific storage S_s is decisive. The latter is defined as volume of water that a unit volume of a (confined) aquifer releases from storage under a unit decline in hydraulic head and is a function of the deformability of the porous medium and the compressibility of water c_w. For linearly-elastic, isotropic ground, the specific storage is

$$S_s = \gamma_w \left(\frac{3(1-2\nu)}{E} + n_g \cdot c_w \right) \quad , \qquad \text{(5-4)}$$

where γ_w, n_g, ν and E denotes the unit weight of water, the porosity of the saturated ground, its Poisson's ratio and its modulus of elasticity, respectively [108]. The lower both permeability and stiffness of the ground, the more lead-time a drainage measure requires (Eqs. (5-4) and (5-3)). Table 5.2 lists the characteristic values of specific storage S_s, permeability K_g as well as the resulting ratio K_g/S_s for typical lithologies.

The influence of the ratio K_g/S_s is discussed by means of Figure 5.3b showing the degree of pore pressure relief M_{eff} as a function of time t (using a logarithmic scale) for several ratios K_g/S_s (again considering ideal drainage of a subsea tunnel, inset in Fig. 5.3a). The curves equally decrease over time and a 10 times lower ratio K_g/S_s takes 10 times longer to reach the same degree of pore pressure relief (compare point B to D in Fig. 5.3b and see Eq. (5-3)).

Consider as an example a weak rock ($E = 1$ GPa, $\nu = 0.25$, $n_g = 0.2$ with $c_w = 4.8 \cdot 10^{-10}$ Pa^{-1}, $\gamma_w = 10$ kN/m^3 inserted in Eq. (5-4)), where the specific storage becomes $S_s = 1.6 \cdot 10^{-5}$ m^{-1}. In case this rock is highly fissured ($K_g = 1 \cdot 10^{-4}$ m/s), a ratio of $K_g/S_s \approx 10$ results. Practically steady conditions ($M_{eff} = 99.9$ %) are reached after only 0.17 h (point A in Fig. 5.3b). Only if the weak rock appears in unfavourable combination with low permeability (*e.g.* $K_g = 1 \cdot 10^{-8}$ m/s due to fissures filled with clayey silt), a considerable lead-time of more than 1000 h is required (point B in Fig. 5.3b).

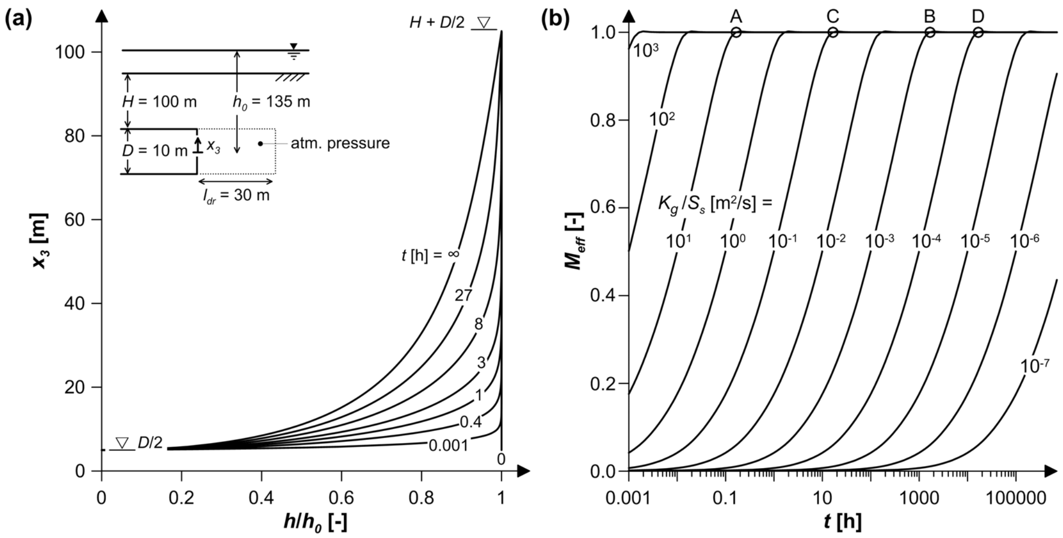

***Figure 5.3** Time-dependent pore pressure relief when considering ideal advance drainage: (a) Normalized hydraulic head distribution h/h_0 above the tunnel face starting at initial condition (t = 0) at several time steps up to stationary conditions ($t = \infty$; K_g/S_s = 0.1) and (b) degree of pore pressure relief M_{eff} as a function of the time t on a logarithmic scale for several ratios of permeability to specific storage K_g/S_s*

More generally, less than 13 h lead-time is required for ratios $K_g/S_s \geq 0.1$ (point C in Fig. 5.3b). This range covers the typical permeable lithologies, *i.e.* is valid for permeability of up to $K_g = 10^{-6}$ m/s in a ground of average specific storage ($S_s \approx 10^{-5}$ m^{-1}; see Table 5.2). However, time-dependency becomes decisive in clayey formations, where a very long lead-time would be necessary in order to reach a practically steady head field (*e.g.* for point D in Fig. 5.3b nearly two years). Note, that in such low-permeability ground presumably vacuum lances are installed which in turn accelerate pore pressure relief. Furthermore in unfissured rock, permeability is obviously lower as well (see Table 5.2), but as in sound rock face stability is no issue, this case is of no interest for our concern.

5.2.4 Effect of axial drainage arrangements

5.2.4.1 Degree of pore pressure relief

A common drainage scheme in tunnelling is drilling axial boreholes from the face (Fig. 5.2c with drainage borehole number n, length l_{dr} and diameter d_{dr}). Dimensional analysis and considering the structure of Eq. (5-3) shows that the degree of pore pressure relief M_{eff} (Eq. (5-2)) may be non-dimensionally expressed as

$$M_{eff} = f\left(\frac{H_w}{D}, \frac{H}{D}, \frac{tK_g}{S_s D^2}, \frac{l_{dr}}{D}, \frac{d_{dr}}{D}, n\right) \quad . \tag{5-5}$$

The seepage flow domain extends either up to the ground surface H (subaqueous tunnels) or up to the groundwater table H_w. The upper boundary of the numerical model is thus located at distance $T = \min(H, H_w)$ above the tunnel crown and Eq. (5-5) simplifies *for a given drainage scheme* to

$$M_{eff} = f\left(\frac{T}{D}, \frac{tK_g}{S_s D^2}\right) \quad . \tag{5-6}$$

Figure 5.4 shows the degree of pore pressure relief M_{eff} as a function of the dimensionless time-factor $tK_g/(S_sD^2)$ on a logarithmic scale for the example of a subsea tunnel and considering n = 2, 6 and 12 boreholes of fixed length and diameter (inset in Fig. 5.4). The curves for all axial drainage arrangements nearly coincide, despite the different seepage area, and require a lead-time of $tK_g/(S_sD^2) \approx 100$ ("n = 2, 6, 12" in

Fig. 5.4). The pore pressure relief caused by ideal drainage measure is faster and requires less lead-time ($\Delta tK_g/(S_sD^2) \approx$ 50 for $M_{eff} \approx$ 1 in Fig. 5.4).

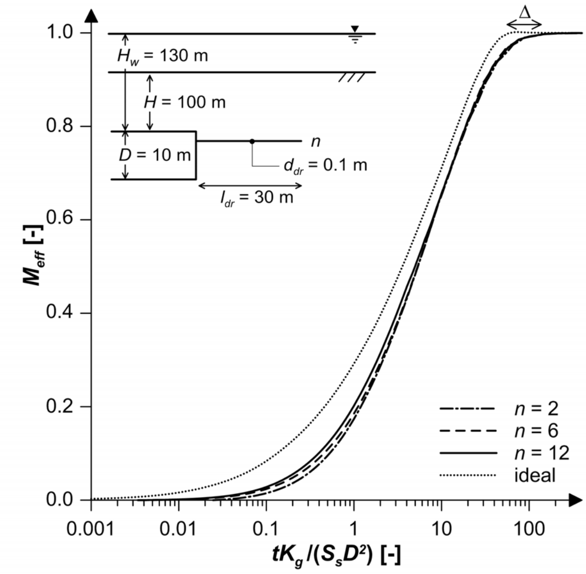

Figure 5.4 *Degree of pore pressure relief M_{eff} as a function of the dimensionless time-factor $tK_g/(S_sD^2)$ on a logarithmic scale (drainage schemes see Fig. 5.2c)*

5.2.4.2 Lead time for face stability

Regarding face stability at a given support pressure, a drainage measure should reach nearly stationary conditions at least in the vicinity of the tunnel face, while far away, the hydraulic head may still decrease with time. The left-hand part of Figure 5.5 shows the hydraulic head field in the vicinity of a tunnel example (Fig. 5.5a). The equipotential line highlighted in white is practically at steady-state conditions for high degree of pore pressure relief M_{eff} (compare Fig. 5.5c to b). The destabilizing gradients increase*, i.e.* the line gets closer to the face, with decreasing M_{eff} (Fig. 5.5d). Figure 5.5e quantifies the face support pressure s that is needed for stability as a function of the ground cohesion c for several M_{eff}. The support pressure is calculated as described in Section 2.2, but with introducing the pore pressure field at a time t into the limit equilibrium equations (an approximation, which is sufficiently accurate for our purpose of comparison; for more details see *e.g.* Eisenstein and Samarasekera [110]). At a degree of pore pressure relief of $M_{eff} \geq$ 90%, virtually the same support as at steady state is required (less than 3% deviation; Fig. 5.5e) and the design nomograms provided in Chapter 2 are applicable. Therefore, we target such degree of pore pressure relief.

For $n = 2$, 6 and 12 boreholes from the face, Figure 5.6 shows the dimensionless time $tK_g/(S_sD^2)$ that must elapse in order that pore pressure relief reaches M_{eff} of 90 or 95%, and plots it as a function of dimensionless distance T/D (see inset in Fig. 5.6a).

Pore pressure relief requires more time with larger seepage flow domain (compare point A to C in Fig. 5.6a), however for distance $T/D \geq 20$ the increase is small (compare point B to C in Fig. 5.6a). The smaller the seepage area of the drainage measure, the more time is required reaching the target degree of pore pressure relief; though differences within the drainage schemes are – if any – rather small (compare point C to D in Fig. 5.6a). For lower degree of pore pressure relief, the results nearly coincide for all borehole numbers (Fig. 5.6b). Summarizing, a time-factor of about $tK_g/(S_sD^2) \geq 58$ provides the target degree of pore pressure relief of 90% independently of the axial drainage arrangements and cover or water head (Fig. 5.6b; for $M_{eff} = 95\%$ it is about $tK_g/(S_sD^2) \geq 80$ in Fig. 5.6a).

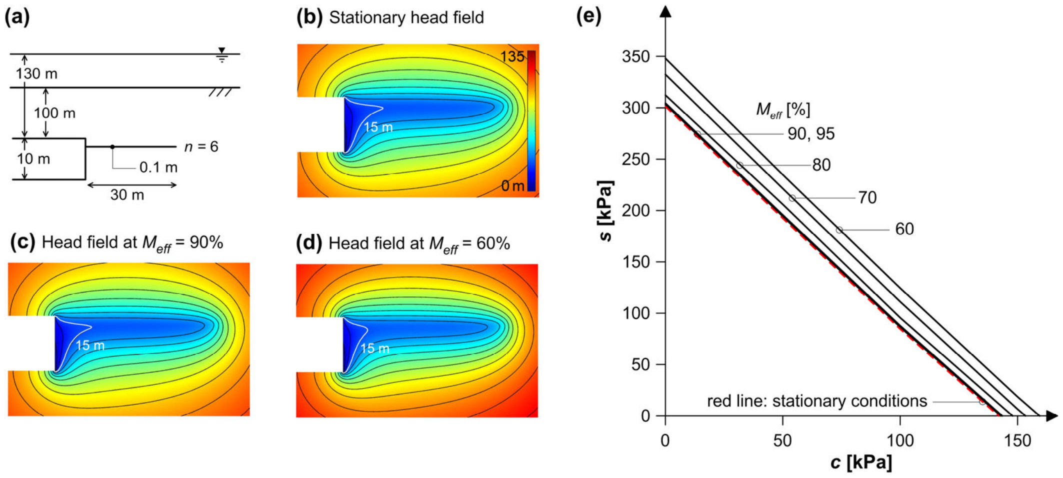

Figure 5.5 *(a) Tunnel example, (b-d) hydraulic head field and (e) required face support pressure s as a function of the ground cohesion c for selected degree of pore pressure relief M_{eff} (other parameter according to Table 5.1)*

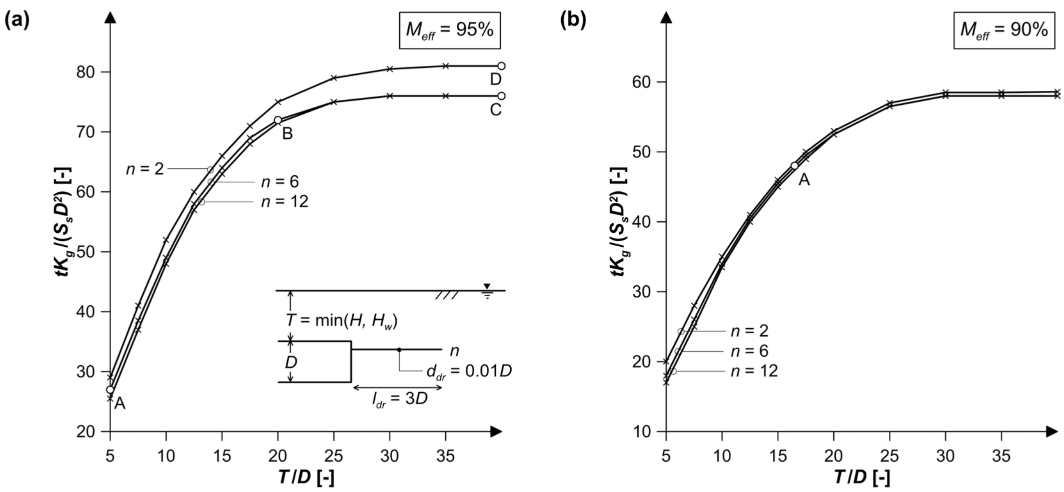

Figure 5.6 *Time-factor $tK_g/(S_sD^2)$ as a function of normalized distance T/D when considering n = 2, 6 and 12 axial drainage boreholes (Fig. 5.2c) for a degree of pore pressure relief M_{eff} = 95 (a) and 90% (b)*

5.2.4.3 Application example

Consider as an example excavating a circular tunnel in frequently fissured rock with silty infillings after having drilled six advance drainage boreholes (Table 5.3) and assume that we know the face support required for stability at steady-state conditions in the fault zone soon to be encountered. We want to determine the required lead-time which provides a degree of pore pressure relief of 90%, *i.e.* allows us to stay with our known face support. Entering Figure 5.6 for the target degree of pore pressure relief and distance of seepage flow domain (M_{eff} = 90%; T/D = 16.4) results in $tK_g/(S_sD^2)$ = 48 (point A in Fig. 5.6b). Thus t = 48 S_sD^2/K_g = 2.1 days after having drilled the drainage boreholes, the hydraulic head in the vicinity of the tunnel face reaches nearly stationary conditions. (Please note that this corresponds with the exact numerical computation for the tunnel example of Table 5.3, which results in a lead-time of 2 days. Thus Figure 5.6 is valid for a wide range of tunnel diameters as long as the drainage geometry is according to the inset (*i.e.* l_{dr}/D = 3 and d_{dr}/D = 0.01; see also Eq. (5-5)).

This seemingly long period must be put into perspective of tunnelling practice: The first drainage boreholes (here: length of 15 m) are drilled in safe distance of the fault zone and require about 1 day of drilling operation. Assuming a daily advance of 2 m in conventional tunnelling, it takes about 4 days until the recommended minimum borehole length of 7 m is reached (minimum borehole length of about 1.5D; *cf.* Section 2.3.3 or Zingg [62]). The drilling operation of the next stage of drainage boreholes requires another day, which gives a sum of 7 days and the required lead-time has passed before entering into the fault zone.

Table 5.3 *Parameters for the application example*

Problem layout		
Depth of cover	H	82 m
Elevation of water table	H_w	100 m
Tunnel diameter	D	5 m
Hydraulic properties of the ground		
Permeability	K_g	$2{\cdot}10^{-7}$ m/s
Specific storage	S_s	$3{\cdot}10^{-5}$ 1/m
Drainage boreholes		
Diameter	d_{dr}	0.05 m
Length	l_{dr}	15 m
Number	n	6

5.3 Groundwater drawdown

5.3.1 Problem

In case of sensitive hydrogeological conditions, the maximum drawdown in water table might be limited. Drainage boreholes increase the seepage area and therefore increase the drawdown in water table. Thus the maximum admissible groundwater drawdown may limit the number and/or length of drainage boreholes, which in turn necessitates higher support pressures for face stability (*cf.* Chapter 2). On the other hand and if there are no restrictions to groundwater drawdown, the lowered hydraulic head favours face stability and less support pressure is required. This section analyses the additional groundwater drawdown caused by axial drainage boreholes drilled from the tunnel face at stead-state conditions.

5.3.2 Computational model

The seepage flow analyses are performed for the example of a cylindrical tunnel (Fig. 5.7) in a homogeneous, isotropic porous medium obeying Darcy's law. The tunnel lining is impervious (no-flow boundary condition); both face and drainage boreholes are considered as seepage faces under atmospheric pressure (drainage boreholes of sufficient capacity). The distance L is chosen large enough not to affect the amount of drawdown in the vicinity of the tunnel face [111]. The hydraulic head at the far-field boundaries is taken equal to the initial water table H_w, except for the initial groundwater surface (abcd in Fig. 5.7), where a no-flow condition is assigned. The seepage flow domain comprises both the lower, saturated region underneath the water table and the overlying, unsaturated ground. The permeability is assumed to drop sharply at p = 0 (to 1/100 of the saturated conductivity according to the residual flow method of Desai and Li [112]; *cf.* [88], [108]) and the free surface is defined as the surface on which pore pressure is equal to atmospheric pressure ($p = 0$). The maximum drawdown ΔH_w ahead of the tunnel face is evaluated (Fig. 5.7).

The hydraulic head field is determined by numerical, three-dimensional steady-state seepage analyses for the following drainage schemes: no advance drainage (Fig. 5.2a), ideal advance drainage (Fig. 5.2b) and advance drainage via axial boreholes from the tunnel face (Fig. 5.2c).

Table 5.4 summarizes the parameters for the comparative analyses.

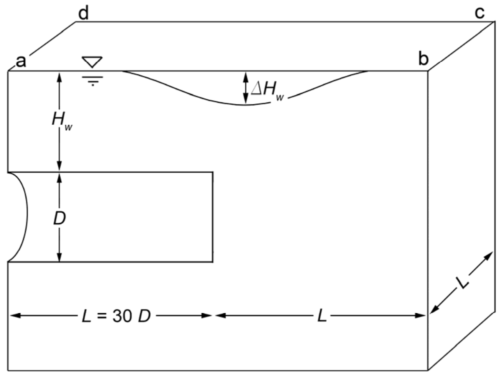

Figure 5.7 *Problem setup for the comparative analysis of the tunnel example*

Table 5.4 *Parameters for the comparative analyses*		
Problem layout		
Elevation of water table	H_w	10-100 m
Tunnel diameter	D	10 m
Ideal drainage		
Length	l_{dr}	10,20,30,50 m
Drainage boreholes		
Diameter	d_{dr}	0.1 m
Length	l_{dr}	30 m
Number	n	2,6,12

5.3.3 Borderline cases

The relative drawdown in water table is minimal, if drainage occurs solely via the tunnel face (Fig. 5.2a) and maximal for ideal advance drainage (Fig. 5.2b). For dimensional reasons, the drawdown ΔH_w may be expressed *for a given drainage scheme* as

$$\frac{\Delta H_w}{H_w} = f\left(\frac{H_w}{D}\right) . \tag{5-7}$$

In case of ideal advance drainage (Fig. 5.2b), the extent l_{dr}/D of the drained area ahead of the face appears as additional dimensionless parameter. The relative drawdown decreases with increasing initial water head (compare point A to B in Fig. 5.8, see also *e.g.* [111]).

The results agree well with Anagnostou [108] who quantified the drawdown due to the seepage area of the tunnel face only (compare line $l_{dr} = 0$ in Fig. 5.8 to the grey crosses taken from Fig. 13 of [108]). For low initial water head, groundwater level decreases below the tunnel roof due to the drainage action of the face ($\Delta H_w/H_w > 1$). For a high initial water head of 10 times the tunnel diameter, the groundwater level decreases to $\Delta H_w/H_w = 0.2$ in case of very long ideal drainage area (point C in Fig. 5.8), and is thus five times higher than for minimum seepage area (point B for no advance drainage in Fig. 5.8).

5.3.4 Effect of distinct drainage boreholes

Figure 5.9 shows the groundwater drawdown in the presence of 2, 6 and 12 axial drainage boreholes (locations after Fig. 5.2c) as a function of the initial water head. The groundwater drawdown is bounded by the borderline cases of no boreholes and ideal drainage up to $l_{dr} = 3D$ ahead of the face.

The increased seepage area due to the axial drainage boreholes leads to a more pronounced drawdown of groundwater; however does not decrease the water table as much as ideal drainage. Doubling the borehole number does not affect the head as much as starting with advance drainage at all (*e.g.* for $H_W/D = 4$ in Fig. 5.9: compare point A to B vs. C to D). However, the additional drawdown of water table due to the axial boreholes is substantial. For an example of $H_W/D = 4$, the drawdown in water table is about three times larger with advance drainage boreholes than without (compare point D to A in Fig. 5.9). The drawdown decreases clearly with increasing initial head, while the share of the advance drainage stays about the same (compare ratios of E over F to D over A in Fig. 5.9). For initial head $H_W/D > 10$, the groundwater drawdown is less than 4-12% of the initial water table for all considered drainage schemes.

In case a specific drawdown of the water table is not admissible, the number of drainage boreholes has to be reduced (which in turn of course requires a higher support pressure for face stability, see nomograms of Chapter 2) or the pore pressure relief has to be limited considering other measures such as sealing grouting or ground freezing.

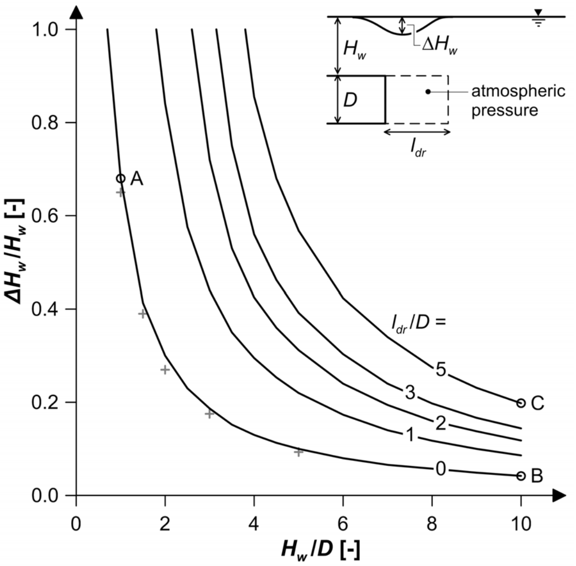

***Figure 5.8** Relative groundwater drawdown $\Delta H_w/H_w$ as a function of the initial water table H_w/D when considering ideal drainage areas of variable length l_{dr} (parameters according to Table 5.4)*

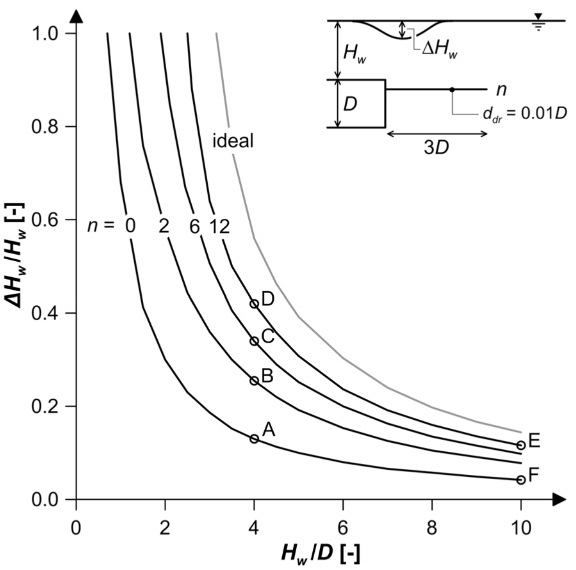

***Figure 5.9** Relative groundwater drawdown $\Delta H_w/H_w$ as a function of the initial water table H_w/D when considering several axial advance drainage borehole schemes (n = 2, 6 and 12 boreholes at location of Fig. 5.2c; other parameters according to Table 5.4)*

5.4 Settlements

5.4.1 Problem and approach

Water table drawdown may be inadmissible (or limited) not only due to environmental reasons, but also due to potential settlement of the ground surface. We limit ourselves here to a rough assessment of maximum settlement by means of the constrained modulus[5] E_S (*e.g.* [113]). When assuming linear-elastic behaviour of the ground (Hooke's law) and considering the change of effective stresses $\Delta\sigma'$ equal to the change in pore water pressure Δp [65], the settlement u_S at the ground surface is

$$u_S = \int \varepsilon \, dx_3 = \int \frac{\Delta\sigma'}{E_S} dx_3 = \int \frac{\Delta p}{E_S} dx_3 \ , \tag{5-8}$$

where ε and x_3 denote the strain of the ground and the vertical coordinate, respectively. The settlement is calculated at the location of the maximum drawdown of water table (see Section 5.3.2) and considers the change in pressure from ground surface down to well below the tunnel invert, where pressure distribution approximates again to the initial, hydrostatic distribution (compare solid to dashed lines and integration area Δp highlighted in grey in Fig. 5.10).

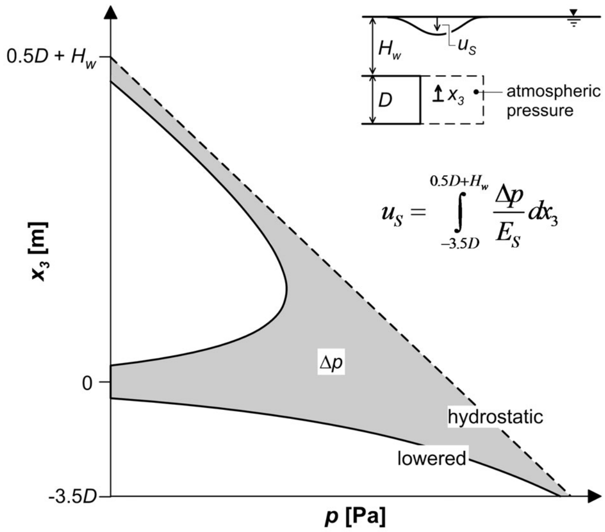

Figure 5.10 *Pore pressure distribution p along a vertical line at the location of maximum groundwater drawdown ΔH_w showing the pore pressure relief Δp (highlighted in grey) between initial conditions (dashed line) and the pressure prevailing after drainage (solid line)*

5.4.2 Effect of drainage boreholes

Figure 5.11 shows the surface settlement u_S (multiplied by the constrained modulus E_S of the ground) as a function of the normalized water head for the axial drainage borehole layouts ($n = 2$, 6 and 12 boreholes at location of Fig. 5.2c) as well as the reference cases ("none" and "ideal"). The solid lines indicate drawdown of water table, the dashed lines no drawdown (see later Section 5.4.2.1). Expectedly, the settlement-factor increases with increasing initial head and with increasing number of advance drainage boreholes.

Consider as an example a deep tunnel in very weak rock ($D = 10$ m, $H_W = 100$ m, $E_S = 500$ MPa). With six axial drainage boreholes, considerable surface settlement of

[5] The constrained modulus E_S is found directly from one-dimensional consolidation test (oedometer) and may be expressed related to the Young's Modulus E and the Poisson's ratio ν by $E_S = E(1\text{-}\nu)/((1+\nu)(1\text{-}2\nu))$.

6.7 cm would have to be expected (point A in Fig. 5.11a). But as the draining action of the tunnel face causes already an extensive deformation of 4 cm (point B in Fig. 5.11a), the drainage boreholes trigger relatively small additional settlements, which might be acceptable for the benefit of face stability. In particular, the required face support pressure with advance drainage is only 8 kPa (assuming ground cohesion of 100 kPa, additional ground parameters see Table 4.4; nomograms provided in Chapter 2 when taking account of the water drawdown according to Fig. 5.9). But without advance drainage, a high support pressure of 314 kPa is necessary. Such values are barely feasible in conventional tunnelling even by heavy face bolting (*cf*. Section 2.5.1). Thus advance drainage proves feasibility of that tunnelling example provided that considerable surface settlement is accepted (else, ground improvement *e.g.* by grouting would be required).

5.4.2.1 Comparison to no drawdown of groundwater table

In case where water is recharged *e.g*. by a direct link to an adjacent lake, no groundwater drawdown takes place. To draw a comparison, the computational model described in Section 5.3.2.1 was used but with fixed initial hydraulic head as boundary condition at ground surface (*i.e.,* at abcd in Fig. 5.7).

Without drawdown, pore pressure relief takes place only in the vicinity of the tunnel face. Thus the surface settlements decrease compared to the case without groundwater drawdown (compare dashed to solid lines in Fig. 5.11). The difference in drawdown slightly increases with increasing hydraulic head due to the larger area of influence (compare *e.g.* points E/F = 1.09 to C/D = 1.14 in Fig. 5.11).

When considering the previous tunnel example (Section 5.4.2), surface settlements considering six axial drainage boreholes decrease to 5.8 cm, while the draining action of the tunnel face causes deformation of 3.7 cm (Fig. 5.11a). On the other hand, the required face support pressure slightly increases to 30 kPa with advance drainage and to 340 kPa without drainage boreholes (nomograms provided in Chapter 2).

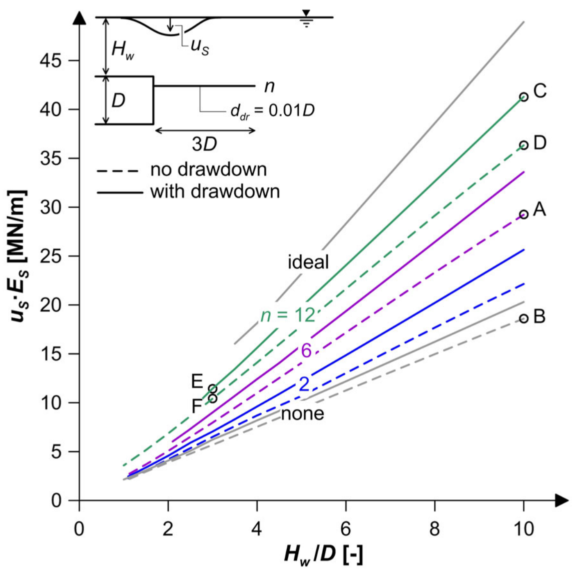

Figure 5.11 *Ground settlement* u_S *multiplied by the constrained modulus* E_S *as a function of the normalized initial water table* H_w/D *when considering several axial advance drainage borehole arrangements (*n *= 2, 6 and 12 boreholes at location of Fig. 5.2c; other parameters according to Table 5.4)*

5.5 Water discharge

5.5.1 Problem

In cases of a highly permeable ground, water inflow from the tunnel face and the boreholes is substantial and appropriate pumping capacity needs to be installed on construction site. The admissible pumping rate may limit the number and/or length of the drainage boreholes, which in turn necessitates higher support pressures for face stability (*cf.* Chapter 2) or requires additional measures such as sealing grouting. This section analyses steady-state inflow from both tunnel face and axial drainage boreholes assuming sufficient capacity (computational model see Section 5.3.2).

5.5.2 Effect of drainage boreholes

We first consider the favourable case of groundwater drawdown (drainage schemes see Fig. 4.25). Figure 5.12 shows the cumulated discharge[6] of all seepage area on logarithmic scale for the considered reference cases and axial advance drainage schemes (the solid lines indicate drawdown of water table, the dashed lines no drawdown; see later Section 5.5.2.1). Water inflow increases with increasing initial head and proves adequate accordance with previous investigations (grey crosses in Fig. 5.12 with values taken from Fig. 9 of Anagnostou [108]. The values of that previous investigation are slightly higher, which is probably due to the smaller model size leading to higher gradients.).

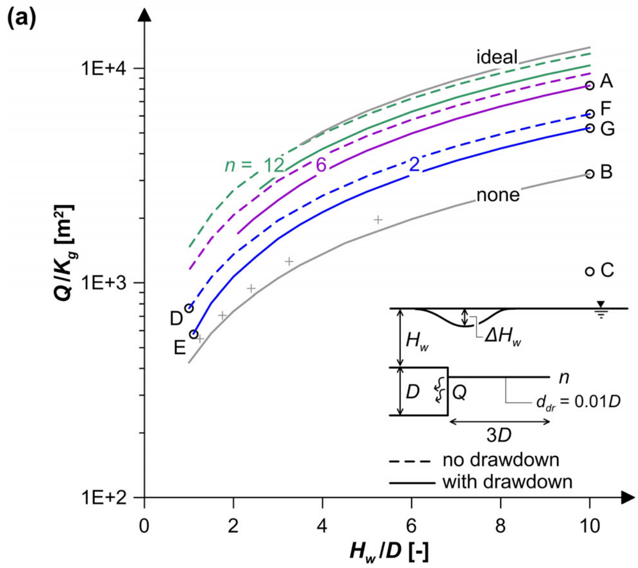

Figure 5.12. *Water discharge Q divided by the permeability of the ground K_g (on a logarithmic scale) as a function of normalized initial water table H_w/D when considering several axial advance drainage borehole arrangements (n = 2, 6 and 12 boreholes at location of Fig. 5.2c; other parameters according to Table 5.4)*

Drilling six advance drainage boreholes creates nearly twice the seepage area compared to no advance drainage (135.1 to 78.5 m^2, respectively). Due to the spatial distribution of this seepage area, the discharge collected from face and boreholes is even multiplied by a factor of 2.6 (compare point A to B in Fig. 5.12). The total water discharge increases with increasing number of boreholes and may necessitate larger pumping capacity than without advance drainage boreholes. On the other hand, advance drainage reduces the discharge at the tunnel face by over 60% (compare C to B in Fig. 5.12, where point C

[6] Please note that the values of cumulated discharge are conservative estimates and presumably higher than the discharge values measured on site, since the computation does not consider any excavation-induced permeability reduction in the vicinity of the tunnel (*cf.* [106], [114]).

indicates discharge at the tunnel face when considering six boreholes), thus improves working conditions at the face provided that the water is discharged immediately from the drainage boreholes.

5.5.2.1 Comparison to no drawdown of groundwater table

In case where water is recharged *e.g*. by direct connection to an adjacent lake, no groundwater drawdown takes place and larger inflow of water is expected. To draw a comparison, the computational model described in Section 5.3.2 was used but with fixed initial hydraulic head as boundary condition at ground surface (*i.e.,* at abcd in Fig. 5.7).

Without drawdown, water discharge is higher due to the higher gradients prevailing (compare dashed to solid lines in Fig. 5.12). The smaller the initial water head, the larger is the difference (*e.g*. for two axial boreholes 16-32%, compare D/E = 1.32 to F/G = 1.16 in Fig. 5.12). The larger the seepage area (*i.e*. the number of boreholes), the larger is the difference in discharge between the cases with and without groundwater drawdown.

5.6 Conclusions

The lead-time, *i.e.* the time needed until practically steady hydraulic conditions are reached after having installed a drainage arrangement, is evaluated as time-factor $tK_g/(S_sD^2)$ (depending on the hydraulic ground properties of specific storage S_0 and permeability K_g as well as on the tunnel diameter D and the time t). The considered drainage arrangements of several axial boreholes drilled from the face show similar time-dependent behaviour and reach after $tK_g/(S_sD^2) \geq 58$ a pore pressure relief, which is so close to stationary conditions that the nomograms of Chapter 2 can be used to assess face stability. From a practical point of view, the lead-times for most of the permeable lithologies are short enough that they may not be decisive, because drilling operation for the boreholes will probably take more time. Only in clayey formations ($K_g << 10^{-6}$ m/s) operationally decisive lead-times are required (note that this is typically the range where vacuum lances are installed in order to increase drainage effectiveness; *i.e.* the lead-time decreases).

Care should be taken concerning the hydraulic parameters of the ground, where ratio of permeability K_g to specific storage S_s is decisive for the lead-time of a drainage measure (a decrease by factor of 10 necessitates a 10 times longer lead-time). The specific storage S_S may be expressed as a function of the modulus of elasticity of the ground (*i.e.* the lower the stiffness of the ground, the more lead-time is required). In literature, its value varies only marginal within the common permeable lithologies for tunnelling ($S_s \approx 10^{-5}$ m^{-1}). But permeability K_g may vary heavily even in small space by several decimal power and should therefore thoroughly be determined.

Groundwater drawdown resulting from advance drainage measures increases with increasing seepage area (*i.e*. with number and length of boreholes) and decreases with increasing initial water head. The considered drainage arrangements of 2 to 12 axial drainage boreholes multiplies groundwater drawdown by a factor of 2 to 3 compared to the drainage action of only the tunnel face.

The potential settlement of the ground surface is estimated assuming linear-elastic ground behaviour and considering the pressure reduction induced by the drainage measure. It shows the considerable settlement due to drainage measures, which however might be acceptable if settlement due to open-face tunnelling is acceptable at the first place. The settlement due to groundwater drawdown is 10-15% larger than the settlement due to local pore water pressure relief only (*i.e*. no groundwater drawdown).

The total amount of water inflow increases substantially due to advance drainage boreholes and is obviously even higher when assuming no groundwater drawdown. However, advance drainage reduces the inflow at the face, thus improves working conditions at the tunnel face provided that the water is discharged immediately from the drainage boreholes.

6 On the stabilizing effect of drainage on tunnel support in grouted fault zones

6.1 Introduction

Previous investigations of Anagnostou and Kovári [40] considered two borderline cases of drainage measures of grouting bodies: a “grouting body without drainage” and an “ideally drained grouting body”. The *grouting body without drainage* refers to the case of a low-permeability grouting body, where the tunnel excavation does virtually not affect the hydraulic head in the untreated ground (Fig. 6.1a). The hydraulic head difference between the in situ head and the excavation boundary is thus dissipated mainly within the grouted body leading to seepage forces f_s, which are high if the thickness of the grouted zone is small and the tunnel is located well below the water table. The *ideally drained grouting body* refers to the assumption of complete pore pressure relief within the grouting body (Fig. 6.1b) thus the seepage forces develop in the untreated ground in safe distance from grouting body and tunnel. However, large inflows may be encountered due to the abandoned sealing effect of the grouting body.

The chapter in hand extends the investigation of Anagnostou and Kovári [40] with point to following aspects of drainage measures: (i) the effect of ideal drainage of only the inner part of the grouting body; (ii) the effect induced by ideal drainage of an area larger than the subsequent constructed grouting body, and (iii) the consideration of the pore pressure relief resulting from specific arrangements of drainage boreholes instead of assuming ideal drainage.

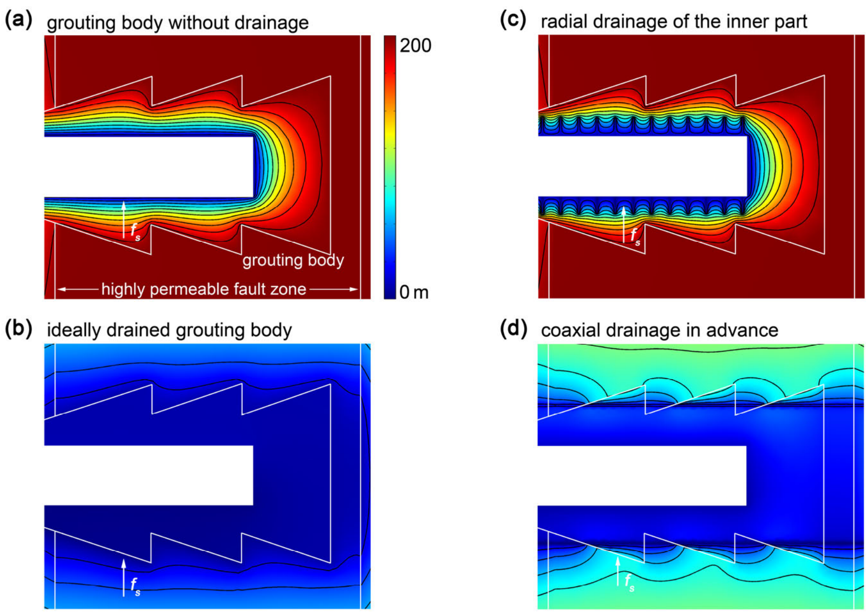

Figure 6.1 *Hydraulic head field when considering (a) the grouting body without drainage, (b) the ideally drained grouting body (c), radial drainage of the inner part of the grouting body and (d) coaxial drainage of the grouting body*

Radial drainage boreholes arranged in the inner part of the grouting body (Fig. 6.1c) relieve the pore pressure close to the excavation boundary and decrease both the deformation and the risk of inner erosion. They thus may be the method of choice in cases where the grouting body is intended to maintain its outer sealing effect, but where possible poor injection works in the inner part of the grouting body require a controlled pressure relief in order to keep the high hydraulic gradients in safe distance to the excavation boundary. However, the seepage forces develop concentrated in the outer shell of the grouting body and may there lead to local overstressing.

In case where for example the water head prevailing renders impossible grouting operation due to maximum feasible injection pressure, drainage in advance of the injection works is an option (*e.g.* by means of boreholes coaxial to the tunnel axis in Fig. 6.1d). The pore pressure relief resulting from the drainage measure increases the shear resistance of the ground (pre-consolidation) prior to grouting. The seepage forces develop in safe distance from the tunnel and, depending on the location of the axial drainage boreholes, also from the grouting body. However, potentially large inflows may develop due to the drainage measures.

The chapter is organized as follows: Section 6.2 explains the modelling concept for calculation of the characteristic line, *i.e.* the stress-displacement behaviour of the excavation boundary when assuming ideal drainage. The results of the analytical solutions considering ideal drainage before and after grouting are presented in Section 6.3. Section 6.4 explains the modelling concept of considering specific drainage borehole arrangements by hydraulic-mechanical coupled FE-modelling. The results (Sections 6.5 and 6.6) quantify the stabilizing effect of several different drainage borehole arrangements drilled after as well as in advance of grouting and place emphasis on the effect of number, length and location of boreholes. Section 6.6 finishes with an example of a fault zone of limited extend and quantifies the pre-consolidation effect of drainage boreholes being drilled in advance of grouting. Finally, Section 6.7 summarizes the findings with focus on the difference between consideration of the analytical solution assuming ideal drainage and consideration of the several different drainage borehole arrangements.

6.2 Modelling ideal drainage

6.2.1 Static system, initial and boundary conditions

The static system for the stability analysis of a deep, circular tunnel through a grouted fault zone of infinite length is considered as made up by three elements: the tunnel lining support pressure, the grouting body and the untreated, surrounding ground (Fig. 6.2; [40]).

The untreated ground is considered as hollow cylinder with an outer radius at infinity and an inner radius b coinciding with the boundary to the grouting body. The state of initial stresses is assumed to be homogeneous and isotropic. The external boundary of the ground is subjected to the effective initial stress σ_0', which magnitude equals to the effective overburden pressure.

The injection body is a thick-wall cylinder with an inner radius a and an outer radius b. Injection is assumed not to lead to any substantial changes in the stress state and thus the stresses acting after injection are equal to the initial stresses and the stress state is still homogeneous and isotropic (for details see Anagnostou and Kovári [40]). The stress state immediately prior to the tunnel excavation is taken as reference state for deformations. At the excavation boundary $r = a$, a uniform lining support pressure σ_a is assumed and at $r = b$, effective pressure σ_b' is acting.

Ideal drainage up to radius $r = l$ is considered as pore pressure relief to atmospheric pressure and thus the hydraulic boundary at the drainage radius l is assumed as a seepage faces (atmospheric pressure at $r = l$). The far-field boundary condition assumes an undisturbed head field (pressure is equal to the initial pressure; $p = p_0$) for the area beyond the radius $r \geq R$, where R is taken equal to the depth of the tunnel below the water table.

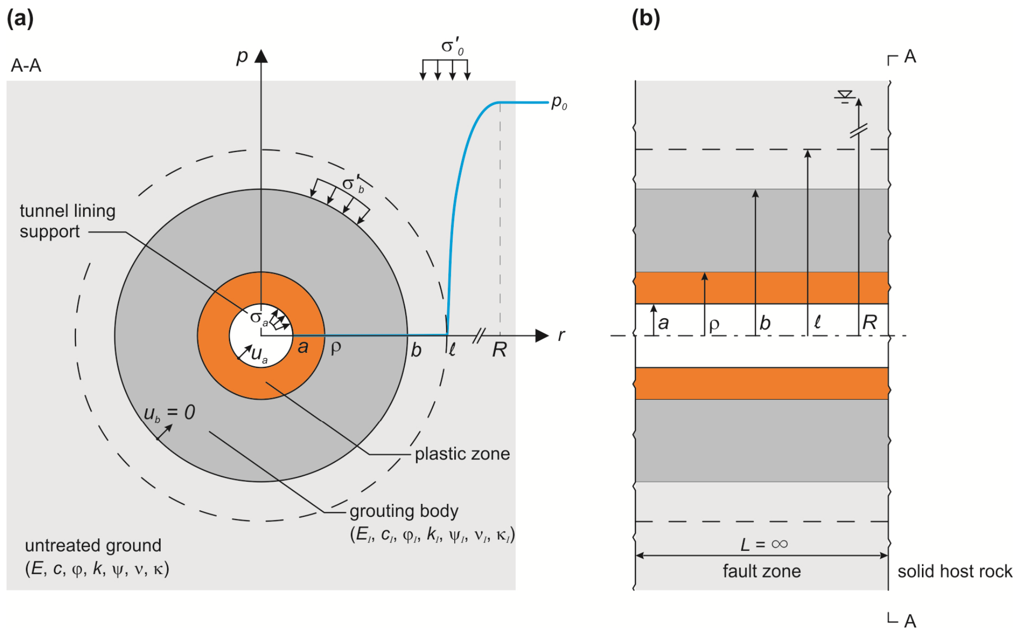

***Figure 6.2** Computational model of tunnel excavation in a grouting body when considering ideal drainage up to radius $r = l$ in an infinite long fault zone: (a) cross section, (b) longitudinal section*

6.2.2 Material properties

The ground (both untreated and grouted) is assumed to be a homogeneous and isotropic porous material with linear-elastic, perfectly-plastic behaviour obeying the principle of effective stress, the Mohr-Coulomb yield criterion and Darcy's law. The seepage forces are equal to the gradient of the pore water pressure field (assumption of deep tunnel; [40]).

The material parameters of the untreated ground have no subscript, the ones of the injection body are denoted with subscript I (effective cohesion c_I, angle of internal friction φ_I, Young's Modulus E_I, Poisson's ratio ν_I, uniaxial compressive strength f_{cI}, angle of dilatancy ψ_I, loosening factor κ_I, material constant m_I, and permeability k_I).

The material constant is defined as

$$m = \frac{1 + \sin\varphi}{1 - \sin\varphi} \quad . \tag{6-1}$$

The uniaxial compressive strength is interrelated by the cohesion and the friction angle:

$$f_c = \frac{2c\cos\varphi}{1 - \sin\varphi} \quad ; \tag{6-2}$$

the loosening factor may be expressed depending on the dilatation angle [40]

$$\kappa = \frac{1 + \sin\psi}{1 - \sin\psi} \quad . \tag{6-3}$$

The permeability of the grouting body is assumed to be several times lower than the one of the untreated ground. The higher the initial ground permeability, the higher is the feasible reduction (*e.g.* for cement grouts and highly permeable ground upmost to a factor 1000; [115]).

Please note that the permeability of the grouting body is assumed to remain constant during plastification (Fig. 6.3a). An increase in permeability, which is possible during plastification due to micro-cracks developing within the plastic zone, would lead to a shift of the hydraulic boundary condition up to radius $r = \rho$, which increases the hydraulic gradients acting in the outer zone of the grouting body and in turn may lead to additional overstressing, *i.e.* an even larger plastic zone (Fig. 6.3b). On the other hand and if grouting would not be able to fill all joints, stress redistribution and joint closure around the tunnel could lead to a decrease in permeability, which in turns increases the hydraulic gradients close to the tunnel face (Fig. 6.3c; *cf.* [116], [114], [117], [118]).

The stiffness of the grouting body is assumed to be considerably higher than the one of the untreated ground. After injection work, no displacement of the outer boundary of the grouting body is assumed ($u_b = 0$).

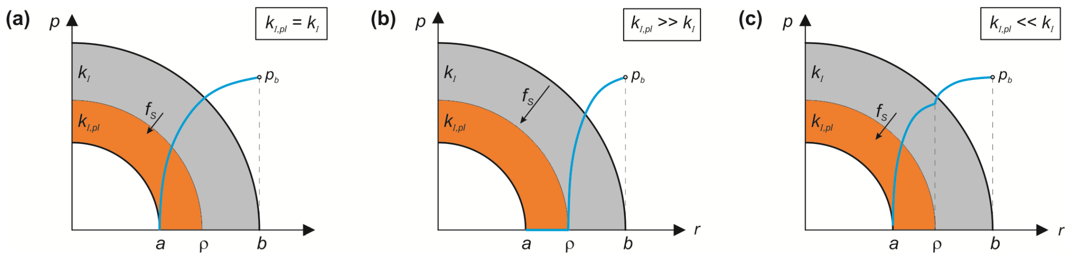

***Figure 6.3** Schematic sketch of pore pressure distribution p in a grouting body considering (a) uniform permeability, (b) an increased permeability due to plastification and, (c) a decreased permeability due to stress redistribution*

6.2.3 Solution method and dimensioning criterion

Due to the various assumptions been made, the system is rotational symmetric to the tunnel axis. As the length of the fault zone is assumed to be infinite (which is a conservative assumption in case encountering short fault zones; [40]), plane strain conditions apply.

Each independent structural element of the static system is described by means of its characteristic line (also known as "ground response curve") expressing the interdependence between radial stress σ and radial displacement u. The characteristic line for the total structure is achieved by providing the mechanical requirement of equilibrium and compatibility at the boundaries between adjacent elements; *i.e.* continuity of both radial stress and displacement. The system can be subdivided any further (*e.g.* into an elastic and a plastic zone, see Fig. 6.2) and reassembled to the overall system providing continuity at the interfaces.

Each's element stiffness and bearing capacity influences the stress distribution in the overall static system. Some parameters are pre-determined in a specific tunnelling situation (the mechanical properties of the untreated ground, the initial stress state prior to any measure, the water pressure); some may be chosen by the engineer: the tunnel lining support, the diameter and the material properties of the grouting body and the drainage measures.

In tunnelling practice, tunnel linings provide typically a support of $\sigma_a < 1$ MPa. Grouting bodies with a diameter corresponding to two or at most three times the tunnel diameter proved to be adequate [34]. Injections usually allow uniaxial compressive strength up to $f_{cI} = 4\text{-}5$ MPa (strength of lean concrete). When the strength of the grouting body is inadequate or the load too high, the grouting body plastifies up to the plastic radius ρ (Fig. 6.2). An extensive plastification may lead to loosening of the grouting body, which impairs its sealing effect, and/or may lead to inner erosion. Thus limiting plastification constitutes another dimensioning criterion, which is in the following referred to as "degree of plastification"

$$\lambda = \frac{\rho - a}{b - a} \quad , \tag{6-4}$$

i.e., the share of the plastic zone ρ of the extent of the grouting body (b - a).

The derivation of all analytical equations considering ideal drainage measures, as well as the matlab-codes used for this study, are given in Zingg [62].

6.3 Effect of ideal drainage of the grouting body

The effect of ideal drainage is discussed by means of the application example of Figure 6.4. Similar to the degree of plastification (Eq. (6-4)), a "degree of drainage" is introduced, which quantifies the share of the drained part of the grouting body:

$$\eta = \frac{l - a}{b - a} \quad . \tag{6-5}$$

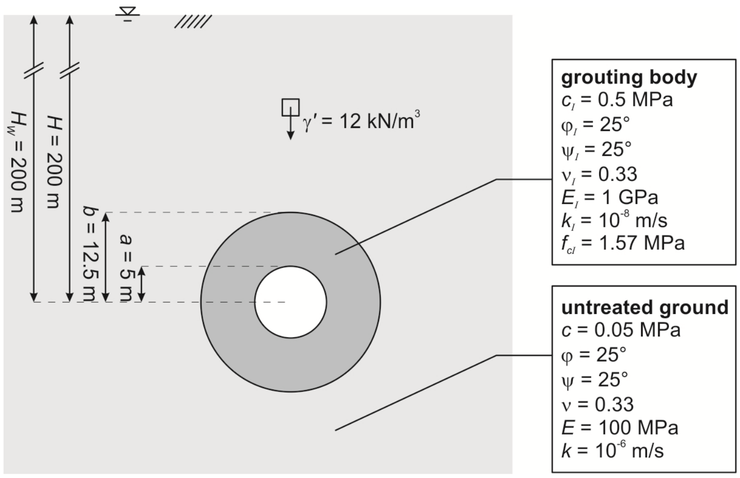

Figure 6.4 *Problem layout of the tunnel example*

6.3.1 Ideal drainage after grouting

6.3.1.1 Characteristic line

Figure 6.5 shows the characteristic line of our tunnel example considering several degrees of drainage η. The case of the grouting body without drainage represents the upper borderline case (red line for $\eta = 0$ in Fig. 6.5). The lining support pressure σ_a steeply decreases for small displacement of the excavation boundary u_a, but then stays nearly constant. In other words, the grouting body is too weak and the excavation boundary tends to close the opening completely for a lining support pressure of less than $\sigma_a = 1$ MPa.

Increasing the degree of drainage favours both support and displacement of the excavation boundary (indicated by black lines for $0 < \eta < 1$ in Fig. 6.5). For very low displacement, the characteristic lines coincide (which is due to the assumption of a very stiff grouting body with $u_b = 0$: "the total load acting on a stiff grouting body will be equivalent to σ_0 irrespectively of any drainage"; [40]). But with increasing displacement, ideal drainage decreases the required support pressure. The case of an ideally drained grouting body represents the lower boundary (green line for $\eta = 1$ in Fig. 6.5).

To give an example, assume the profile in our tunnel example to allow for a displacement of $u_a = 0.2$ m. An ideal drainage degree of $\eta = 0.2$ decreases the lining support pressure by about 30% compared to the upper boundary of no drainage (compare points A to B in Fig. 6.5). Increasing the degree of drainage lowers the required support, but with decreasing effect (compare point A to B to C in Fig. 6.5). A drainage degree of $\eta > 0.6$ finally provides no additional benefit and the lines coincide with the characteristic line of and ideally drained grouting body (point D in Fig. 6.5).

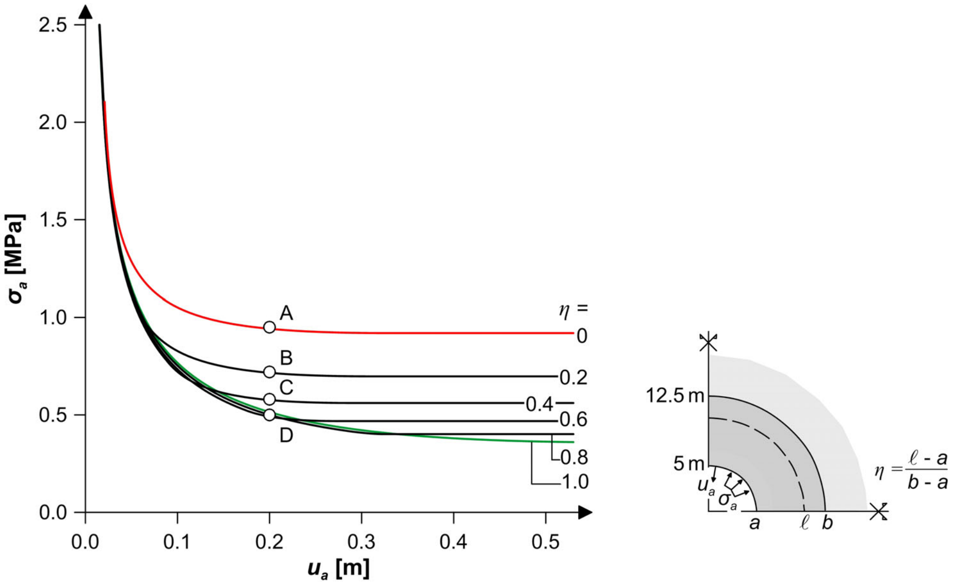

Figure 6.5 *Characteristic lines for several degrees η of drainage after grouting (parameters see Fig. 6.4)*

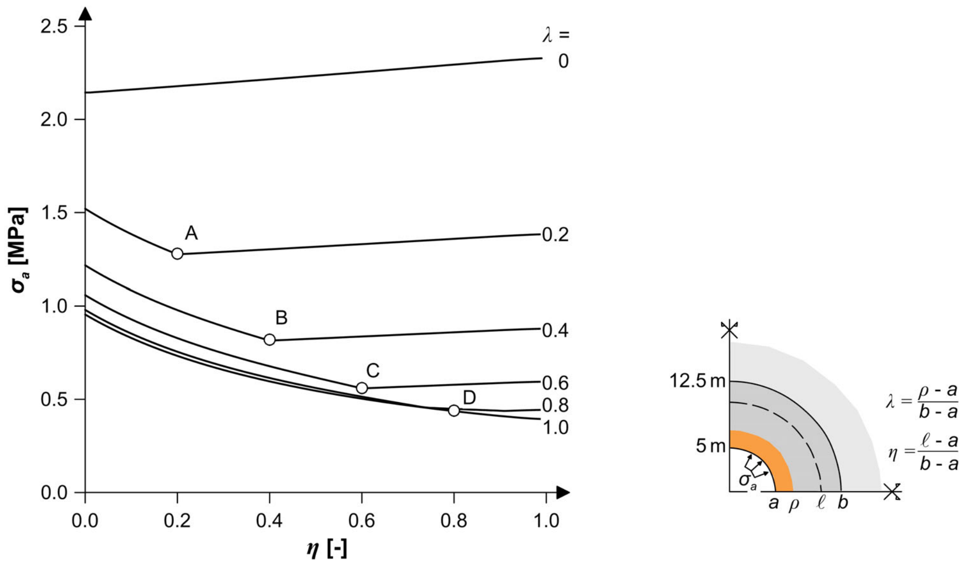

Figure 6.6 *Support pressure σ_a as a function of the degree η of drainage after grouting and for several degrees of plastification λ (parameters see Fig. 6.4)*

6.3.1.2 Radius of drainage and plastification

The lining support pressure σ_a as a function of the degree of drainage η is shown in Figure 6.6 when considering several degrees of plastification λ of the grouting body. For grouting bodies at purely elastic stress state ($\lambda = 0$ in Fig. 6.6), the support pressure increases with increasing drainage degree. On the other hand for a fully plastified grouting body ($\lambda = 1$ in Fig. 6.6), the support pressure decreases with increasing drainage degree, *i.e.* drainage is tentatively unfavourable for stability. For a partially plastified grouting body ($0 < \lambda < 1$ in Fig. 6.6), a combination thereof is observed: the required support pressure first decreases, then increases. The lowest support pressure is required at the point of discontinuity $\lambda = \eta$ (points A-D in Fig. 6.6) and thus represents the optimal drainage degree. A higher drainage degree offers no benefit in terms of support, but on the contrary is tentatively unfavourable for the stability of the grouting body due to the risk of inner erosion caused by high gradients prevailing in the outer ring of grouting body.

6.3.1.3 Required strength of grouting body

In the course of pre-dimensioning, the engineer might have determined the admissible degree of plastification $\lambda = 0.6$ and now needs to quantify both strength and lining support pressure for grouting bodies fulfilling that requirement (Fig. 6.7). The necessary uniaxial compressive strength f_{cI} depends linearly on the support pressure σ_a. Drainage degrees smaller than the degree of plastification require a higher support or strength, respectively ($\eta < \lambda = 0.6$ in Fig. 6.7).

In case of choosing a drainage degree equal to the degree of plastification ($\eta = \lambda = 0.6$), the grouting body is stable for the combination of strength $f_{cI} = 1.65$ MPa and support pressure $\sigma_a = 0.5$ MPa (point A in Fig. 6.7). If only a support pressure of $\sigma_a = 0.25$ MPa is provided, the strength of the grouting body has to be increase to $f_{cI} = 2.24$ MPa (point B in Fig. 6.7).

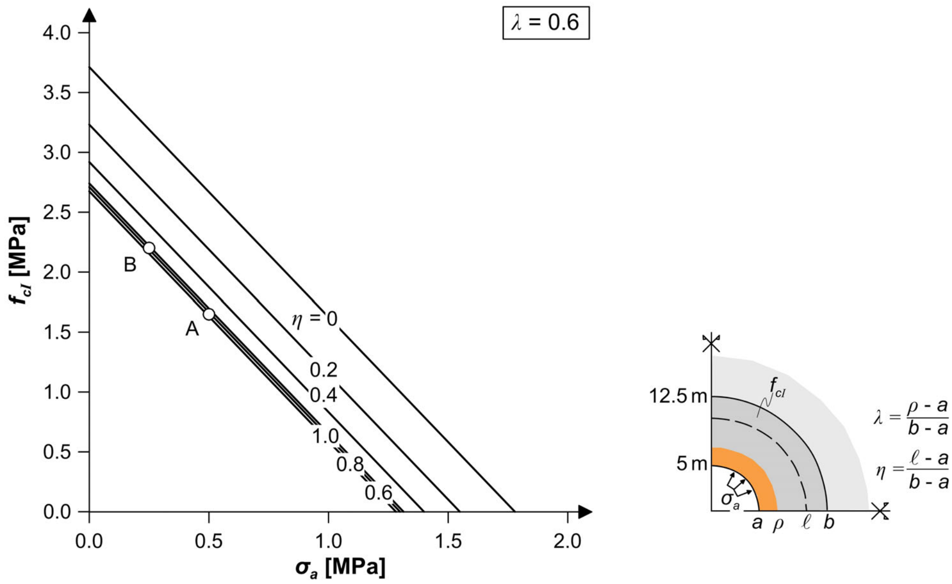

Figure 6.7 *Required uniaxial compressive strength f_{cI} as a function of the support pressure σ_a for several degrees η of drainage after grouting (parameters see Fig. 6.4)*

6.3.1.4 Parametric study

A parametric study was conducted concerning the lining support pressure σ_a as a function of the degree of plastification λ when varying the decisive design parameters of a grouting body: the geometry (b/a), the required uniaxial compressive strength (f_{cI}) and the degree of drainage η (Table 6.1). The results are shown in Figure 6.8. (Note that the marginal deviation in lining support pressure at the onset of plastification (*i.e.,* at $\lambda = 0$) is due to the slow increase in support pressure with increasing degree of drainage η; *cf.* Fig. 6.6.)

Drainage of the inner part of the grouting body decreases the required lining support pressure only if a plastification of at least 10% of the grouting body is admissible. For lower degree of plastification, the lining support pressures coincide for all considered parameters (compare plots for $\lambda < 0.1$ in Fig. 6.8).

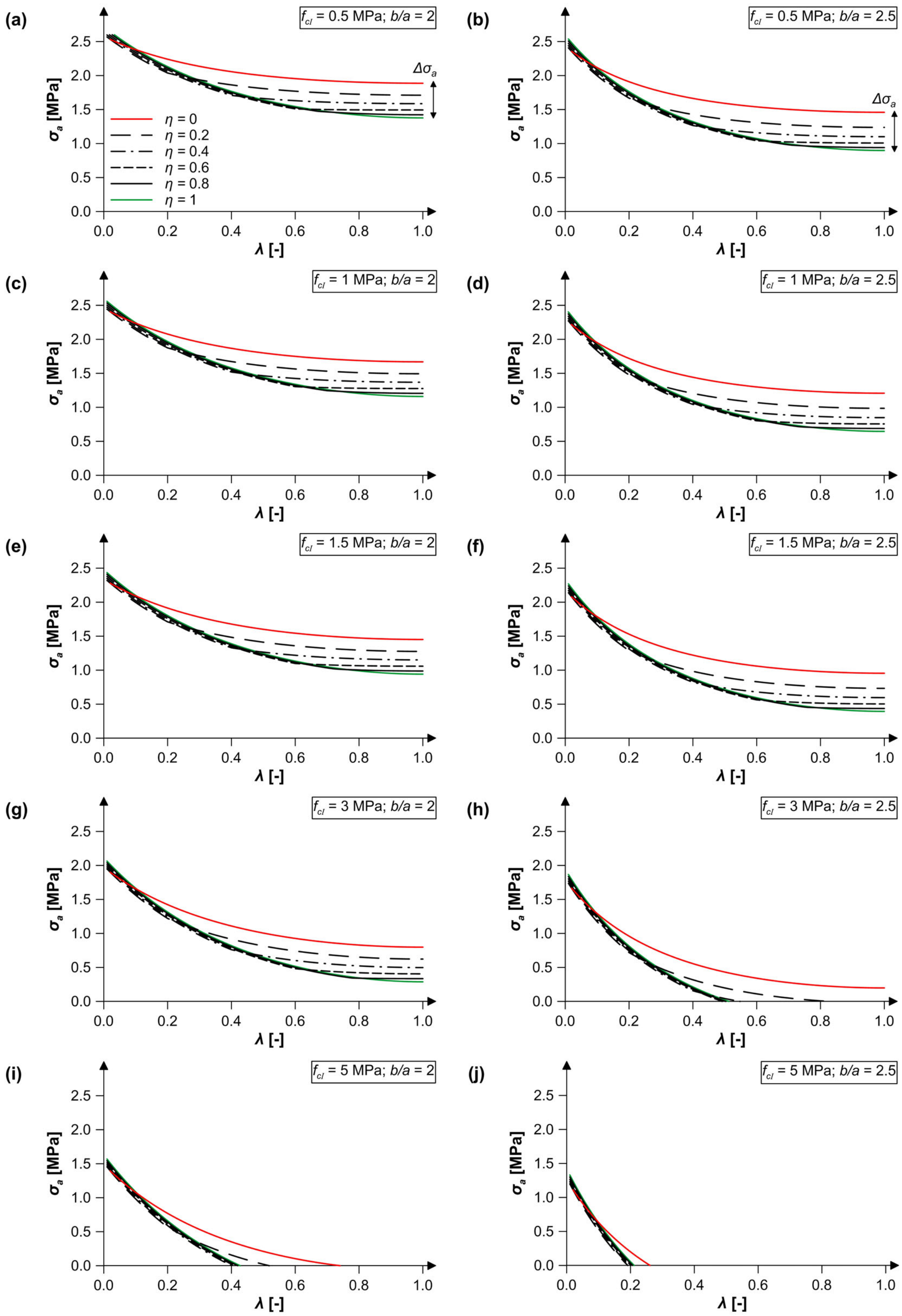

Figure 6.8 *Required lining support pressure* σ_a *as a function of the degree of plastification* λ *for the parametric study of Table 6.1*

In case of aiming at a degree of plastification of $\lambda = 0.3$, the required lining support pressures coincide for all degree of drainage $\eta \geq 0.2$ independently of the size or the stiffness of the grouting body in our parametric study (compare Fig. 6.8 for $\lambda = 0.3$). For higher degree of plastification, the required support clearly depends on the degree of drainage. An increase of degree of drainage from $\eta = 0$ to 0.2 decreases the required support more than an increase from $\eta = 0.6$ to 0.8 (in evidence *e.g.* for $\lambda = 1$ in Fig. 6.8b).

A drainage degree of $\lambda = 0.8$ necessitates a value of lining support pressure comparable to the one required in case of a completely drained grouting body ($\lambda = 1$), but with benefit of (at least some) sealing effect.

The bigger the grouting body, the larger are the differences in support pressure required when considering minimum or maximum drainage degree (compare *e.g.* $\Delta\sigma_a$ of Fig. 6.8a to 6.8b).

Grouting bodies of $b/a = 2$ are only expedient when having high compressive strength ($f_{cI} > 3$ MPa for our tunnel example, Fig. 6.8). Otherwise, they do not allow for a practically feasible support pressure of about $\sigma_a < 1$ MPa, even for full plastification (see *e.g.* Fig. 6.8c). Of course, the support pressure decreases with increasing strength and size of the grouting body (compare *e.g.* Fig. 6.8i to 6.8j).

Table 6.1 *Problem layout of the parametric study of Figure 6.8*

Problem layout		
Total stresses, in-situ	σ_0	4.4 MPa
Pore water pressure, in-situ	p_0	2.0 MPa
Radius of tunnel excavation	a	5 m
Radius of influence for seepage flow	R	200 m
Ratio of permeability of grouting body to untreated ground	k_I/k	0.01
Poisson's ratio of grouting body	ν_I	0.33
Angle of internal friction equal to angle of dilatancy	$\varphi_I = \psi_I$	25°
Variable design parameters for grouting body		
Degree of drainage	η	0-1
Degree of plastification	λ	0-1
Ratio of radii of grouting body to excavation	b/a	2, 2.5
Uniaxial compressive strength	f_{cI}	0.5-5 MPa

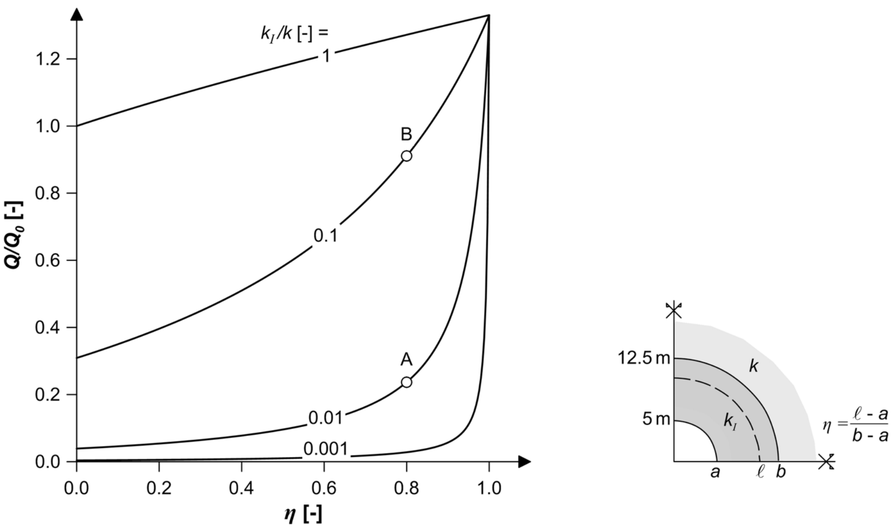

Figure 6.9 *Inflow Q (normalized with the inflow when considering untreated ground Q_0) as a function of the degree η of drainage after grouting when considering several permeability ratios k_I/k (other parameters see Fig. 6.4)*

6.3.1.5 Water inflow

One intention of injection measures may be reducing the water inflow into the tunnel. Figure 6.9 shows the normalized inflow as a function of the degree of drainage η. In case of equal permeability of grouting body and untreated ground ($k_I/k = 1$ in Fig. 6.9), the inflow linearly increases with increasing degree of drainage η (*i.e.* increasing radius of drainage l). The lower the permeability ratio and the lower the degree of drainage, the higher is the sealing effect of the injection body.

Consider as an example ideal drainage of 80% of the grouting body (η = 0.8 in Fig. 6.9). In case grouting reduces the permeability to 1/100 of the initial value, inflow is reduced considerably to $Q/Q_0 = 0.23$ (point A in Fig. 6.9). But in case sealing grouting is less successful and decreases permeability only to 1/10, water inflow is only reduced to 90% of the inflow collected in untreated ground (point B in Fig. 6.9).

6.3.2 Ideal drainage in advance of grouting

6.3.2.1 Characteristic line

Figure 6.10 compares the characteristic line for drainage *prior* or *after* grouting. Drainage in advance of grouting is clearly favourable concerning stresses and displacement of the excavation boundary.

Assume as an example a feasible tunnel support of $\sigma_a = 0.8$ MPa. The displacements in case of drainage in advance of grouting are 6 cm (point C in Fig. 6.10) and correspond to a degree of plastification of 32% (aiming at a lower degree of plastification would require an increase of the strength or the diameter of the grouting body – or to install a higher tunnel support). Drainage after grouting leads to 8.5 cm displacement (point D in Fig. 6.10), which is about 50 % more than with drainage prior to grouting.

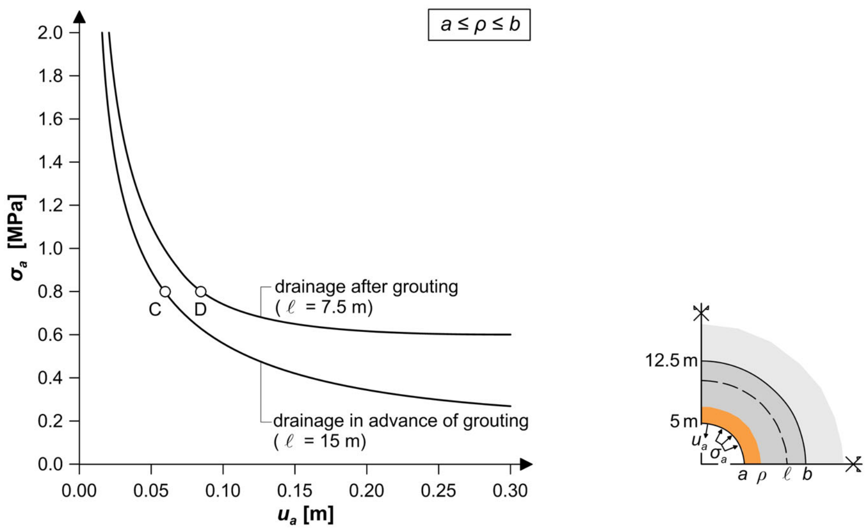

Figure 6.10 *Comparison of the characteristic lines of drainage in advance of grouting to drainage after grouting (parameters see Fig. 6.4)*

6.3.2.2 Dimensioning aids

Anagnostou and Kovári [40] provide dimensioning aids allowing a simple and fast pre-dimensioning of grouting bodies in “dry” fault zones in the form of normalized nomograms for variable parameters to be chosen by the engineer (*e.g*. geometry, stiffness, lining support pressure etc.). These dimensioning aids apply for drainage in advance of grouting when using σ'_{bDR} according to Eq. (6-7) of Zingg [62] instead of σ'_b in Figures 5.3-1 to 5.3.4 of Anagnostou and Kovári [40].

6.3.3 Assumption of stiff grouting body

In our analytical model, we assume the grouting body to be very stiff and thus experiencing no displacement at its outer boundary ($u_b = 0$ at $r = b$; *cf.* [40]). But displacements u_b during plastification depend on the stresses acting at $r = b$ and the stiffness of the grouting body (*i.e.* size *b*/*a*, strength f_{cI} and degree of plastification λ). Lines C and D in Figure 6.11 indicate a displacement of about $u_b = 8$ cm for our tunnel example in the worst-case of full plastification of the grouting body ($\lambda = 1$), virtually independent of drainage in advance or after grouting. This displacement is only 6 ‰ of the radius of the grouting body. By neglecting it, the analytical model marginally overestimates the stresses acting on the grouting body, *i.e.* the solution is slightly safe-side concerning stresses and displacement of the excavation boundary.

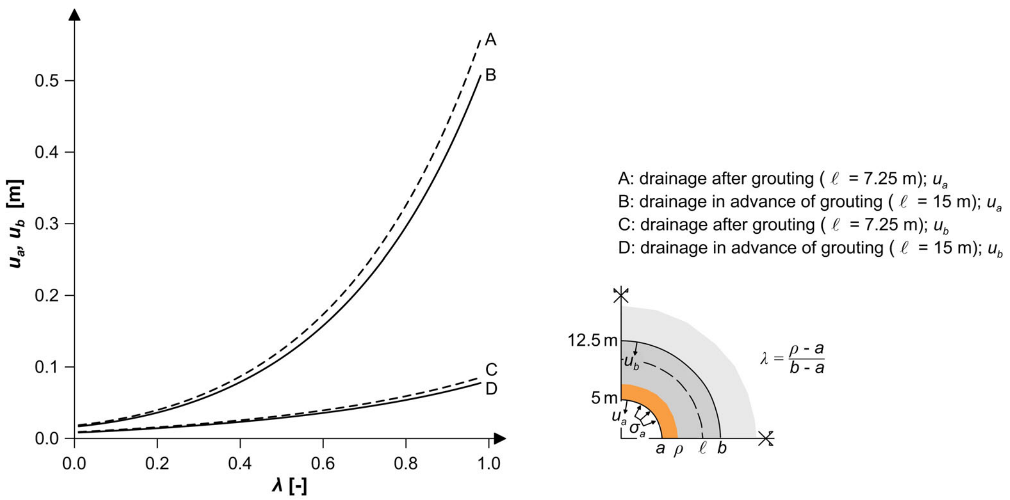

Figure 6.11 *Displacement of the inner (u_a) and outer (u_b) boundary of the grouting body as a function of the degree of plastification λ for drainage in advance and after grouting (parameters see Fig. 6.4)*

6.4 Modelling specific drainage borehole arrangements

6.4.1 Problem and approach

In the previous sections, complete pore pressure relief due to ideal drainage was assumed. We stay with the tunnel example of Figure 6.4, but now, the pore pressure relief resulting from specific borehole arrangements will be considered and the characteristic lines are determined by FE-modelling.

6.4.2 Arrangement of drainage boreholes

Pore pressure relief resulting from several different borehole arrangements are investigated. For drainage in advance of grouting, drainage boreholes coaxial to the tunnel axis are considered. For drainage subsequent to construction of the grouting body, radial drainage borehole arrangements are studied.

The borehole arrangements considered for drainage *in advance of grouting* can be grouped in three drainage layouts (Fig. 6.12): Layout A considers drainage boreholes of diameter 10 cm evenly spaced around the circumference of $r = l$ ($l \geq b$; Fig. 6.12a). Layout B comprises lateral drainage boreholes of 10 cm diameter each, arranged in horizontal centre distance l to the tunnel axis and of vertical spacing y_{DR} (Fig. 6.12b). For the purpose of comparison, ideal drainage is modelled assuming pore pressure relief within the radius $r = l$ ($l \geq b$; Fig. 6.12c). The geometric values are given in the table within Figure 6.12.

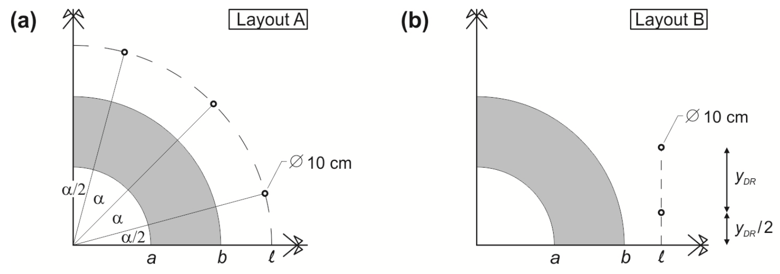

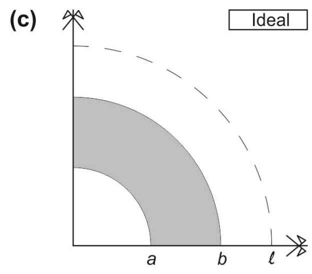

Number n of boreholes in cross-section:

	a [m]	b [m]	y_{DR} [m]	ℓ [m]
n = 4	5.0	10.0	10.0	12.0
	5.0	12.5	10.0	14.8
	5.0	15.0	10.0	17.6
n = 8	5.0	10.0	8.7	11.4
	5.0	12.5	10.9	14.2
	5.0	15.0	12.9	16.9
n = 16	5.0	10.0	4.0	10.9
	5.0	12.5	5.3	13.8
	5.0	15.0	6.4	16.3

Figure 6.12 *Drainage layouts considered for drainage in advance of grouting: a) coaxial drainage boreholes evenly spaced along the circle line $r = l$ ("layout A"), (b) lateral arrangement of coaxial drainage boreholes ("layout B") and (c) ideal drainage of the area $l \geq b$*

Figure 6.13 shows the group of borehole arrangements considered for *drainage measures after grouting*. Ideal drainage (Fig. 6.13a) assumes pore pressure relief within the radius $r = l$ ($a \leq l \leq b$) and serves for the purpose of comparison to the analytical solution. The two-dimensional layout simulates drainage slits of 10 cm diameter, which are evenly spaced at sector angle α around the circumference (Fig. 6.13b; plane strain conditions). Both length l ($a \leq l \leq b$) and number n of boreholes per cross-section are investigated (n = 1-60). The three-dimensional drainage layout (Fig. 6.13c) simulates 12 drainage boreholes (α = 30°) of 10 cm diameter each. The study considers several length of boreholes *l* ($a \leq l \leq b$) and varies the spacing *e* of the boreholes coaxial to the tunnel axis from 1.25 to 10 m.

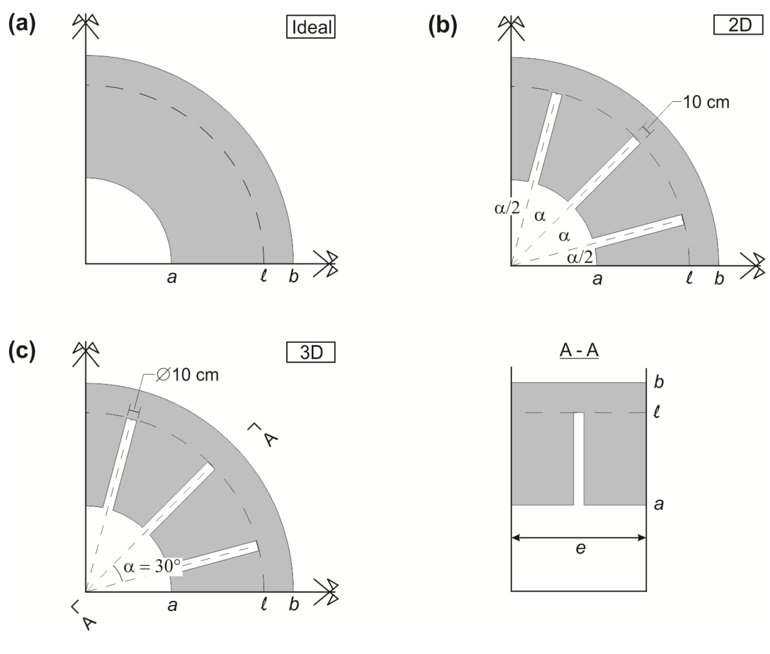

Figure 6.13 *Drainage layouts considered for drainage after grouting: (a) ideal drainage of area $l \leq b$, (b) radial drainage slits considered in the two-dimensional model (plane strain) and (c) radial drainage boreholes considered in the three-dimensional model*

6.4.3 Computational model

Figure 6.14 shows the problem layout for a representative drainage arrangement. As in the previous sections, it considers a deep, circular tunnel of radius a and the grouting body in form of a thick-walled cylinder of outer radius b in plane strain condition. The ground (both untreated and injected) is considered as an elasto-plastic porous medium obeying the principle of effective stresses, Coulomb's failure criterion and Darcy's law. Associated flow rule is assumed. The initial stress state of untreated ground is assumed to be homogeneous and isotropic; the magnitude of the effective initial stress σ_0' equals to the effective overburden pressure. The initial water pressure p_0 acts at a radial distance R from the tunnel, with R being equal to the height of the undisturbed water table above the tunnel. The lining support pressure σ_a is assumed uniform along the excavation boundary $r = a$. The boundaries of excavation and drainage boreholes represent seepage faces of atmospheric pressure ($p = 0$). At the axis of symmetry, a no-flow boundary-condition is assumed and no normal displacement is allowed.

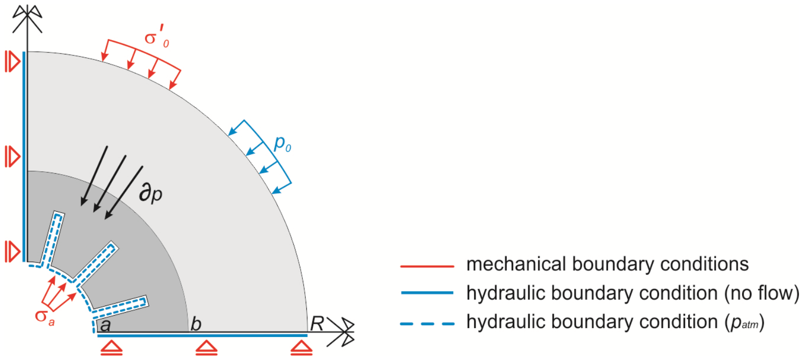

Figure 6.14. *Computational model for the numerical analyses*

The FE-model considers the sequential coupling of hydraulic analysis influencing the mechanic analysis by augmenting the effective stresses in the equations of the mechanical equilibrium by the spatial gradients of fluid pressure ∇p (*e.g.* Potts [119]). The used FE-code (Comsol [55]) enables manual coupling of hydraulic and mechanical analysis. The implementation was verified by comparison to results of a built-in routine in the FE-code of Abaqus (steady-state consolidation; [120]) and Hydmec [121]. Additionally, the FE-Model was validated by comparing the characteristic lines of the analytical and numerical model by Zingg [62].

The computational steps are described for drainage in advance and after grouting separately (see below).

6.4.3.1 Computational steps: drainage in advance of grouting

Figure 6.15 shows the sequence of computational steps simulating drainage in advance of constructing the grouting body and subsequent excavation of the tunnel for representative drainage layout A. The hydraulic step H1 calculates the hydraulic head field due to the drainage measure. The mechanical step M1 serves for initialisation of the stresses in the untreated ground. Step M2 incorporates the spatial derivative of the pore pressure field resulting from step H1, considers the initial stresses of step M1 and calculates the increased stresses due to consolidation. In step H2, the pore pressure field when considering the changed permeability due to the grouting body is computed. Step M3 considers the pore pressure field resulting from step H2 and the initial stresses of step M2, and computes the stress-field after injection (no displacements allowed at the future excavation boundary). The last hydraulic step H3 calculates the pore pressure field due to excavation. The final mechanical step M4 (considering the initial stresses of step M3 and pore pressure field of step H3) simulates the excavation of the tunnel by step-by-step reduction of σ_a. For evaluation of the displacements u_a at the excavation boundary, step M4 is considered only.

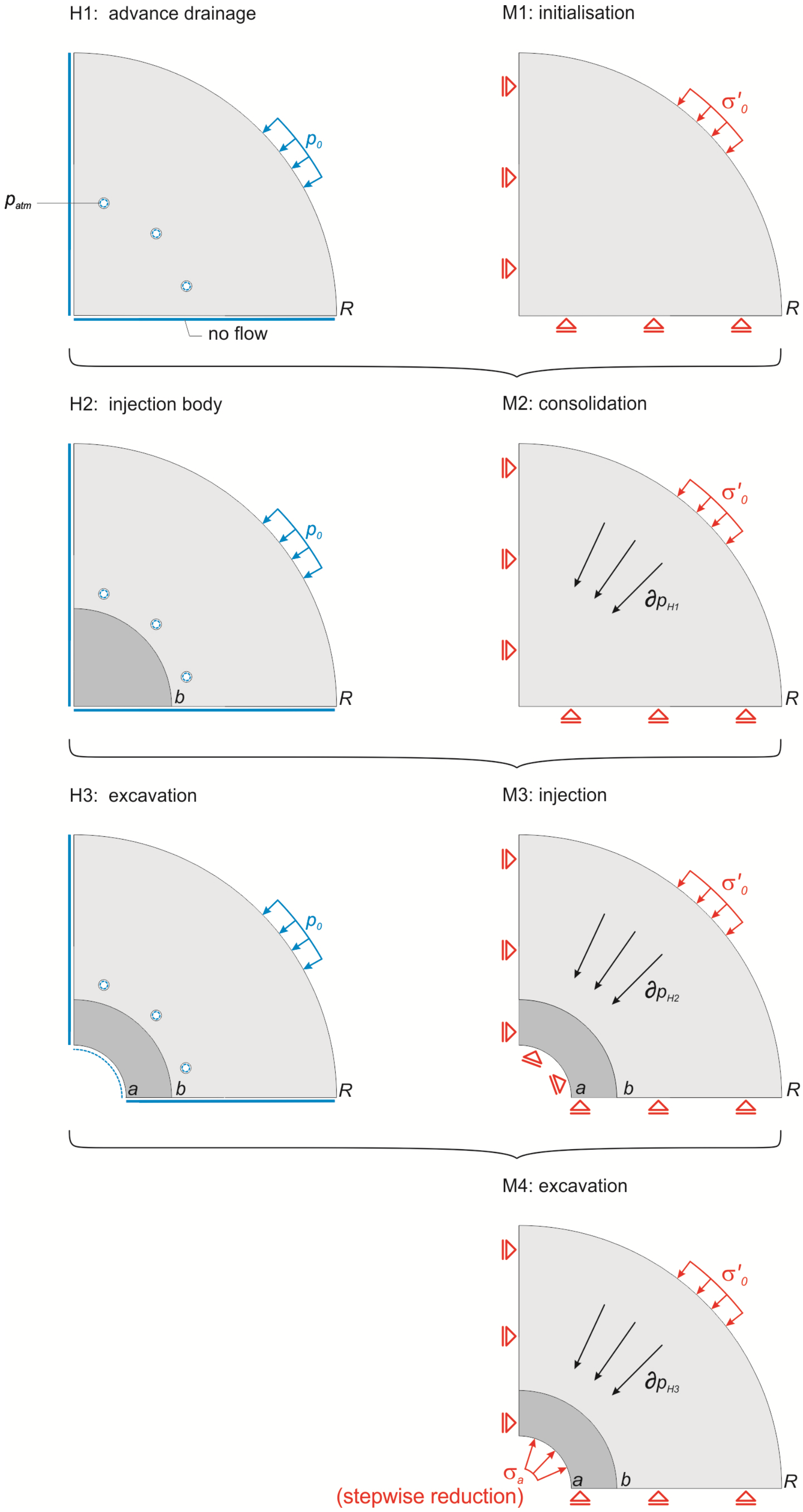

Figure 6.15 *Computational steps of the numerical model simulating drainage in advance of grouting and subsequent excavation of the tunnel*

6.4.3.2 Computational steps: drainage after grouting

Figure 6.16 depicts the sequence of computational steps simulating the grouting body with subsequent drainage and excavation of the tunnel for a representative drainage layout. The only hydraulic step H calculates the hydraulic head field due to excavation and drainage measure, which are assumed to take place simultaneously. Mechanical step M1 is used for initialisation of the stresses acting in the untreated ground and the grouting body. Step M2 incorporates the spatial derivative of the pore pressure field resulting from step H, considers the initial stresses of step M1 and calculates the increased stresses due to consolidation. At the future excavation boundary a no displacements are allowed. Still incorporating the spatial derivative of the pore pressure field resulting from step H, but considering the initial stresses of step M2, the final step M3 calculates the excavation of the tunnel by stepwise reduction of σ_a. For evaluation of displacements u_a at the excavation boundary, step M3 is considered only.

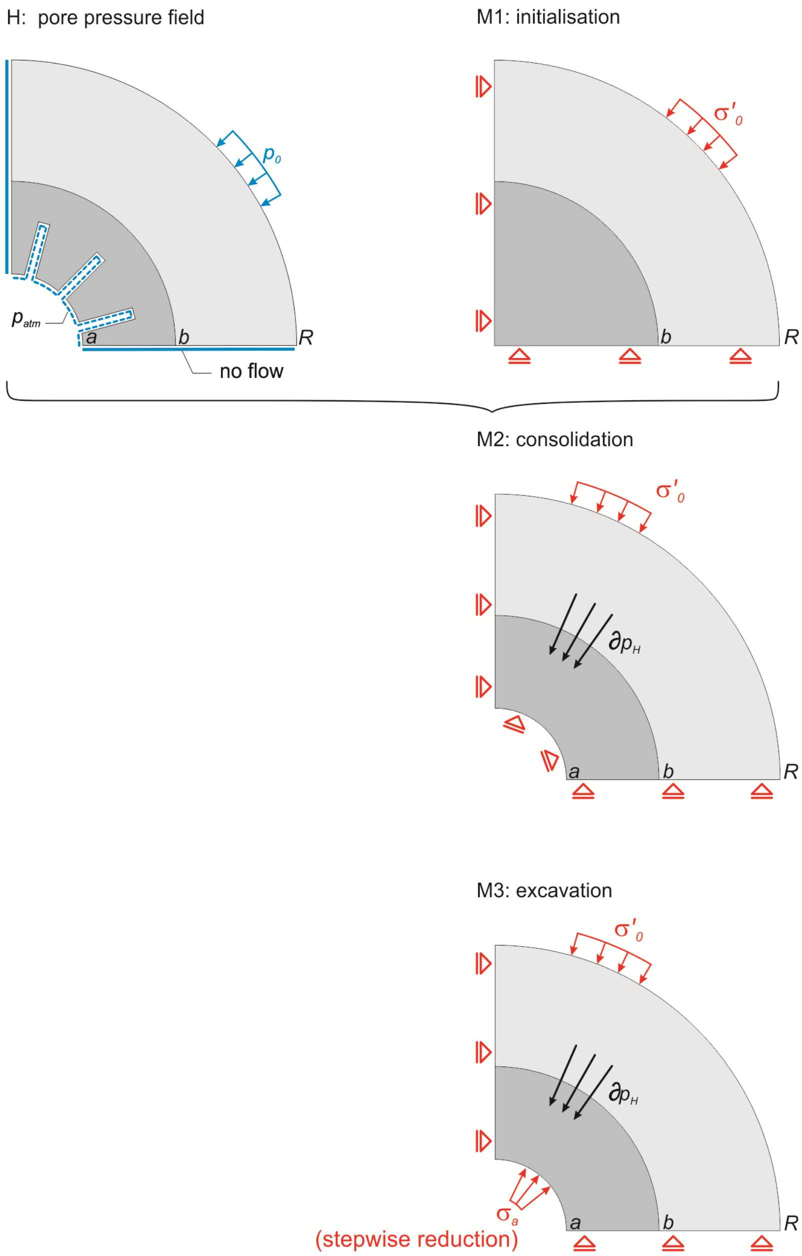

Figure 6.16 *Computational steps of the numerical model simulating drainage after grouting and subsequent excavation of the tunnel*

6.5 Effect of drainage borehole arrangements drilled after grouting

6.5.1 Drainage slits (2D-model)

6.5.1.1 Number of drainage slits

Figure 6.17 shows the hydraulic head field of the two-dimensional drainage layouts (Fig. 6.13b) for variable number n of drainage slits of length l =11 m, as well as for the belonging boundary cases without and with ideal drainage. In the grouting body without drainage, pore water pressure dissipates mainly within the grouting body and nearly 2 MPa of water pressure acts on the outer boundary of the grouting body (Fig. 6.17a). In case of 4 drainage slits, the pressure is slightly reduced to p_b = 1.9 MPa, but the number of drainage slits is too small to relief pressure overall within the grouting body (Fig. 6.17b). Increasing the drainage number to n =12 (Fig. 6.17d; p_b = 1.75 MPa) provides a good approximation to the ideally drained case (Fig. 6.17f; p_b = 1.6 MPa), where very high hydraulic gradients act within the outer ring of the grouting body.

The pore pressure relief within the grouting body is plotted in Figure 6.18 as a function of the number n (or the sector angle α, respectively) of drainage slits. The pressure decreases steeply for low number of drainage slits and then levels out for larger amounts. Increasing the number of drainage slits above n = 20 (α < 18°) offers marginal utility concerning pore pressure relief, but would require an extremely high drilling effort in tunnelling practice. However, even very dense drainage slits (n = 60 or α = 6°) do not relief pressure as much as ideal drainage (point A in Fig. 6.18).

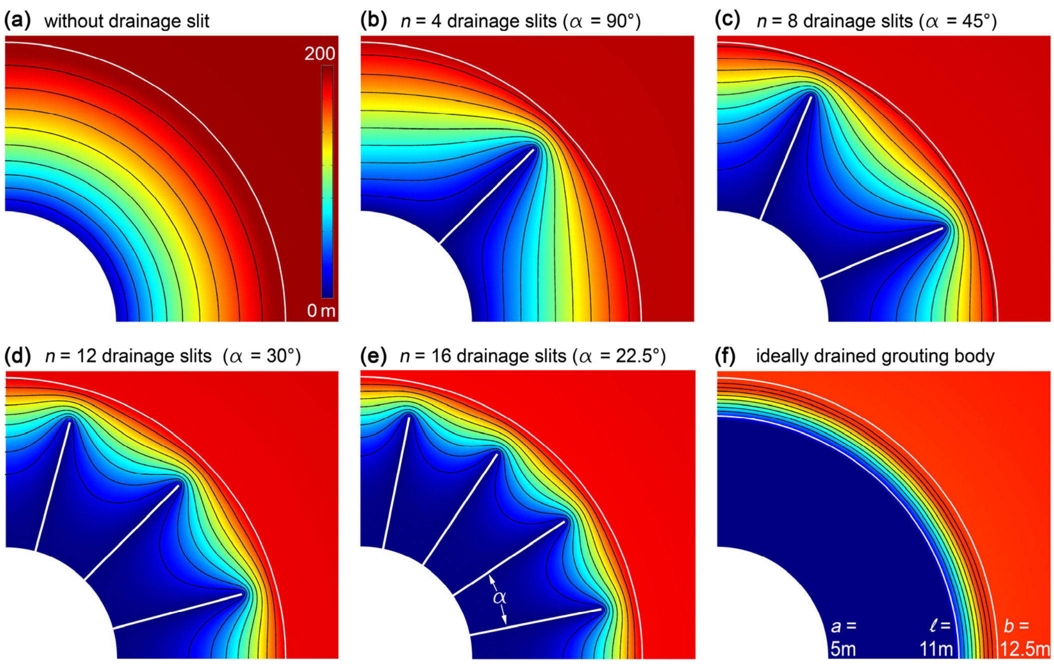

Figure 6.17 *Hydraulic head fields for several number n of drainage slits installed after grouting (η = 0.8; parameters see Fig. 6.4)*

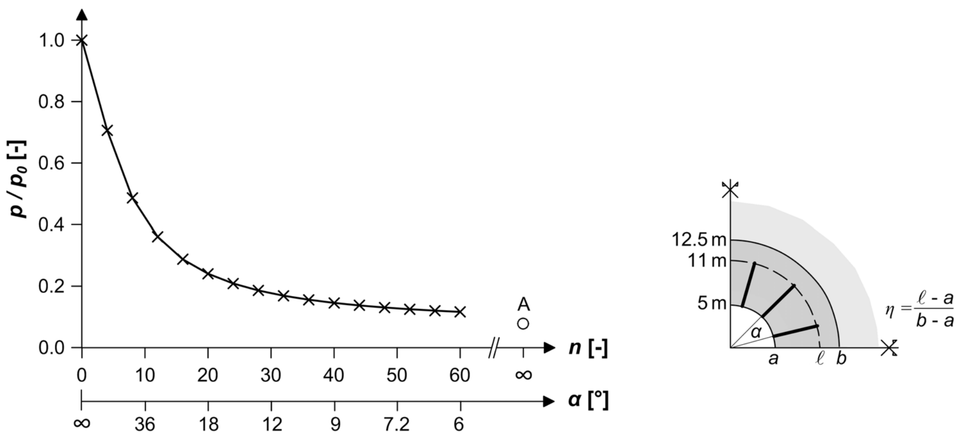

***Figure 6.18** Average pore pressure p in the grouting body normalized with the initial pressure p_0 as a function of the number n (or the sector angle α) of drainage slits installed after grouting (η = 0.8; parameters see Fig. 6.4)*

6.5.1.2 Plastic zones

During the stepwise reduction of the lining support pressure σ_a, a plastic zone develops starting from the inner boundary of the grouting body (orange area in Figs. 6.19 and 6.20b). The very high gradients between the outer boundary of the grouting body and the end of the drainage borehole (Fig. 6.19 and 6.20a) might lead to local overstressing of the grouting body.

In case of ideal drainage, an inner plastic zone appears at σ_a = 1.2 MPa (Fig. 6.19b). At a lining support pressure of σ_a = 0.45 MPa, plastification starts also from the outer, highly stressed boundary b of the grouting body (Fig. 6.19c). With decreasing lining support pressure (σ_a = 0.44 MPa in Fig. 6.19c), an outer plastic zone grows towards the excavation boundary. After merging of these two plastic zones, plastification may propagate outwards into the untreated ground.

In case of drainage boreholes, a second plastic zone develops from the outer boundary of the grouting body for lower support pressures (σ_a = 0.58 MPa in Fig. 6.20c), but in contrast to ideal drainage starting from local spots instead of the full ring (compare Fig. 6.19 to Fig. 6.20). A further decrease of lining support leads to plastic “bridges” between the inner and the outer plastic zone (Fig. 6.20d; σ_a = 0.57 MPa).

For our study, full plastification (*i.e.*, a degree of plastification λ = 1) is defined as the state where the first bridge between outer and inner plastic zone develops.

6.5.1.3 Required lining support pressure

The results of a parametric study into the effects of the numbers of drainage slits (n = 4, 8, 12, 16), the degrees of drainage (η = 0.4, 0.8, 1) and the size of grouting body (b/a = 2 and 2.5) is shown in Figure 6.21. The lower borderline case of the ideally drained grouting body is plotted in red; the upper borderline case of no drainage slits is shown in green.

As an example, we assume a maximum admissible degree of plastification of λ = 0.5 for a mid-size grouting body of b/a = 2.5, which is drained to a degree of η = 0.8 (Fig. 6.21b). In the best-case of ideal drainage, a lining support pressure of σ_a = 0.7 MPa would be required (A in Fig. 6.21b). The effect of 12-16 drainage slits nearly coincides with ideal advance drainage (σ_a = 0.7-0.73 MPa). In case of 8 drainage slits, the required support increases by 17% (to σ_a = 0.81 MPa; B in Fig. 6.21b). The case of only four drainage slits requires 50% more lining support pressure than the ideal case (compare C to A in Fig. 6.21b).

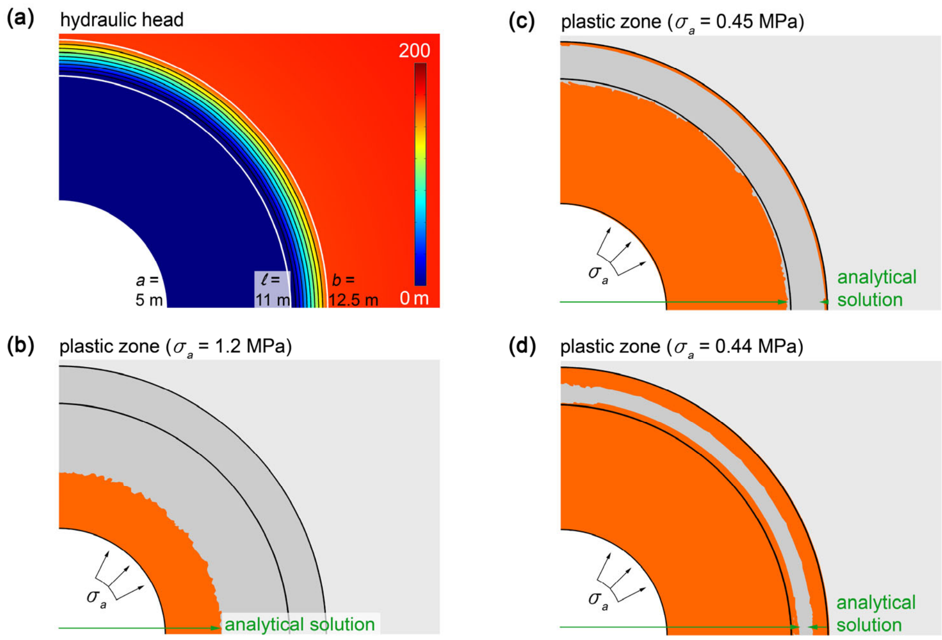

Figure 6.19 *(a) Hydraulic head fields and development of plastic zones for decreasing support pressure for ideal drainage after grouting: (b) single plastic zone for σ_a = 1.2 MPa, (c) second plastic zone for σ_a = 0.45 MPa and (d) σ_a = 0.44 MPa (extent of plastic zones according to the analytical model indicated with green arrows; parameters see Fig. 6.4)*

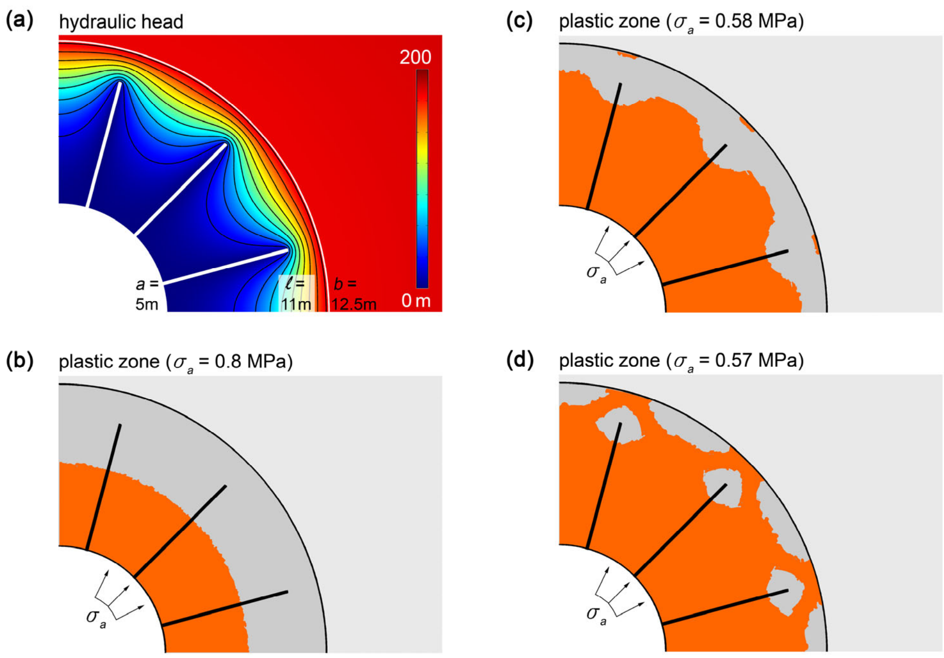

Figure 6.20 *(a) Hydraulic head fields and development of plastic zones for decreasing support pressure when considering drainage slits after grouting: (b) inner plastic zone for σ_a = 0.8 MPa, (c) additional plastic spots for σ_a = 0.58 MPa and (d) plastic "bridges" for σ_a = 0.57 MPa (η = 0.8; parameters see Fig. 6.4)*

The same trends apply overall in Figure 6.21. The higher the number of drainage slits, the better is of course the approximation to the ideal solution. However, 12 or more drainage slits provide a good approximation to the ideal solution (about 10-20% accuracy). For low degree of plastification up to $\lambda = 0.4$ (which is about the admissible degree of plastification in tunnelling practice for reasons of safety and usability), the required support pressures for both drainage lengths virtually coincide (less than 5% deviation for both $\eta = 0.4$ and 0.8).

The smaller the grouting body, the higher has to be the degree of drainage to allow for pressure relief at small drainage slit numbers. Otherwise (and as shown in Figures 6.21d and e for four drainage slits), the drainages have no effect on the required support. On the other hand and assuming slits piercing the entire grouting body ($\eta = 1$), already 4 drainage slits allow a considerable reduction of pore pressures and the lines for higher drainage numbers nearly coincide, independently of the size of the grouting body (Fig. 6.21c and 6.21f).

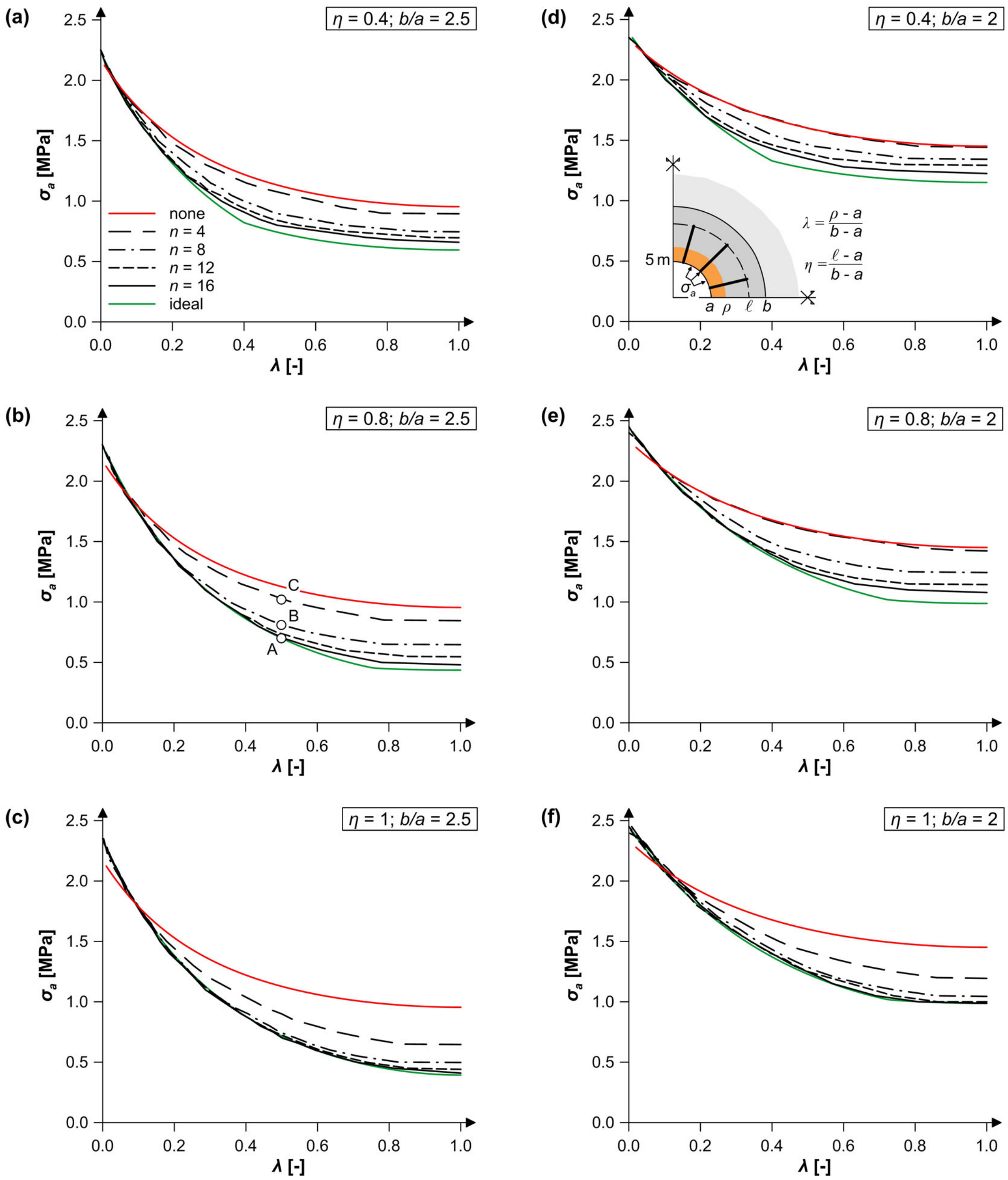

Figure 6.21 *Required lining support pressure σ_a as a function of the degree of plastification λ for drainage after grouting considering several numbers n of drainage slits, three degrees of drainage η and two sizes of grouting body b/a ($b = 12.5$ and 10 m; drainage layout see Fig. 6.13b; other parameters see Fig. 6.4)*

6.5.1.4 Inflow

Figure 6.22 shows the normalized inflow as a function of the degree of drainage η. Without any drainage measure ($\eta = 0$ in Fig. 6.22), the grouting body considerably reduces the inflow to about 4% of the inflow in untreated ground. The inflow increases with growing seepage area, *i.e.* with increasing number n of drainage slits and/or increasing degree of drainage η. The inflow considering drainage slits is lower than in the borderline case of ideal drainage (compare 'ideal' to other lines in Fig. 6.22). Reason is that although the seepage area increases when considering drainage slits compared to ideal drainage, the thereon acting hydraulic gradients are considerably smaller (see also Fig. 6.17).

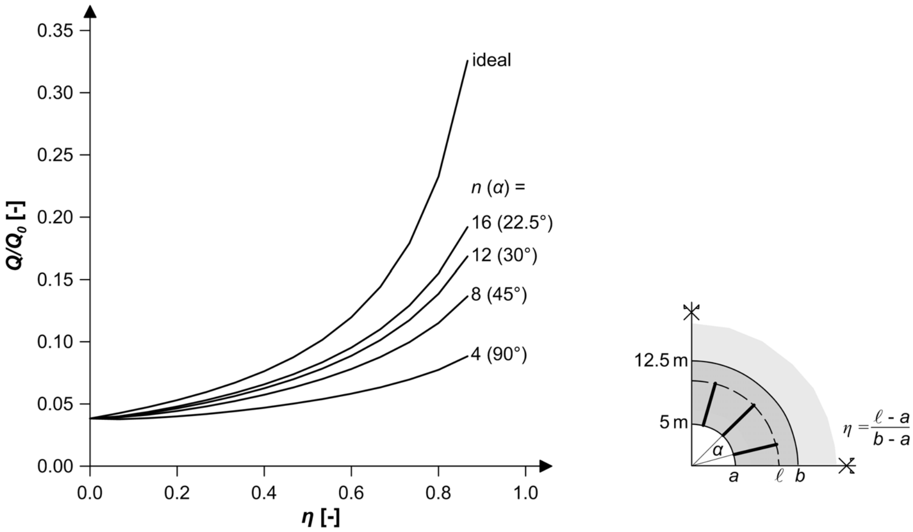

Figure 6.22 *Inflow Q collected from all boundaries of excavation and drainage (normalized with the inflow when considering untreated ground Q_0) as a function of the degree η of drainage after grouting (drainage layout see Fig. 6.13b; parameters see Fig. 6.4)*

6.5.2 Drainage boreholes (3D-model)

According to the results of the two-dimensional model, twelve drainage slits approximate the solution of ideal drainage reasonably well (Section 6.5.1.1). Thus we limit our considerations to 12 drainage boreholes in cross-section of the three-dimensional model and focus on the effect of axial borehole distance e and borehole length l (see Fig. 6.13c).

6.5.2.1 Axial borehole distance

Figure 6.23 shows the hydraulic head fields in the cross section (r.h.s.) and in the longitudinal section to the tunnel axis (l.h.s.) for the example of 11 m long boreholes. It is self-evident that the hydraulic head field of the drainage slits in the two-dimensional model (see Fig. 6.17d) is approximated best by a very small axial borehole distance e (*e.g.*, $e = 2.5$ m in Fig. 6.23a). But this is not expedient keeping in mind the required drilling effort for tunnelling practice. An almost homogeneous hydraulic head field in both radial and axial direction develops when keeping the axial distance e about equal to the middle centre-distance of the boreholes m (Fig. 6.23b with $e \approx m = 0.5(l+a) \cdot \tan\alpha = 4.6$ m). In case of longer axial borehole distance, the benefit of the number of drainage boreholes will be lost and the hydraulic head distribution in the axial direction is less favourable than in the radial (see Δr for $e = 10$ m in Fig. 6.23d).

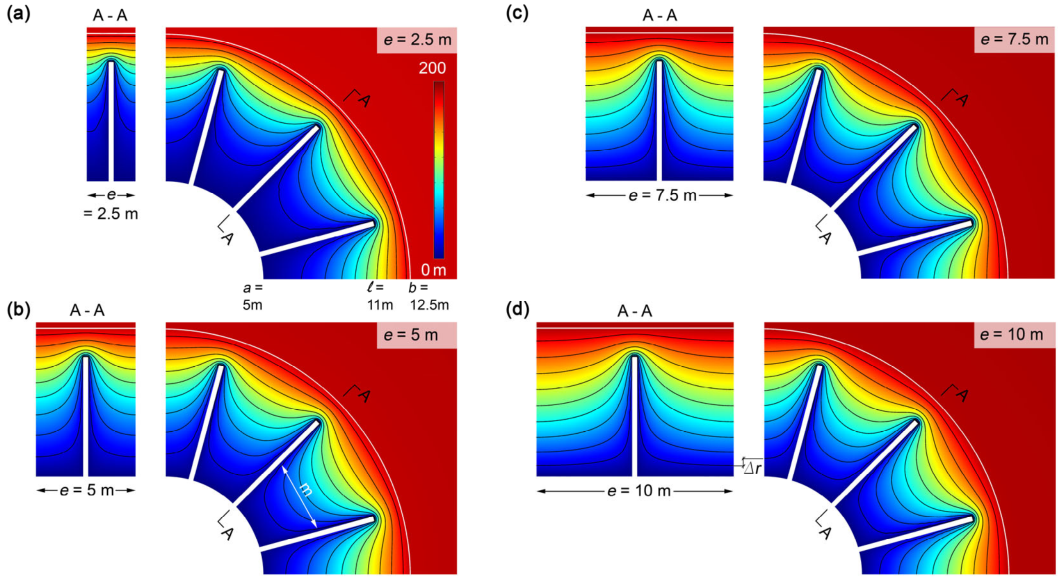

Figure 6.23 Hydraulic head field for 12 drainage boreholes drilled after grouting for several axial spacings e (drainage layout of Fig. 6.13c; other parameters see Fig. 6.4)

6.5.2.2 Required lining support pressure

A parametric study into the effects of the axial borehole spacing (e = 1.25-10 m; Fig. 6.13c) and borehole length (l = 11 m and 12.5 m or η = 0.8 and 1, respectively) was conducted. The required lining support pressure σ_a as a function of the degree of plastification λ is shown in Figure 6.24. Again, the lower borderline case of the ideally drained grouting body is plotted as green line; the upper borderline case of no drainage boreholes is shown as red line.

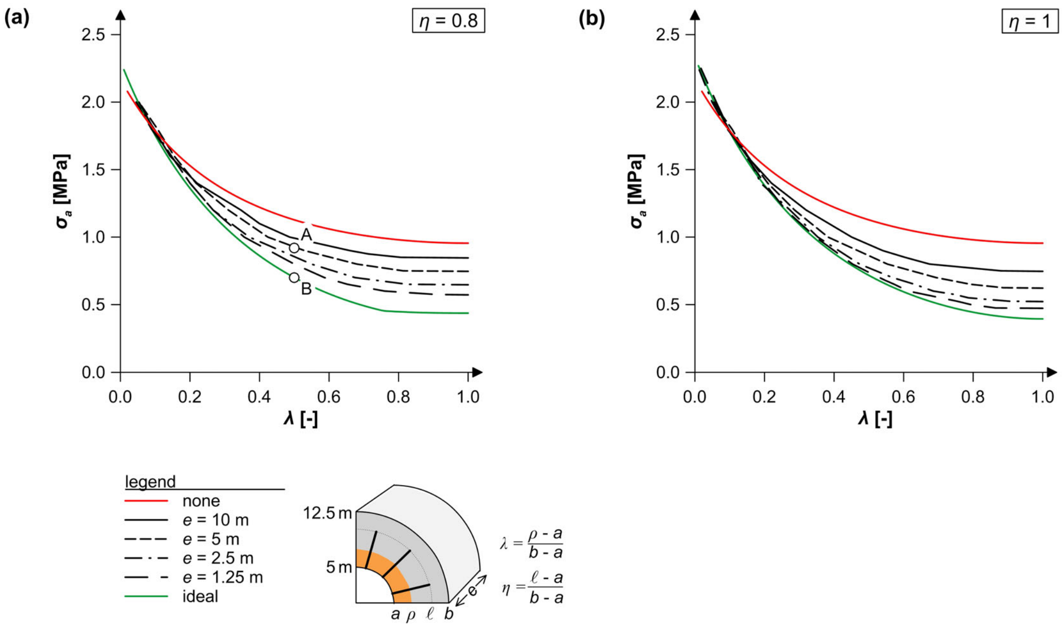

Figure 6.24 Required lining support pressure σ_a as a function of the degree of plastification λ for drainage after grouting. Drainage borehole arrangement of Figure 6.13c with variable axial spacing e for two degree of drainage η (parameters see Fig. 6.4)

An axial borehole distance of $e = 1.25$ m shows nearly the same support-plastification line as the two-dimensional case (compare Fig. 6.24a to Fig. 6.21b). In case of full degree of drainage ($\eta = 1$), this dense drainage layout nearly coincides with the ideal line (compare dotted to green line in Fig. 6.24b).

For larger axial borehole distance, the deviation to the case of ideal drainage increases fast. Assuming a maximum admissible degree of plastification of $\lambda = 0.5$, a lining support pressure $\sigma_a = 0.92$ MPa is required (point A in Fig. 6.24a for $\eta = 0.8$, $e = 5$ m), which is 30 % more than when considering ideal drainage ($\sigma_a = 0.7$ MPa, point B in Fig. 6.24a). However for the practical relevant ranges of plastification, the deviation to the ideal solution diminishes to only 3-12% (for $\lambda = 0.2$ and 0.3, respectively).

6.5.2.3 Comparison of characteristic lines

Assume a maximum feasible lining support pressure of $\sigma_a = 0.75$ MPa for the tunnel example of Figure 6.4. The engineer has to choose from the drainage arrangements sketched as insets A to D in Figure 6.25, all of them considering 12 boreholes, and wants to know the belonging displacements of the excavation boundary u_a including the degree of plastification λ.

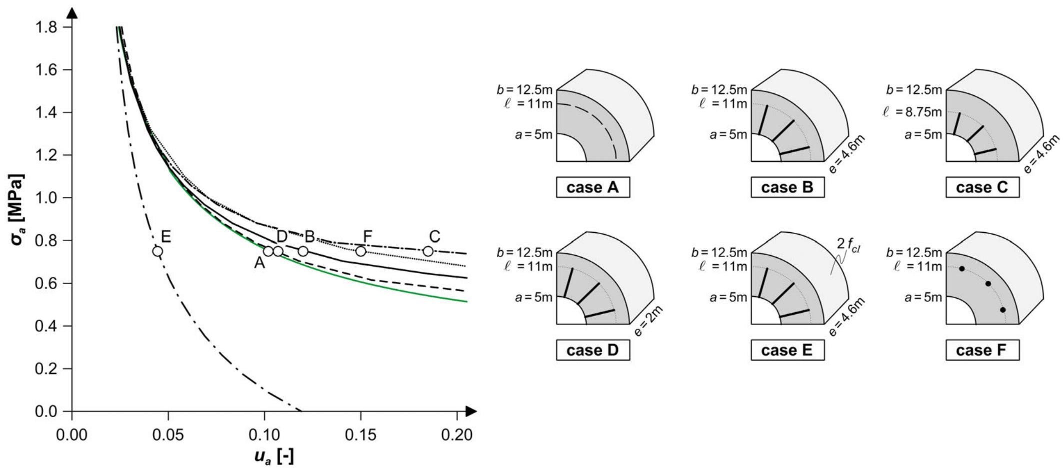

Figure 6.25 *Characteristic lines when considering several different drainage borehole arrangements after grouting (see insets; parameters see Fig. 6.4)*

The lower borderline case of ideal drainage leads to 10 cm displacement of the excavation boundary (point A in Fig. 6.25) and the degree of plastification is $\lambda = 0.46$ (see *e.g.* Fig. 6.20). Nearly the same values of deformation and plastification can be obtained with borehole arrangement of inset D, where radial boreholes are drilled every second tunnel meter (point D in Fig. 6.25; $u_a = 11$ cm, $\lambda = 0.48$).

Increasing the axial borehole distance to 4.6 m (leading to an almost homogeneous head field as discussed in Section 6.5.2.1), a slightly higher displacement results (point B in Fig. 6.25; $u_a = 12$ cm). The degree of plastification is $\lambda = 0.53$ (see Fig. 6.24a). Shorter drainage boreholes would increase deformation considerably (inset and point C in Fig. 6.25; $u_a = 18$ cm, $\lambda = 0.79$).

In case the 12 drainage boreholes were arranged coaxial to the tunnel axis (see inset F in Fig. 6.25), 25% more displacement and plastification than in the radial arrangement result (compare point B to point F in Fig. 6.25 with $u_a = 15$ cm, $\lambda = 0.65$).

Although displacements of all considered drainage layouts are relatively small, the engineer might aim for a lower degree of plastification for safety reasons. Note that this would only be possible (for all other parameters remaining unchanged) by an increase in uniaxial compressive strength of the grouting body (inset and point E in Fig. 6.25 for twice the uniaxial compressive strength of Fig. 6.4; $u_a = 4$ cm, $\lambda = 0.15$).

6.5.2.4 Inflow

Figure 6.26 shows the normalized inflow as a function of the degree of drainage η for several axial borehole distances (e = 1.25-10 m; borehole layout of Fig. 6.13c). The inflow increases with increasing seepage area; *i.e.* smaller axial borehole distance e and increasing degree of drainage η. The inflow is reduced to less than 20% of the inflow in untreated ground for all considered axial distances and – due to reduced seepage area of the drainage boreholes – reduced remarkably compared to the ideally drained case (compare line “ideal” to the other lines in Fig. 6.26).

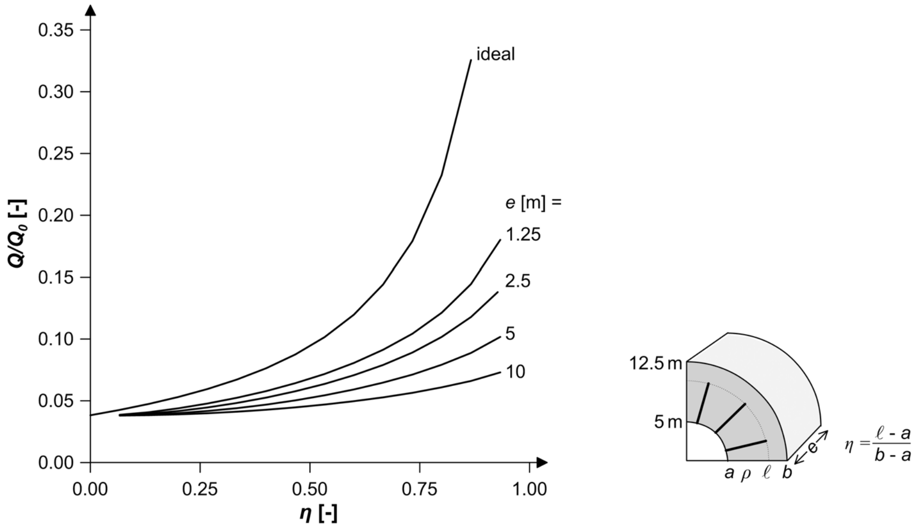

Figure 6.26 *Inflow Q collected from all boundaries of excavation and drainage (normalized with the inflow when considering untreated ground Q_0) as a function of the degree η of drainage after grouting for drainage layout of Figure 6.13c with variable axial spacing e (parameters see Fig. 6.4)*

6.6 Effect of drainage boreholes drilled in advance of grouting

6.6.1 Layout A: circular borehole arrangements

6.6.1.1 Number of drainage boreholes

The effect of the number of advance drainage boreholes is discussed by means of the borehole layout A with circle line at l =15 m (see Fig. 6.12a).

Figure 6.27 shows the hydraulic head field (l.h.s.) and the plastic zones when assuming a lining support pressure $\sigma_a = 0.4$ MPa (r.h.s.) for several borehole numbers n. The borderline cases of no and ideal advance drainage are added for comparison. The pore pressure relief is evident when comparing the hydraulic head field considering no boreholes to the case of only two advance drainage boreholes (compare l.h.s. of Fig. 6.27a to b). The plastic zone is considerably smaller, too and shows a slightly oval shape due to the lateral location of drainage (compare orange area indicating the plastic zone in r.h.s. of Fig. 6.27b to a). Increasing the borehole number reduces the plastic radius and leads to an even shape of the plastic zone for $n \geq 8$ (r.h.s. of Fig. 6.27).

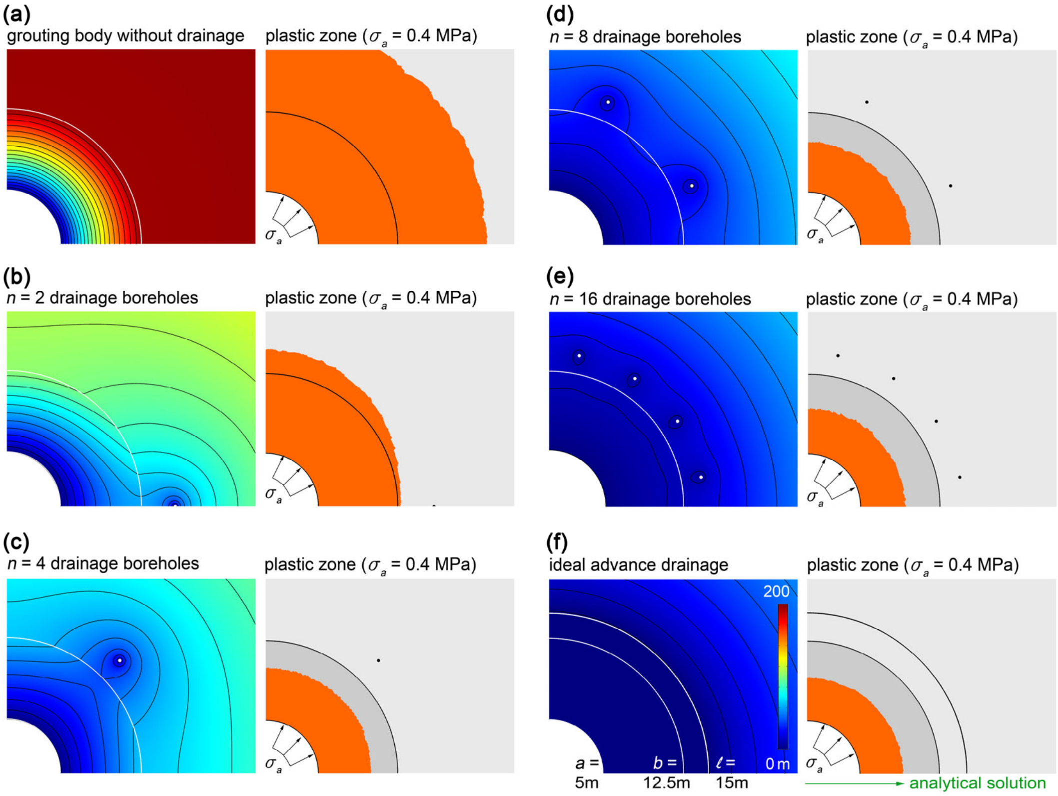

Figure 6.27 *Hydraulic head fields (l.h.s.) and plastic zones for a support pressure of σ_a = 0.4 MPa (r.h.s.) when considering several numbers n of drainage boreholes drilled in advance of grouting (extent of plastic zones according to the analytical model indicated with green arrows; drainage layout A of Fig. 6.12a; parameters see Fig. 6.4)*

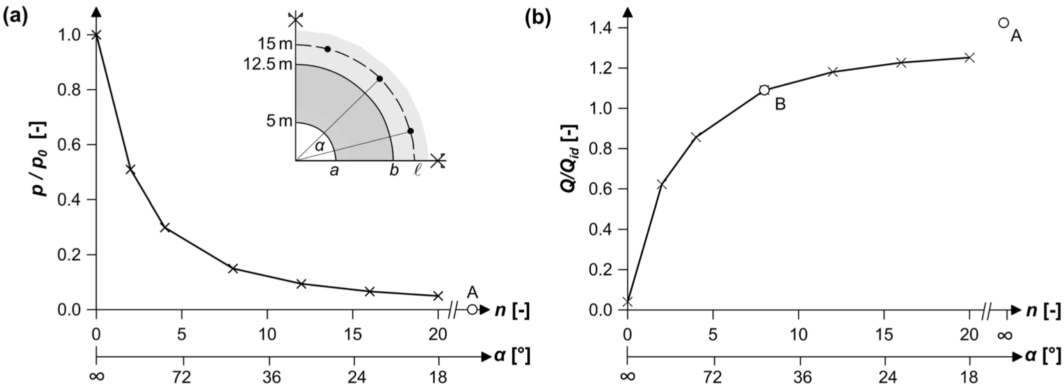

Figure 6.28 *(a) Water pressure acting on the grouting body p (normalized with the initial pressure p_0) and (b) inflow Q collected from all boundaries of excavation and drainage (normalized with the inflow Q_{id} which considers ideal drainage up to $r = l$) as a function of the number n (or the sector angle α) of drainage boreholes drilled in advance of grouting (drainage layout A; parameters see Fig. 6.4)*

The average normalized pore pressure acting on the grouting body is plotted as a function of the number n (or the sector angle α, respectively; Fig. 6.28a). Already a small number of drainage boreholes decreases the pore pressure clearly, while increasing the borehole number $n > 8$ provides marginal additional benefit. A large borehole number ($n = 20$) nearly reliefs the pressure as much as ideal drainage in advance of grouting (point A in Fig. 6.28a).

The normalized inflow increases with increasing seepage area (*i.e.* increasing borehole number), but does not reach the values as when assuming ideal drainage (point A in Fig. 6.28b). In the case of 8 advance drainage boreholes, the inflow is by 25% lower than when assuming ideal advance drainage in advance of grouting (compare point B to A in Fig. 6.28b).

The characteristic lines for n = 2-20 drainage boreholes drilled in advance of grouting are shown in Figure 6.29. The lower borderline case of the ideally advanced drained grouting body is plotted in green; the upper borderline case of no drainage is shown as red line. For borehole number $n \geq 16$, the characteristic lines virtually coincide with the one of ideal advance drainage (compare black to green lines in Fig. 6.29). Assuming a feasible lining support pressure of $\sigma_a = 0.4$ MPa, the displacement of the excavation boundary considering ideal advance drainage is $u_a = 14$ m (point A in Fig. 6.29). In case of 8 advance drainage boreholes, a 20 % higher displacement results (point B in Fig. 6.29; $u_a = 17$ cm). In case of only 4 drainage boreholes, the deformation increases (point C in Fig. 6.29; $u_a = 25$ cm) and for two drainage boreholes, the system is close to failure (point D in Fig. 6.29; u_a = 85 cm).

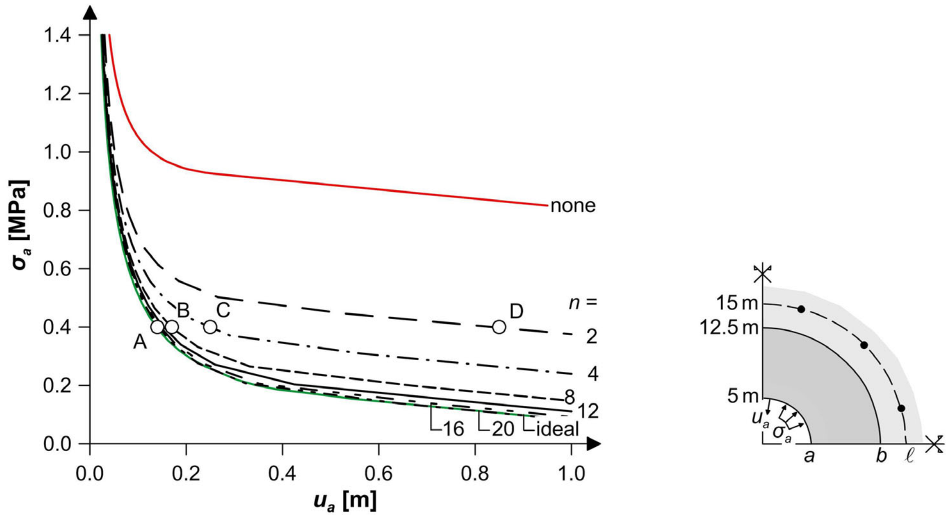

Figure 6.29 *Characteristic lines for several drainage borehole numbers n drilled in advance of grouting (drainage layout A; parameters see Fig. 6.4)*

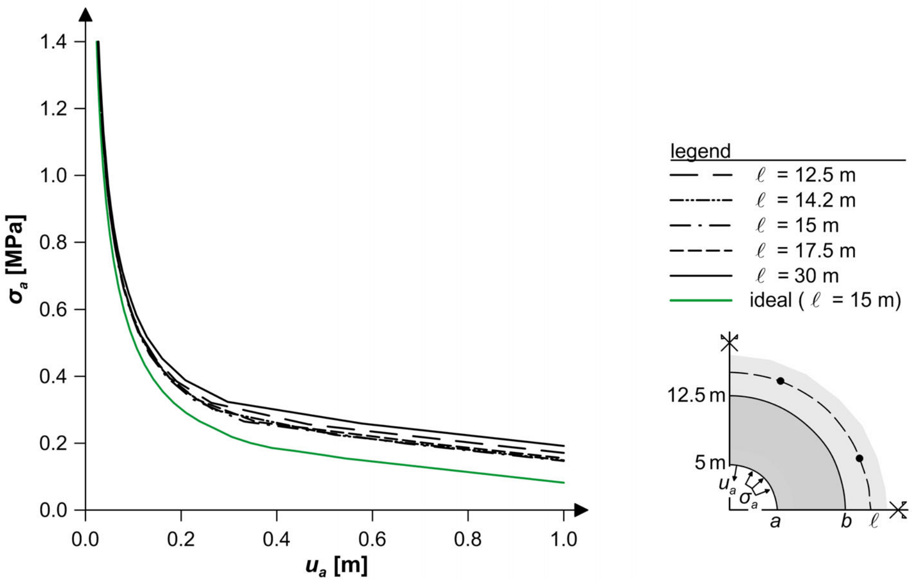

Figure 6.30 *(a) Characteristic lines for several circle lines l when considering drainage in advance of grouting (layout A of Fig. 6.12a with n = 8; other parameters see Fig. 6.4)*

6.6.1.2 Circle line of drainage boreholes

Figure 6.30 shows the characteristic lines when considering 8 drainage boreholes at several distances between grouting body and drainage boreholes, here referred to as “circle line l”. At too large circle line, the boreholes are not able to relief the pore pressure close to the grouting body, leading to unfavourable characteristic lines (*e.g.* line $l = 30$ m in Fig. 6.30a). On the other hand at very small circle line, the drainage boreholes cannot be fully effective due to the close permeability interface to the grouting body and thus do not offer additional benefit in terms of stresses and displacements (*e.g.* line $l = 12.5$ m in Fig. 6.30a).

A parametric study was conducted to determine the circle line for common sizes of grouting bodies ($b/a = 2\text{-}3$) and $n = 4$, 8 and 16 boreholes of borehole layout A (Fig. 6.12a and Table 6.2). It showed low sensitivity to the value of circle line, as long as the boreholes are arranged roughly 1-2 m outside of the grouting body (note that the ratio of permeability of grouting body to untreated ground $k_I/k \leq 0.1$ proved therefore to be negligible). A recommendation of circle line l normalized with the tunnel radius a is given in Figure 6.31.

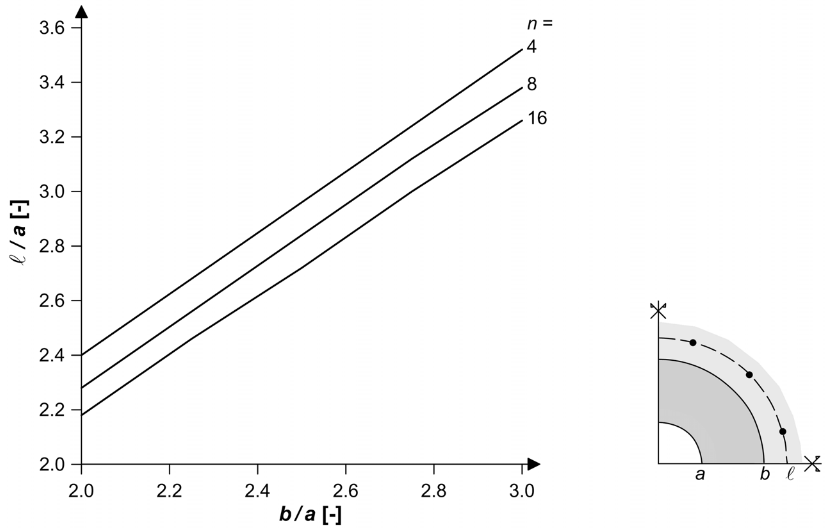

Figure 6.31 *Recommended circle line l as a function of the size of the grouting body b (normalized with tunnel radius a) for drainage via borehole number n in advance of grouting (drainage layout A)*

***Table 6.2** Problem layout of the parametric study of Figure 6.31*		
Problem layout		
Total stresses, in-situ	σ_0	4.4 MPa
Pore water pressure, in-situ	p_0	2.0 MPa
Radius of tunnel excavation	a	5 m
Radius of influence for seepage flow	R	200 m
Ground and grouting body		
Effective cohesion	c	0.05 MPa
Angle of eff. internal friction	φ	25 °
Angle of dilatancy	ψ	25 °
Poisson’s ratio	v	0.33
Young’s modulus	E	100 MPa
Uniaxial compressive strength	f_{cI}	1.5 MPa
Poisson’s ratio of grouting body	v_I	0.33
Angle of internal friction equal to angle of dilatancy	$\varphi_I = \psi_I$	25 °
Variable design parameters		
Number of drainage boreholes	n	4,8,12
Circle line	l	10-50 m
Ratio of radii of grouting body to excavation	b/a	2, 2.5,3
Ratio of permeability of grouting body to untreated ground	k_I/k	0.1-0.001

6.6.1.3 Required lining support pressure

The results of a parametric study into the effects of the number of drainage boreholes ($n = 4$, 8, 16) and the size of grouting body ($b = 10$, 12.5 and 15m, *i.e.* $b/a = 2$, 2.5 and 3) is evaluated in Figure 6.32 showing the required lining support pressure of σ_a as a function of the degree of plastification λ. The lower borderline case of the ideal advance drainage of the grouting body is shown as green line; the upper borderline case of no drainage measure is shown as red line.

The effect of every advance drainage borehole arrangement is remarkable with respect to lining support or degree of plastification and similar for all sizes of grouting bodies (compare Fig. 6.32a to b to c). Consider a maximum admissible degree of plastification $\lambda = 0.5$ for a mid-size grouting body ($b/a = 2.5$ in Fig. 6.32b). In the case of ideal advance drainage, a lining support pressure of $\sigma_a = 0.5$ MPa would be required (point A in Fig. 6.32b; note that this value is 30 % lower than when considering ideal drainage *after* grouting; point A in Fig. 6.21b). The model of ideal drainage is adequate with 10% accuracy in the case of 16 boreholes, and with still 20% accuracy for 8 boreholes ($\sigma_a = 0.55$ and 0.6 MPa for $n = 16$ and 8, respectively; Fig. 6.32b). In case of 4 boreholes, accuracy decrease to 32% ($\sigma_a = 0.66$ MPa at point B in Fig. 6.32b; see also later in Section 6.6.3 for an application example).

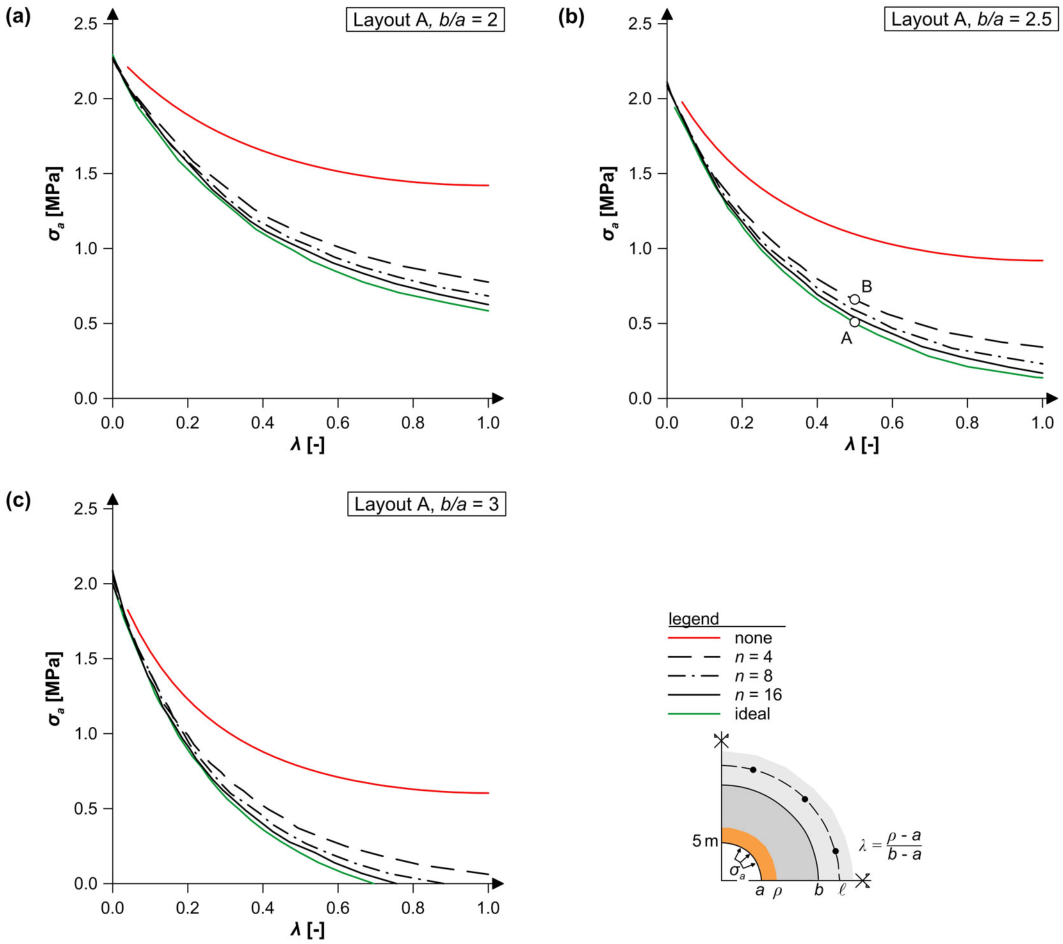

Figure 6.32 *Required lining support pressure* σ_a *as a function of the degree of plastification* λ *for drainage in advance of grouting when considering three sizes of grouting bodies* b/a *(*$b = 10$*, 12.5 and 15 m; drainage layout A of Fig. 6.12a; other parameters see Fig. 6.4)*

6.6.2 Layout B: lateral borehole arrangements

6.6.2.1 Effect of Layout B compared to Layout A

In tunnelling practice, a circular arrangement of boreholes might not be possible due to the limited accessibility for drilling. An option might be a lateral arrangement of drainage boreholes (layout B of Fig. 6.12). Figure 6.33 compares the hydraulic head field (l.h.s.) and the plastic zone when assuming a lining support pressure $\sigma_a = 0.4$ MPa (r.h.s.) of layout A to layout B for the example of $n = 8$ advance drainage boreholes. Layout B lowers the hydraulic head lateral of the grouting body similar to layout A, but is less effective above the tunnel roof (l.h.s. of Fig. 6.33). The plastic zone is therefore marginally more extended in vertical direction and the displacements are distinguished into "roof" and "lateral" (r.h.s. of Fig. 6.33b). The average degree of plastification is $\lambda = 0.8$, which is 20% higher than for layout A ($\lambda = 0.67$; compare r.h.s. of Fig. 6.33).

The characteristic line confirms the advantage of layout A compared to layout B (Fig. 6.34). When assuming a maximum admissible support pressure of $\sigma_a = 0.4$ MPa, the lower borderline case of ideal advance drainage has a displacement of only $u_a = 14$ cm (point C in Fig. 6.34). The displacements increase for layout A by 20% and by additional 50% for layout B ($u_a = 17$ and 24 cm for point A and B in Fig. 6.34). The differences in characteristic lines due to the egg-shaped plastic zone (denoted as "roof" and "lateral" according to Fig. 6.33b) appear only for very low support pressure close to failure of the grouting body, while for lower displacement, both lines coincide.

Hereinafter, the study considers the worst-case of displacements at the tunnel roof.

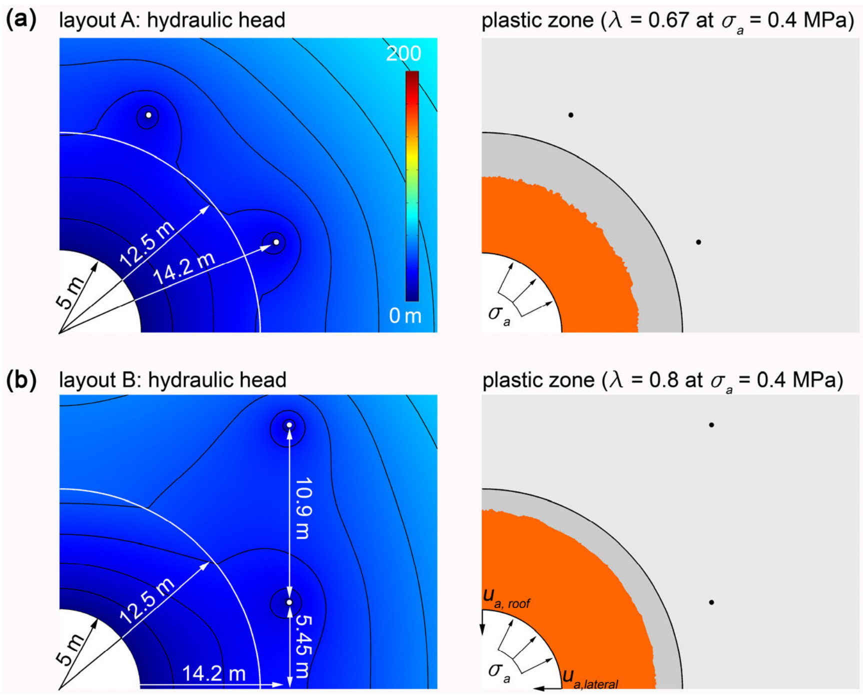

Figure 6.33 *Hydraulic head field (l.h.s.) and plastic zone for a support pressure of $\sigma_a = 0.4$ MPa (r.h.s.) when (a) considering drainage in advance of grouting by means of borehole layout A and (b) layout B ($n = 8$; other parameters see Fig. 6.4)*

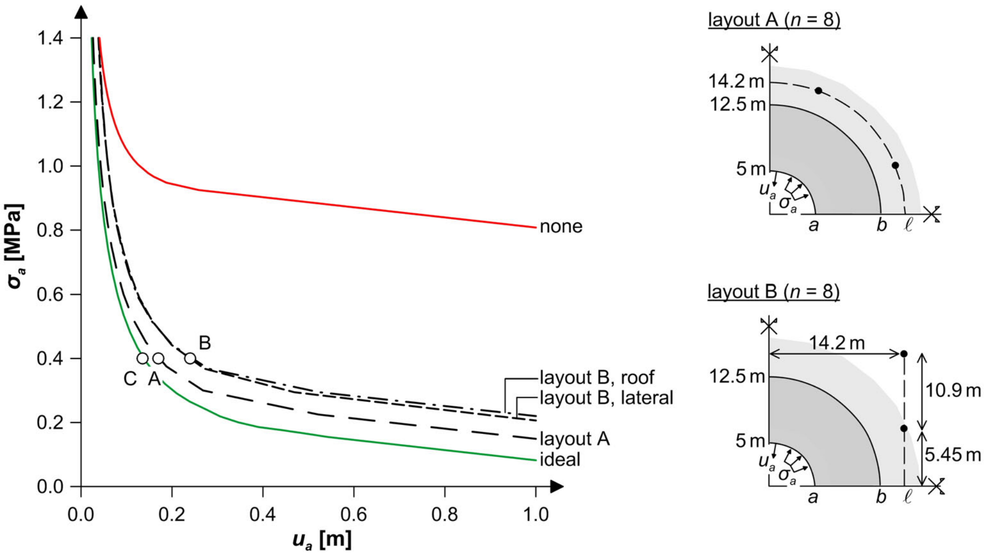

Figure 6.34 *Characteristic lines for drainage in advance of grouting by means of borehole layout A and B (other parameters see insets and Fig. 6.4)*

6.6.2.2 Required lining support pressure

As in Section 6.6.1.3, the required lining support pressure σ_a as a function of the degree of plastification λ is evaluated in Figure 6.35 for variable borehole number n (drainage layout B of Fig. 6.12b) and for three sizes of the grouting body ($b = 10$, 12.5 and 15 m, *i.e.* $b/a = 2$, 2.5 and 3). The lower borderline case of ideal advance drainage is indicated for comparison as green line; the upper borderline case of no advance drainage measure is shown as red line.

Comparing the results of layout A (Fig. 6.32) to layout B (Fig. 6.35) proves the trend discussed in the previous section: layout B might allow easier accessibility than layout A. But layout A provides benefit in terms of stresses and displacements at the excavation boundary. Section 6.6.3 examines these effects by means of an application example.

6.6.3 Application example

Consider planning a grouting body at a depth and in a ground shown in the tunnel example of Figure 6.4. The uniaxial compressive strength of the grouting body is limited to 1.5 MPa; its size to maximum $b/a = 2.5$. The lining will provide a support pressure of $\sigma_a = 0.6$ MPa. For safety reason, maximum half of the grouting body is allowed to plastify (degree of plastification $\lambda = 0.5$). Without drainage measures, the grouting body will fail (see *e.g.* red lines in Fig. 6.32a or b). Which drainage arrangements allow a stable grouting body within these parameters – and what are the displacements to be expected at the excavation boundary?

First, the lateral drainage borehole arrangements are studied (layout B). Figure 6.35 shows that a small grouting body requires higher lining support pressure than $\sigma_a = 0.6$ MPa, but a grouting body of size $b/a = 2.5$ might be an option. The limits of admissible plastification $\lambda = 0.5$ is only fulfilled for $n = 16$ advance drainage boreholes (point B in Fig. 6.35b). The displacement of the excavation boundary is $u_a = 12$ cm (point B in Fig. 6.36e).

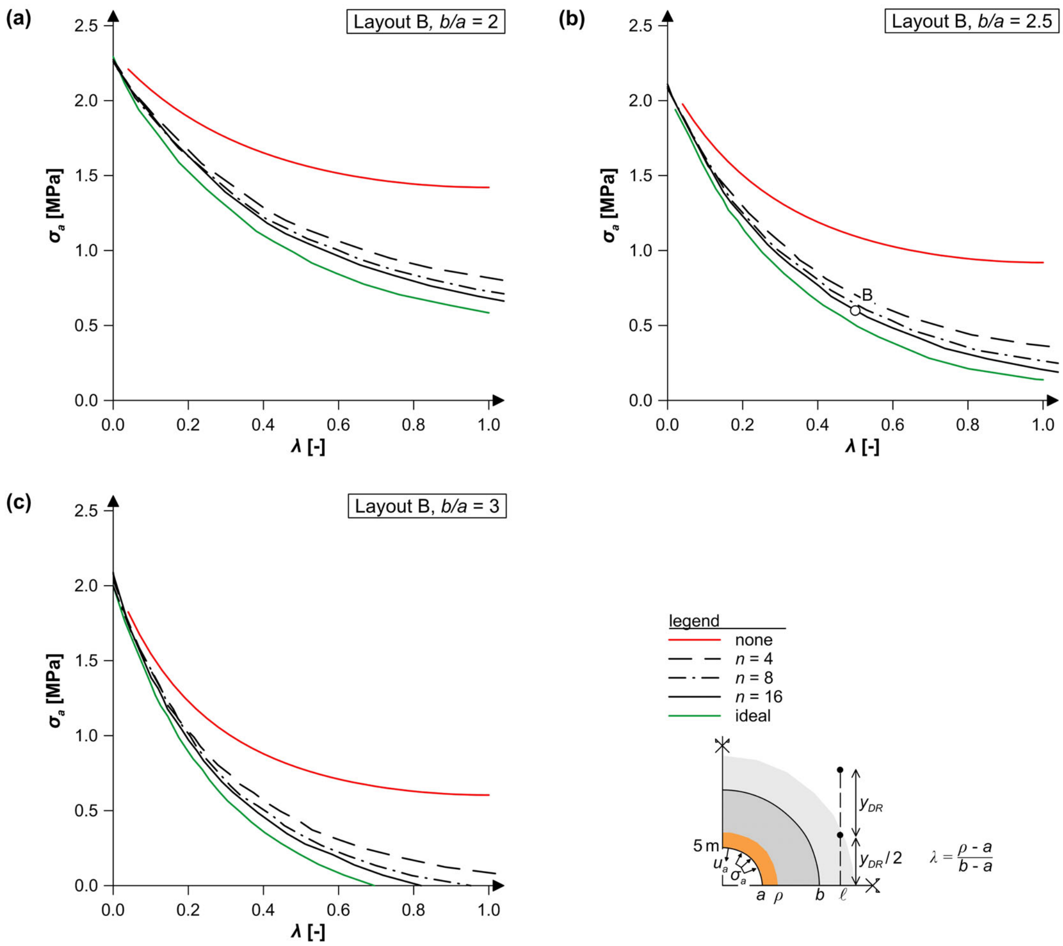

***Figure 6.35** Required lining support pressure σ_a as a function of the degree of plastification λ for drainage in advance of grouting considering three sizes of grouting bodies b/a (b = 10, 12.5 and 15 m; drainage layout B of Fig. 6.12b; other parameters see Fig. 6.4)*

Advance drainage considering borehole layout A is supposed to be more favourable. But still, only a grouting body of size $b/a = 2.5$ enables the lining support pressure of $\sigma_a = 0.6$ MPa (see Fig. 6.32). The degree of plastification is $\lambda = 0.46$ and 0.5 for $n = 16$ and 8 drainage boreholes, respectively (about point A in Fig. 6.32b). The displacement of the excavation boundary is $u_a = 9$ and 10 cm (point A in Fig. 6.36e), *i.e.* 20% less than for drainage layout B.

Summarizing, both drainage layouts A and B allow for construction of a stable grouting body. The option of choice is presumably drainage layout A with 8-16 drainage boreholes. The circle line for the advance drainage boreholes is $l = 13.6 - 14.2$ m (Fig. 6.31), the size of the grouting body $b = 12.5$ m ($b/a = 2.5$). If preferring drainage layout B, 20% larger displacements had to be considered, while the degree of drainage was about the same.

(Please note that drainage boreholes drilled after grouting is no option within the demanded parameters of the application example. According to Figure 6.24, only the theoretical, ideal drainage measure allows for a support of $\sigma_a = 0.6$ MPa – and still for a too high degree of plastification of $\lambda > 0.6$.)

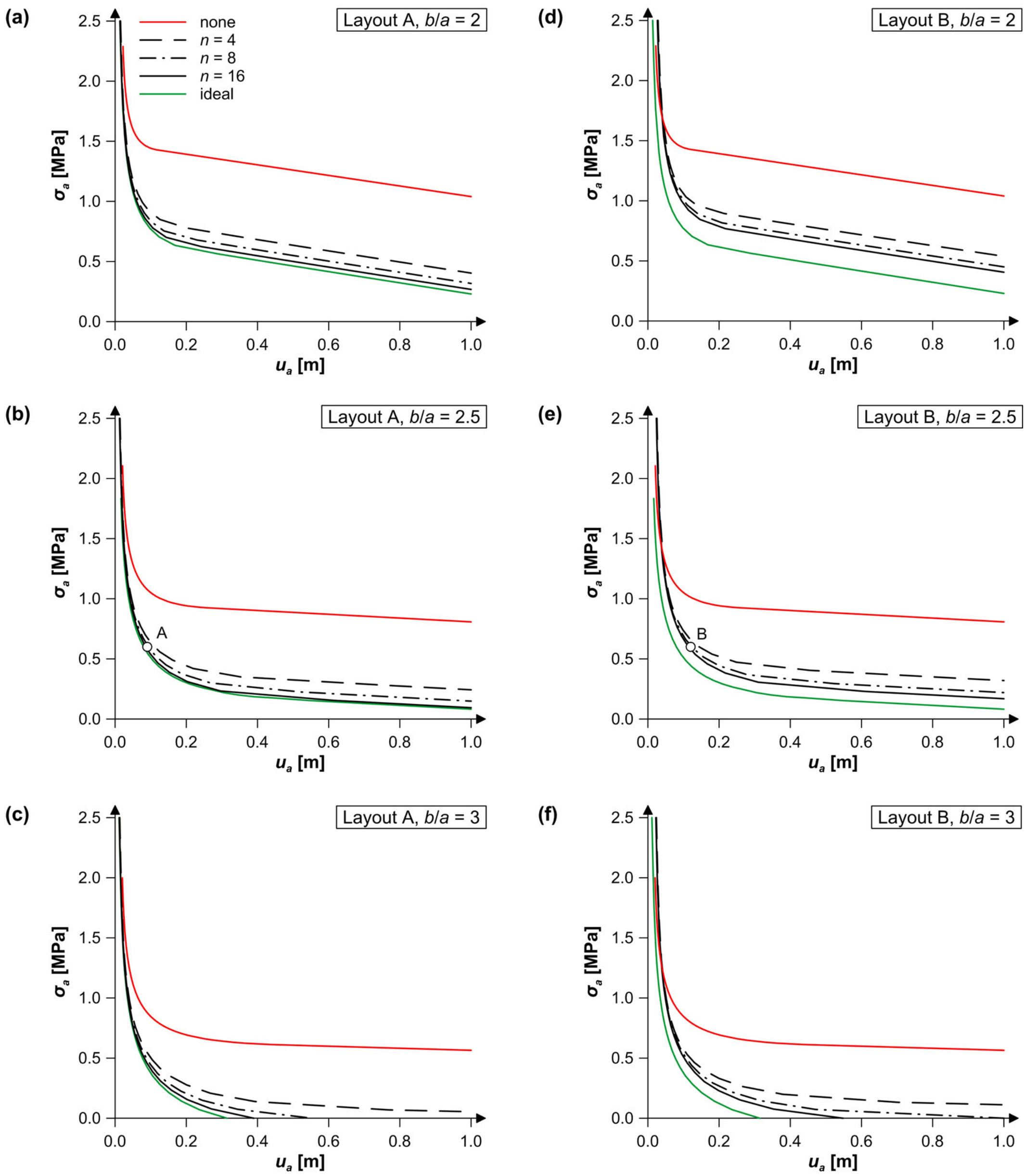

Figure 6.36 *Characteristic lines for drainage in advance of grouting considering three sizes of grouting bodies b/a (b = 10, 12.5 and 15 m; drainage layouts of Fig. 6.12; other parameters see Fig. 6.4)*

6.6.4 Effect of fault zone of limited extent

Anagnostou and Kovári [40] described that in fault zone of limited extent, a “stabilizing wall-effect” might be observed. Triggered by the deformation occurring within the fault zone, shear stresses develop at the interface to the stiffer host rock. Other than in the previous sections considering a fault of unlimited extent, where the effective stresses increased by about the amount of pressure relief induced by drainage, the increase in effective stresses is therefore diminished by the wall-effect. The stresses acting on the grouting body are lower, which is favourable in terms of stability.

For detailed explanation including parametric studies, reference is made to Anagnostou and Kovári [40]. Here, we limit ourselves to one single example of fault zone without intending an in-depth study, but still extend the previous investigations in three aspects: (i) by considering a fault zone running axis-parallel to the tunnel; (ii) by taking account of the possibly different permeability of fault zone and host rock; and (iii) by considering specific borehole arrangements drilled in advance of grouting.

The exemplary fault zone of 60 m width runs axis-parallel to the tunnel and has a vertical interface to the solid host rock (Fig. 6.37). The width of the fault zone is chosen such as it is supposed to trigger a visible wall effect (in fault zones normal to the tunnel axis, this is the case for zones up to an extent of about 8 times the radius of the grouting body; [40]). The problem layout, the approach and the properties of both fault zone and grouting body are the ones of our previous tunnel example; the only difference being that the ground model additionally considers the properties of the solid host rock (denoted with subscript H in Fig. 6.37).

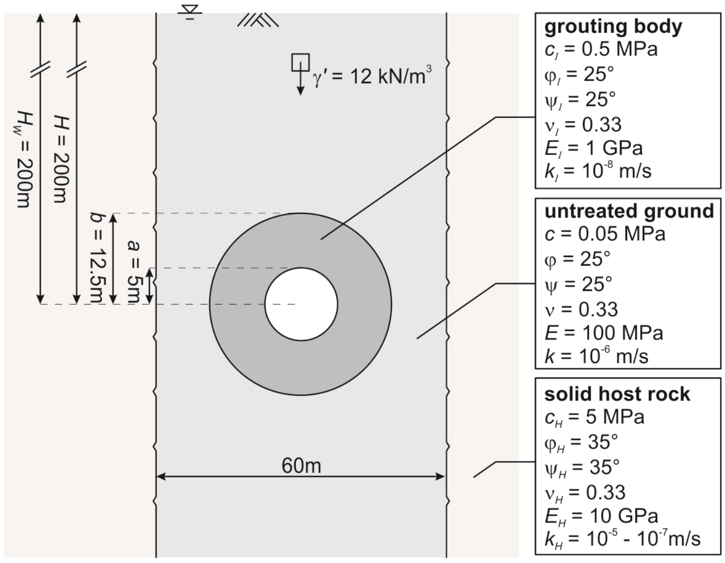

Figure 6.37 *Problem layout considering a fault zone of limited extent*

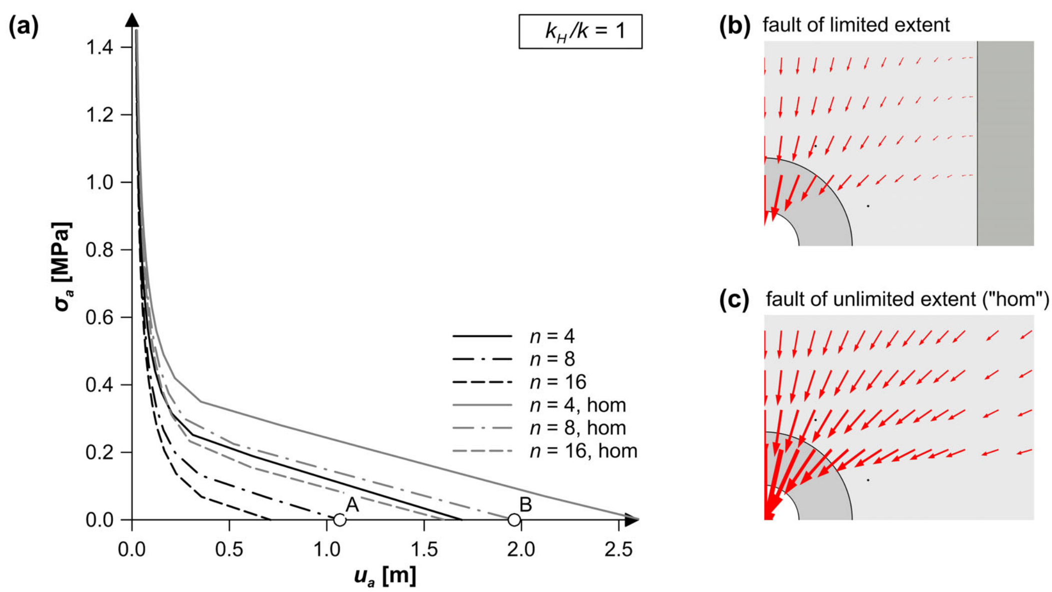

Figure 6.38 *(a) Comparison of characteristic lines for drainage in advance of grouting considering a fault of limited and a fault of unlimited extent. Displacement vectors (b) in a fault of limited extent and (c) in a fault of unlimited extent (drainage layout A of Fig. 6.12a; k_H/k = 1, other parameters see Fig. 6.37)*

6.6.4.1 Host rock and fault zone of uniform permeability

First we consider ground and host rock of uniform permeability (*i.e.,* $k_H/k = 1$) and quantify the wall-effect due to the different rock properties of fault zone and solid host rock for $n = 4$, 8 and 16 drainage boreholes drilled in advance of grouting (borehole layout A of Fig. 6.12a). Comparison is drawn to the previously discussed results of a fault of unlimited extent (Section 6.6.1).

Figures 6.38b and 6.38c illustrate the wall-effect by means of the displacement vectors which develop when considering 8 advance drainage boreholes. In a fault of unlimited extent, deformations are high and occur also in some horizontal distance to the tunnel axis (Fig. 6.38c). In a fault of limited extent, the deformation diminishes with decreasing distance to the interface of fault zone to host rock (Fig. 6.38b), where shear stresses, triggered by the deformation in the fault zone, act against the displacement. The reduction in effective stresses acting on the grouting body sums up to about 10% (after drainage and subsequent grouting: $\sigma_b' = 3.8$ MPa in a fault of unlimited extent, $\sigma_b' = 3.4$ MPa in the fault of limited extent).

Figure 6.38a shows the characteristic lines for both a fault of limited and unlimited extent (the latter denoted as “hom”). The displacement of the excavation boundary is clearly favourable when considering the limited fault zone (compare black to grey lines in Fig. 6.38). For the example of 8 drainage boreholes and considering no lining support pressure, the displacement is 50% smaller than in fault of unlimited extent (compare point A to B in Fig. 6.38a). The stabilizing wall-effect increases with larger number of drainage boreholes, *i.e.* increased seepage area (compare dashed grey to black line in Fig. 6.38a). Of course, the characteristic lines coincide for high support pressure, *i.e.* allowing virtually no displacement.

6.6.4.2 Host rock and fault zone of different permeability

The effect of host rock and fault permeability is discussed for 8 drainage boreholes drilled in advance of grouting (Fig. 6.39). Figure 6.40 compares three permeability ratios of host rock to fault zone: the left column shows the case of a low-permeability fault ($k_H/k = 10$); the middle column the case of uniform permeability ($k_H/k = 1$) and the right column the case of a high-permeability fault ($k_H/k = 0.1$). The top-line shows the overall hydraulic head field, the second line the enlargement in vicinity of the tunnel, the third line the plastic zone for a lining support pressure of $\sigma_a = 0.4$ MPa when considering drainage borehole layout B. The bottom line shows the characteristic lines for both layout A and B. It includes for comparison the lower borderline case of ideal drainage in advance of grouting as green line ($l = 15$ m in Fig. 6.12c); the upper borderline case of no drainage measure is shown as red line.

In uniformly permeable ground ($k_H/k = 1$), the hydraulic head dissipates uniformly in both rock and fault zone (Fig. 6.40b and e). The characteristic lines when considering drainage measures are clearly favourable (compare *e.g.* ideal drainage of Fig. 6.40k to 6.36b). The previously discussed lower efficiency of layout B (Section 6.6.2.2) is no longer of relevance: borehole layouts A and B are equivalent (Fig. 6.40k). However, when assuming no lining support ($\sigma_a = 0$), the displacement considering borehole layouts A and B is by factor 2.5 larger than when assuming ideal drainage in advance of grouting (compare black to green line in Fig. 6.40k).

In case of a low-permeability fault ($k_H/k = 10$), pore pressure relief takes place within the fault zone (Fig. 6.40a). The hydraulic gradients acting on the grouting body are higher (compare Fig. 6.40d to e), thus the plastic zone is larger than in ground of uniform permeability (compare Fig. 6.40g to h). Therefore, the characteristic lines are less favourable (Fig. 6.40j). The stress-displacement behaviour of both the considered drainage layouts A and B are very similar with small advantage for layout A (compare dotted-dashed to dashed line in Fig. 6.40j). Note that the deviation to the case of ideal drainage is substantial (compare black to green lines in Fig. 6.40j).

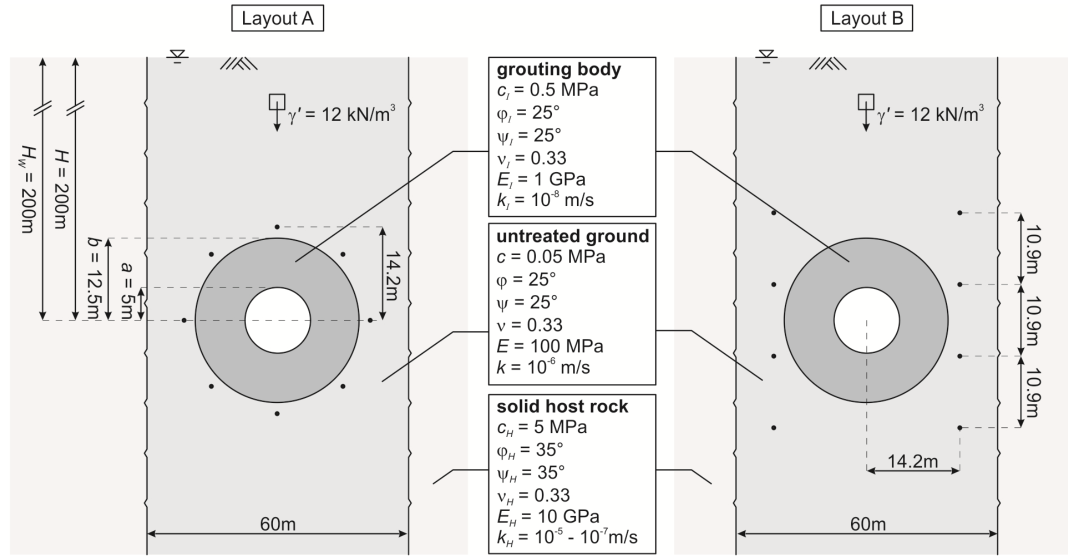

Figure 6.39 *Problem layout when considering a fault zone of limited extent for drainage borehole layout A (l.h.s.) and layout B (r.h.s.)*

The most favourable situation is the case of a high-permeability fault ($k_H/k = 0.1$). Pore pressure relief takes place within the (less permeable) host rock and very low gradient act on and within the grouting body (Fig. 6.40c and f). The plastic zone is smaller and has an egg-shape in case considering layout B (compare Fig. 6.40i to h). However, drainage layouts A and B are equivalent in terms of stability and both the characteristic lines are very close to the case of ideal drainage for lining support pressures larger than $\sigma_a = 0.1$ MPa (compare black to green lines in Fig. 6.40l).

Note that the characteristic line of the upper borderline case (*i.e.* a grouting body without drainage boreholes; red lines in Fig. 6.40jkl) is virtually unaffected of the ratio k_H/k, as pore pressure relief takes place mainly within the grouting body and thus does not lead to significant consolidation of the untreated ground, which in turn would trigger the favourable wall-effect.

Summing up, the wall-effect developing in case of advance drainage measures in the exemplary fault of 60 m width is clearly favourable for the stability of grouting bodies. 8 boreholes drilled in advance of grouting may decrease displacements by more than 50% compared to a fault of unlimited extent. The effects of drainage layout B is almost equal to layout A. The permeability ratio of solid host rock to fault zone is a key factor for the hydraulic head field and needs to be considered when determining the characteristic line considering drainage in advance of grouting in a fault of limited extent. The model of ideal drainage in advance of grouting proved to be adequate only for a fault zone of higher permeability than the host rock ($k_H/k \leq 0.1$).

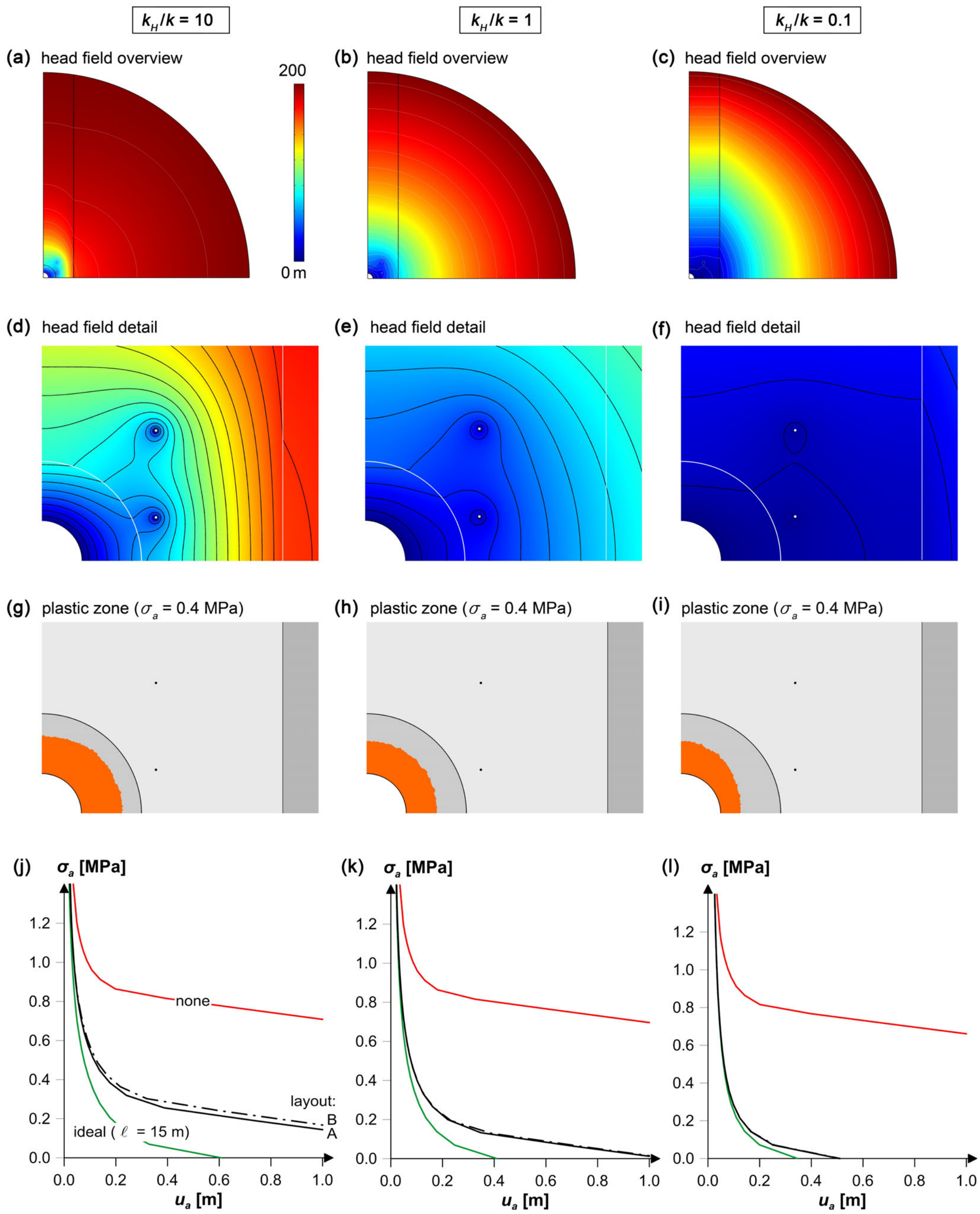

Figure 6.40 *Three permeability ratios of host rock to fault zone k_H/k presented in three columns comprising: (a-c) overall hydraulic head field, (d-f) detail of hydraulic head, (g-i) plastic zones for a support pressure of σ_a = 0.4 MPa, and (j-l) characteristic lines when considering drainage in advance of grouting in a fault zone of limited extent (Fig. 6.39)*

6.7 Conclusions

The chapter in hand showed that drainage measures considerably increase the stability of grouting bodies in water-bearing fault zones. Considerations were limited to an exemplary deep tunnel without claiming general validity. However, there is no reason to doubt that the analytical solutions of ideal drainage represent lower limits for pre-dimensioning grouting bodies and that the accuracy will be in a comparable range when considering specific borehole arrangements similar to the ones discussed above.

6.7.1 Analytical solution of ideal drainage

6.7.1.1 Drainage after grouting

Equations have been derived for the displacement at the excavation boundary u_a, which is a function of the geometry of the grouting body b/a, the degree of drainage η, the degree of plastification λ, the material properties of the grouting body (effective cohesion c_I, Young's Modulus E_I, angle of internal friction φ_I, angle of dilatancy ψ_I, Poisson's ratio ν_I), the ratio of permeability of grouting body to untreated ground k_I/k, the in-situ pore pressure p_0 and the lining support pressure σ_a.

Ideal drainage does increase the stability of the grouting body only if at least some moderate plastification is allowed ($\lambda > 0.1$). In a fully elastic grouting body, drainage is tentatively unfavourable for stability. Other measures to increase the stability of grouting bodies (for a given degree of plastification) is to increase the size b/a, the uniaxial compressive strength f_{cI} or the lining support pressure σ_a.

The optimal drainage degree is equal to the degree of plastification ($\eta = \lambda$). A larger drainage area does not affect stability, but might involve the risk of inner erosion due to the high gradients prevailing in the outer ring of the grouting body.

Limiting the degree of drainage to $\eta < 0.8$ ensures the sealing effect of a grouting body, which is 100 times less permeable than the untreated ground, and inflow is reduced to 20% of the value without considering any grouting body.

6.7.1.2 Drainage in advance of grouting

Drainage in advance of grouting decreases both displacements and stresses at the excavation boundary in comparison to drainage after grouting. The displacement at the excavation boundary u_a are a function of the geometry of the grouting body b/a, the degree of plastification λ, the material properties of the grouting body (effective cohesion c_I, Young's Modulus E_I, angle of internal friction φ_I, angle of dilatancy ψ_I, Poisson's ratio ν_I) and the lining pressure σ_a, but not of the radius of advance drainage l. Dimensioning aids developed in previous studies apply for drainage in advance of grouting when using σ'_{bDR} according to Eq. (6-7) of Zingg [62] instead of σ'_b in Figures 5.3-1 to 5.3-4 of Anagnostou and Kovári [40].

The model-assumption of a very stiff grouting body ($u_b = 0$) may marginally overestimate the displacements at the excavation boundary.

6.7.2 Specific drainage borehole arrangements

6.7.2.1 Drainage borehole arrangements drilled after grouting

Considering ideal drainage after grouting by means of the analytical solution represents the lower limit for the stress-displacement behaviour at the excavation boundary. 12 drainage slits in the cross-section (two-dimensional consideration) approximate ideal drainage conditions with 5% accuracy for a degree of plastification of $\lambda = 0.5$ and with

10% accuracy for higher plastification. A small grouting body requires longer drainage slits than a large grouting body to account for the same pore pressure relief.

When arranging 12 boreholes such as they lead to a spatial uniform hydraulic head field (three-dimensional consideration with about an equal spacing between the boreholes in radial and axial direction; $e \approx m$ in Fig. 6.23b), up to 12% higher displacements result than in the borderline case of ideal drainage for a degree of plastification of $\lambda \leq 0.3$ (30% accuracy for $\lambda = 0.5$). For better accordance, the axial spacing has to decrease. Virtually unaffected of the axial distance, the sealing effect of the grouting body leads to less than 20% of the water inflow in untreated ground.

6.7.2.2 Drainage borehole arrangements drilled in advance of grouting

Considering ideal drainage in advance of grouting by means of the analytical solution determines the lower limit of the characteristic line when considering specific advance drainage borehole arrangements. A minimum of 8 coaxial drainage boreholes, arranged evenly distributed around a circle line of a radius which is 1-2 m larger than the grouting body (layout A), leads to a uniform shape of the plastic zone. An additional increase in borehole number provides marginal additional benefit in terms of pore pressure relief. The model of ideal drainage is adequate for consideration of the stress-displacement behaviour at the excavation boundary up to $\lambda \leq 0.5$ with 20% accuracy in case of 8 drainage boreholes and with 10% for 16 boreholes. A lateral borehole arrangement (layout B) may be preferred due to accessibility and drilling operation, but it increases the displacements by about 20-30% compared to the circumferential arrangement of layout A.

The smaller seepage area of individual advance drainage boreholes decreases the water inflow considerably compared to ideal drainage (*e.g.* by 25% for 8 boreholes).

For a fault of limited extent, favourable shear stresses develop at the interface to the solid rock due to consolidation induced by advance drainage. Displacements may decrease by more than 50% when considering 8 drainage boreholes drilled in advance of grouting. The permeability ratio of solid host rock to fault zone needs to be considered when determining the characteristic line. Good accordance to the case of ideal drainage was found only for fault zones of higher permeability than the host rock.

7 Residual water pressure on the tunnel lining considering permanent drainage measures

7.1 Introduction

Permanent drainage measures may be applied in cases of a tunnel crossing water-bearing Karst formations or fault zones. For instance, the Tunnel Engelberg in Switzerland runs through a limestone section with water-bearing joints or karstic systems at 540 m elevation of water table. The 80 cm thick lining collapsed due to high water pressures caused by a severe storm in 2005 ([122], [47]). Subsequently, extensive measures were designed to allow immediate drainage of water in case of heavy inflow (Fig. 7.1). Ring-shaped drainage gaps of 0.5 m width were arranged in the lining every 4-6 m. In addition, 6 radial, 4-6 m long drainage boreholes were drilled each cross section (tunnel and drainage boreholes of 8.5 m and 11.8 cm diameter, respectively). The drainage gaps were designed such as they were able to withstand the rock pressure (*i.e.* adequate frequency, width and thickness) and the diameter of the boreholes was chosen large enough to allow for sufficient water discharge. That kind of drainage concept was applied also to several Swiss hydropower caverns.

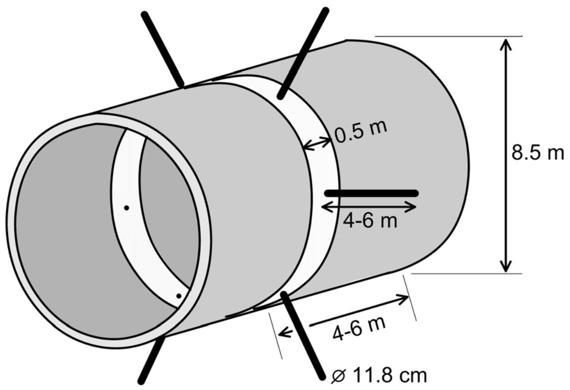

Figure 7.1 *Schematic sketch of drainage measures at Tunnel Engelberg, Switzerland (after Ingenieurgemeinschaft LSE Steilrampe [122])*

Chapter 7 focuses on following drainage layouts: radial drainage boreholes drilled through (Fig. 7.2a) or ring-shaped drainage gaps arranged in the impermeable tunnel lining (Fig. 7.2b). The permanent drainage measures increase the water inflow, but relief the water pressure acting on the lining. The distinct drainage spots offer better accessibility for maintenance and servicing than a drainage layer all around the tunnel, which may become decisive in case of high and/or permanent water inflow: potential accumulation of floating debris (*e.g.* sintering, limescales, sulphide and aluminium hydroxides) may lead to clogging of the drainage layer and/or the gravel pack and endanger the lining stability due to water pressure developing.

Section 7.2 describes the computational model including a dimensional analysis, which shows the dependencies of the residual relative water pressure (and water discharge) on the tunnel diameter, the area of seepage flow, the drainage borehole number and both diameter and length of boreholes drilled radially through the tunnel lining. Section 7.3 discusses the effect of each of these parameters successively by means of a tunnel example. A parametric study considering drainage boreholes or ring elements provides more general results, which are edited as dimensioning charts (Section 7.4) and discussed by means of an application example in Section 7.5.

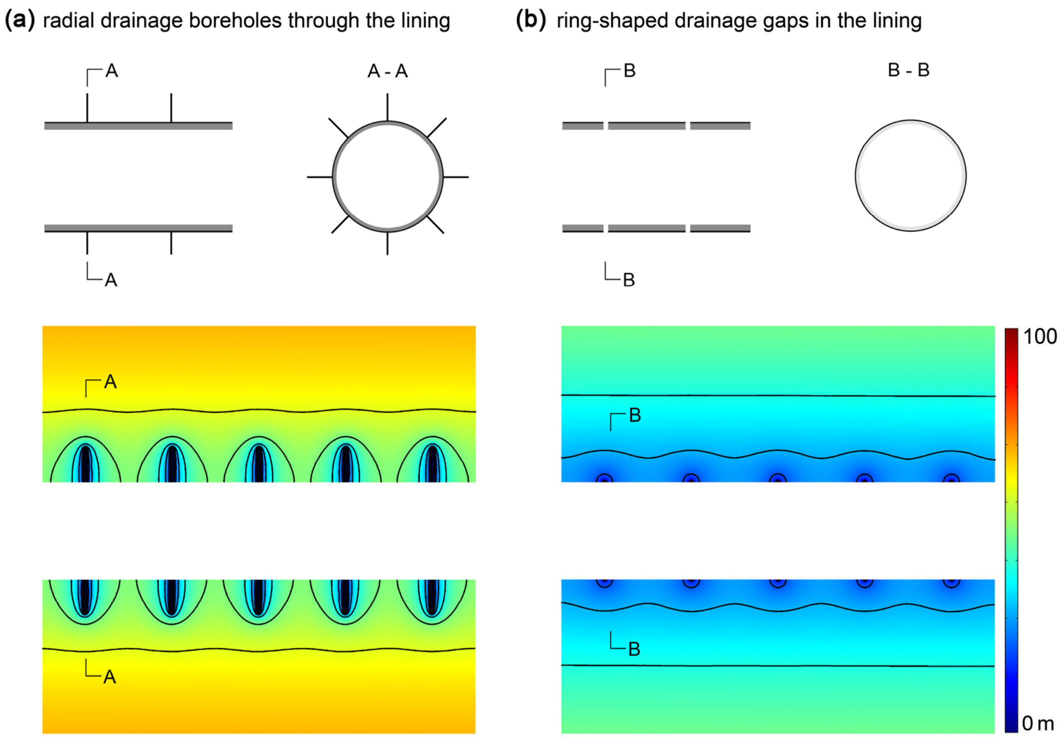

Figure 7.2 *Schematic sketch of longitudinal and lateral section with surface plots of the hydraulic head field along the tunnel axis for two permanent drainage measures*

7.2 Computational model

The three-dimensional, numerical seepage flow analyses consider a cylindrical tunnel of radius a, located in distance T below water table and ground surface, in a homogeneous, isotropic porous medium obeying Darcy's law at steady-state conditions (Fig. 7.3). The hydraulic head at the far-field boundaries is taken equal to the initial hydraulic head and the water table is assumed to remain constant (no drawdown) in spite of the drainage action (conservative assumption, *cf.* Section 5.3). The tunnel lining is considered as impermeable (no-flow boundary condition) and the drainage surfaces are taken as seepage faces of atmospheric pressure (sufficient hydraulic capacity of drainage boreholes assumed).

The seepage field is determined taking account of specific, permanent drainage layouts consisting either of n equally spaced, radial drainage boreholes or of ring-shaped drainage gaps, respectively (Fig. 7.4). The axial borehole distance $e \approx (\pi/n)(a+l_{dr})$ was determined such that an about uniform pore pressure relief is achieved (maximum residual pressure between the boreholes is about equal in axial and circumferential direction).

Table 7.1 summarizes the parameter values of the tunnel example.

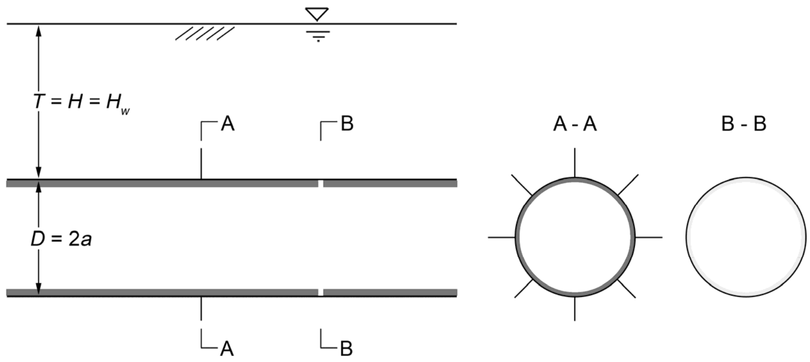

Figure 7.3 *Problem layout of the comparative analysis*

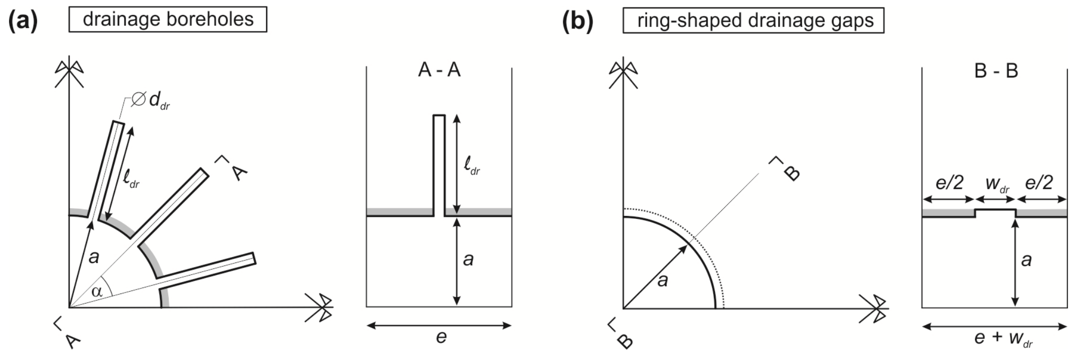

Figure 7.4 *Drainage layouts of (a) number n radial drainage boreholes each cross-section arranged in axial borehole distance $e \approx (\pi/n)(a+l_{dr})$ and (b) ring-shaped drainage gaps*

Table 7.1 *Parameters for the comparative analyses*		
Problem layout		
Depth of cover (T=H=H_w)	T	100 m
Tunnel radius	a	5 m
Drainage boreholes		
Number in each cross-section	n	4, 8, 12, 16
Sector angle	α	22.5-90 °
Length	l_{dr}	2 m
Diameter	d_{dr}	0.1 m
Axial distance	e	$(a+l_{dr})\cdot\pi/n$
Ring-shaped drainage gaps		
Width	w_{dr}	3, 6, 20, 50 cm
Axial distance	e	1-160 m

7.2.1 Dimensional analysis

The maximum water pressure p acting on the tunnel lining may be normalized with the initial pressure p_0 and expressed as a function of the geometrical parameters of the seepage field and of the drainage layout (for details see Zingg [62]). In case of individual drainage boreholes (Fig. 7.4a) and taking account of the dependencies of the axial distance $e = f(l_{dr}, a, n)$ according to Table 7.1, dimensional analysis leads to

$$\frac{p}{p_0} = f\left(\frac{T}{a}, n, \frac{l_{dr}}{a}, \frac{d_{dr}}{a}\right) \quad . \tag{7-1}$$

In case of ring-shaped drainage gaps (Fig. 7.4b), the functional dependencies are

$$\frac{p}{p_0} = f\left(\frac{T}{a}, \frac{w_{dr}}{a}, \frac{e}{a}\right) \quad . \tag{7-2}$$

The water discharge Q collected from the drainage boreholes or ring elements (averaged per linear metre) is normalized with the inflow Q_0, which denotes the inflow per tunnel meter into a permeable tunnel without additional drainage measures

$$Q_0 = \frac{2\pi k p_0}{\rho_w g \ln\left(T/a\right)} \quad , \tag{7-3}$$

with ρ_w and g denoting the unit weight of water and the acceleration due to gravity, respectively. By doing so, the dependency of the ground permeability k can be omitted and the functional dependencies are the same as in Eqs. (7-1) and (7-2).

7.3 Effect of drainage boreholes

7.3.1 Spacing of drainage boreholes

Figure 7.5 shows the normalized residual water pressure p/p_0 acting on the tunnel lining (l.h.s.) and the normalized inflow Q/Q_0 (r.h.s.) as a function of the drainage borehole number n (or the sector angle α, respectively) for the tunnel example of Table 7.1.

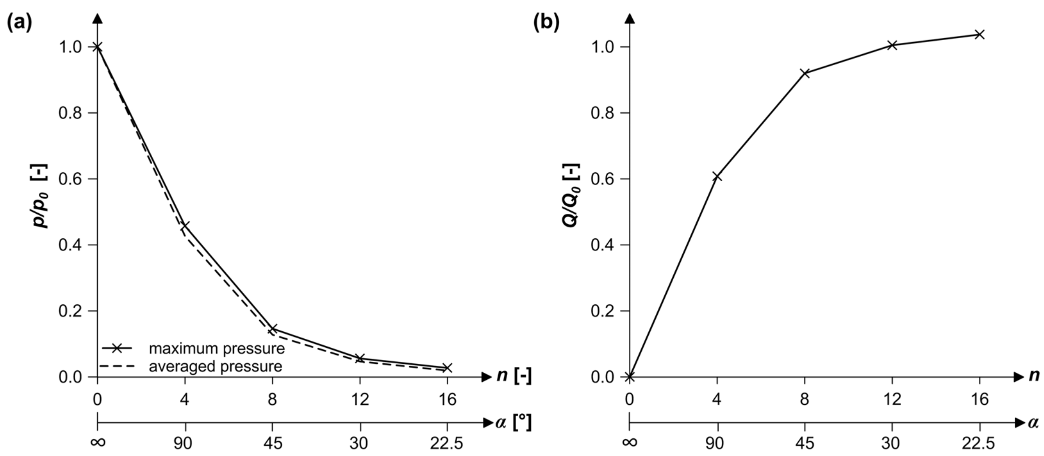

Figure 7.5 *(a) Normalized residual water pressure p/p_0 on the tunnel lining and (b) normalized water discharge from the boreholes Q/Q_0 as a function of the number n of drainage boreholes or the sector angle α (drainage layout of Fig. 7.3a; other parameters according to Table 7.1)*

Already 4 boreholes each drainage cross-section reduce the water pressure to 43% of the initial value (solid line in Fig. 7.5a). 8 drainage boreholes decrease the pressure to $p/p_0 = 13\%$, but increasing the drainage number to more than 12 boreholes provides a marginal benefit in terms of residual water pressure ($p/p_0 < 5\%$). The deviation between the solid and dashed line (indicating the maximum and the averaged water pressure within the boreholes, respectively) is negligible for our purposes, which is why only the maximum water pressure will be considered below.

Water discharge increases considerably with increasing seepage area, *i.e.* with increasing borehole number (to $Q/Q_0 = 0.6$ and 0.92 for $n = 4$ and 8, respectively in Fig. 7.5b). For even more drainage boreholes, more discharge is collected than when assuming a permeable tunnel lining ($Q/Q_0 > 1$).

7.3.2 Seepage flow domain

Figure 7.6 shows the normalized residual water pressure p/p_0 acting on the tunnel lining (l.h.s.) and the normalized inflow Q/Q_0 (r.h.s.) as a function of the distance T between tunnel crown and upper boundary of the seepage flow domain.

The residual water pressure slightly decreases with increasing seepage flow domain, mainly in case of small drainage borehole number (compare curves for $n = 4$ to 16 for $T/a < 20$ in Fig. 7.6a). However, even for only 4 drainage boreholes the value of residual pressure at $T/a = 10$ is only about $0.1p_0$ higher than at $T/a = 80$; and at $T/a = 20$, the deviation is merely $0.05p_0$, which is negligible compared to the total amount of pressure relief (compare points A to C and B to C in Fig. 7.6a, respectively). For 12 drainage boreholes, the residual pressure is less than 8% of the initial water pressure, independently of the size of the seepage flow domain.

Accordingly, in the case of 4-8 drainage boreholes, water discharge marginally increases with the distance T (Fig. 7.6b). If the boreholes are very closely spaced ($n \geq 12$) and thus induce great poressure relief, slightly increased inflow is observed for small seepage area $T/a < 10$ (boundary effect similar to $T/D < 5$ in Section 2.4.2). Overall, the size of the seepage flow domain has a very small to even negligible effect on the normalized water discharge.

7.3.3 Diameter of drainage boreholes

Figure 7.7 shows the normalized residual water pressure p/p_0 on the tunnel lining (l.h.s.) and the normalized inflow Q/Q_0 (r.h.s.) as a function of the normalized diameter d_{dr} of the drainage boreholes.

Even a very small drainage borehole of 1.5 cm diameter leads to a considerable relief in water pressure ($d_{dr}/a = 0.003$ in Fig. 7.7a). The residual water pressure decreases and the water discharge increases with increasing seepage area, *i.e.* increasing borehole diameter. Boreholes larger than $d_{dr}/a = 0.02$ (*i.e.* 10 cm diameter in our tunnel example) provide a marginal utility in terms of water pressure and discharge. The increase of the seepage area due to 16 relatively thin drainage boreholes leads to more discharge than when assuming a permeable tunnel lining ($Q/Q_0 > 1$ for $d_{dr}/a \geq 0.01$ in Fig. 7.7b).

7.3.4 Length of drainage boreholes

Finally, the effect of the normalized length l_{dr} of the drainage boreholes is shown in Figure 7.8 in terms of the normalized residual water pressure p/p_0 on the tunnel lining (l.h.s.) and the normalized inflow Q/Q_0 (r.h.s.).

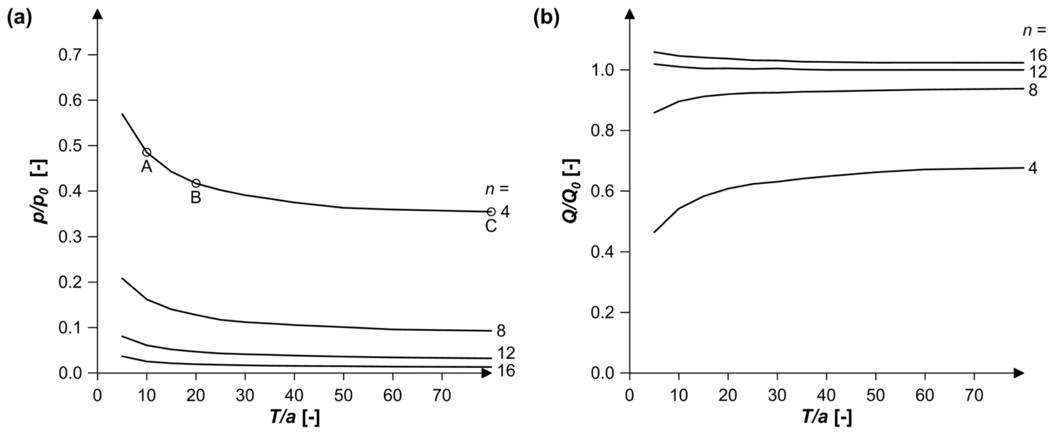

Figure 7.6 *(a) Normalized residual water pressure* p/p_0 *on the tunnel lining and (b) normalized water discharge from the boreholes* Q/Q_0 *as a function of the normalized distance* T *(drainage layout of Fig. 7.3a; other parameters according to Table 7.1)*

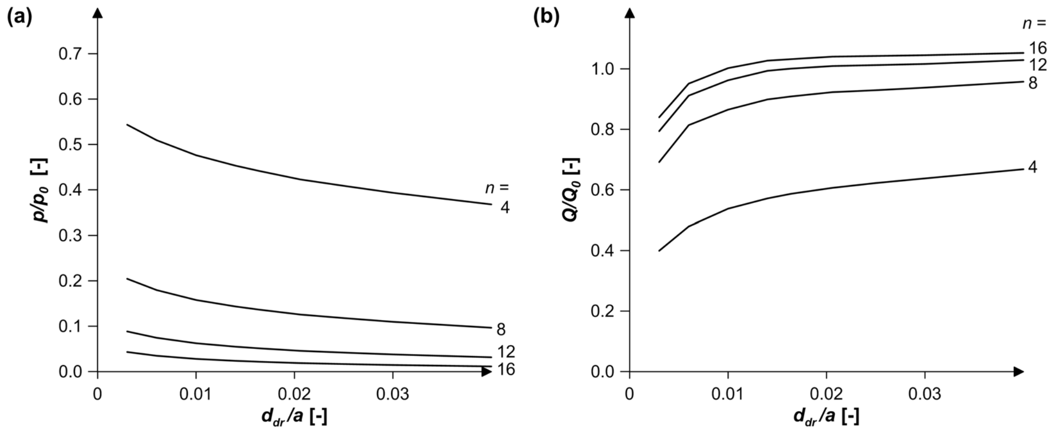

Figure 7.7 *(a) Normalized residual water pressure* p/p_0 *on the tunnel lining and (b) normalized water discharge from the boreholes* Q/Q_0 *as a function of the normalized borehole diameter* d_{dr} *(drainage layout of Fig. 7.3a; other parameters according to Table 7.1)*

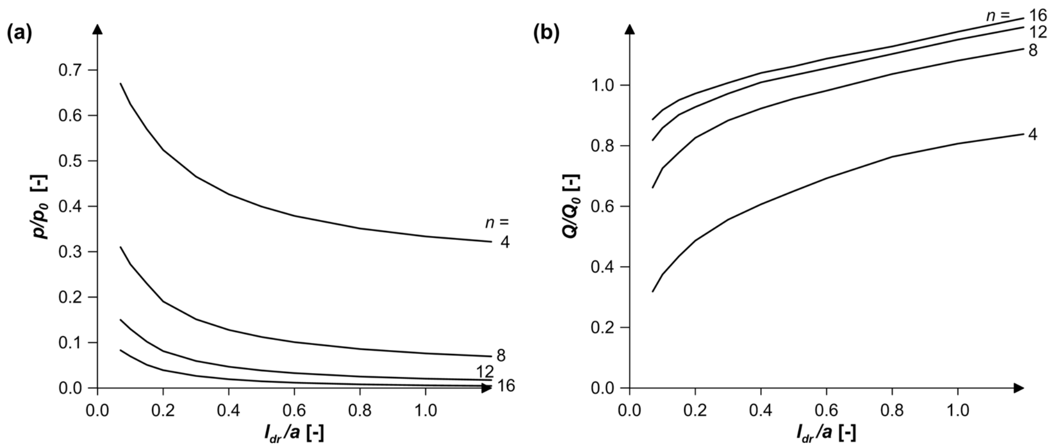

Figure 7.8 *(a) Normalized residual water pressure* p/p_0 *on the tunnel lining and (b) normalized water discharge from the boreholes* Q/Q_0 *as a function of the normalized borehole length* l_{dr} *(drainage layout of Fig. 7.3a; other parameters according to Table 7.1)*

The residual water pressure decreases and the water discharge increases with increasing borehole length. However, boreholes longer than $l_{dr}/a = 0.4$ to 0.6 provide only additional benefit for water pressure relief, but still lead to an increase of water discharge. Thus the choice of the appropriate drainage borehole length is based on a balance of benefits in terms of pore pressure relief and costs of high water discharge.

7.4 Parametric study

A parametric study was conducted into the effect of drainage borehole number n, diameter d_{dr}, length l_{dr}, as well as into the effect of ring-shaped drainage gaps of width w_{dr} at axial distance e considering several sizes of seepage area T (Table 7.2). The results are edited as dimensioning charts and given in Appendix II. The use of these dimensioning charts will be shown by means of an application example in Section 7.5.

***Table 7.2** Values for the parametric study*

Problem layout		
Normalized size of seepage area	T/a	10-80
Drainage boreholes (layout of Fig. 7.4a)		
Number (each cross-section)	n	4, 8, 12, 16
Normalized length	l_{dr}/a	0.01-1.2
Normalized diameter	d_{dr}/a	0.006-0.04
Ring-shaped drainage gaps (layout of Fig. 7.4b)		
Normalized width	w_{dr}/a	0.06-0.1
Normalized axial distance	e/a	0.2-30

7.4.1 Drainage boreholes

The graphs of the normalized residual water pressure on the tunnel lining (Fig. II.1) expectably decrease with increasing borehole length, diameter, number and size of seepage area. Correspondingly, the normalized water discharge out of the boreholes increases with increasing borehole length, diameter, number and (for small n or small T/a) also with increasing size of seepage area (Fig. II.2). As expected, the graphs for variable T/a coincide for great drainage-induced pressure relief (see *e.g.* graphs for $n = 8$ in Fig. II.2c). However, in case of many and very long drainage boreholes around a shallow tunnel ($n \geq 12$; $l_{dr}/a \geq 0.8$; $T/a \leq 20$), the distance between drainage boreholes and upper boundary of seepage flow is considerably reduced and the inflow increases due to the boundary effect (see *e.g.* graph for $n = 12$ and $T/a = 10$ in Fig. II.2a).

Note that comparative calculation showed very well agreement of the results in hand with previous research (*e.g.* of Beruchashvili [53]; *cf*. Section 1.2.3).

7.4.2 Ring-shaped drainage gaps

Ring-shaped drainage gaps lead to a decrease below 70% of the initial water pressure in cases where the axial spacing is smaller than about 5 times the tunnel diameter ($e/a \leq 5$ in Fig. II.3). A residual water pressure of less than 30% of the initial pressure requires densely arranged elements of at least $e/a \leq 2.2$ or 1.2, respectively, depending on the width of the drainage gap (compare Fig. II.3d to II.3a).

Correspondingly, the inflow decreases with increasing axial distance, decreasing width of the ring-shaped drainage gaps and size of seepage area (Fig. II.4).

7.5 Application example

The normalized charts allow for easy pre-dimensioning of the residual water pressure (and water discharge to take account of) due to drainage measures. Consider, for example, a tunnel with horse-shoe cross-section of about 8x9 m, located 300 m below the water table in a ground of permeability $k = 5 \cdot 10^{-6}$ m/s. The final lining shall withstand a residual water head of maximum 60 m. Drainage measures are either boreholes of 10 cm diameter or ring-shaped drainage gaps of maxium 20 cm width. Which drainage layout does allow for such a pressure relief and to what amount of water inflow?

The form of the tunnel is of subsidiary importance, as long as the tunnel lining is impervious (see also Nasberg and Ilyushin [44]). Therefore, we approximate the tunnel by a cylindrical tunnel of an equivalent radius of 4.5 m.

First, we consider ring-shaped drainage gaps. In our example is $T/a = 66$, *i.e.* we have to interpolate between the curves for $T/a = 60$ and 80 in Figures II.3 and II.4. The aimed residual water pressure corresponds to $p/p_0 \leq 0.2$. Small ring elements require a very dense axial spacing ($e/a \leq 1$ according to Fig. II.3a and II.3b), and leads to a discharge of 0.55 Q/Q_0, which is in absolute terms an inflow of 1.2 l/sm (Fig. II.4b and Eq. (7-3)). Ring elements of 18 cm width and of axial spacing of 5.4 m would provide for the desired pressure relief ($e/a \leq 1.2$ in Fig. II.3c for $p/p_0 = 0.2$). This corresponds to a water inflow of 1.5 l/s every linear metre (0.68 Q/Q_0 in Fig. II.4c).

The effectiveness of the drainage boreholes in terms of the residual water pressure on the lining for $d_{dr}/a = 0.022$ in our example is evaluated by means of Figure II.1c: 8 drainage boreholes of $l_{dr}/a = 0.2$ allow for a pore pressure relief to $p/p_0 = 0.14$ and lead to water discharge of $Q/Q_0 = 0.85$ (Fig. II.2c). In absolute terms, this means for our tunnel example 8 radial drainage boreholes of 10 cm diameter and 0.9 m length in each cross section. The axial spacing is 2.2 m ($\approx (a+l_{dr}) \cdot \pi/n$), the residual water pressure 42 m, and the inflow 1.9 l/sm.

As from the standpoint of installation and maintenance the drainage boreholes are more convenient than ring-shaped drainage gaps, the designing engineer chooses probably the drainage boreholes.

7.6 Conclusions

Radial drainage boreholes are a very effective measure to reduce the residual water pressure on the tunnel lining. Already 4 drainage boreholes each cross section and of the same length as the tunnel radius allow for reducing the initial water pressure by about 50%. 12 drainage boreholes each cross-section even lower the water pressure to less than 20% of the initial pressure, independently of the drainage diameter, the borehole length or the area of the seepage field. On the other hand, water discharge increases considerably to at least 60% of the inflow into a permeable tunnel in case of 4 drainage boreholes, and to maximum 115% in case of 12 drainage boreholes.

Ring-shaped drainage gaps decrease the water pressure to less than 30% in case they are spaced along the tunnel axis every 1-2 times the value of the tunnel radius. The water discharge increases to 47-66% of the inflow assuming a permeable tunnel. Lower residual water pressures require denser spaced and/or wider ring-shaped drainage gaps, which in turn may endanger overall stability of the tunnel lining.

Note that both permanent drainage measures consider stationary conditions, sufficient drainage capacity, an impermeable tunnel lining, homogeneously permeable ground and no drawdown in groundwater table. Considering transient behaviour would increase both pressure and inflow especially at early drainage stages in medium permeable ground (*cf*. Section 5.2). Taking account of the hydraulic capacity of the drainage boreholes could lead to an increase of the residual water pressure (*cf*. Chapter 4). A tunnel lining of at least some hydraulic permeability would lower the residual water pressure, but increase the amount of water discharge. Heterogeneousl ground could lead to favourable or unfavourable pressure distributions, depending on location (and permeability) of the ground layer in relation to the drainage measure. However, permanent drainage measures are located at highly permeable spots, i.e. they are able to induce a wide pore pressure relief (*cf*. Chapter 3). The drawdown in water table, finally, is favourable in terms of bot pressure and inflow (*cf*. Section 5.3).

8 Concluding remarks

In this research project, the effects of drainage measures for two particularly important problems of tunnelling through water-bearing ground have been investigated systematically and comprehensively: the stability of the tunnel face and stability of grouting bodies. Drainage measures improve the stability and deformation behaviour of underground openings decisively by relieving the pore pressure which in turn, (i) reduces the magnitude of the seepage forces acting on the ground, and (ii) increases the effective stress and thus the resistance of the ground to shearing.

The first part of the report focused on face stability, which was analysed through limit equilibrium computations taking account of the numerically-determined seepage flow conditions prevailing in the ground after the implementation of a drainage measure. The findings were summarized within the respective chapters. The main contributions may be summarized as follows:

- A design equation was developed (Chapter 2), which allows a quick assessment to be made of tunnel face stability considering the effects of various advance drainage schemes and thus representing a very valuable design aid for tunnel engineers. The coefficients that appear in the equation can be depicted using dimensionless nomograms worked out by analysing the computational results of a comprehensive parametric study incorporating a wide parameter range in a homogeneous ground.
- In ground of non-uniform permeability, the drainage boreholes should be arranged so that they lower the pressure in and around critical barrier layers; they will then be are as effective as in homogeneous ground. Various critical situations in terms of the orientation, elevation and thickness of ground layers of different permeability to the surrounding rock were set out in Chapter 3. Also, the suitability of using an equivalent homogeneous anisotropic model for calculating the seepage flow condition was shown in the case of thin layered ground.
- The application range of drainage measures is restricted due to feasibility aspects related to the drainage boreholes themselves (associated with their hydraulic capacity and casings; Chapter 4), the ground permeability in combination with the construction process (the lead-time required for pore pressure relief) or environmental constraints (admissible groundwater drawdown, settlement or inflow; Chapter 5). An equivalent conductivity model taking account of pipe-flow hydraulics within the borehole allowed a determination to be made of the potential loss of pore pressure relief in the surrounding ground with regard to the hydraulic capacity of the borehole. Also, Chapters 4-5 discussed the potential loss of pore pressure relief in the surrounding ground due to the aforementioned factors and showed the applicability limits of the design nomograms of Chapter 2.

The second part of the report focused on the stability of grouting bodies in geological fault zones under high hydrostatic pressure. The relationship between support pressure and displacement of the excavation boundary was investigated by considering the ground as a porous, elasto-plastic medium obeying the principle of effective stress, Coulomb's failure criterion and by taking into account the seepage forces developing in the presence of a series of different drainage measures. The findings were summarized within Chapter 6. The main contributions may be summarized as follows:

- For the virtual case of ideal drainage (either in advance of grouting or after grouting), existing analytical solutions were extended to consider an arbitrary radius of the drained zone.
- The effectiveness of realistic drainage schemes was studied by means of hydraulic-mechanical coupled FE-modelling considering the pore pressure relief resulting from the individual boreholes. The computational results provide valuable information about the number, length, spacing and location of drainage boreholes.
- Drainage (either in advance of grouting or after grouting) increases the stability of the grouting body considerably, both for ideal drainage and for specific arrangements of drainage boreholes. The analytical solutions for the case of ideal drainage provide a

lower limit for the lining support pressure and displacement at the excavation boundary. Chapter 6 shows under which conditions these solutions can be used in the case of realistic drainage schemes for the pre-dimensioning of grouting bodies in engineering practice.

The third part of the report focused on the effect of permanent drainage measures on the residual water pressure on the impermeable tunnel lining and on the discharge of water resulting from the drainage measures. A comprehensive parametric study was worked out, considering the ground as a porous medium obeying Darcy’s law at stationary conditions in the presence of drainage boreholes or ring-shaped drainage gaps. The findings were summarized within Chapter 7. The main contribution may be summarized as follows:

- Design charts are provided, which allow a quick assessment of the residual water pressure and of the inflow resulting from several different drainage layouts and thus represent a useful design aid for tunnel engineers.

There are still a number of open questions concerning drainage measures in tunnelling, which merit further investigation (see also Zingg [62]). From the point of view of engineering practice, special emphasis is recommended to place on the selection and handling of casings allowing for pore pressure relief. This is a demanding task on site and solutions are often found only by trial and error. A more detailed investigation into the design of casings (with materials and shapes providing high stiffness and torque, but still offering adequate spacing for pore pressure relief; the hydraulic behaviour of inflow into casings when taking account of local losses at the openings etc.) and execution aspects of drilling and insertion would be of relevance for drainage application in tunnelling practice.

Appendices

I Nomograms of face support

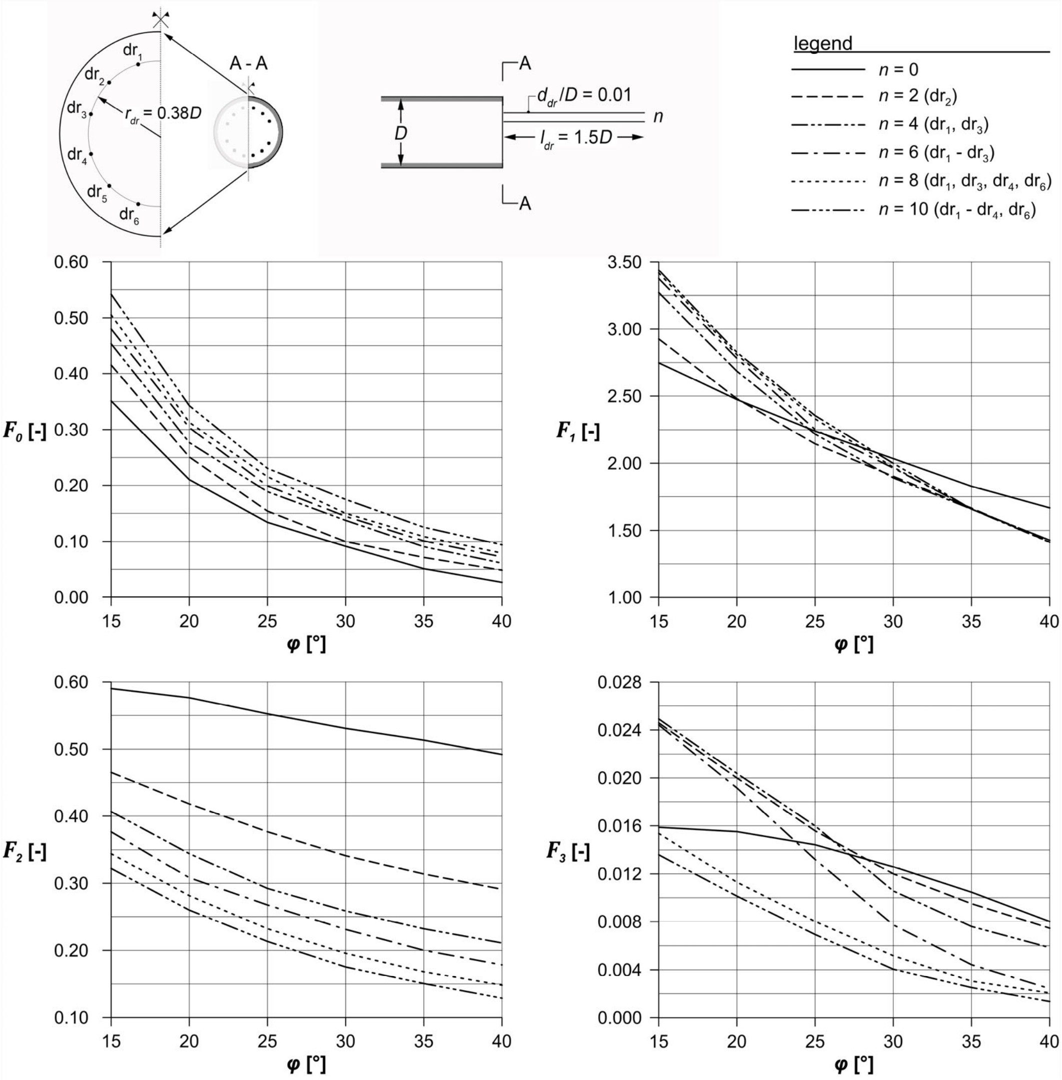

Figure I.1 *Nomograms for the coefficients F_0 to F_3 in the case of drainage via boreholes from the tunnel face (l_{dr}/D = 1.5; variable: number n of boreholes)*

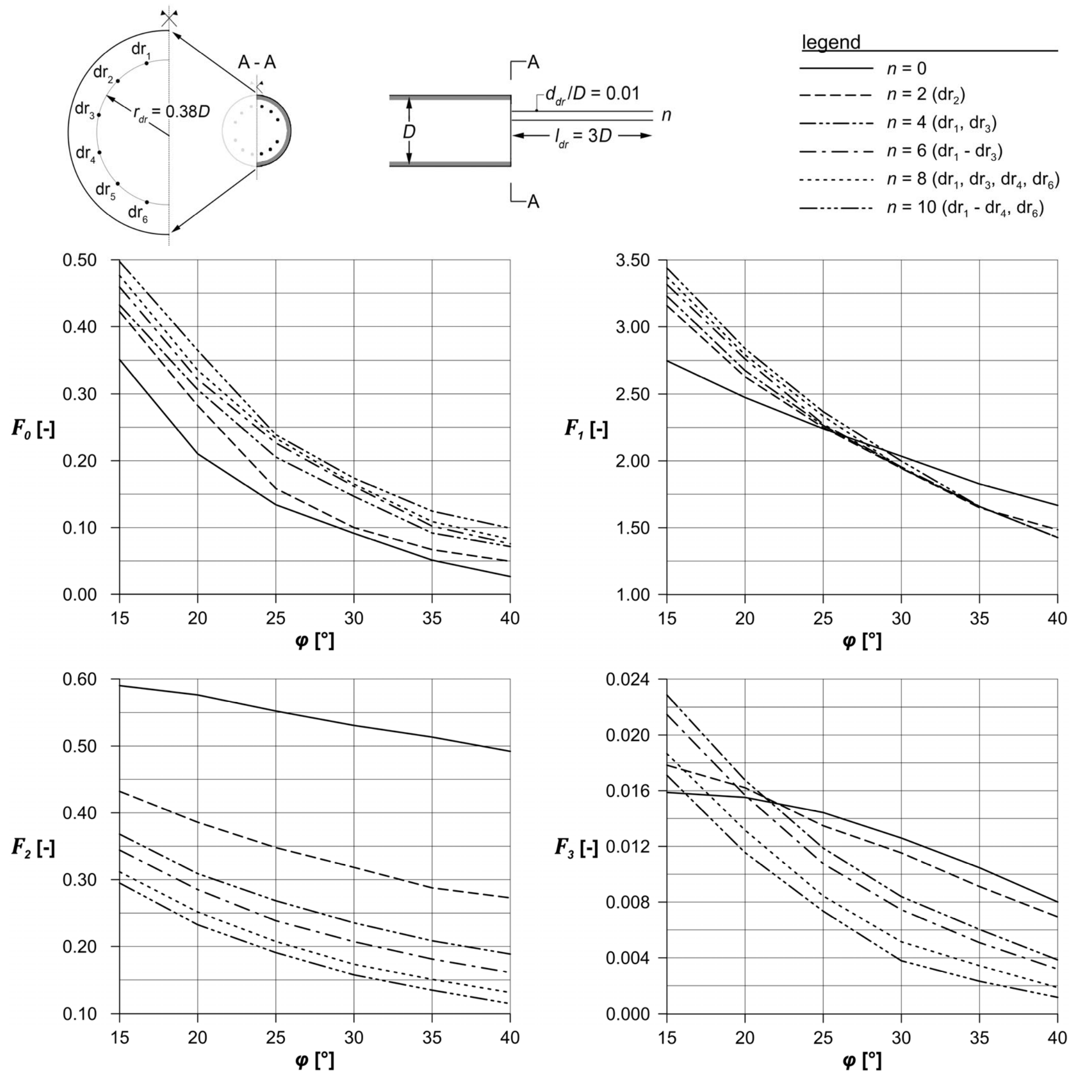

***Figure I.2** Nomograms for the coefficients F_0 to F_3 in the case of drainage via boreholes from the tunnel face (l_{dr}/D = 3; variable: number n of boreholes)*

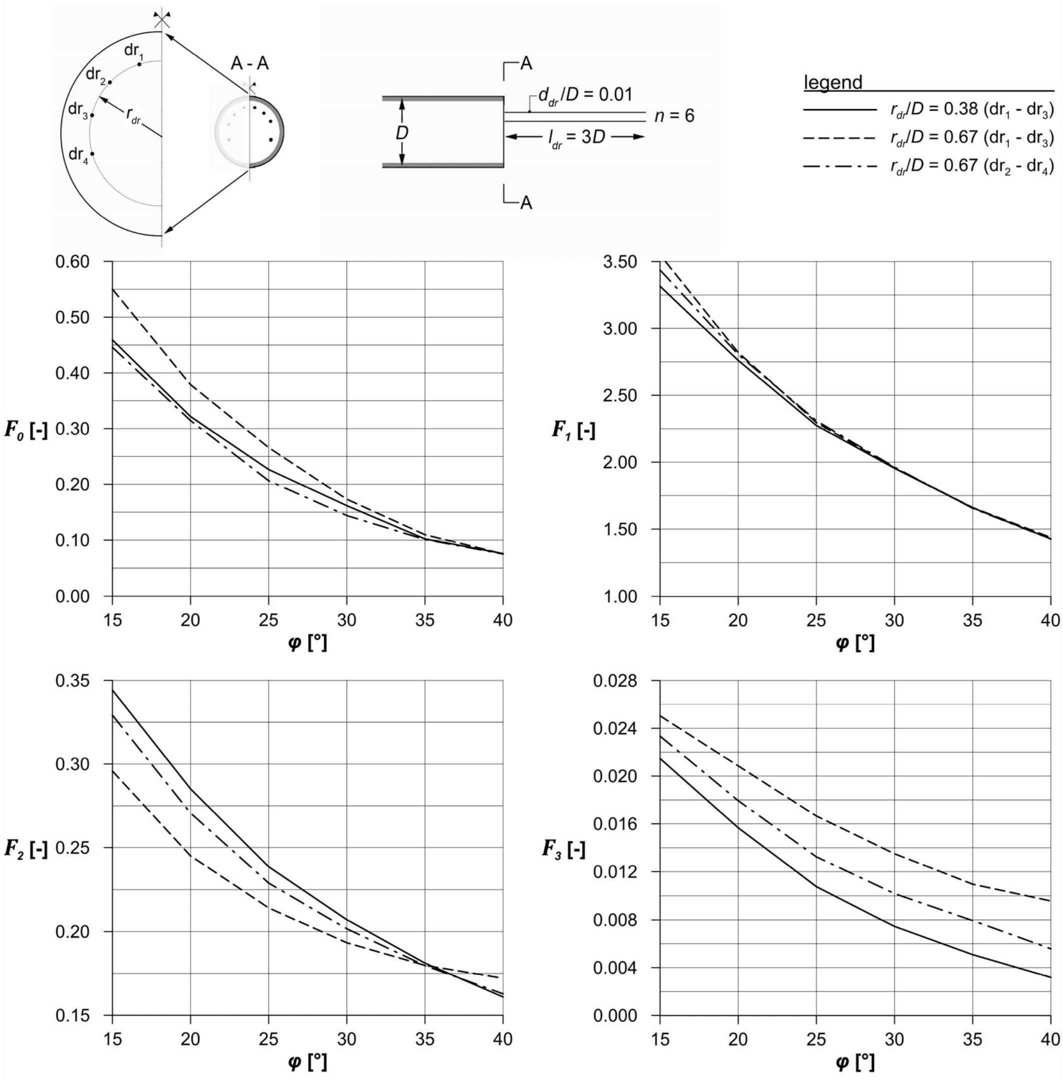

***Figure I.3** Nomograms for the coefficients F_0 to F_3 in the case of drainage via boreholes from the tunnel face (n = 6; variable: borehole location r_{dr}/D)*

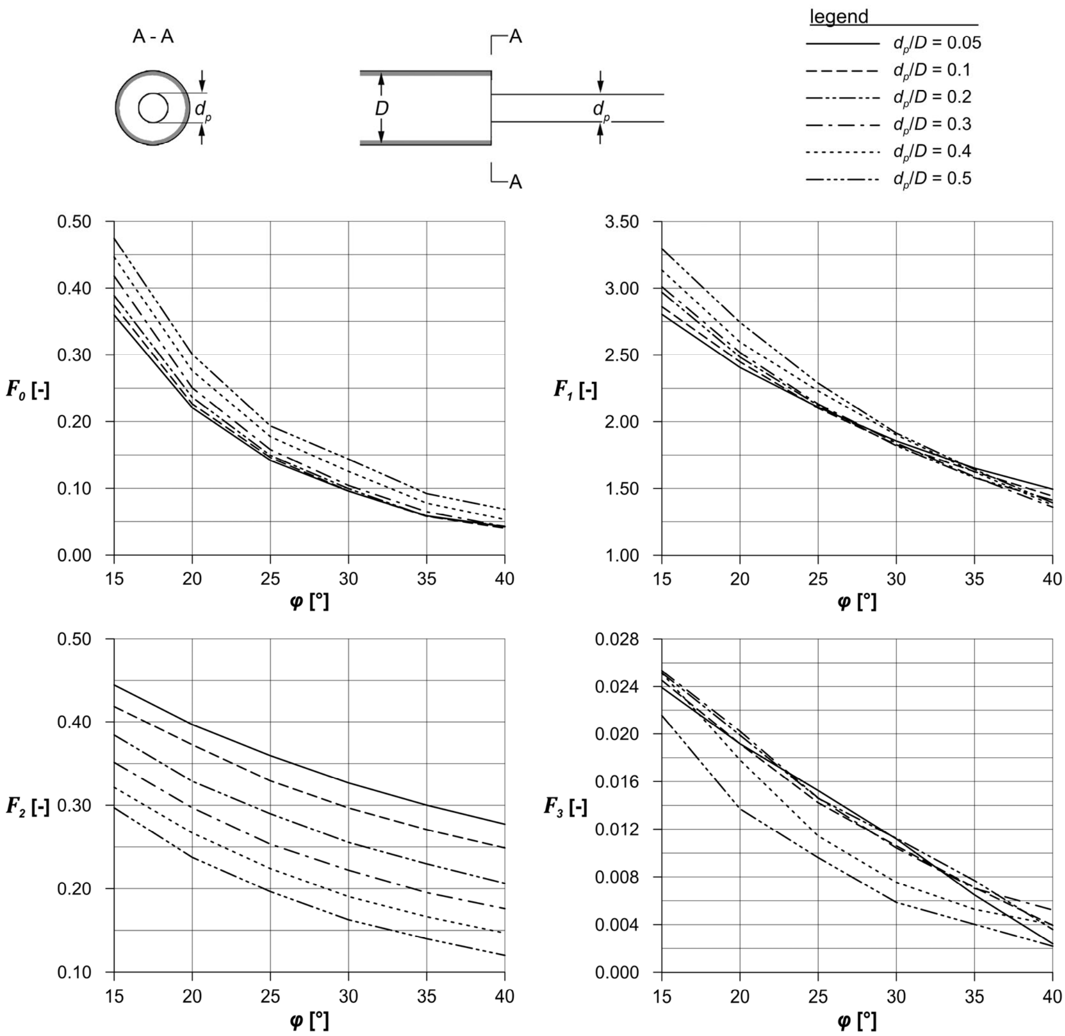

Figure I.4 *Nomograms for the coefficients F_0 to F_3 in the case of drainage via a co-axial pilot tunnel (variable: normalized pilot tunnel diameter d_p/D)*

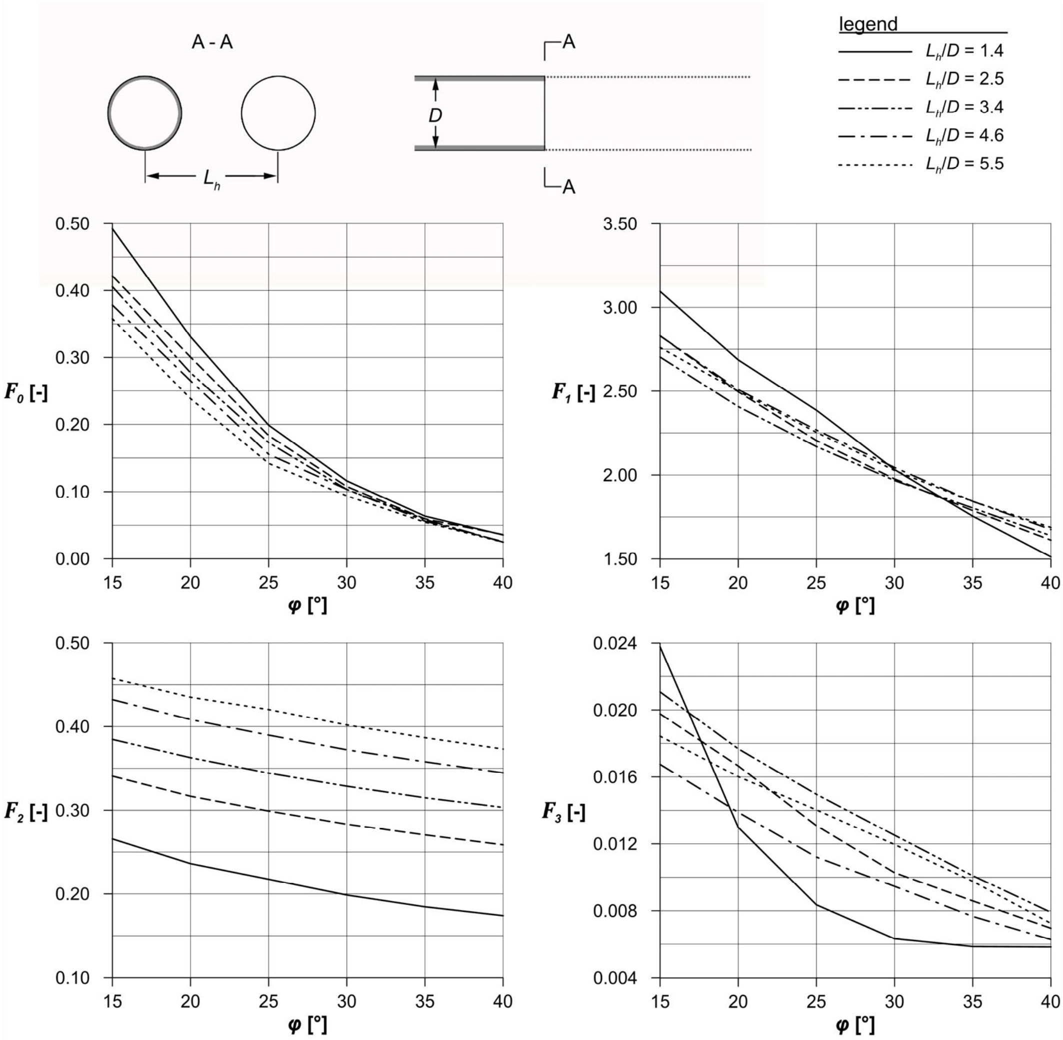

***Figure I.5** Nomograms for the coefficients F_0 to F_3 in the case of drainage via the first tube of a twin tunnel (variable: centre distance L_h/D)*

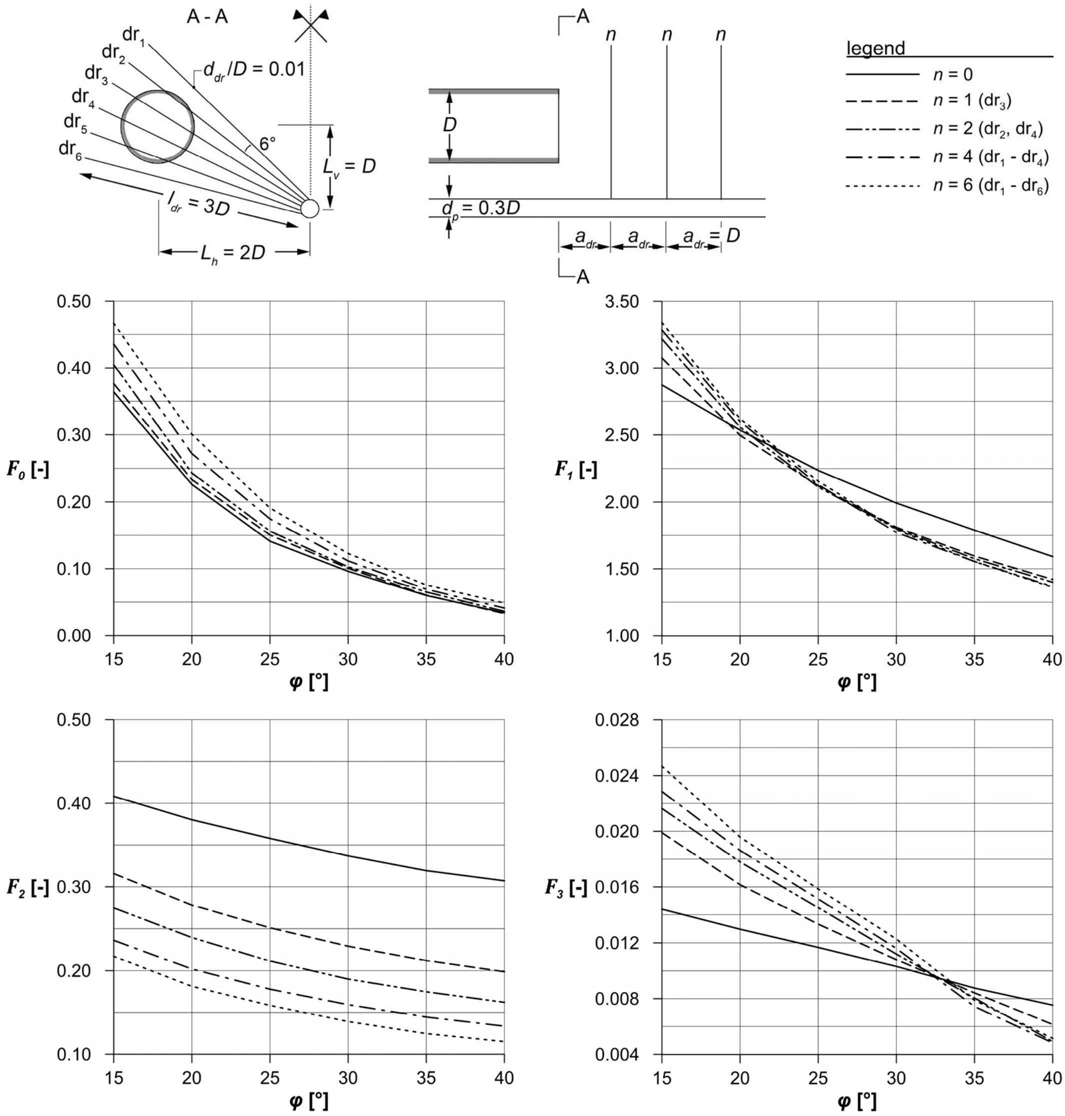

Figure I.6 *Nomograms for the coefficients F_0 to F_3 in the case of drainage via drainage curtains from an external pilot tunnel with permeable boundary (variable: number n of drainage boreholes)*

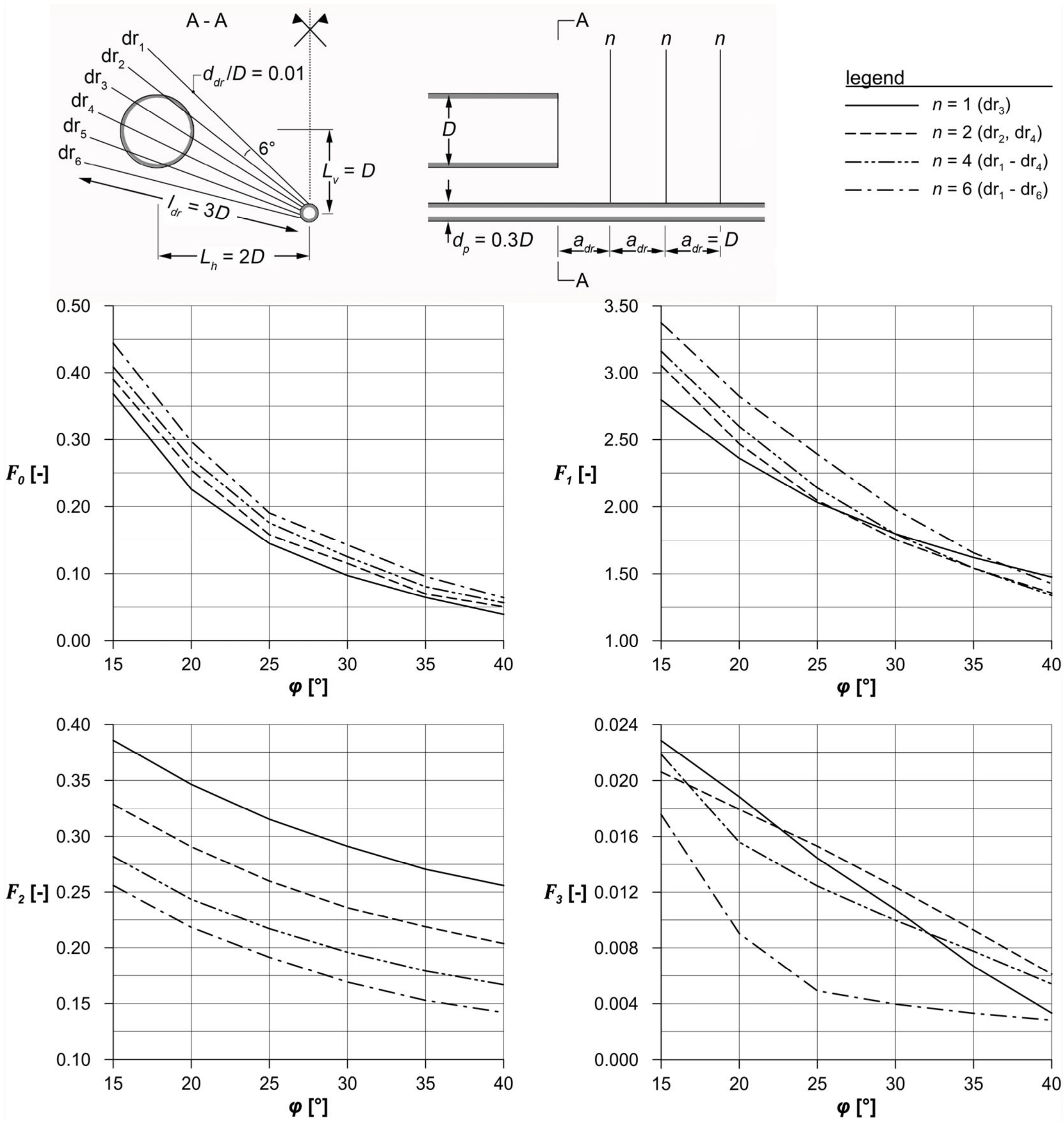

Figure I.7 *Nomograms for the coefficients F_0 to F_3 in the case of drainage via drainage curtains from an external pilot tunnel with impermeable boundary (variable: number n of drainage boreholes)*

II Dimensioning charts of residual water pressure and water discharge

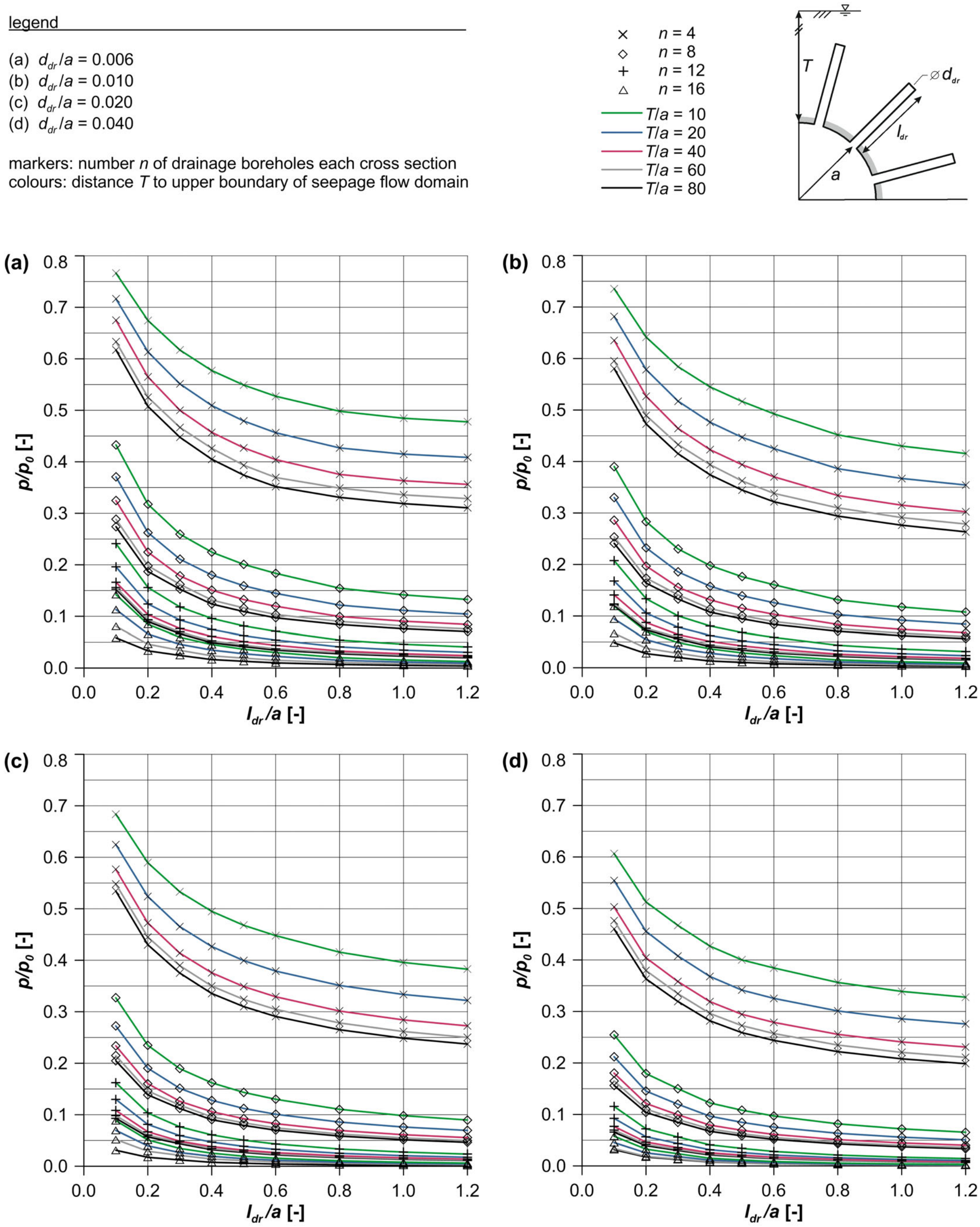

Figure II.1 *Normalized residual water pressure* p/p_0 *on the tunnel lining as a function of the normalized borehole length* l_{dr} *(axial borehole distance* $e \approx (\pi/n)(a+l_{dr})$*)*

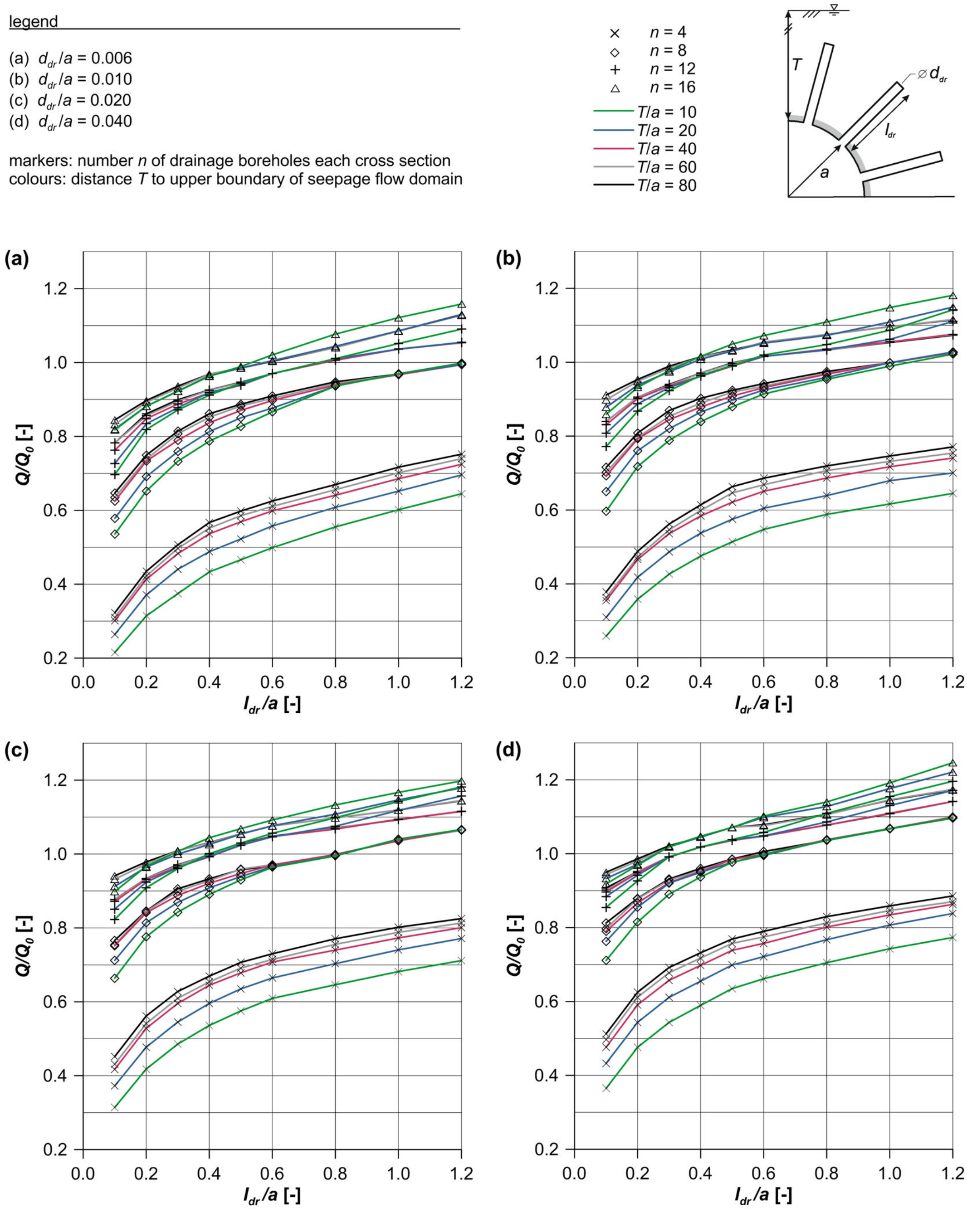

***Figure II.2** Normalized water discharge from the boreholes Q/Q_0 as a function of the normalized borehole length l_{dr} (axial borehole distance $e \approx (\pi/n)(a+l_{dr})$)*

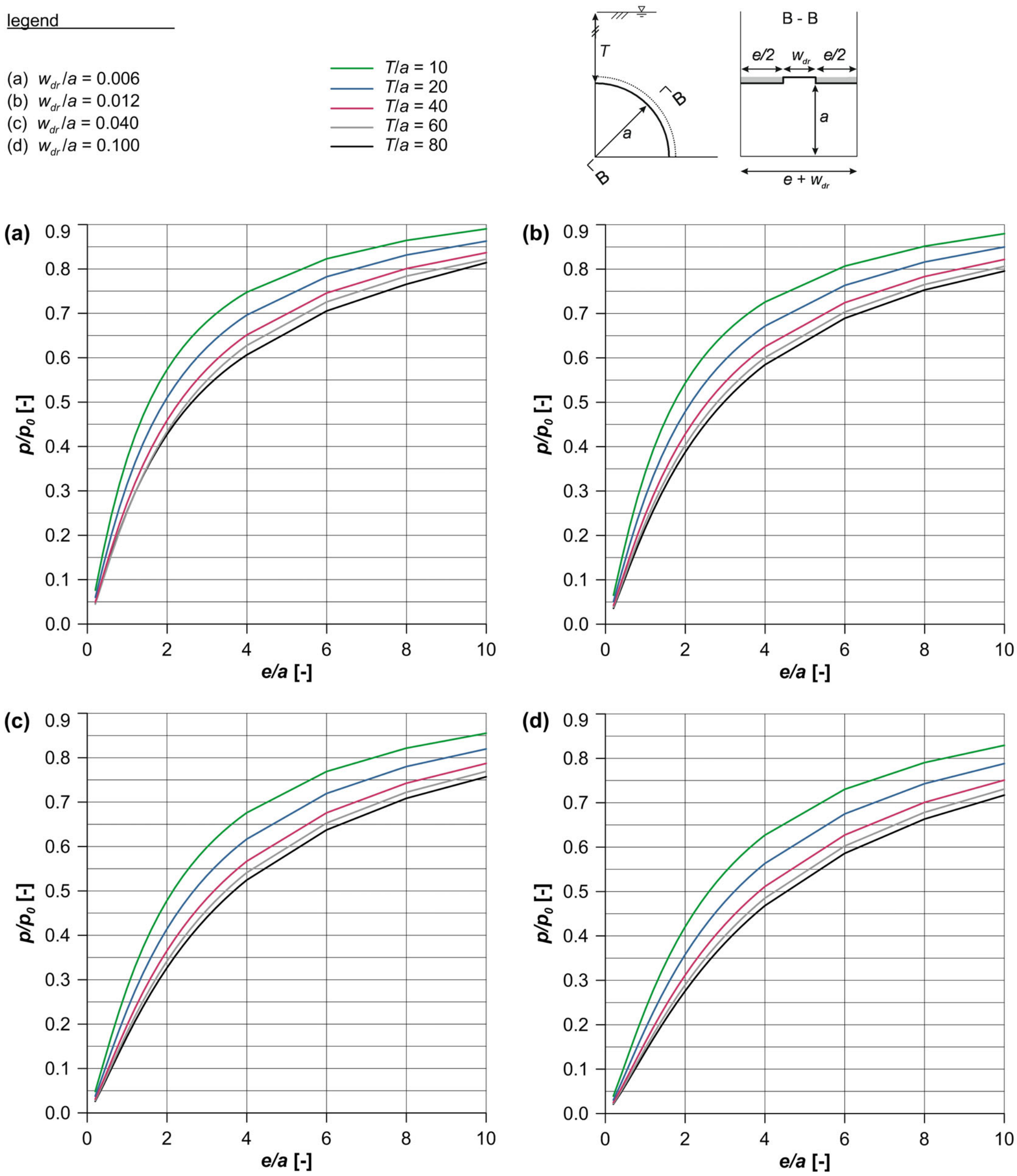

Figure II.3 *Normalized residual water pressure p/p_0 on the tunnel lining as a function of the normalized axial distance e*

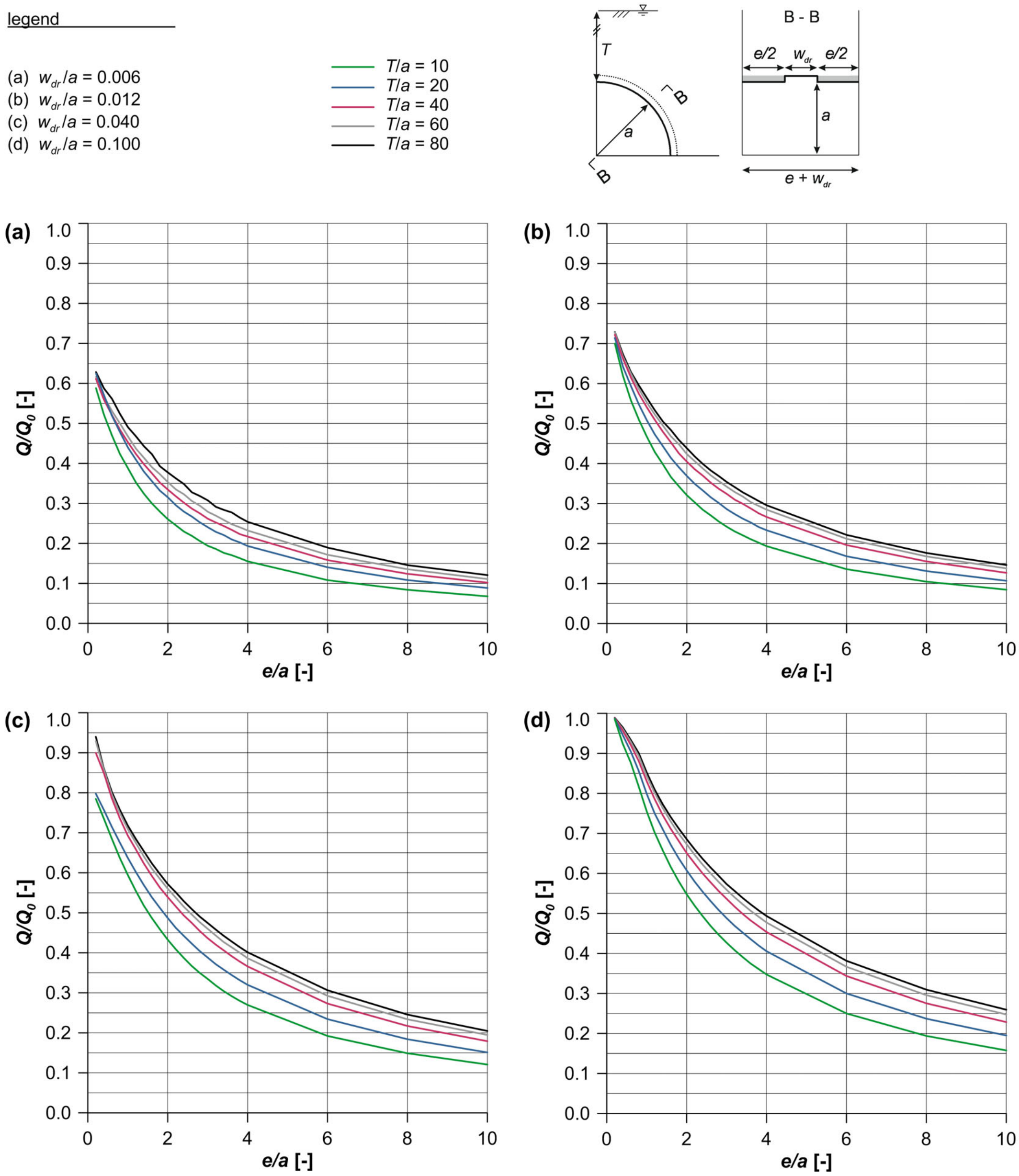

Figure II.4 *Normalized water discharge from the boreholes Q/Q_0 as a function of the normalized axial distance e*

Notation

Latin symbols

a	radius of the tunnel
a_{dr}	distance of drainage curtains
a_i	fraction of layer i
B	average hydraulic head of a specific drainage scheme at time t
b	radius of the grouting body
c	effective cohesion of the (untreated) ground
c_H	effective cohesion of the solid host rock
c_I	effective cohesion of the injection body
c_w	compressibility of water
D	diameter of the tunnel
D'	side length of equivalent square tunnel cross-section
d_b	diameter of grouted borehole
d_{dr}	diameter of drainage borehole
d_L	thickness of a layer
d_{lin}	thickness of the lining
d_p	diameter of pilot tunnel
E	Young's modulus of the (untreated) ground
e	axial distance of drainage boreholes
E_H	Young's modulus of the solid host rock
E_I	Young's modulus of the injection body
E_S	constrained modulus of the ground
$f(...)$	function of ...
$F_0 - F_3$	coefficients provided by nomograms
f_c	uniaxial compressive strength
f_{cI}	uniaxial compressive strength of the injection body
f_s	seepage force
g	acceleration due to gravity
H	depth of cover
h	hydraulic head
$\bar{h}$	normalized hydraulic head
h_0	initial hydraulic head (depth of the tunnel axis underneath the water table)
$\bar{h}_0$	normalized initial hydraulic head
$h_{e,i}$	energy head at point i
h_V	head loss in drainage borehole
H_w	elevation of water table (with respect to the tunnel crown)
i_{adm}	admissible hydraulic head gradient
I_x	hydraulic head gradient of the drainage borehole
k	permeability
k_1	permeability of layer 1
k_2	permeability of layer 2
K_g	permeability of the ground
k_H	permeability of the solid host rock
k_I	permeability of the injection body
k_L	permeability of a layer
k_{lower}	permeability of the lower formation
k_n	equivalent permeability normal to stratified layers

k_p	equivalent permeability parallel to stratified layers
$k_{s,eq}$	equivalent sand roughness of drainage borehole wall
k_{upper}	permeability of the upper formation
K_x	equivalent permeability in x-direction
$K_{x,pipe}$	equivalent permeability in drainage borehole considering pipe flow
k_z	permeability of a zone
L	centre distance
l	circle line of the drainage measure
l_{dr}	length of drainage boreholes
$l_{dr,char}$	characteristic length of drainage boreholes
L_h	horizontal centre distance
L_v	vertical centre distance
M_{eff}	degree of pore pressure relief of a drainage scheme at time t
m	average radial distance of drainage boreholes
m_I	material constant of the injection body
n	number of drainage boreholes (or drainage slits)
n_b	bolt density
$N_{c\omega}$	cohesion influence coefficient for wedge angle ω
n_g	porosity of saturated ground
$N_{h\omega}$	seepage flow influence coefficient for wedge angle ω
$N_{\gamma\omega}$	weight influence coefficient for wedge angle ω
p	pore water pressure
p_0	initial pore water pressure
p_{atm}	atmospheric pressure (seepage face)
Q	discharge of water, water inflow
Q_0	water inflow in untreated ground
Q_{id}	water inflow when considering ideal drainage
r	coordinate in radial direction
R	radius of the hydraulic head field
r_{dr}	distance of boreholes from tunnel axis
Re	Reynolds number
R_s	percentage of seepage face area on the drainage shell surface
s	effective face support pressure
s_0	effective face support pressure for cohesionless ground
s_{nomo}	effective face support pressure according to the nomograms
s_{max}	maximum effective face support pressure
S_s	specific storage coefficient
s_ω	support pressure for wedge angle ω
T	distance of the upper boundary of the seepage flow domain to the tunnel crown
t	time
u	radial displacement
u_a	radial displacement of the excavation boundary ($r = a$)
u_b	radial displacement of the outer boundary of the grouting body ($r = b$)
u_S	settlement of ground surface
v_x	average flow velocity coaxial to the drainage borehole
w_{dr}	width of ring-shaped drainage gaps
x	(local) coordinate parallel to the drainage borehole
x_1	(global) horizontal coordinate parallel to the tunnel axis
x_2	(global) horizontal coordinate perpendicular to the tunnel axis
x_3	(global) vertical coordinate
x_b	coordinate along to the drainage borehole casing

x_f	position of tunnel face
x_{If}	distance of interface of a layer to tunnel face
x_s	spacing between slots or perforations in borehole screens
z	(local) vertical coordinate of the drainage borehole; geodetic height
z_b	position of bottom edge of a layer
z_I	distance of tunnel axis to interface of a layer

Greek symbols

α	sector angle between drainage boreholes/slits
γ'	submerged unit weight of the ground
γ_d	dry unit weight of the ground
γ_w	unit weight of water
ε	strain
η	degree of drainage; $\eta = (l\text{-}a)/(b\text{-}a)$
κ_I	loosening or dilatation factor of the injection body
λ	degree of plastification; $\lambda = (\rho\text{-}a)/(b\text{-}a)$
λ_p	coefficient of lateral stress in prism
λ_w	coefficient of lateral stress in wedge
ν	Poisson's ratio of the (untreated) ground
ν_H	Poisson's ratio of the solid host rock
ν_I	Poisson's ratio of the injection body
ρ	radius of the plastic zone
ρ_w	unit density of water
σ	stress
σ'_b	effective radial stress at the outer boundary of the grouting body (at $r = b$)
σ_a	radial stress at the excavation boundary (at $r = a$); lining support pressure
τ_m	bond strength
υ	kinematic viscosity of water
φ	angle of effective internal friction of the (untreated) ground
φ_H	angle of effective internal friction of the solid host rock
φ_I	angle of effective internal friction of the injection body
χ	ratio of idealized square tunnel cross-section side length to tunnel diameter
ψ	angle of effective dilatancy of the untreated ground
ψ_H	angle of effective dilatancy of the solid host rock
ψ_I	angle of effective dilatancy of the injection body
ω	angle between face and inclined slip plane
ω_{cr}	critical angle ω

References

[1] Nilsen, B., 1999. Key factors determining stability and water leakage of hard rock subsea tunnel, in: Amadei, Kranz, Scott, Smeallie (Eds.), Rock Mechanics for Industry. Balkema, Rotterdam, Vail, 593-599.

[2] Nilsen, B., 2011. Cases of instability caused by weakness zones in Norwegian tunnels. Bulletin of Engineering Geology and the Environment 70, 7-13.

[3] Nilsen, B., Palmström, A., 2001. Stability and water leakage of hard rock subsea tunnels, in: Adachi, T., Tateyama, K., Kimura, M. (Eds.), Modern Tunneling Science and Technology. Swets & Zeitlinger, Kyoto, Japan, 497-502.

[4] Wang, T.T., Wang, W.L., Lin, M.L., 2004. Harnessing the catastrophic inrush of water into New Yungchuen Tunnel in Taiwan, ITA-AITES World Tunnel Congress (WTC2004), Singapore, pp. 1-8.

[5] Hong, E.-S., Park, E.-S., Shin, H.-S., Kim, H.-M., 2010. Effect of a front high hydraulic conductivity zone on hydrological behavior of subsea tunnels. KSCE Journal of Civil Engineering 14, 699-707.

[6] Fulcher, B., Bell, M., Garshol, K., 2008. Pre-excavation drilling and grouting for water control and ground improvement in highly variable ground conditions at the Arrowhead Tunnels project, North American Tunneling Conference (NAT2008). SME Inc. Littleton, San Francisco, USA, 749-765.

[7] Sellner, P., Janotta, M., Koinig, J., 2008. Systematic drainage measures in the tunnel construction - experiences in the Neogene Sections of the Investigation Tunnels for the Koralm Tunnel. Geomechanik und Tunnelbau 1, 287-293.

[8] Pellet, F., Descoeudres, F., Egger, P., 1993. The effect of water seepage forces on the face stability of an experimental mircotunnel. Canadian Geotechnical Journal 30, 363-369.

[9] Anagnostou, G., Kovári, K., 1996. Face stability conditions with Earth Pressure Balanced shields. Tunnelling and Underground Space Technology 11(2), 165-173.

[10] de Buhan, P., Cuvillier, A., Dormieux, L., Maghous, S., 1999. Face stability of shallow circular tunnels driven under the water table: a numerical analysis. International Journal for Numerical and Analytical Methods in Geomechanics 12, 79-95.

[11] Broere, W., 2001. Tunnel face stability & new CPT applications, Civil Engineering. Technische Universiteit Delft, Delft, 208p.

[12] Vermeer, P.A., Ruse, N.M., Marcher, T., 2002. Tunnel heading stability in drained ground. Felsbau 20, 8-18.

[13] Droniuc, N., Magnan, J.P., Al Hallak, R., 2004. The stability of tunnel face accounting for the effects of groundwater, Numerical Models in Geomechanics (NUMOG IX). Pande & Pietruszczak, London, 433-438.

[14] Lee, I.-M., Nam, S.-W., 2001. The study of seepage forces acting on the tunnel lining and tunnel face in shallow tunnels. Tunnelling and Underground Space Technology 16, 31-40.

[15] Fellner, D., Gärber, R., 2004. Hydrogeological aspects for the design of deep seated tunnels. Lombardi AG (www.lombardi.ch; last access 01.06.2016), 15p.

[16] Höfle, R., Fillibeck, J., 2007. Time dependent deformation and stability of tunnel faces in fine-grained soils under groundwater, in: Eberhardsteiner, E. (Ed.), ECCOMAS Thematic Conference on Computational Methods in Tunnelling (EURO:TUN 2007), Vienna.

[17] Ströhle, P., Vermeer, P.A., 2009. Die Stabilität der Ortsbrust bei strömendem Grundwasser, Kolloquium Bauen in Boden und Fels. TAE, Ostfildern 2010, 117-123.

[18] Lu, X., Wang, H., Huang, M., 2014. Upper Bound Solution for the face stability of shield tunnel below the water table. Mathematical Problems in Engineering 2014, 11.

[19] Perazzelli, P., Leone, T., Anagnostou, G., 2014. Tunnel face stability under seepage flow conditions. Tunnelling and Underground Space Technology 43, 459-469.

[20] Lee, I.-M., Nam, S.-W., Ahn, J.-H., 2003. Effect of seepage forces on tunnel face stability. Canadian Geotechnical Journal 40, 342-350.

[21] Lee, I.-M., Lee, J.-S., Nam, S.-W., 2004. Effect of seepage force on tunnel face stability reinforced with multi-step pipe grouting. Tunnelling and Underground Space Technology 19, 551-556.

[22] Anagnostou, G., Cantieni, L., Nicola, A., Ramoni, M., 2010. Face stability assessment for the Lake Mead Intake No 3 Tunnel, Tunnel Vision Towards 2020, ITA-AITES World Tunnel Congress (WTC2010), Vancouver.

[23] Brekke, T.L., Selmer-Olsen, R., 1965. Stability problems in underground constructions caused by montmorillonite-carrying joints and faults. Engineering Geology 1, 3-19.

[24] Chang, Y., Swindell, R., Bogdanoff, I., Lindström, B., Termén, J., Starsec, P., 2005. Study of tunnelling through water-bearing fracture zones. Baseline study on technical issues with NE-1 as reference. SKB, Stockholm, Sweden.

[25] Anagnostou, G., 2010. Some rock mechanics aspects of subaqueous tunnels, EUROCK 2009: Rock Engineering in Difficult Ground Conditions - Soft Rocks and Karst, Dubrovnik, 3-14.

[26] Könz, P., 1968. Sickerströmung im Hauptdolomit beim Stollenbau der Engadiner Kraftwerke, Einfluss der Felsanisotropie in der Durchlässigkeit. Mitteilungen der Schweizerischen Gesellschaft für Bodenmechanik und Fundationstechnik, 75, p. 8.

[27] Barla, G., 2000. Lessons learnt from the excavation of a large diameter TBM tunnel in complex hydrogeological conditions, GeoEng2000. Technomic Publishing Company, Inc, Melbourne, Australia, 938-996.

[28] Bezrodny, K.P., Vlasov, S.N., Matsegora, A.G., 1992. Crossing tectonic faults in tunnel construction. Gidrotekhnicheskoe Stroitel'stvo 12, 24-27.

[29] Dahlø, T.S., Nilsen, B., 2002. Stability and rock cover in Norwegian hard rock sub-sea tunnels, Norwegian subsea tunnels 2002.

[30] Shi, C., Cao, C., Lei, M., Yang, W., 2015. Face stability analysis of shallow underwater tunnels in fractured zones. Arabian Journal of Geoscience 9, 11p.

[31] Theiler, A., Zingg, S., Anagnostou, G., 2013. Analysis of a demanding historical tunnel: Albula, ITA-AITES World Tunnel Congress (WTC2013), Geneva, 2022-2029.

[32] Sturk, R., Stille, B., 2008. Advanced Ground Freezing at the Hallandsås Project, Sweden. Geomechanik und Tunnelbau 1, 512-517.

[33] Ponimatkin, P.U., 1972. Analysis of a circular tunnel lining, considering the seepage through the lining and the consolidation-grouted zone. Gidrotekhnicheskoe Stroitel'stvo 3, 35-38.

[34] Kovári, K., 1992. Die Machbarkeit der Piora Mulde beim Gotthard-Basistunnel. In: Die Alptransit-Basistunnel Gotthard und Lötschberg, SIA Dok D085, 55-62.

[35] Adachi, T., Tamura, T., Indraratna, B., Knovel, J.C., 2005. Chapter 12: Undersea tunnel-effect of drainage and grouting. Elsevier Geo-Engineering Book Series. Elsevier, Vol. 3, 327-355.

[36] Egger, P., Ohnuki, T., Kanoh, Y., 1982. Bau des Nakama-Tunnels. Kampf gegen Bergwasser und vulkanisches Gestein. Rock Mechanics, Suppl. 12, 275-293.

[37] Egger, P., 1988. Ground improvement measures for crossing large, heavily water-bearing zone. Tunnels and Water, Serano (ed), Balkema, Rotterdam, 985-990.

[38] Fukuchi, G., 1989. Report on Session 4: Underwater tunnels. Seikan tunnel and water. Tunnels and Water, Serano (ed), Balkema, Rotterdam, 1189-1194.

[39] Soriano, A, Oteo, C.S., Serrano, J.M., 1989. Effects of previous soil improvement with high pressure grouting in subaquatic tunnels. Tunnels and Water, Serano (ed), Balkema, Rotterdam, 839-845.

[40] Anagnostou, G., Kovári, K., 2003. The stability of tunnels in grouted fault zones. Mitteilungen des Inst. für Geotechnik der ETH Zürich. Vol. 220. vdf Hochschulverlag AG.

[41] Anagnostou, G., Kovári, K., 2005. Tunnelling through geological fault zones. International Symposium on Design, Construction and Operation of Long Tunnels, Taipei, Taiwan, 509-520.

[42] Bilfinger, W., 2005. Impermeabilization versus drainage - some considerations regarding lining loads. Felsbau 23, 55-61.

[43] Indraratna, B., Jian Chu, K., 2005. Ground Improvement - Case Histories, in: Hudson, J.A. (Ed.), Elsevier Geo-Engineering Book Series. Elsevier, Oxford.

[44] Nasberg, V.M., Ilyushin, V.F., 1973. Seepage analysis of grouted tunnels and shafts. Gidrotekhnicheskoe Stroitel'stvo 11, 39-45.

[45] Lee, C.F., Sijing, W., Zhifu, Y., 1996. Geotechnical aspects of rock tunnelling in China. Tunnels and Deep Space 11, 445-454

[46] Alija, S., Torrijo, F.J., Quinta-Ferreira, M., 2013. Geological engineering problems associated with tunnel construction in karst rock masses: The case of Gavarres tunnel (Spain). Engineering Geology 157, 103-111.

[47] Anagnostou, G., Ehrbar, H., 2013. Tunnelling Switzerland. vdf, Zürich. p. 118.

[48] Nasberg, V.M., Ilyushin, V.F., 1975. Consideration of groundwater pressure on linings of pressure tunnels and shafts. Gidrotekhnicheskoe Stroitel'stvo 6, 34-38.

[49] Shin, J.H., Addenbrooke, T.I., Potts, D.M., 2002. A numerical study of the effect of groundwater movement on long-term tunnel behaviour. Géotechnique 52, 391-403.

[50] Shin, J.-H., 2008. Numerical modeling of coupled structural and hydraulic interactions in tunnel linings. Structural Engineering and Mechanics 29, 1-16.

[51] Arjnoi, P., Jeong, J.-H., Kim, C.-Y., Park, K.-H., 2009. Effect of drainage conditions on porewater pressure distributions and linig stresses in drained tunnels. Tunnelling and Underground Space Technology 24, 376-389.

[52] Hong, E.-S., Shin, H.-S., Kim, H.-M., Park, C., Park, E.-S., 2007. Numerical study on horizontal pre-drainage system using horizontal directional drilling in subsea tunnelling. Chinese Journal of Rock Mechanics and Engineering 26, 3697-3703.

[53] Beruchashvili, G.A., 1973. Experimental verification of relations for the analysis of a drain well system, by the electrohydrodynamic analogy method. Gidrotekhnicheskoe Stroitel'stvo No. 3, 29-32.

[54] Bukhairov, R.K., 1992. Seepage calculation of drainage. Gidrotekhnicheskoe Stroitel'stvo 26, 25-28.

[55] Anagnostou, G., Schuerch, R., Ramoni, M., 2014. TBM tunnelling in complex rock formations. Ch. 15 in: Proc. XV MIR Conference "Interventi e opere nelle formazioni complesse", Torino, 307-331.

[55] COMSOL®. Subsurface Flow and Geomechanics Module (Comsol Multiphysics 4.4-5.1). COMSOL 1998-2016.

[56] Zingg, S., Anagnostou, G., 2016. An investigation into efficient drainage layouts for the stabilization of tunnel faces in homogeneous ground. Tunnelling and Underground Space Technology, Volume 58, 49–73.

[57] Anagnostou, G., Zingg, S., 2013. On the stabilizing effect of advance drainage in tunnelling. Geomechanics and Tunnelling, Vol. 6, No. 4, 338–354.

[58] Zingg, S., Anagnostou, G., 2012. The effects of advance drainage on face stability in homogeneous ground, ITA-AITES World Tunnel Congress, WTC 2012, Bangkok.

[59] Zingg, S., Anagnostou, G., 2013. Effect of tunnel diameter on the efficiency of advance drainage with respect to face stability. TU-Seoul 2013, International Symposium on Tunnelling and Underground Space Construction for Sustainable Development, Seoul, Korea, 277-280.

[60] Zingg, S., Bronzetti, D., Anagnostou, G., 2013. Face stability improvement by advance drainage via pilot tunnel. ITA-AITES World Tunnel Congress, WTC 2013, Geneva, 701-708.

[61] Zingg, S., Anagnostou, G., 2012. Tunnel face stability in narrow water-bearing fault zones. ISRM International Symposium, Eurock 2012, Stockholm.

[62] Zingg, S., 2016. Static effects and aspects of feasibility and design of drainages in tunnelling. PhD-Thesis No. 23729 at ETH Zurich.

[63] Anagnostou, G., 2012. The contribution of horizontal arching to tunnel face stability. Geotechnik 35, 34-44.

[64] Janssen, H.A., 1895. Versuche über Getreidedruck in Silozellen. Zeitschrift des Vereines Deutscher Ingenieure, p. 1045.

[65] Terzaghi, K., Jelinek, R., 1954. Theoretische Bodenmechanik. Berlin: Springer-Verlag.

[66] Anagnostou, G., Kovári, K., 1994. The face stability of slurry-shield driven tunnels. Tunnelling and Underground Space Technology 9(2), 165-174.

[67] Perazzelli, P., Anagnostou, G., 2011. Comparing the limit equilibrium method and the numerical stress analysis method of tunnel face stability assessment. In: TC28 – IS Roma, 7th Int. Symp. on ‘‘Geotechnical Aspects of Underground Construction in Soft Ground’’, 16–18 May 2011, Roma, Italy.

[68] Wongsaroj, J., 2005. Three-dimensional finite analysis of short- and long-term ground response to open face tunnelling in stiff clay. Ph.D. Thesis, Cambridge University.

[69] Mair, R.J., 2008. Tunnelling and geotechnics: new horizons. Géotechnique 58, No. 9, 713-720.

[70] Franzen, T.,Celestino, T.B., 2002. Lining of tunnels under groundwater pressure. ITA- AITES Downunder 2002, Vol. 1, 481-487.

[71] Celestino, T.B., Giambastiani, M., Bortolucci, A.A., 2001. Water inflows in tunnels: back-analysis and role of different lining system. Proc. 2001 World Tunnelling Congress (WTC2001), VII, Milano, pp. 547-554.

[72] Anagnostou, G., Serafeimidis, K., 2007. The dimensioning of tunnel face reinforcement, Underground Space – the 4th Dimension of Metropolises, ITA-AITES World Tunnel Congress (WTC2007), Prague, 291-296.

[73] Atwa, M., Magnan, J.-P., Leca, E., 2000. Analyse des écoulements d'eau autour des tunnels en cours de construction et à long terme. Laboratoire central des Ponts et Chaussées, Paris.

[74] Sieber Cassina und Handke AG, IG PV Alvra, 2014. Neubau Albulatunnel II, Bauprojekt Raibler-Formation, Aufschlüsse und Färbversuche Albulatunnel I vom 22.07.2014 (not published).

[75] McDonald, J., Burger, W., 2009. Lake-Mead-Zulauftunnel Nr. 3. Tunnel 4, 43-48.

[76] Feroz, M., Jensen, M., Lindell, J.E., 2007. The Lake Mead Intake 3 water tunnel and pumping station, Las Vegas, Nevada, USA, in: Taylor, M.T., Townsend, J.W. (Eds.), Rapid Excavation and Tunneling Conference (RETC2007). Society for Mining Metallurgy and Exploration, Toronto, 647-662.

[77] Anagnostou, G., 2014. Some critical aspects of subaqueous tunnelling, ITA-AITES World Tunnel Congress (WTC2014). Muir Wood Lecture, Brazil, pp. 1-20.

[78] Nicola, A., Nickerson, J., Bono, R., Donadoni, N., Anagnostou, G., Schürch, R., Zingg, S., 2014. Lake Mead Intake Tunnel No. 3 – A step beyond the limits, Swiss Tunnel Congress, Lucerne, 166-173.

[79] Ferrari, A., Pedrazzini, S., 2008. Experiences with TBM drives in the Gotthard Base Tunnel, Bodio section. www.lombardi.ch (last access 01.06.2016).

[80] Hennings, F., 1908. Projekt und Bau der Albulabahn, Denkschrift. Kommissions-Verlag von F. Schuler.

[81] Kovári, K., Anagnostou, G., 1996. Design of grouting cylinder for a deep alpine tunnel. 2nd International Conference on Ground Improvement Geosystems. Japanese Society of Soil Mechanics and Foundation Engineering, Tokyo, 165-170.

[82] Brierley Associates, 2011. Lake Mead Intake #3. Relocated Tunnel Alignment. Geotechnical Interpretive Report, 555p.

[82] Nickerson, J., Bono, R., Cimiotti, C., Moonin, E., 2015. Lake Mead Intake No. 3 - TBM tunneling at high pressures, Rapid excavation and tunneling conference (RETC 2015). SME, New Orleans, 936-946.

[83] Smith, K., 2015. Reviewing the legacy of Lake Mead. North American Tunneling Journal Feb/March 2015, 10-19.

[84] Faulkner, D.R., Jackson, C.A.L., Lunn, R.J., Schlische, R.W., Shipton, Z.K., Wibberley, C.A.J., Withjack, M.O., 2010. A review of recent developments concerning the structure, mechanics and fluid flow properties of fault zones. Journal of Structural Geology 32, 1557-1575.

[85] Evans, J.P., Forster, C.B., Goddard, J.V., 1997. Permeability of fault-related rocks, and implications for hydraulic structure of fault zones. Journal of Structural Geology 19, 1393-1404.

[86] Micarelli, L., Benedicto, A., Wibberley, C.A.J., 2006. Structural evolution and permeability of normal fault zones in highly porous carbonate rocks. Journal of Structural Geology 28, 1214-1227.

[87] Ganarod, G.V., Braathen, A., Willemoes-Wissing, B., 2008. Predictive permeability model of extensional faults in crystalline and metamorphoric rocks; verification by pre-grouting in two sub-sea tunnels, Norway. Journal of Structural Geology 30, 993-1004.

[88] Bear, J., Zaslavsky, D., Irmay, S., 1968. Physical principles of water percolation and seepage. United Nations Educational, Scientific and Cultural Organisation (UNESCO), Paris.

[89] Louis, C., 1967. Strömungsvorgänge in klüftigen Medien und ihre Wirkung auf die Standsicherheit von Bauwerken und Böschungen im Fels, in: Leussink, H. (Ed.). Veröffentlichungen des Institutes für Bodenmechanik und Felsmechanik der Universität Fridericiana in Karlsruhe, Karlsruhe.

[90] Atkinson, T.C., 1977. Diffuse flow and conduit flow in limestone terrain in the Mendip Hills, Somerset (Great Britain). Journal of Hydrology 35, 93-110.

[91] Jeannin, P.-Y., 2001. Modeling flow in phreatic and epiphreatic karst conduits in the Hölloch cave (Muotatal, Switzerland). Water Resources Research, 37(2), 191– 200.

[92] Halford, K.J., 2000. Simulation and interpretation of borehole flowmeter results under laminar and turbulent flow conditions. Seventh International Symposium on Logging for Minerals and Geotechnical Applications, U.S. Geol. Surv., Golden, Colo., 24– 26 Oct.

[93] Shoemaker, W.B., Cunningham, K.J., Kuniansky, E.L., Dixon, J., 2008. Effects of turbulence on hydraulic heads and parameter sensitivities in preferential groundwater flow layers. Water resources research Vol. 44, W03501.

[94] Shoemaker, W.B., Kuniansky, E.L., Birk, S., Bauer, S, 2008. Documentation of a conduit flow process (CFP) for MODFLOW-2005, U.S. Geol. Surv. Tech. Methods Rep., Book 6, Chap. A24.

[95] Birch, S., Donahue, R., Biggar, K.W., Sego, D.C., 2007. Prediction of flow rates for potable water supply from directionally drilled horizontal wells in river sediments. J. Environ. Eng. Sci., 6, 231-245.

[96] Chen, C., Wan, J., Zhan, H., 2003. Theoretical and experimental studies of coupled seepage-pipe flow to a horizontal well. Journal of Hydrology 281, 159-171.

[97] Wang, W., Zhang, G., 2007. Numerical simulation of groundwater flowing to horizontal seepage wells under a river. Hydrogeology Journal, 15, 1211-1220.

[98] Li, Z., Huang, Y., Wang, J., Zi, Q., 2012. 3-D FEM seepage simulation of channel with drain pipes. Applied Mechanics and Materials Vol. 137, 198-204.

[99] Colebrook, C.F., White, C.M., 1937. Experiments with fluid friction in roughened pipes, Proceedings of the Royal Society of London. Series A, Mathematical and Physical. The Royal Society, 367-381.

[100] Bollrich, G., 2000. Technische Hydromechanik, 5 Ed. Verlag Bauwesen, Berlin.

[101] Siwoń, Z., 1987. Solutions for lateral inflow in perforated conduits. Journal of Hydraulic Engineering, 113(9), 1117-1132.

[102] Ouyang, L.-B., Arbabi, S., Aziz, K., 1998. A single-phase wellbore-flow model for horizontal, vertical, and slanted wells. SPE Journal, June, 124-133.

[103] Clerno, T., 2006. Flow in perforated pipes: a comparison of models and experiments. SPE Productions and Operations, May, 302-311.

[104] Theis, C.V., 1935. The relation between the lowering of the piezometric surface and the rate and duration of discharge of a well using groundwater storage. Transactions, American Geophysical Union, Vol 16, 519-524.

[105] Coli, M., Pinzani, A., 2014. Tunnelling and hydrogeological issues: a short review of the current state of the art. Rock Mechanics and Rock Engineering 47, 839-851.

[106] Heuer, R.E., 1995. Estimating rock tunnel water inflow (I), in: Williamson, G., Gowring, I.M. (Eds.), Rapid Excavation and Tunneling Conference RETC. Society for Mining, Metallurgy, and Exploration, Inc., San Francisco, 41-60.

[107] Heuer, R.E., 2005. Estimating rock tunnel water inflow - II, in: Hutton, J.D., Rogstad, W.D. (Eds.), Rapid Excavation and Tunneling Conference RETC. Society for Mining, Metallurgy, and Exploration, Inc., Seattle, 394-407.

[108] Anagnostou, G., 1995. The influence of tunnel excavation on the hydraulic head. International Journal for Numerical and Analytical Methods in Geomechanics 19, 725-746.

[109] Younger, P.L., 1993. Simple generalized methods for estimating aquifer storage parameters. Quarterly Journal of Engineering Geology 26, 127-136.

[110] Eisenstein, Z., Samarasekera, L., 1992. Stability of unsupported tunnels in clay. Can. Geotech. J. 29, 609–613.

[111] Arn, T., 1989. Numerische Erfassung der Strömungsvorgänge im geklüfteten Fels, Institut für Bauplanung und Baubetrieb, Fels- und Untertagbau. Eidgenössische Technische Hochschule Zürich, Zürich.

[112] Desai, C.S., Li, G.C., 1983. A residual flow procedure and application for free surface flow in porous media. Advances in Water Resources 6, 27-35.

[113] El Tani, 2001. Surface displacements due to pressure modifications induced by tunnels. Modern Tunneling Science and Technology, 77–82.

[114] Moon, J., Fernandez, G., 2010. Effect of excavation-induced groundwater level drawdown on tunnel inflow in a jointed rock mass. Engineering Geology 110, 33-42.

[115] Greenwood, D.A., Thomson, G.H., 1984. Ground stabilisation: deep compaction and grouting. Thomas Telford Limited, London.

[116] Mas Ivars, D., 2006. Water inflow into excavations in fractured rock – a three-dimensional hydro-mechanical numerical study. International Journal of Rock Mechanics & Mining Sciences 43, 705-725.

[117] Moon, J., Fernandez, G., 2010. Excavation-induced hydraulic conductivity reduction around a tunnel – Part 1: guideline for estimate of ground water inflow rate. Tunnelling and Underground Space Technology 25, 560-566.

[118] Moon, J., Fernandez, G., 2010. Excavation-induced hydraulic conductivity reduction around a tunnel – Part 2: verification of proposed method using numerical modelling. Tunnelling and Underground Space Technology 25, 567-574.

[119] Potts, D.M., Zdravkovic, L., 1999. Finite Element Analysis in Geotechnical Engineering: Volume One - Theory. Thomas Telford, London. Chapter 10.

[120] Abaqus, 2014. Dassault Systèmes, Providence, USA.

[121] Anagnostou, G., 1991. Untersuchungen zur Statik des Tunnelbaus in quellfähigem Gebirge. Dissertation 9553, ETH Zurich.

[122] Ingenieurgemeinschaft LSE Steilrampe, 2007. Tunnel Engelberg. Tunnelausbau in der Quintnerkalk-Strecke. Kurzbericht über die Konzepterarbeitung (Plan Nr. 981.6-R-6) im Auftrag der Zentralbahn.

Projektabschluss

Schweizerische Eidgenossenschaft
Confédération suisse
Confederazione Svizzera
Confederaziun svizra

Eidgenössisches Departement für
Umwelt, Verkehr, Energie und Kommunikation UVEK
Bundesamt für Strassen ASTRA

FORSCHUNG IM STRASSENWESEN DES UVEK

Version vom 09.10.2013

Formular Nr. 3: Projektabschluss

erstellt / geändert am: 30.11.2016

Grunddaten

Projekt-Nr.:	FGU 2010/004
Projekttitel:	Statische Auswirkung, Machbarkeit und Ausführungsaspekte von Gebirgsdrainagen im Untertagbau
Enddatum:	November 2016

Texte

Zusammenfassung der Projektresultate:

Das Forschungsprojekt fördert das vertiefte Verständnis der statischen Auswirkungen von Drainagemassnahmen auf drei grundlegende, tunnelbauliche Problemstellungen durch wasserführendes Gebirge von geringer Festigkeit: die Stabilität der Ortsbrust, die Stabilität und Verformungen eines Injektionskörpers, sowie die Belastung einer Tunnelschale durch das Bergwasser. Es werden Dimensionierungshilfen zur Verfügung gestellt, die dem praktizierenden Ingenieur die Planung und Ausführung erleichtern können.

Die Untersuchung der Ortsbrust umfasst:
- die Beurteilung der Ortsbruststabilität für verschiedene vorauseilende Drainageanordnungen mittels Grenzgleichgewichtsbetrachtungen und unter Berücksichtigung der numerisch ermittelten Sickerströmung;
- die Ausarbeitung von Dimensionierungs-Nomogrammen für verschiedene, praxisnahe Drainageanordnungen;
- die Berücksichtigung einer Reihe von Faktoren, die die Wirksamkeit von Drainagemassnahmen limitieren können, da sie die Porenwasserdruckreduktion begrenzen (z.B. Ort, Anzahl und Länge von Bohrlöchern; die hydraulische Kapazität der Bohrungen; die zulässige Grundwasserspiegelabsenkung usw.)

Die Studie des Injektionskörpers quantifiziert:
- die stabilisierende Wirkung der theoretischen, idealen Drainage auf Ausbauwiderstand und Plastifizierung eines Injektionskörpers mittels analytischer Lösungen;
- den stabilisierenden Effekt von praxisnahen Drainageanordnungen, die vor und nach der Injektionsmassnahme gebohrt werden und inner- oder ausserhalb des Injektionskörpers angeordnet sind (hydraulisch-mechanisch gekoppelte FE-Modellierung);
- die Genauigkeit und somit die Anwendbarkeit der analytischen Lösungen im Rahmen der Vorprojektierung von drainierten Injektionskörpern.

Die Untersuchung zum Tunnelausbau beinhaltet:
- die Quantifizierung des Restwasserdruckes auf den Tunnelausbau sowie der Wassermenge, die sich infolge verschiedener, permanenter Drainagemassnahmen einstellen;
- die Aufbereitung dieser Resultate in Form von Dimensionierungsdiagrammen.

Forschung im Strassenwesen des UVEK: Formular 3 Seite 1 / 3

Schweizerische Eidgenossenschaft
Confédération suisse
Confederazione Svizzera
Confederaziun svizra

Eidgenössisches Departement für
Umwelt, Verkehr, Energie und Kommunikation UVEK
Bundesamt für Strassen ASTRA

Zielerreichung:

Das Projekt hat die statischen Effekte von Drainagemassnahmen detailliert untersucht, darauf basierend Hilfsmittel für die Praxis ausgearbeitet und somit die im Forschungsgesuch gesteckten Ziele fast vollkommen erreicht.
Bei instabilen Drainagebohrlöchern werden Hüllrohre nötig. Im Projekt wird aufgezeigt, was die statischen Effekte von Hüllrohren sind und welcher Mantelflächenanteil aus Sicht der Ortsbruststabilität mindestens drainieren sollte. Von praktischer Bedeutung ist jedoch auch der Umgang mit diesen Hüllrohre auf den Baustellen und so sind weitere, praxisorientierte Untersuchungen in diesem Gebiet zu empfehlen (Material- und Formwahl, sodass viel Drainagefläche vorhanden ist und die Hüllrohre dennoch genügend (Torsions-)steif sind; baupraktische Ausführung von Bohren und Einführen der Rohre; Berücksichtigung von Zutrittsverlusten beim hydraulischen Verhalten usw.).
Die im Zwischenbericht (Juni 2012) erwähnte Problemstellung "Verklemmen der TBM" umfasst die Modellierung des laufenden TBM-Vortriebs und dessen Interaktion mit der vorauseilenden Drainage. Nach Rücksprache mit der BK wurde diese Problemstellung zu Gunsten der vertieften Betrachtung der übrigen Problemstellungen nicht weiter bearbeitet. Dennoch ist diese Fragestellung für Tunnelprojekte durch wasserführendes druckhaftes Gebirge von Bedeutung und sollte daher untersucht werden.

Folgerungen und Empfehlungen:

Das Forschungsprojekt zeigt auf, dass bereits 6 Drainagebohrungen, gebohrt ab der Ortsbrust und mit einer minimalen Länge von 1.5 Tunneldurchmessern, die Ortsbruststabilität massiv erhöhen. Im heterogen durchlässigen Baugrund sollten die Drainagen so angeordnet sein, dass sie durch geringdurchlässige Baugrundschichten hindurch reichen und damit den Porenwasserdruck vor und hinter diesen potentiellen hydraulischen Barrieren absenken können. Die hydraulische Kapazität sowie die tolerierbare Vorlaufzeit von Drainagemassnahmen begrenzen den Bereich der Baugrunddurchlässigkeit (ungefähr 10exp-7 bis 10exp-5 m/s), für welche Drainagebohrungen empfohlen werden können. Die statisch erforderlichen offenen Flächenanteile für Hüllrohre werden quantifiziert, ebenso Wasseranfall, Grundwasserspiegelabsenkung und Setzung infolge Drainage.
Weiter wird belegt, dass die analytischen Lösungen der idealen Drainage von Injektionskörpern für die praktische Vordimensionierung ausreichend genau sind, wenn beispielsweise
- entweder 12 radiale Drainagen innerhalb des Injektionskörpers gebohrt werden,
- oder mindestens 8 koaxiale Bohrungen ausserhalb des Injektionskörpers angeordnet werden.

Das Projekt quantifiziert die hydraulische Belastung des Tunnelausbaus auf z.B. gut 10% des initialen Wasserdrucks, wenn 8 radiale Drainagebohrungen (mit gegebener Länge, Axialabstand und Durchmesser) angeordnet werden.

Publikationen:

- Zingg, S., 2016. Static effects and aspects of feasibility and design of drainages in tunnelling. PhD-Thesis No. 23729 at ETH Zurich.
- Zingg, S., Anagnostou, G., 2012. The effects of advance drainage on face stability in homogeneous ground, ITA-AITES World Tunnel Congress, WTC 2012, Bangkok.
- Zingg, S., Anagnostou, G., 2012. Tunnel face stability in narrow water-bearing fault zones. ISRM International Symposium, Eurock 2012, Stockholm.
- Zingg, S., Anagnostou, G., 2013. Effect of tunnel diameter on the efficiency of advance drainage with respect to face stability. TU-Seoul 2013, International Symposium on Tunnelling and Underground Space Construction for Sustainable Development, Seoul, Korea, 277-280.
- Zingg, S., Anagnostou, G., 2016. An investigation into efficient drainage layouts for the stabilization of tunnel faces in homogeneous ground. Tunnelling and Underground Space Technology, Volume 58, 49–73.
- Zingg, S., Bronzetti, D., Anagnostou, G., 2013. Face stability improvement by advance drainage via pilot tunnel. ITA-AITES World Tunnel Congress, WTC 2013, Geneva, 701-708

Der Projektleiter/die Projektleiterin:

Name: Anagnostou   Vorname: Georg

Amt, Firma, Institut: Institut für Geotechnik, ETH Zürich

Unterschrift des Projektleiters/der Projektleiterin:

Forschung im Strassenwesen des UVEK: Formular 3   Seite 2 / 3

Schweizerische Eidgenossenschaft
Confédération suisse
Confederazione Svizzera
Confederaziun svizra

Eidgenössisches Departement für
Umwelt, Verkehr, Energie und Kommunikation UVEK
Bundesamt für Strassen ASTRA

FORSCHUNG IM STRASSENWESEN DES UVEK

Formular Nr. 3: Projektabschluss

Beurteilung der Begleitkommission:

Beurteilung:

Die Forschungsarbeiten sind sehr detailliert durchgeführt worden. Die verschiedenen Aspekte der Drainage auf die Ortsbruststabilität, auf die Stabilität eines Injektionskörpers und auf die Tunnelverkleidung wurden durch umfangreiche Parameterstudien analysiert. Auch wenn gewisse Fragestellungen nicht vertieft werden konnten, die in der ursprünglichen Zielsetzung vorgesehen waren, so resultiert auf der anderen Seite aus der Arbeit eine sehr systematische und gründliche Analyse der betrachteten Aspekte. Damit darf man den grössten Teil der Thematik als erschöpfend bearbeitet betrachten.

Umsetzung:

Die Untersuchungen wurden durch sehr umfangreiche Parameterstudien vorgenommen. Damit konnten einerseits eine Vielzahl von Parametern studiert und ihre Einflüsse belegt werden, andererseits wurden damit auch die Voraussetzungen geschaffen für Dimensionierungshilfen (Nomogramme etc), die eine rasche, unkomplizierte und trotzdem korrekte Umsetzung der Resultate in die Praxis ermöglichen.

weitergehender Forschungsbedarf:

Weiterer Forschungsbedarf besteht in der Erweiterung der Untersuchungen auf TBM Vortriebe und in der Umsetzung auf bautechnische Vorgaben, die allenfalls bis zur Spezifikation von Materialeigenschaften reichen könnten.

Einfluss auf Normenwerk:

Einzelne Erkenntnisse, wie zB Anzahl und Anordnung von Drainagebohrungen, können bei der Überarbeitung der SIA Normen 198 ff berücksichtigt werden.

Der Präsident/die Präsidentin der Begleitkommission:

Name: Amberg   Vorname: Felix

Amt, Firma, Institut: Amberg Engineering AG

Unterschrift des Präsidenten/der Präsidentin der Begleitkommission:

Forschung im Strassenwesen des UVEK: Formular 3   Seite 3 / 3

Verzeichnis der Berichte der Forschung im Strassenwesen

Das Verzeichnis der in der letzten Zeit publizierten Schlussberichte kann unter www.astra.admin.ch (Forschung im Strassenwesen → Downloads → Formulare) heruntergeladen werden.